High resolution climatic modelling in the Amazon-Andes transition region : understanding climate-forest interaction and its implication for rainfall patterns

Juan Pablo Sierra Perez

THÈSE

Pour obtenir le grade de

DOCTEUR DE L'UNIVERSITÉ GRENOBLE ALPES

École doctorale : STEP - Sciences de la Terre de lEnvironnement et des Planètes
Spécialité : Sciences de la Terre et de l'Univers et de l'Environnement
Unité de recherche : Institut des Géosciences de lEnvironnement

Modélisation climatique à haute résolution dans la région de transition Amazonie-Andes: comprendre l'interaction climat-forêt et ses implications pour les régimes pluviométriques

High resolution climatic modelling in the Amazon-Andes transition region: understanding climate-forest interaction and its implication for rainfall patterns

Présentée par :

Juan Pablo SIERRA PEREZ

Direction de thèse :

Jhan Carlo ESPINOZA VILLAR Université Grenoble Alpes	Directeur de thèse
Clémentine JUNQUAS CHARGEE DE RECHERCHE, Université Grenoble Alpes	Co-encadrante de thèse

Rapporteurs :

Francina DOMINGUEZ
PROFESSEUR, University of Illinois Urbana-Champaign
Vincent DUBREUIL
PROFESSEUR DES UNIVERSITES, Université de Rennes 2

Thèse soutenue publiquement le **2 décembre 2022**, devant le jury composé de :

Jhan Carlo ESPINOZA VILLAR DIRECTEUR DE RECHERCHE, IRD délégation Sud-Est	Directeur de thèse
Francina DOMINGUEZ PROFESSEUR, University of Illinois Urbana-Champaign	Présidente
Laurent LI DIRECTEUR DE RECHERCHE, CNRS délégation Ile-de-France Sud	Examinateur
Vincent DUBREUIL PROFESSEUR DES UNIVERSITES, Université de Rennes 2	Rapporteur
Fabien MAUSSION PROFESSEUR ASSISTANT, University of Innsbruck	Examinateur
Thierry LEBEL DIRECTEUR DE RECHERCHE EMERITE, IRD délégation Sud-Est	Examinateur
Jean-Martial COHARD MAITRE DE CONFERENCES HDR, Université Grenoble Alpes	Examinateur

Invités :

Clémentine JUNQUAS
Chargé de Recherche, IRD

Agradecimientos

La realización material de esta investigación ha sido posible gracias al financiamiento por parte del proyecto AMANECER, el cual hace parte a su vez del programa del gobierno francés Make Our Planet Great Again (MOPGA). Por esta razón quiero agradecerle al gobierno francés, y particularmente al Institut de Recherche pour le Développement (IRD) y a la Agence Nationale de la Recherche (ANR) quienes han trabajado en el desarrollo de la ciencia en los países del hemisferio sur y particularmente en Suramérica. Agradezco también a la Université Grenoble Alpes, al Institut des Géoscienses de l'Environnement y en particular al personal académico y administrativo École Doctorale Sciences de la Terre de l'Environnement por generar un ambiente agradable y fructífero para las discusiones académicas. Agradezco a los equipos C2H y CryoDyn, y particularmente a Thomas Condom, Jean E. Sicart y Antoine Rabatel, quienes aportaron siempre nuevas perspectivas.

La conceptualización y las preguntas científicas abordadas en esta tesis han sido, en gran parte, el resultado de la reflexión y la trayectoria académica de mi director de tesis Jhan Carlo Espinoza. Agradezco enormemente a Jhan Carlo por compartir conmigo su amor por la ciencia, la horología y, por supuesto, la buena cervecería. También quisiera expresar mi profundo agradecimiento a mi co-directora de tesis, Clementine Junquas. Su capacidad para ver siempre el potencial de nuestras ideas y discusiones ha definido en gran medida el alcance y curso de este trabajo. Además. quisiera agradecerle a ella por permitirme conocer un poco mas de la cultura de este bello país que es Francia.

Las discusiones y reflexiones conjuntas con personas de otros laboratorios e institutos han enriquecido significativamente este trabajo. Mis agradecimientos especiales al profesor Jan Polcher del Laboratoire de Météorologie Dynamique por sus interesantes e incisivos comentarios que llevaron este trabajo por caminos inesperados. Gracias también al profesor Vincent Moron del Centre Européen de Recherche et d'Enseignement des Géosciences de l'Environnement, quien estuvo siempre dispuesto a escuchar nuestras ideas y a compartir su gran conocimiento acerca de la dinámica atmosférica. Así mismo, me quiero agradecer al profesor Fabien Maussion de la University of Innsbruck por su tiempo e interés en este trabajo. Como siempre, mi especial gratitud con la profesora Paola Arias de la Universidad de Antioquia por siempre creer en mi y por su importante influencia en mi formación investigador.

Quiero agradecer a los miembros del jurado de tesis: Fabien Maussion, Francina Dominguez, Thierry Lebel, Vincent Dubreuil, Laurent Li, Jean-Martial Cohard, por aceptar ser parte de esta aventura, por su tiempo y su interés.

Finalmente, me siento infinitamente afortunado de todas las experiencias vividas en estos tres años como doctorante, pero sobre todo por haber conocido personas tan especiales como mis amigos boliviano-peruano-ecuatoriano-alemano-indio-mexicano-franceses. Muchas gracias por enseñarme de sus culturas, su deliciosa gastronomía y por haber hecho de este tiempo en Grenoble algo inolvidable. Gracias especiales a mi esposa, Tatiana, por compartir el mundo conmigo y por que su amor ha sido mi fuente de energía en los días mas agotadores. Finalmente, gracias infinitas

a mi familia, desde la distancia logran llenarme de felicidad y motivación. Gracias a mi madre, Zilah, y a mi padre Mauricio por creer siempre en mi, y a mis hermanas Ana María y María Fernanda por que sin saberlo siempre me han llenado de buena energía.

Remerciements

La réalisation matérielle de cette recherche a été rendue possible grâce au financement du projet AMANECER, qui fait partie du programme MOPGA (Make Our Planet Great Again) du gouvernement français. C'est pourquoi je tiens à remercier le gouvernement français, et en particulier l'Institut de Recherche pour le Développement (IRD) et l'Agence Nationale de la Recherche (ANR) qui ont œuvré pour le développement de la science dans les pays du Sud et notamment en Amérique du Sud. Je remercie également l'Université Grenoble Alpes, l'Institut des Géosciences de l'Environnement et en particulier le personnel académique et administratif de l'École Doctorale Sciences de la Terre de l'Environnement pour avoir créé un environnement agréable et fructueux pour les discussions académiques. Je remercie les équipes du C2H et de CryoDyn, et en particulier Thomas Condom, Jean E. Sicart et Antoine Rabatel, qui ont toujours apporté de nouvelles perspectives.

La conceptualisation et les questions scientifiques abordées dans cette thèse ont été, dans une large mesure, le résultat de la réflexion et du parcours académique de mon directeur de thèse Jhan Carlo Espinoza. Je tiens tout particulièrement à remercier Jhan Carlo pour avoir partagé avec moi son amour de la science, de l'horlogerie et, bien sûr, de la bonne bière. Je tiens également à exprimer ma profonde reconnaissance à ma codirectrice de thèse, Clémentine Junquas. Sa capacité à toujours voir le potentiel de nos idées et de nos discussions a largement défini la portée et le déroulement de ce travail. De plus, je tiens à la remercier de m'avoir permis d'en apprendre un peu plus sur la culture de ce beau pays qu'est la France.

Les discussions et réflexions communes avec des personnes d'autres laboratoires et instituts ont considérablement enrichi ce travail. Je remercie tout particulièrement le professeur Jan Polcher du Laboratoire de Météorologie Dynamique pour ses commentaires intéressants et incisifs qui ont amené ce travail dans des directions inattendues. Merci également au Professeur Vincent Moron du Centre Européen de Recherche et d'Enseignement des Géosciences de l'Environnement, qui était toujours prêt à écouter nos idées et à partager sa grande connaissance de la dynamique atmosphérique. Je tiens également à remercier le professeur Fabien Maussion de l'Université d'Innsbruck pour le temps et l'intérêt qu'il a accordés à ce travail. Comme toujours, je tiens à remercier tout particulièrement le professeur Paola Arias de l'université d'Antioquia pour avoir toujours cru en moi et pour son influence importante sur ma formation en recherche.

Je tiens à remercier les membres du jury de thèse : Fabien Maussion, Francina Dominguez, Thierry Lebel, Vincent Dubreuil, Laurent Li, Jean-Martial Cohard, pour avoir accepté de faire partie de cette aventure, pour leur temps et leur intérêt.

Enfin, je me sens infiniment chanceux pour toutes les expériences que j'ai vécues au cours de ces trois années de doctorat, mais surtout pour avoir rencontré des personnes aussi spéciales que mes amis boliviens, péruviens, équatoriens, allemands, indiens, mexicains et français. Merci beaucoup de m'avoir fait découvrir vos cultures, votre délicieuse gastronomie et d'avoir rendu ce séjour à Grenoble

inoubliable. Je remercie tout particulièrement ma femme, Tatiana, pour avoir partagé le monde avec moi et pour son amour qui a été ma source d'énergie lors des journées les plus épuisantes. Enfin, un merci infini à ma famille, qui, de loin, parvient à me remplir de bonheur et de motivation. Merci à ma mère, Zilah, et à mon père Mauricio d'avoir toujours cru en moi, et à mes sœurs Ana María et María Fernanda de m'avoir rempli, sans le savoir, de bonnes énergies.

Abstract

A warming climate, more frequent dry and wet extreme events and an unstoppable deforestation currently threaten the largest rainforest in the world. The Amazon forest holds rich and biodiverse ecosystems, and its vegetation acts as a source of water vapor to the atmosphere and as an atmospheric carbon sink. Thus, this tropical forest is an active component of the Earth climate system. Amazonian moisture sustains rainfall in the Amazon itself and in different regions of the South American continent such as the tropical Andes, a place containing numerous glaciers and fragile mountainous ecosystems. Concurrently, high erosion rates associated with heavy rainfall in the eastern side of the Andes produce the sediments that fertilize the Amazon lowlands. In this way, the Amazon and the tropical Andes conform an entangled bio-geophysical system. The main question of this thesis is how the Amazonian deforestation could impact the hydro-climatic connectivity in the Amazon-Andes system.

To address this question, we perform simulations with the Weather Research and Forecasting (WRF) regional climate model using a control (forced with present land-use conditions) and a deforestation experiment (forced with observed 1992-2002 deforestation rates projected to the year 2050). For a better representation of the land surface-atmosphere processes, we couple WRF with the land surface model ORganising Carbon and Hydrology In Dynamic EcosystEms (ORCHIDEE) in some sections of the thesis.

Our modelling results suggest that, in the current land-use conditions, the land cover heterogeneity in the southern Amazon (dominated by the coexistence of tropical rainforest and cropland/grassland) is crucial for the establishment of the rainy season onset. During the dry-to-wet transition period, thermally driven shallow convection is developed over crops. Nonetheless, large-scale subsidence inhibits convection over the region except over forested areas which present higher convective potential energy. We hypothesize that the large-scale flow transports the upward wind anomalies initialized over croplands toward forested areas, triggering deep convection over these zones. Deforestation reduces the forest area and therefore the land-surface heterogeneity, what could hinder the early development of deep convection and delay the wet season onset. Changes in the wet season (December-to-February) atmospheric circulation regimes reinforce the idea of a late arrival of the rainy season.

Amazonian forest loss generates profound changes in the austral summer regional atmospheric circulation, surface energy and hydrological balances at different time scales. At intra-seasonal scale, deforestation weakens the South Atlantic Convergence Zone and decreases its frequency of occurrence at the beginning of the wet season. Similarly, the north-south flow of the South American Low-Level Jet (SALLJ) is weaker under deforested conditions and exhibits a delayed activity. At seasonal scale, deforestation reduces the surface net radiation and evapotranspiration. Hence, the troposphere is colder and drier causing a rainfall depletion and wide subsidence anomaly over the Amazon basin. The subsidence anomaly increases the mid-upper tropospheric stability and reduces precipitation also in the western part of the southern tropical Andes. Over the Amazon-Andes transition region, deforestation decreases rainfall over the cleared areas of the Amazon lowlands

during daytime and over the eastern Andean hillsides during nighttime. Using high-resolution simulations, we trace the evolution of the regional-scale deforestation signal to its impact at local scale in the Bolivian inter-Andean valleys. Deforestation reduces nighttime precipitation in the valleys of Zongo and Huarinilla in -30% as a result of a decreased entry of the SALLJ moist winds from Amazon towards the Andean summits. This rainfall reduction can seriously impact the hydrology of the region.

Résumé

Le réchauffement du climat, des événements extrêmes plus fréquents et la déforestation incessante menacent la plus grande forêt tropicale du monde. La forêt amazonienne abrite des écosystèmes biodiversifiés et sa végétation sert de source de vapeur d'eau pour l'atmosphère et de puits de carbone atmosphérique. Cette forêt tropicale est donc un composant actif du système climatique. L'humidité amazonienne alimente les précipitations en Amazonie même et dans différentes régions du continent sud-américain comme les Andes tropicales, où se trouvent de nombreux glaciers et des écosystèmes montagneux fragiles. Parallèlement, les taux d'érosion associés aux précipitations intenses sur le versant oriental des Andes produisent les sédiments qui fertilisent les basses terres amazoniennes. De cette façon, l'Amazonie et les Andes tropicales forment un système biogéophysique entrelacé. La question centrale de cette thèse est de savoir comment la perte de la forêt amazonienne pourrait avoir un impact sur la connectivité hydroclimatique dans le système Amazone-Andes.

Pour répondre à cette question, nous effectuons des simulations avec le modèle climatique régional WRF en utilisant une expérience de contrôle et une de déforestation. Pour une meilleure représentation des processus surface terrestre-atmosphère, nous couplons WRF avec le modèle de surface terrestre ORCHIDEE dans certaines sections de la thèse.

Nos résultats suggèrent qu'actuellement, l'hétérogénéité de la couverture terrestre dans le sud de l'Amazonie (dominée par la coexistence de la forêt tropicale et des cultures/prairies) est cruciale pour le début de la saison des pluies. Pendant la période de transition sec-humide, une convection peu profonde d'origine thermique apparaît sur les cultures. La subsidence à grande échelle empêche la convection dans la majorité de la zone, sauf dans les zones forestières qui présentent une énergie potentielle de convection plus élevée. Les anomalies de vent ascendant initialisées sur les terres cultivées pourraient être transportées par le flux à grande échelle et déclencher une convection profonde sur les zones forestières. La déforestation réduit la surface des forêts, ce qui pourrait entraver le développement précoce de la convection profonde et retarder le début de la saison humide. Les changements dans les régimes de circulation atmosphérique de la saison humide (décembre à février) renforcent l'idée d'une arrivée tardive de la saison des pluies.

La déforestation amazonienne génère changements dans la circulation atmosphérique régionale de l'été austral, les bilans d’énergie de surface et hydrologiques à différentes échelles de temps. À l'échelle intra-saisonnière, un affaiblissement et une diminution de la fréquence des événements de la Zone de Convergence de l'Atlantique Sud au le début de la saison humide sont observés dans le scénario de déforestation. De même, la circulation du South American Low-Level Jet (SALLJ) est plus faible avec la déforestation. À l'échelle saisonnière, la déforestation réduit le rayonnement net de surface et l'évapotranspiration. La troposphère est donc plus froide et sèche, ce qui entraîne une diminution des précipitations et une anomalie de subsidence dans le bassin amazonien. Dans la région de transition entre l'Amazonie et les Andes, la déforestation réduit les précipitations sur les zones défrichées pendant la journée et sur les collines des Andes

orientales pendant la nuit. En utilisant des simulations à haute résolution, nous traçons l'évolution du signal de déforestation à l'échelle régionale jusqu'à son impact à l'échelle locale dans les vallées interandines boliviennes. Nos résultats montrent que la déforestation réduit les précipitations nocturnes dans la vallée du Zongo d'environ -30% en raison d'une entrée réduite des vents humides SALLJ de l'Amazonie vers les hautes terres andines. Cette réduction des précipitations peut avoir un impact sérieux sur l'hydrologie de la région.

Contents

1

General context and the objective of the thesis

Contents

1.1 Tropical rainforest and the hydrological cycle

Every year, on average, about 40.000 km^3 of water evaporated over the oceans are transported by the winds toward the continents. Equally distributed over terrestrial areas, this moisture quantity generates ~268 mm per year (mm y^{-1}) of rainfall. Nevertheless, the average annual precipitation over land is about 779 mm per year, what implies that nearly 511 mm y^{-1} or, in other words, more than 60% of terrestrial precipitation is derived from the sum of evaporation and transpiration (the release of water vapor from plant leaves during the photosynthesis) within the continents (Trenberth et al. 2011). The surface water available for evapotranspiration (the sum of direct evaporation and vegetation transpiration) depends on the surface characteristics and vegetation. In general, the main contributor for terrestrial evapotranspiration is transpiration, and rainforests exhibit the highest transpiration rates with respect to other land surface covers (Bonan 2015). In this way, tropical rainforests act as a water source to the atmosphere (Zhang et al. 2001; Jasechko et al. 2013). Thus, within the tropics, air parcels travelling over forested surfaces generate twice or more rainfall than air parcels moving over non-forested lands (Spracklen et al. 2012). In this sense, forest plays an important role in the continental hydrology and helps to sustain the wet conditions necessary for its own existence (Ampuero et al. 2020).

1.2 The Amazon rainforest as a tipping element of the Earth system

The Amazon, the major tropical forest in the world, has been recognized as one ‘tipping element’ of the Earth system. A tipping element is defined as a large-scale component of the Earth system that might pass a ‘tipping point’, a critical threshold at which a small perturbation can alter the state or development of the system (Lenton et al. 2008). Two tipping points have been identified that could drive the Amazon ecosystem toward a savanna-like state: (i) clearing more than 40% of the Amazon basin, and (ii) a global warming between 3° and 4°C (Lenton et al. 2008). Currently, 17% of the Amazon basin has been deforested (Figure 1.1). At the same time, the region has warmed about 1 to 1.5°C during the past century (Victoria et al. 1998; Jiménez-Muñoz et al. 2013). Thus, simultaneously, we are getting close to these

critical thresholds. Moreover, the interaction between global warming and large-scale forest loss may increase the probability of irreversible changes in the ecosystem (Wongchuig et al. 2021).

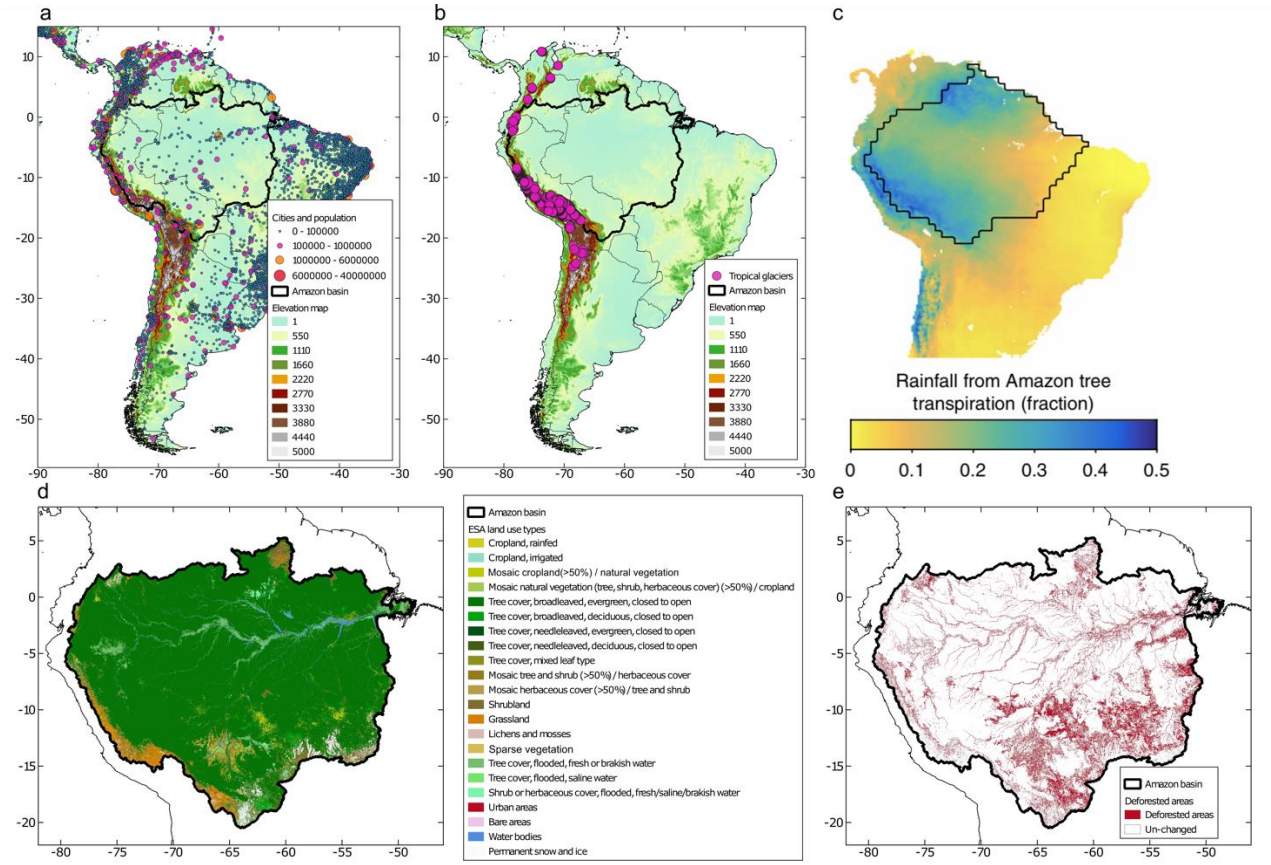

Fig. 1.1 Elevation map (m.a.s.l.) on South America and location of the Amazon basin (black line). **a** Location of cities in South America. Blue dots represent very small cities (less than 100.000 habitants), magenta dots represent small cities (between 100.000 to 1.000.000 habitants), orange dots represent medium cities (between 1.000.000 to 6.000.000 habitants) and red dots represent big cities (>6.000.000 habitants). **b** Location of tropical glaciers (magenta dots) in South America. **c** Fraction of mean annual rainfall that has been transpired by trees in the Amazon basin. **d** Observed land cover for the year 1992. **e** Deforested areas for the year 2020. Data source for the digital elevation model is the USGS 30 ARC-second Global Elevation Data, GTOPO30. Population dataset comes from https://simplemaps.com/data/world-cities. Glacier dataset is obtained from the Randolph Glacier Inventory (available at https://nsidc.org/data/nsidc-0770/versions/6#anchor-1). Data source for South American land cover is the European Space Agency Climate Change Initiative ESA-CI available at https://www.esa-landcover-cci.org/. Figure c modified from Staal et al. (2018)© Copyright Springer Nature.

The degradation of the Amazonian rainforest is associated with several impacts on the functioning of the ecosystem including the disruption of the river flow regulation and its sediment transport toward Amazon lowlands, alterations of the atmospheric carbon sequestration or reductions in the atmospheric moisture transport toward La Plata basin, the Andean cities and the Andean tropical glaciers (Marengo et al. 2004; Arraut

et al. 2012; Sagredo and Lowell 2012; Rabatel et al. 2013; Poveda et al. 2014; Figure 1.1). Moisture originated in the Amazon basin contributes to 30-50% of the total annual rainfall over the southern tropical Andes (between 5°-20°S) and the western Amazon (Figure 1.1c). Over these regions in particular, population is highly concentrated (Figure 1.1 a) and most of the tropical glaciers are located (Figure 1.1b). Thus, Amazonian forest degradation might generate serious impacts on the water resources for Andean cities and for the existence of tropical glaciers, among others. Analyzing the potential impacts of the undergoing Amazonian deforestation on the regional climate is a major issue in order to better understand the associated risks of our current development strategies as a society.

1.3 Why it is still important to explore the impacts of Amazonian deforestation on the regional climate?

Although the majority of studies on tropical deforestation have focused on the Amazon, computational constraints have limited the geographical domains, the time period lengths, and the horizontal resolutions used by the climate models (D'Almeida et al. 2007; Spracklen et al. 2018). As a result, two types of modeling works cover most of the scientific literature developed so far: (i) small-scale deforestation studies with realistic deforestation experiments which use high-resolution regional climate models, but covering limited areas and short time periods (e.g. Silva Dias and Regnier 1996; Dolman et al. 1999; Walker et al. 2009; Khanna et al. 2017), or (ii) large-scale deforestation experiments with regional or global climate models, coarse spatial resolutions and unrealistic deforestation scenarios (e.g. Lean and Rowntree 1997; Costa and Foley 2000; Voldoire and Royer 2004). With the recent advances of computational sciences, high resolution simulations with more realistic deforestation scenarios and a better representation of land-atmosphere processes are becoming more frequent (e.g. Ramos da Silva et al. 2008; Lejeune et al. 2015; Alves et al. 2017; Eiras-Barca et al. 2020; Ruiz-Vásquez et al. 2020; Jiang et al. 2021). However, these studies still present some important limitations. First, deforestation scenarios are in general too simplistic and tend to ignore the real complexity of the land-use change (e.g. replacing forest areas with a unique type of land surface cover; Akkermans et al. 2014). Secondly, many works use fixed sea surface temperatures and neglect the possible ocean-atmosphere interactions in deforestation experiments (e.g. Voldoire

and Royer 2005; Schneider et al. 2006; Nobre et al. 2009). Third, the use of regional climate models, even with enhanced spatial resolutions present the inherent constraint of fixed boundary conditions (prescribed winds and moisture entering into the analyzed spatial domain) that inhibit the deforestation influence on larger spatial scales (Hasler et al. 2009; Medvigy et al. 2011; Badger and Dirmeyer 2016). Fourth, despite the new generation climate models have spatial resolutions of the scale of dozens of kilometers, this resolution is not enough to represent some important land-atmosphere processes such as convection. This is particularly important in the Amazon, where almost 80% of the annual precipitation is produced by deep convection (Greco et al. 1990). Finally, the majority of the literature on the impacts of Amazonian deforestation is focused mainly on annual and seasonal scales. Except for a few studies (e.g. Polcher 1995; Medvigy et al. 2011; Eghdami and Barros 2020), the effects of forest clearance on the atmospheric phenomena at an intra-seasonal level remain poorly understood.

In order to deal with some of the above-mentioned limitations, the AMazon ANdEs ConnEctivity (AMANECER) project, which is part of the French national project Make Our Planet Great Again (MOPGA) and looks for taking action against global warming, has addressed part of its efforts to analyzing the impacts of Amazonian deforestation on the regional climate. Previous AMANECER publications have identified the particular vulnerability of the Amazon-Andes transition region to the rainforest loss and the lack of studies regarding the potential impacts of Amazonian deforestation in the existent hydroclimatic connection between the Amazon rainforest and the Andes (Ampuero et al. 2020; Pabón-Caicedo et al. 2020; Armijos et al. 2020a; Poveda et al. 2020; Gutierrez-Cori et al. 2021). The Amazon-Andes transition region is recognized by its high fraction of rainfall originated from the Amazon rainforest evapotranspiration, by its huge biodiversity and by its intense current deforestation rates (Myers et al. 2000; Staal et al. 2018; Lovejoy and Nobre 2019). Therefore, this PhD thesis is addressed to gain a better understanding of the potential impacts of Amazon deforestation on the hydroclimatic connectivity between the Amazon and the Andes at different time scales.

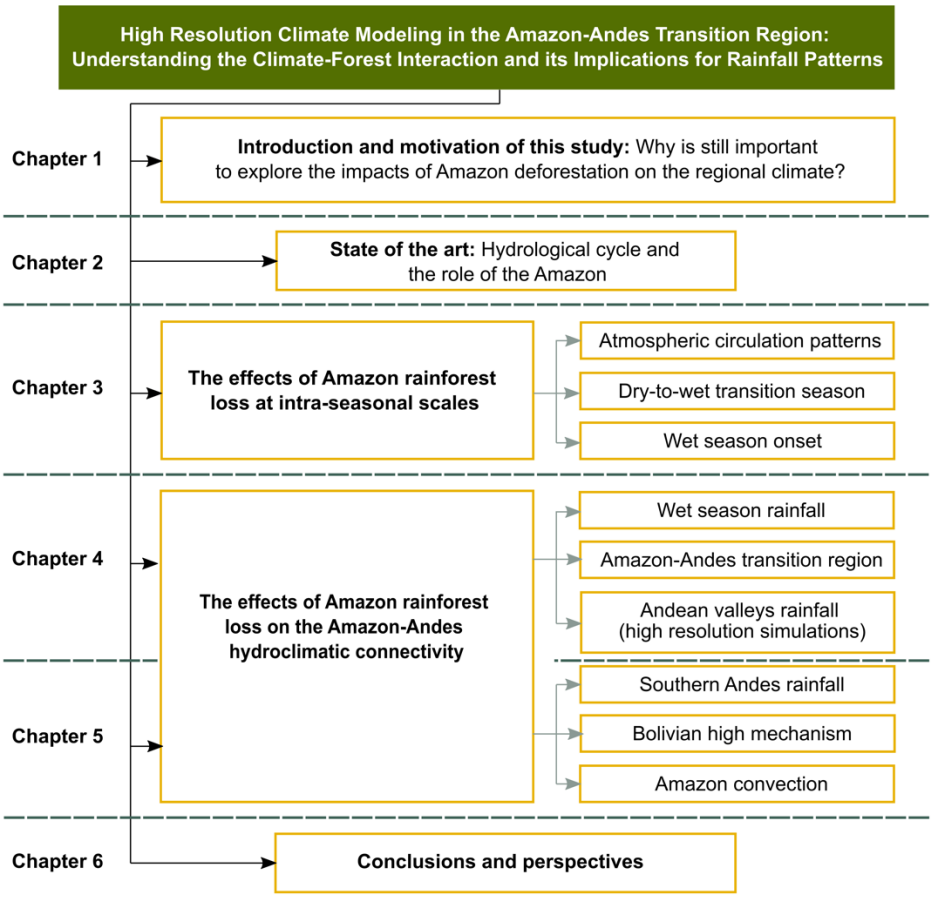

Fig. 1.2 Schematic structure of this thesis.

This manuscript is organized in six chapters as illustrated in Figure 1.2. In the first chapter (this chapter), we describe the motivation for this thesis and a general introduction regarding the problem of tropical deforestation, as well as the main 'holes' in the current knowledge of Amazonian deforestation. Chapter 2 is dedicated to present the current state of the art of deforestation in the Amazon basin. In this chapter we describe the role of the Amazon rainforest in the Earth climate system, the basic climatic conditions in the Amazon basin, the recent observed environmental changes in the catchment, as well as the observed and projected impacts of the rainforest loss. In Chapter 3 we analyze the impacts of Amazonian deforestation on the regional atmospheric circulation and its associated rainfall at intra-seasonal time scales. Additionally, we explore the different role of pasture and forest on the onset of the wet season in the southern Amazon. We end this chapter with the assessment of the impacts of forest loss on the onset and development of the wet season using a weather typing approach. Chapters 4 and 5 are addressed to study the potential impacts of the

rainforest clearance on the hydroclimatic connectivity between the Amazon and the tropical Andes. While Chapter 4 is focused on the deforestation induced changes in the Amazon-Andes transition region rainfall, as well as the perturbations in precipitation over an instrumented Andean valley using high resolution convective permitting simulations, Chapter 5 looks for evaluate the effects of Amazonian deforestation on the relationship between southern tropical Andes rainfall, the Bolivian High and the Amazonian convection. Finally, Chapter 6 discusses the general conclusions and the potential research topics for future works.

2

The Amazon as an essential component of the Earth climate system

Contents

2.1 Generalities of the world's largest tropical rainforest

The Amazon basin is located between 20°S and 5°N. It extends over seven countries and encompasses ~5.8 million km^2, nearly 33% of South America (Figure 1.1). The Amazon basin presents a strong longitudinal topographic gradient, with surface elevations above 6000 m.a.s.l. in the west, and lowlands almost at sea level in the east (Figure 1.1). This heterogenous landscape, in conjunction with the low rainfall seasonality and high rainfall rates over the western part, and the vast sediment production there help to explain the huge biological diversity found within the watershed (Hoorn et al. 2010; Rangel et al. 2018; Cadena et al. 2021).

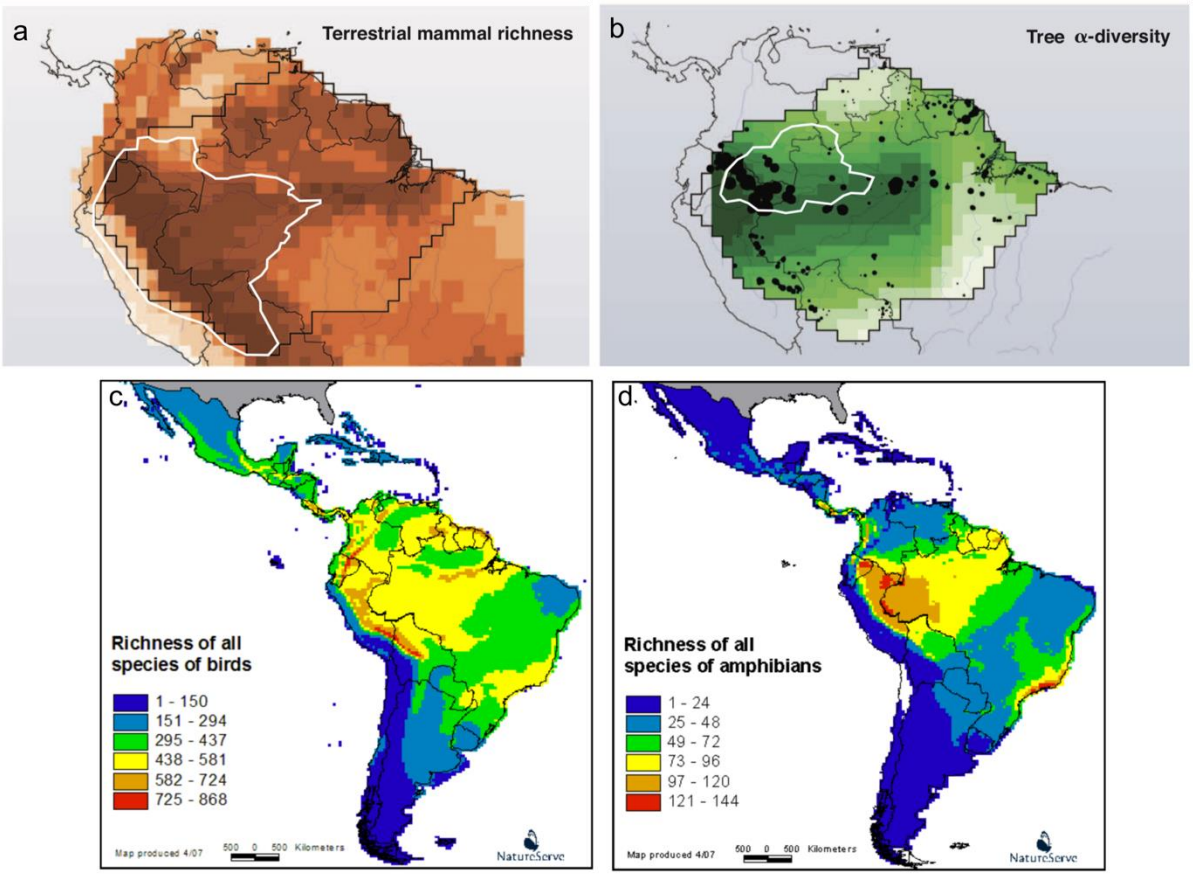

Fig. 2.1 Current Amazonian diversity patterns in terms of: **a** terrestrial mammal richness (lightest color means 2-10 species, darkest color means 89-109 species), **b** tree α-diversity, c bird richness and d amphibian richness. White polygons in **a** and **b** correspond to areas with rich soils and areas with least severe water storage, respectively. Black dots in b represent the observed local tree α-diversity on 1 ha. Figures modified from Hoorn et al. (2010) © Copyright AAAS.

Beyond the borders of this huge basin, it extends the largest rainforest on Earth, which holds about 50% of global tropical rainforest (Malhi and Grace 2000), around 30% of world vascular plants (Dirzo and Raven 2003; Raven et al. 2020), and nearly one third of world vertebrates and arthropods (Jenkins et al. 2013; Stork 2018). The Amazonian region, particularly the western part, is considered one of the most biodiverse terrestrial ecosystems in the world (Myers et al. 2000; Ceballos and Ehrlich 2006; Killeen et al. 2007b; Hoorn et al. 2010; Figure 2.1). On the other hand, the Amazon forest is one of the major sources of global terrestrial evapotranspiration (Fisher et al. 2011). High transpiration is closely related to an intense vegetation activity. Therefore, Amazonian forests account for near 15% of terrestrial photosynthesis (Field et al. 1998) and uptake one-quarter of the total annual atmospheric carbon sequestered by land (Pan et al. 2011). Thus, the Amazon acts as an atmospheric carbon sink, offsetting around 10% of global fuel emissions (Phillips et al. 2009; Pan et al. 2011).

2.2 Climatic features of the Amazon

2.2.1 The mean annual climate patterns

The Amazon watershed exhibits a large rainfall spatial variability, with values ranging from less than 300 mm per year over Andean highlands, to more than 6000 mm per year at northwestern Amazon (Espinoza et al. 2009b). Particularly, annual precipitation over the Amazon rainforest is considerably high and varies between 1500-3500 mm per year (Salati and Vose 1984; Laurent 2002; Figure 2.2a). Thus, the Amazon rainforest is recognized as one of the world's major convective centers. All year long, moist laden easterly winds enter to the Amazon basin from the Atlantic Ocean (Espinoza et al. 2009b; Arraut et al. 2012; Satyamurty et al. 2013; Figure 2.2a). Once inland, these humid and warm winds gain extra moisture as a consequence of the high evapotranspiration rates of the Amazonian rainforest (Zemp et al. 2014; Figure 2.2b). Although most of the atmospheric water in the Amazon comes from the Atlantic Ocean (Satyamurty et al. 2013), trees evapotranspiration allows this water to precipitate and to be evapotranspirated several times (Zemp et al. 2014; Staal et al. 2018). In consequence, observations and models estimate that between 25-35% of Amazonian precipitation is previously transpired by local forest (Eltahir and Bras 1994; Trenberth 1999; Dirmeyer et al. 2009). Amazonian moisture not only sustains rainfall in the Amazon rainforest itself, but also in neighboring regions such as La Plata basin,

the eastern flank of the tropical Andes and the Andean Altiplano (Garreaud et al. 2003; Van Der Ent et al. 2010; Martinez and Dominguez 2014; Zemp et al. 2014). Through evapotranspiration, Amazonian rainforest acts as an energy source to the atmosphere. Thanks to its low albedo (the reflective capacity of a surface), tropical rainforests present high net surface radiation values, or in other words, high energy available to evaporate, transpire and conduct heat to the soil underground. Most of this available energy is consumed in the sum of evaporation of water from the soil and tree canopy, or transpiration through the tree leaves (von Randow et al. 2004; Bonan 2015). The energy removed from the surface via latent heat fluxes is subsequently released as water vapor condenses (Pielke 2001; Costa et al. 2021). This energy liberation warms the troposphere and engines the regional atmospheric circulation (Gill 1980; Eltahir 1996; Gedney and Valdes 2000; Rodwell and Hoskins 2001).

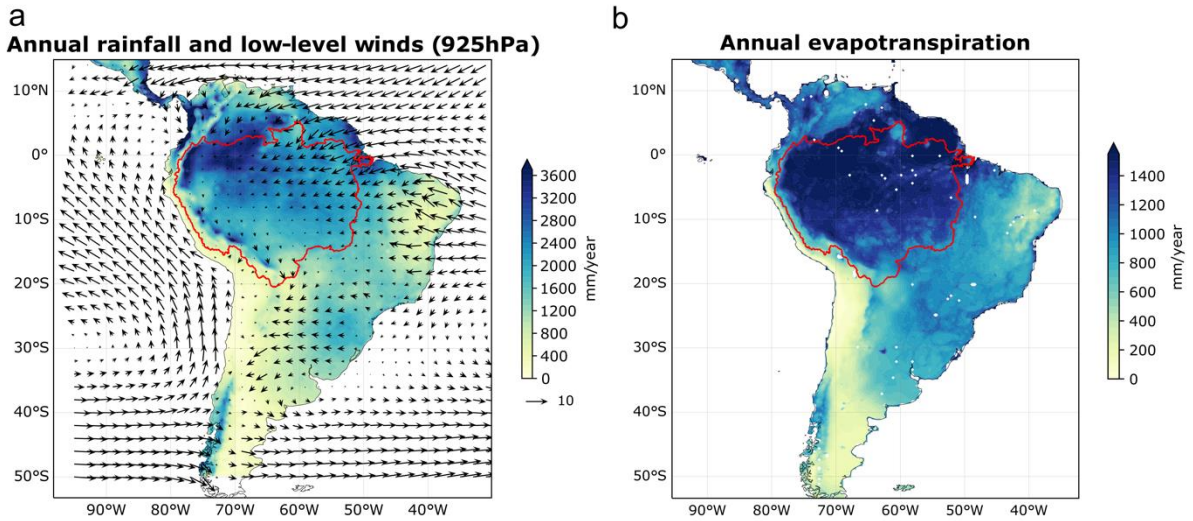

Fig. 2.2 Annual mean climatology for: **a** rainfall (shaded, in mm year^{-1}) and low-level 925hPa wind (vectors, in m s^{-1}) for the period 1981-2020 from Climate Hazards Group InfraRed Precipitation with Station data (CHIRPS) version 2 and the European Centre for Medium-Range Weather Forecast (ECMWF) ERA5 reanalysis, respectively; **b** evapotranspiration (mm year^{-1}) for the period 1980-2020 from the Global Land Evapotranspiration Amsterdam Model (GLEAM). Location of the Amazon basin is shown in red thick line.

The western Amazonia/eastern Andes is the rainiest area in the basin and one of the rainiest regions in the world (Figueroa and Nobre 1990; Espinoza et al. 2015; Figure 2.2a). Intense precipitation there produces large runoff and erosion rates (Moquet et al. 2011; Pepin et al. 2013), controlling the sediment and nutrient load for rivers downstream in the watershed (Vauchel et al. 2017; Armijos et al. 2020a). Sediments are transported by Amazon River tributaries from the Andes toward Amazon lowlands

and the Atlantic Ocean, conforming the largest sedimentary land-sea discharge and delivering about 20% of the global freshwater streamflow to the oceans (Salati and Vose 1984; Barthem et al. 2004; Callède et al. 2010; Armijos et al. 2020a). At the same time, rainfall over the eastern tropical Andes is sustained by moisture exported from the Amazon lowlands and transported by the trade winds (Falvey and Garreaud 2005; Poveda et al. 2006; Builes-Jaramillo and Poveda 2018). This exchange of atmospheric water, runoff and sediments shapes the entangled Andes/Amazon bio-geophysical system (Poveda et al. 2006; Espinoza et al. 2020; Figure 2.3).

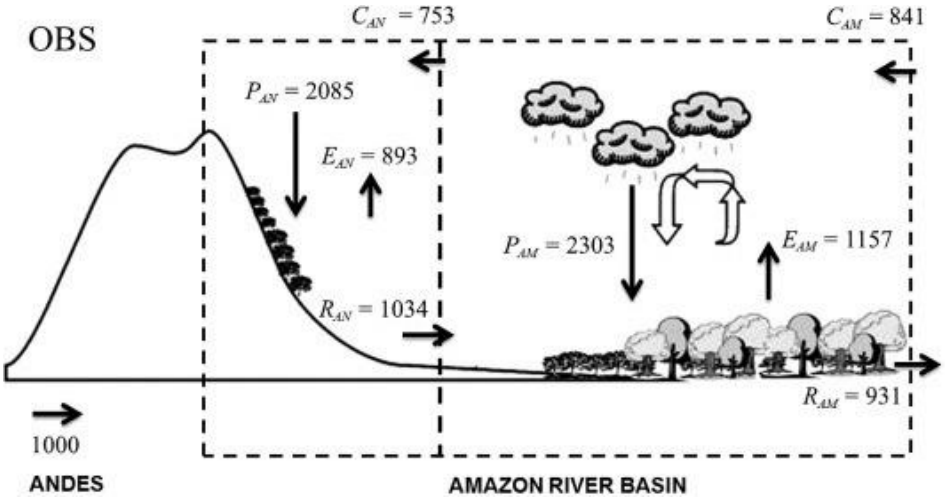

Fig. 2.3 Illustration of the components of the surface water balance and the atmospheric water balance in the Andes and Amazonia subregions of the Amazon River basin for the observation data sets (combination of satellite, reanalysis, models and in-situ measurements). Values are in units of mm yr−1. The arrow convention in the bottom left represents 1,000 mm yr−1. Figure modified from (Builes-Jaramillo and Poveda 2018) © Copyright AGU.

2.2.2 Seasonal climatology in the Amazon basin

Seasonality of solar radiation exerts a strong control on the atmospheric circulation and rainfall over tropical South America. As a result of its large size, encompassing parts of the northern and southern hemispheres, there is a north-south contrast in the hydro-climatological annual cycle within the basin (Horel et al. 1989; Figueroa and Nobre 1990).

During austral winter (June-August), the warming of the northern hemisphere develops a Hadley-type circulation (a latitudinal movement of the winds at different levels in the atmosphere) over tropical South America, with the ascending (descending) branch

and heavy precipitation (dry conditions) between 0º-10ºN (20ºS-10ºS; Figures 2.4a-b). Subsidence over the central and southern Amazon is associated with clear-sky conditions, which increases the solar radiation at the surface and enhances evapotranspiration during the dry season (Betts and Silva Dias 2010; Figure 2.4c). Despite the small rainfall rates observed during this season, the deep forest rooting system allows forest to extract water from the deep soil and sustain evapotranspiration (Shuttleworth 1988; Nepstad et al. 1994; da Rocha et al. 2004).

Between September-November, the continental part of the cloud and rainfall band known as the Intertropical Convergence Zone (ITCZ; blue band around 10°N in Figure 2.4a for SON) migrates southward following the solar radiation maximum. As a consequence, more humid and warmer winds enter to the basin from the north Atlantic Ocean (Figure 2.4a), moistening the lower troposphere and the Planetary Boundary Layer (PBL), the lowest part of the atmosphere which is directly influenced by the land surface (Fu et al. 1999). This atmospheric moistening increases the potential energy available for convection in the Amazon and helps to trigger the rainy season onset, in a first stage by the increase of local surface fluxes via rainforest evapotranspiration (Fu and Li 2004; Li and Fu 2004; Wright et al. 2017), and subsequently by the moisture advection from the large-scale circulation (Fu et al. 1999). During these months, about 70% of the regional rainfall comes from the local rainforest transpiration, consisting in the maximum rainfall recycling ratio along the year (Staal et al. 2018). Indeed, measurements from eddy covariance flux towers have demonstrated how the highest evapotranspiration rates lead the rainfall increase during the dry-to-wet transition season in the Amazon (da Rocha et al. 2004; Hasler and Avissar 2007).

The wet season over central and southern Amazon basin occurs in the austral summer (December- February; Figure 2.4b), when the South American Monsoon System (SAMS) is developed. The SAMS is featured by the occurrence of several regional atmospheric phenomena on an intra-seasonal scale, among which are the north-south low-level flow east of the Andes known as the South American Low-Level Jet (SALLJ; Berri and Inzunza 1993; Vera et al. 2006a, b; M Silva et al. 2009), the northwest-southeast band of convective activity extending from the continent towards the tropical south Atlantic, named the South Atlantic Convergence Zone (SACZ; Kodama 1992), and the upper-troposphere anticyclonic circulation known as the Bolivian High (see

Chapter 4 for details of the summer circulation). These atmospheric structures are characterized by low-level northerly winds entering the basin from the north Atlantic Ocean, low-level moisture convergence, intense ascending motion and heavy precipitation in the region that accounts for near 50% of the total annual precipitation (Espinoza et al. 2021). With the widespread precipitation, cloud area increases, and less solar radiation reaches the ground. As a consequence, rainforest evapotranspiration is limited (Vourlitis et al. 2002; Hutyra et al. 2005; Juárez et al. 2007) and the fraction of Amazonian recycled rainfall is minimum during this season (Staal et al. 2018). Groundwater recharge during this season is crucial for sustaining forest evapotranspiration during the next dry season (Juárez et al. 2007; Miguez-Macho and Fan 2012a).

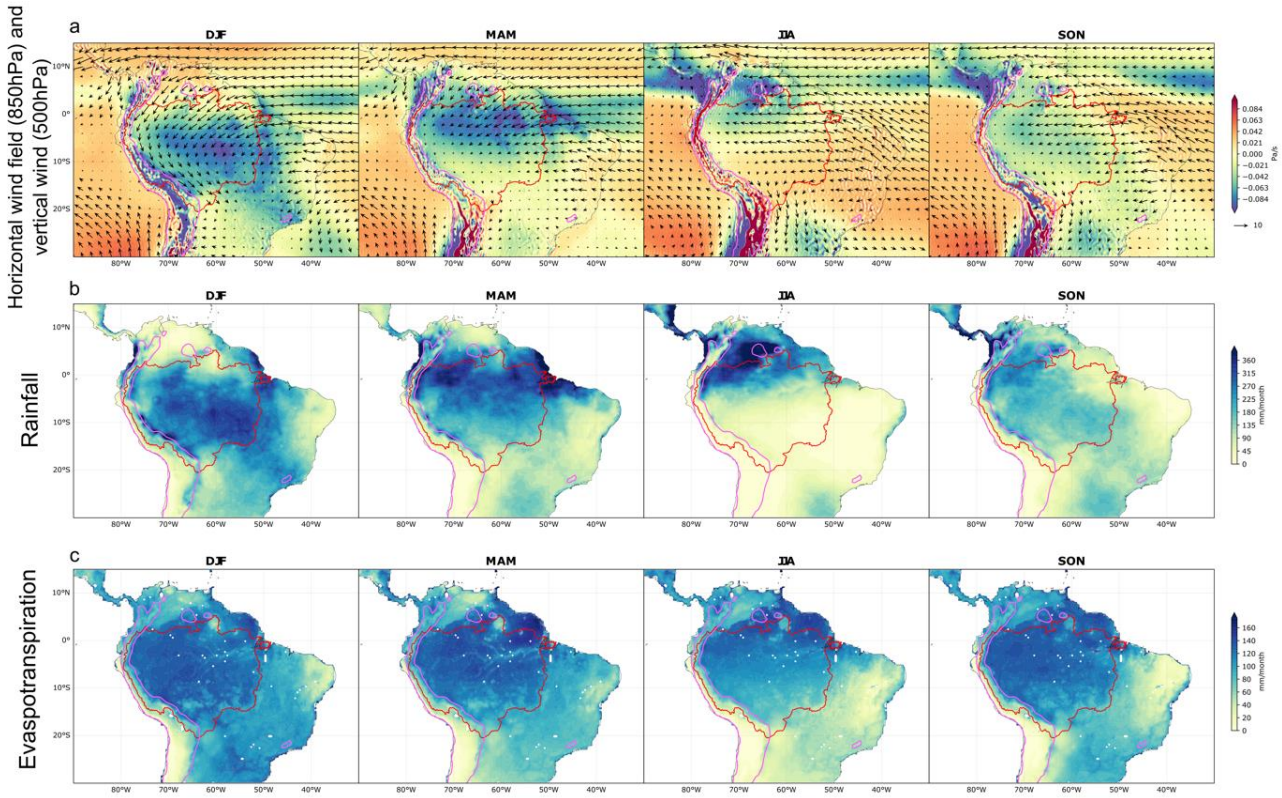

Fig. 2.4 Climatological means by season for: **a** horizontal low-level wind at 850 hPa (vectors, in m s^{-1}) and vertical wind component at 500 hPa (shaded, in Pa s^{-1}) over the period 1980-2020 from ERA5. Red and blue colors indicate descending and ascending motion, respectively; **b** precipitation (shaded, in mm $month^{-1}$) over the period 1981-2020 from Climate Hazards Group InfraRed Precipitation with Station data (CHIRPS) version 2; **c** evapotranspiration (shaded, in mm $month^{-1}$) over the period 1980-2020 from Global Land Evapotranspiration Amsterdam Model (GLEAM). Limits of the Amazon basin is shown in red thick line. Data source for the rainfall dataset is the Data source for the wind dataset is the European Centre for Medium-Range Weather Forecast (ECMWF) ERA5. Data source for the evapotranspiration dataset is the Global Land Evapotranspiration Amsterdam Model.

Precipitation maximum during March-May is observed over the Amazon delta associated with the latitudinal migration of the continental ITCZ (Figure 2.4b; Espinoza Villar et al. 2009a). Associated with large-scale rainfall events, radiosonde and ground-based measurements show dust and aerosols originated from northern Africa are deposited over the central Amazon conforming a potential nutrient source for the local rainforest (Swap et al. 1992; Formenti et al. 2001; Rizzolo et al. 2017). Additionally, the forest canopy produces biogenic aerosols that are transported upward in the atmosphere by convective air masses and are a key ingredient for cloud formation (Pöschl et al. 2010; Pöhlker et al. 2018).

For the above, the Amazon rainforest is considered an essential component of the Earth system (Bonan 2008b; Malhi et al. 2008a). Paleoclimate records suggest that the Amazon rainforest has been part of the climate system for at least the last 55 million years (Maslin et al. 2005). However, current anthropogenic pressures such as deforestation and global warming, as well as climate change and recent trends in extreme events rise the concern on the impacts of the Amazonian degradation on the regional and global climate (Malhi and Wright 2004; Cox et al. 2008; Davidson et al. 2012; Brienen et al. 2015; Marengo and Espinoza 2016).

2.3 Recent environmental change in the Amazon basin

The threats acting on the Amazon are numerous, complex and involve the big problems that humanity faces today. Global warming, the unsustainable consumption of natural resources, food and energy production, and water security are pushing the Amazon ecosystem toward irreversible changes (Tian et al. 2000). In the first half of this subsection we summarize the recent observed trends in the hydroclimate of the Amazon basin. The second part is focused in describing the evolution of deforestation in the Amazon.

2.3.1 Recent observed changes in Amazon hydroclimate

The natural climate variability in the Amazon at inter-annual and inter-decadal scales is closely linked to conditions in the sea surface temperatures (SSTs) over the Pacific and Atlantic oceans (Kousky et al. 1984; Aceituno 1988; Richey et al. 1989; Marengo

1992, 2005; Marengo and Hastenrath 1993; Yoon and Zeng 2010b; Cai et al. 2020). Recent changes in tropical oceanic SSTs have been observed during the last four decades (Servain et al. 2014; Li et al. 2016). The underlying causes of these involve the anthropogenic influence through aerosol (Booth et al. 2012) and greenhouse gases emissions (Du and Xie 2008; Dong et al. 2014). The warming of the North Atlantic and Indian oceans, and the cooling of the central-eastern Pacific have led to an SST dipole and have enhanced the Walker circulation in the period 1992-2011 (McGregor et al. 2014; Figure 2.5). All these changes in oceanic surface conditions and the atmospheric response have perturbated the Amazon hydrology in several ways.

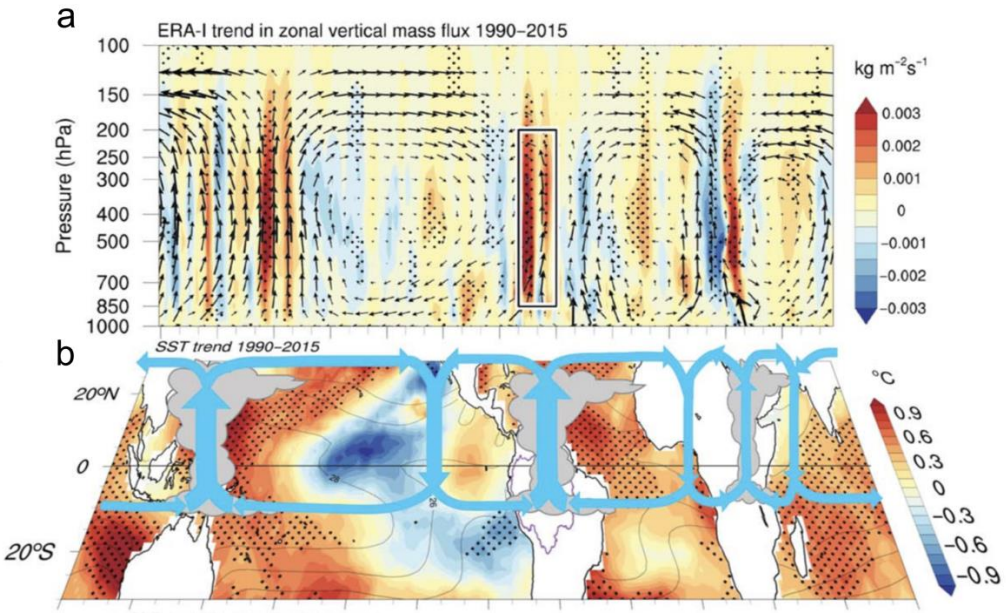

Fig. 2.5 **a** Trends in local Walker circulation (shading) during the wet season (December to February) for the period 1990-2015 based on meridionally averaged (10°S-10°N) zonal vertical mass flux in the ERA-Interim (ERA-I) reanalysis. Vectors represent the wet season climatological zonal wind and the vertical velocity scaled by a factor of -50. **b** Observed wet season SST trends from the Extended Reconstructed SST dataset (ERSST). Schematic representation of the overturning Walker cells in blue. Modified from Barichivich et al. (2018) © Copyright 2018 AAAS.

The hydrological cycle in the Amazon has intensified since the 1990s, with an increase in the frequency of extreme events (Espinoza et al. 2009a; Gloor et al. 2013; Marengo and Espinoza 2016). As a result of the North Atlantic warming, an intensification of the Walker and regional Hadley cells have resulted in an enhanced convection (subsidence) over northern (southern) Amazonia (Arias et al. 2015; Espinoza et al. 2016, 2019b, a, 2021; Wang et al. 2018; Barichivich et al. 2018; Segura et al. 2020; Figure 2.6). As a consequence, a differentiated spatial pattern has emerged over the

basin, with a wetter northwestern Amazon experiencing increased rainfall, streamflow, and frequency of wet days and with a drier southeastern Amazon (Espinoza et al. 2009a; Gloor et al. 2013; Marengo and Espinoza 2016; Barichivich et al. 2018; Haghtalab et al. 2020; Heerspink et al. 2020; Funatsu et al. 2021; Figure 2.6). Whereas the northern part of the basin has experienced 9 extreme floods during the last 20 years, which corresponds to the same number of extreme floods recorded during the whole XXth century (Espinoza et al. 2022), the duration of the dry season over the southern part of the Amazon has increased about 1 month during the period 1979-2011 (Dubreuil et al. 2012; Marengo et al. 2012; Fu et al. 2013; Correa et al. 2021). Consistently, extreme droughts and wild fires have become more frequent in the southern Amazon (Alencar et al. 2015; Marengo and Espinoza 2016), causing an increase in tree's mortality (Brando 2014; Brienen et al. 2015) and releasing tons of carbon dioxide to the atmosphere (Aragão et al. 2018).

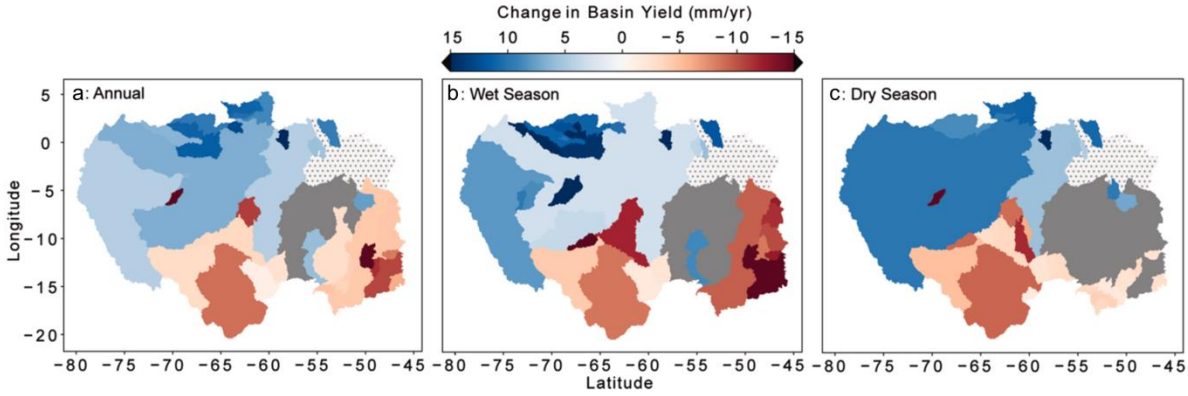

Fig. 2.6 Slope of change in streamflow (mm yr^{-1}) for: a annual, b wet season, and c dry season periods between 1980 and 2014 for a combination of stream gauging stations, satellite precipitation data from the Tropical Rainfall Measuring Mission (TRMM), satellite groundwater estimations from the Gravity Recovery and Climate Experiment (GRACE) and evapotranspiration estimates from the Moderate Resolution Imaging Spectroradiometer (MODIS). Sub basins are drawn as polygons. Catchment areas in solid gray have no significant trend at the p=0.1 level. Stipple patterned areas fall outside the catchments. Modified from Heerspink et al. (2020) © Copyright 2020 Elsevier.

At present, the Amazon forest acts as a carbon sink (Pan et al. 2011; Ballantyne et al. 2012; Le Quéré et al. 2013), and it soils and trees store about 150-250 PgC (Malhi et al. 2006; Feldpausch et al. 2012). Nevertheless, the observed tree mortality could turn the Amazon into a carbon source, what can generate a positive feedback accelerating climate change (Phillips et al. 2009; Brienen et al. 2015). This phenomenon has been observed under severe dry years as 2005 (Phillips et al. 2009) or 2010 (Lewis et al. 2011). One of the tree's mortality drivers is the air temperature (Toomey et al. 2011).

Water loss from the tree leaves depends on the water pressure difference between the canopy and the surrounding air. Higher temperatures increase tension in the inner conducting tree's vessels and can end in creation of air bubbles and embolism death (Anderegg et al. 2012). On the other hand, temperatures above 28°C cause a damage in the photosynthetic ability of tropical forests (Sastry and Barua 2017). The Amazon has suffered a continuous warming since the beginning of the XXth century (Victoria et al. 1998), with a recent acceleration since 1980 as a consequence of the anthropogenic greenhouse effect (Malhi and Wright 2004). Surface heating is exacerbated by the replacement of forest cover with cropland (Gash and Nobre 1997; Nobre et al. 2016). In this sense, there is a mixture of global and local perturbation signals acting simultaneously over the Amazon ecosystem.

2.3.2 Deforestation evolution in the Amazon basin

Humans are present in the Amazon basin since thousands of years. However, the anthropogenic activity has become an important force for the ecosystem only during recent decades (Fearnside 2005; Davidson et al. 2012). First forest exploitations date back to the XVIth century with the arrival of Portuguese navigators (Cameron 2018). By the XIXth and the beginning of the XXth century, large agricultural plantations spread throughout Central and South America (Pielke et al. 2011). Rubber, sugar cane and coffee plantations cut down millions hectares of forest during this period (Mather 1990; Williams 2000). Five centuries of European colonization deforested a total area slightly larger than Portugal, with deforestation centers concentrated over coast and river areas (da Costa 1988; Machado 1998; Fearnside 2005; Etter et al. 2008).

After 1950, the dynamics and drivers of the Amazonian forest loss changed dramatically. The implementation of settlement policies by the Brazilian government prompted the construction of highways connecting the Amazon with the rest of the country (Schmink and Wood 1992; Aguiar et al. 2007). At the same time, economic incentives boosted the forest clearing in the region until the 1980s (Mahar 1979; Hecht 2005; Fearnside 2005). As a consequence, population in the region increased from 6 million in the 1960s to 25 million in 2010 (Davidson et al. 2012). By the 1990s, the loss of native vegetation start to be dominated by global market forces and the growing demand of beef, soybeans and agricultural products (Becker 2005; Nepstad et al.

2006; Killeen et al. 2007a). However, this model of rural development in the Amazon is outdated, not very productive and has not resulted in wealth creation or better living conditions for the people of the Amazon (Fillion et al. 2009; Kahn et al. 2014; Nobre et al. 2016).

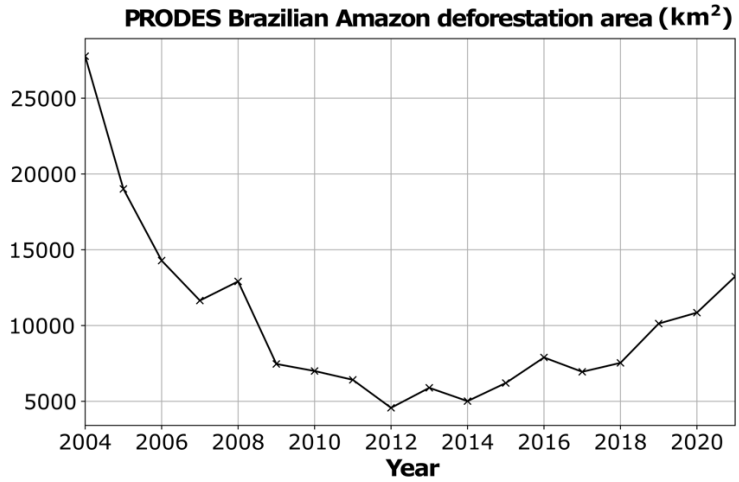

Fig. 2.7 Time evolution of deforestation in the Brazilian Amazon in km^2. Data obtained from the Satellite Deforestation Monitoring Project PRODES.

Between 2004 and 2013, Amazon deforestation rates exhibited a significant reduction of near 80% (Diniz et al. 2015; Assunção et al. 2015; Figure 2.7). Among the causes behind this slowdown in forest loss are the implementation of a satellite monitoring system, law enforcements by the Brazilian government, the creation and expansion of protected areas, and interventions in soy and beef supply chains (Nepstad et al. 2014). Nevertheless, deforestation rates have risen again as a result of policy mechanisms in the Brazilian Amazon, small scale mining and oil palm crops in Peruvian piedmonts, as well as an expansion of the colonization front in Colombia (Asner et al. 2013; Armenteras et al. 2013; Kalamandeen et al. 2018; Amigo 2020). Indeed, 2019 exhibited the largest forest loss in the last decade (Amigo 2020; Silva Junior et al. 2021; Figure 2.7). Converting forest into cropland/grasslands has significant impacts on local and regional climate (Hartmann et al. 2013; Mahowald et al. 2017), as will be described in the next subsection.

2.4 How deforestation in the Amazon impacts the local, regional and global climate?

The loss of the Amazonian tropical forest may generate profound disturbances in the ecological, hydrological and climatic functioning of the Earth system at different scales of time and space. In the present section, we describe the observed changes induced by Amazonian deforestation on the local microclimate. The projected impacts of large-scale deforestation on the regional and global climate are also discussed according to model experiments.

2.4.1 Impacts of the observed deforestation on the Amazon at local and meso scales

Deforestation in the Amazon basin consists mainly in the replacement of natural rainforest by soy croplands or un-irrigated pasture lands for cattle ranching (Davidson et al. 2004; Nepstad et al. 2006, 2014). This land use change modifies the biophysical properties of the surface and perturbs the land-atmosphere energy and water exchanges. Thanks to the scientific effort made in the 1990's and the early 2000's through two field campaigns over forested-deforested paired sites in the Amazon, the Anglo-Brazilian Amazonian Climate Observational Study ABRACOS and the Large-Scale Biosphere Atmosphere LBA project, the local effects of deforestation are now better understood. Deforested areas present different biophysical properties such as changes in albedo, thermal emissivity (effectiveness of a surface in emitting energy as thermal radiation), roughness length (related to the vertical height of surface vegetation) among others (Culf et al. 1995; Wright et al. 1995; Gash and Nobre 1997; von Randow et al. 2004). A brief summary of the observed local-scale effects of deforestation over the Amazon is described in Chapter 4. A more complete description of this can be found in Gash and Nobre (1997).

The conversion of forest to cropland/grassland also involves alterations under a biogeochemical point of view. Amazonian rainforest supports its high productivity, partially thanks to its phosphorus recycling capacity (Cuevas and Medina 1988; Markewitz et al. 2004). In this sense, while forest are more limited by nitrogen, deforested pastures are limited by nitrogen and phosphorus at the same time

(Davidson et al. 2004). In addition, the nitrogen dynamics is also perturbed by deforestation (Davidson et al. 2004; Figueiredo et al. 2019). In-situ measurements found that regrowth forest presents only about half of the nitrogen mineralization compared to undisturbed forest (Figueiredo et al. 2019). On the other hand, the forest loss induces less uptake or even an emission of methane from the vegetation cover (Bustamante et al. 2009), what contributes to the observed rising in the atmospheric concentration of this greenhouse gas (Gulev et al. 2021) .

At local scales, in-situ observations have shown that forest loss leads to a drier and warmer conditions, with a reduced latent heat flux and an enhanced sensible heat flux (Wright et al. 1995; von Randow et al. 2004). As a result, the PBL grows faster and deeper over deforested areas during the dry season (Culf et al. 1996; Gash and Nobre 1997). These local perturbations force thermally driven mesoscale circulations (circulation of the order of 50 km or more), with air masses moving from the forested cooler surrounding areas toward the deforested warmer patches, increasing shallow convection and cloudiness over the deforested land (Cutrim et al. 1995; Chagnon et al. 2004; Negri et al. 2004; Wang et al. 2009). The deforestation-induced mesoscale circulation has been reproduced by climate models (Dias and Regnier 1996; Wang et al. 1996; Baidya Roy and R. 2002), what proves the models potential as tools for understanding the possible impacts of a larger deforestation.

2.4.2 Mesoscale, regional and global effects of Amazonian deforestation

Early modelling studies explored the effect of idealized complete removal of Amazonian rainforest on the regional climate using Global Climate Models (GCMs) or Regional Climate Models (RCMs). Annual reductions (increment) in precipitation and evapotranspiration (surface temperature) are projected by climate models under these deforestation scenarios (Lean and Warrilow 1989; Shukla et al. 1990; Nobre et al. 1991; Dickinson and Kennedy 1992; Henderson-Sellers et al. 1993; Polcher and Laval 1994; Polcher 1995). Since the forest clearance affects deep convection in the Amazon, the high-level tropical outflow of energy is perturbated generating teleconnections with mid and high latitudes (Snyder 2010a). Many works have found a weakening of the regional Hadley cell, what induces a Rossby wave response in the

upper troposphere propagating the deforestation signal outside the tropics (Zhang et al. 1996; Sud et al. 1996; Gedney and Valdes 2000; Badger and Dirmeyer 2016). A similar mechanism was proposed theoretically by Gill (1980). Nevertheless, there are discrepancies among the different studies in the magnitude of the extratropical response to the land-use change in the Amazon and/or in the tropics (Zhang et al. 1996; Werth and Avissar 2002; Hasler et al. 2009). These pioneering studies, as well as studies based on GCMs, have limitations such as the coarse horizontal resolution (grid-cells sizes between 100 km and 500 km), what causes unrealistic deforestations scenarios and masks the differential spatial climatic response to the forest loss forcing.

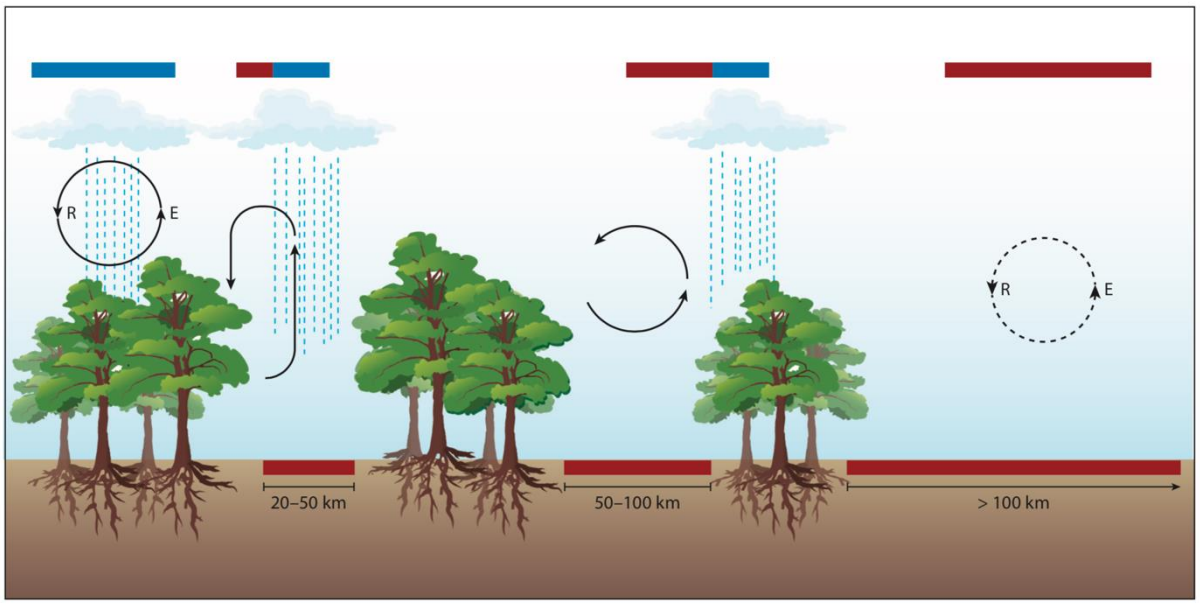

Fig. 2.8 Effects of tropical deforestation on rainfall. Deforestation leads to reduced evapotranspiration (E), resulting in a warmer land surface (red soil). Small patches of deforestation (<100 km) cause atmospheric circulations leading to regions of increased (blue) and decreased (red) rainfall. At larger scales, deforestation reduces rainfall recycling, leading to reduced regional rainfall (P). Adapted from Spracklen et al. 2018 © Copyright 2018 Annual Reviews.

With the advancement of computer science and the improvement of model horizontal resolution, more land-atmosphere feedbacks are now represented by climate models. Mesoscale and local phenomena such as orographic lifting and cumulus convection can be explicitly solved by the new high resolution climate models (Dai 2006; Tai et al. 2021; Junquas et al. 2022). This particularly favors the representation of atmospheric processes in regions with complex topography such as the western Amazon, where the Andes mountain chain stands and where the exchange of water, sediments and nutrients between the Andes and the Amazon lowlands takes place

(Poveda et al. 2006; Builes-Jaramillo and Poveda 2018). In fact, the effects of deforestation on the Amazon-Andes coupled system have been poorly explored and is one of the questions addressed in this thesis. On the other hand, a finer horizontal resolution also makes it possible to implement spatially distributed deforestation scenarios based on observed trends of forest loss in the region (Soares-Filho et al. 2006; Alves et al. 2017; Eiras-Barca et al. 2020). Thanks to the use of more realistic forest clearance scenarios, in conjunction with theoretical works, it is well known now that the impacts of Amazonian deforestation are not linear with respect to the size of the deforested area. Whereas small and medium-scale deforestation (up to a cleared area conforming 20-30% of the total Amazon basin area) increases local convection, rainfall and cloud formation over the cleared areas (Medvigy et al. 2011; Nobre et al. 2016), large-scale deforestation seems to lead to a general rainfall reduction in the region (Lejeune et al. 2015; Lawrence and Vandecar 2015; Figure 2.8). This has led to the development of the 'tipping point' concept (section 1.2), a threshold of deforested area that, if reached and surpassed, dramatic nonlinear precipitation decreases would lead to irreversible and permanent drier conditions in the ecosystem (Avissar 2002). For the Amazon, modelling and observational studies suggest a 40% of total forest loss as a tipping point driving the rainforest toward a savanna dominated ecosystem (Sampaio et al. 2007; Hirota et al. 2011).

In spite of the expected precipitation decrease over Amazonia under large-scale deforestation scenarios, the spatial pattern of rainfall changes within the basin is model-dependent. For this reason, it has been suggested that using high resolution models with state-of-the-art land surface schemes is crucial for the representation of the underlying mechanisms leading the climatic changes (Lejeune et al. 2015). In addition, most works on Amazonian deforestation using climate models have focused on the alterations in the annual mean and/or seasonal climate, while the changes in the underlying intra-seasonal atmospheric phenomena remain poorly studied. Thus, in the following chapters we explore two main scientific questions: first, we are interested in how the Amazonian forest loss impacts the regional and local climate at seasonal and intra-seasonal time scales, and secondly, what are the effects of the Amazonian forest loss on the hydroclimatic coupling between the Amazon and the tropical Andes.

2.5 Regional climate models, lands surface models and configurations used in this thesis

To answer the main scientific questions of this thesis we rely on simulations with different climate models, different configurations, spatial resolutions and geographical domains. In this subsection we present a guide to the details of the configurations and models used in each chapter.

In the first part of the thesis (Chapter 3), which seeks to evaluate the impacts of Amazonian deforestation on the regional atmospheric circulation at intra-seasonal time scales and on the rainy season onset in the southern Amazon. To this, we use the Regional Earth System Model of the Institute Pierre Simon Laplace (RegIPSL). As an Earth system model, RegIPSL couples three different models through the OASIS-MCT coupler (Craig et al. 2017): the Weather Research and Forecasting Model (WRF) for the atmosphere(Skamarock et al. 2008, 2019), the ORganising Carbon and Hydrology In Dynamic EcosystEms (ORCHIDEE) for the land surface (Krinner et al. 2005), and the Nucleus for European Modelling of the Ocean (NEMO) model for the ocean (Madec et al. 1998).

Land surface processes play a key role for determining the surface boundary conditions to the lower atmosphere, the Planetary Boundary Layer, as well as clouds and precipitation processes. Thus, the modeling of surface processes is fundamental for a good representation of atmospheric dynamics (Avissar and Pielke 1989; Chen and Avissar 1994). ORCHIDEE is a complex land surface model that incorporates land-atmosphere interchanges of water, energy and carbon, the competition of different functional types of plants (dynamic vegetation model), and a simple lateral water transfer scheme based on flow direction, topography and channel length. This lateral scheme simulates the water exchange between hydrological transfer units through three reservoirs: the stream, the surface runoff and the drainage. The soil is discretized in ORCHIDEE in 11 layers reaching at least 2 m down within the soil for the representation of the water balance and at least 10 m down for the soil temperature. This model has been used and tested in the Amazon region in previous works (Guimberteau et al. 2012, 2017). For this reason, we select RegIPSL for representing land surface processes under a land-cover forcing such as a

deforestation experiment. This simulation uses spectral nudging at scales above 1200 km over horizontal winds and temperature (von Storch et al. 2000). In this way, we impose a consistency between the lateral boundary conditions and the regional climate model simulated fields. However, the freedom of the model is reduced what can dampen the deforestation signal in the upper parts of the troposphere.

On the other hand, in Chapter 4 we assess the impacts of the rainforest clearance on the hydroclimatic connectivity between the Amazon and the tropical Andes, particularly over the eastern flank of the Andes and certain Andean valleys. This is a region with complex topography, where local processes such as mechanical channeling or thermally induced circulations (anabatic and katabatic winds) are important. Thus, we need to perform high resolution simulations. As a consequence, we implement a different configuration of the model. In this chapter we couple WRF with the land surface model NOAH (Chen and Dudhia 2001) taking advantage of the fact that this configuration has already been used with good results in high resolution simulations over the region of interest (Junquas et al. 2018). However, several tests altering the cumulus convection and PBL parameterizations were performed, aiming a realistic representation of rainfall in the region. Additionally, we activate a wind correction that improves the simulated wind field over complex terrains taking into account the steep topography of the interest region (Jiménez and Dudhia 2012).

The NOAH land surface model also presents a soil depth of 2 m depth but discretized in only four soil layers. A brief summary with the models and the main configuration features used in the present thesis is shown in Table 2.1. In Chapter 5 we compare the outputs of the two model configurations in the assessment of the Amazon deforestation effects on the atmospheric processes that drive rainfall in the upper southern tropical Andes.

Table 2.1 General characteristics of the land surface and atmospheric models used in the thesis

Chapter	**Land surface model**			**Atmospheric model**		
Chapter 3	ORCHIDEE	Soil depth (m)	2	WRF	Version	3.7.1

		Soil layers	11		Spatial domains/ Horizontal resolution (km)	South American continent / 20
					Spectral nudging	Yes
					Wind topographic correction	No
					Cumulus parameterization	Grell Freitas
					PBL parameterization	Meyor Yamada MYNN 2
Chapter 4	NOAH	Soil depth (m)	2	WRF	Version	4.1
		Soil layers	4		Spatial domains/ Horizontal resolution (km)	Tropical northern South America / 15
						Amazon-Andes transition region /5
						Bolivian Andes / 1
					Spectral nudging	No
					Wind topographic correction	Yes
					Cumulus parameterization	Grell 3D
					PBL parameterization	Yonsei University scheme

3

Amazon deforestation impacts on the regional climate at intra-seasonal timescales

Contents

3.1 Introduction

Deforestation can have significant impacts on the climate system at different spatial and temporal scales. As described in Chapter 2, the effects of the Amazonian rainforest loss depend on the size of the deforested patch in non-linear ways. This topic has been extensively explored due to the constant expansion of the forest cleared areas and to the scientific concern about the existence of thresholds in the climatic system which, if surpassed, can drastically change the conditions of the biggest rainforest on Earth and could turn large parts of it into dry savannas (Chapter 1).

Similarly, deforestation effects on the atmospheric conditions vary depending on the analyzed time scale. This time-scale dependency of the deforestation impacts is in general a less explored question, in part due to the large computational resources needed in this regard. For instance, although several studies find a decrease in precipitation and an increase in the surface temperature with large-scale deforestation in the annual mean conditions over the Amazon basin (e.g. Henderson-Sellers et al. 1993; Costa and Foley 2000; Kleidon and Heimann 2000; Lejeune et al. 2015; Eiras-Barca et al. 2020), this deforestation-induced perturbations can be different for a specific season, month or for atmospheric phenomena acting at higher temporal scales (e.g. Badger and Dirmeyer 2016; Eiras-Barca et al. 2020). Regional/continental climatic conditions at a seasonal or monthly scales are averages of more fundamental atmospheric phenomena acting from daily to decadal time scales (e.g. Espinoza et al. 2012, 2021; Moron et al. 2015; Paccini et al. 2018). Therefore, in this chapter we explore how the tropical forest loss can impact these underlying atmospheric states. To our knowledge, it is the first time that the impacts of Amazonian deforestation on atmospheric states acting from daily-to-decadal scales are evaluated. We use the partition of the atmospheric variability into recurrent and well-defined atmospheric situations to assess the potential effects of deforestation on the wet season onset over the southern Amazon. The results of this chapter have been submitted for publication in the journal Climate Dynamics in an article entitled **'Impacts of land-surface heterogeneities and Amazonian deforestation on the wet season onset in southern Amazon'**.

3.2 Impacts of land-surface heterogeneities and Amazonian deforestation on the wet season onset in southern Amazon

Juan P. Sierra, Jhan C. Espinoza, Clementine Junquas, Sly Wongchuig, Jan Polcher, Vincent Moron, Lluís Fita, Paola A. Arias, Anthony Schrapffer, Romain Pennel

Article submitted to the journal Climate Dynamics on the 2nd of August 2022

3.2.1 Introduction

The Amazon rainforest is an important driver in the climate system. Exchanges of water and energy within and through the borders of the largest tropical rainforest in the world help to sustain the atmospheric circulation in the tropics and precipitation in the South American continent (Gill 1980; Eltahir and Bras 1994; Eltahir 1996; Gedney and Valdes 2000; Bonan 2008a; Fisher et al. 2011; Zemp et al. 2014). The constant anthropogenic pressures such as deforestation, global warming and the increase in the extreme weather and climate events during the last decades threaten this mega biodiverse ecosystem and raise the concern on the possible impacts of the Amazonian degradation on the regional and global climate (Malhi and Wright 2004; Cox et al. 2008; Malhi et al. 2008b; Brienen et al. 2015; Shukla et al. 2019; Arias et al. 2021).

During the last six decades, population growth, agriculture and cattle ranching expansion, logging, mining, as well as road and dam building have led to continuous deforestation in the Amazon region (Fearnside 1993; Hutyra et al. 2005; Nepstad et al. 2008; Latrubesse et al. 2017). By the year 2011, around 87% of the Amazon basin was still covered by original forest (Davidson et al. 2012) while it has been reduced to 83% in 2020 (Eiras-Barca et al. 2020). Major clearance areas are located in the southern and eastern parts of the basin conforming the so called ‘arc of deforestation’ (Malhi et al. 2008b; Leite et al. 2011; Davidson et al. 2012). The southern Amazon, which encompasses between 30-40% of the basin, has experienced one of the most rapid agricultural expansion in the world (Salazar et al. 2007; Instituto Nacional De Pesquisas Espaciais 2014). Taking into account that observations and models

estimate that between 24-41% of the Amazonian precipitation originates from local evapotranspiration (Salati et al. 1979; Eltahir and Bras 1994; Dirmeyer and Brubaker 2007; Van Der Ent et al. 2010; Staal et al. 2018; Dominguez et al. 2022), deforestation could have profound implications in the regional hydrology.

The southern Amazonia, defined here as the region between 5°S-15°S and 70°W-50°W (Figure 3.1a-b), is characterized by a strong rainfall annual cycle and a weak evapotranspiration seasonality (Figure 3.2a-b, respectively), both driven by the seasonal warming and the establishment of regional-scale features such as the South American Monsoon System (SAMS) (Horel et al. 1989; Figueroa and Nobre 1990; Liebmann and Marengo 2001; Espinoza et al. 2009a). The dry season in the region occurs between June-August, when rainfall rate is around 1 mm day-1 (Figure 3.2a). As a consequence of water and energy limitations, evapotranspiration is minimum during these months (Juárez et al. 2007; Figure 3.2b). A rapid precipitation increase from August to October characterizes the dry-to-wet transition period (Marengo et al. 2001). At the same time, evapotranspiration rises following the increments in precipitation, incoming solar radiation and net surface radiation (Figures 3.2c and 3.2i; Myneni et al. 2007), what contributes to preconditioning the atmosphere for the arrival of the wet season (Fu and Li 2004; Yin et al. 2014; Wright et al. 2017). Many authors suggest that the evapotranspiration increase during this period can moisten the boundary layer and increase the available potential energy of the lower troposphere (Fu et al. 1999; Fu and Li 2004; Li et al. 2006). Cold fronts entering to Amazonia from the extratropics lift warm and humid surface air over the southern Amazon, and trigger deep convection setting up the wet season onset (Li et al. 2006; Espinoza et al. 2013a). Rainy events associated with cold intrusions during the early wet season warm the atmosphere through diabatic heating driving the reversal of the cross-equatorial flow and enhancing advection of moisture laden winds from the Atlantic Ocean in a positive feedback (Wang and Fu 2002). As a result, the core of the wet season is observed during December-February, when precipitation reaches more than 8 mm day^{-1} (Figure 2a; Marengo et al. 2001; Gan et al. 2004; Yin et al. 2014).

Drier conditions have been reported over the southern Amazon in the recent decades in terms of: (i) an increase in dry days frequency during the dry-to-wet transition period (Espinoza et al. 2019a; Funatsu et al. 2021); (ii) an increase in tree's mortality and

biomass degradation (Brienen et al. 2015); and (iii) shorter wet and larger dry seasons since the 1970's (Phillips et al. 2009; Fu et al. 2013; Debortoli et al. 2015; Arias et al. 2015; Correa et al. 2021). This lengthening of the dry season is related to multiple causes that include alterations in the entrance of cold fronts to the Amazon basin and the latitudinal location of the Southern Hemisphere subtropical jet (Fu et al. 2013), the Atlantic and Pacific sea surface temperatures and its inter-annual/decadal variability (Arias et al. 2015; Marengo et al. 2017), atmospheric circulation changes in the Hadley and Walker cells (Yoon and Zeng 2010a; Barichivich et al. 2018; Agudelo et al. 2019; Espinoza et al. 2021) and the human induced influence of the forest-to-cropland conversion (Butt et al. 2011; Debortoli et al. 2015; Ruiz-Vásquez et al. 2020). Natural forests over the region are vulnerable to a lengthening of the dry season and to reductions in total annual rainfall (Da Silveira Lobo Sternberg 2001; Sombroek 2001; Staver et al. 2011; Guan et al. 2015). Indeed, year-to-year variations in the onset of the wet season affects river flows, fire risk, small-scale agriculture, methane emissions due to alterations of the flood pulse and the inter-annual variability of the global atmospheric CO2 concentrations (Cochrane et al. 1999; Asner 2009; Lee et al. 2011; Chen et al. 2011; Molina-Carpio et al. 2017; Melack et al. 2022). Although in agreement with observations, coupled biosphere-atmosphere models suggest a delay in the date of the wet season onset under deforestation scenarios (Costa and Pires 2010; Boisier et al. 2015; Nobre et al. 2016; Alves et al. 2017; Ruiz-Vásquez et al. 2020), these works are limited by the fact that they are based on the analysis of modeled parameterized rainfall with coarse horizontal resolutions.

Among all the perturbations induced to surface energy and water fluxes by forest loss, deforestation decreases the net radiative energy at the surface, and consequently the evapotranspiration and latent heat flux according to flux-tower and satellite-derived data (von Randow et al. 2004, 2020; Khand et al. 2017; Baker and Spracklen 2019; Oliveira et al. 2019; Laipelt et al. 2020). A reduction in the vegetation's transpiration (the water loss through the plant's leaves) is caused also by the reduced soil-water-uptake capacity of the shorter crop roots (Neill et al. 2013; Caioni et al. 2020). On the other hand, deforestation favors the occurrence of shallow clouds and reduces deep convection activity during the dry and dry-to-wet transition season (Wang et al. 2009). Both evapotranspiration and deep convection during these particular months are important for the onset and evolution of the rainy season. Thus, in this study we

analyze how deforestation can perturb the onset and development of the wet season in southern Amazonia.

A recent study has explored the observed dry season lengthening over the southern Amazon under a pattern recognition framework of weather typing or atmospheric circulation patterns (CPs) approach (Espinoza et al. 2021). The CPs can be understood as regional-scale circulation anomalies which are recurrent and correspond to preferred states of the climate system (Moron et al. 2008, 2015; Espinoza et al. 2021). Espinoza et al. (2021) explained the lengthening of the dry season in the southern Amazonia in terms of an increased frequency of a particular CP linked to enhanced subsidence over southern tropical South America and a decreased occurrence of a CP characterized by the entry of cold intrusions and convective activity over the region (Figure 2 in Espinoza et al. 2021). Taking into account that wind circulation is usually better represented by climate models in comparison with precipitation (Kendon et al. 2012; Flato et al. 2013; Fosser et al. 2015; Pichelli et al. 2021; Ban et al. 2021), using the circulation pattern approach results attractive to explore deforestation experiments with a regional climate model. Therefore, this study evaluates the impacts of Amazonian deforestation on the onset and evolution of the rainy season in the southern Amazon, based on CPs, using a control and a deforested experiment with the Regional Earth System Model of the Institute Pierre Simon Laplace (RegIPSL). This work is organized as follows: the control and deforestation experiments, as well as the data and methods are described in section 3.2.2; section 3.2.3 is dedicated to validating the model in terms of (i) the annual cycle of rainfall and surface fluxes in the southern Amazon, (ii) the regional atmospheric circulation variability through the CPs, and (iii) the conditions in the atmospheric circulation states, rainfall and evapotranspiration during the onset of the wet season; we end the section with a discussion of the role of the land-surface heterogeneities on the development of the wet season onset; in section 3.2.4, we assess the impacts of deforestation on the evolution of the Amazonian wet season; finally, section 3.2.5 discuses and summarizes the main results.

3.2.2 Data and methods

3.2.2.1 Model description

RegIPSL (https://gitlab.in2p3.fr/ipsl/lmd/intro/regipsl/regipsl/-/wikis/home) is an Earth system model that couples the atmospheric model Weather Research and Forecasting Model (WRF), the land surface model ORganising Carbon and Hydrology In Dynamic EcosystEms (ORCHIDEE), and the oceanic model Nucleus for European Modelling of the Ocean (NEMO). The coupling between the different modules of the model is performed by OASIS-MCT (Craig et al. 2017) and input/output is done via the XML-IO-SERVER (XIOS, https://forge.ipsl.jussieu.fr/ioserver). However, the present work does not use the oceanic component.

The atmospheric regional climate model WRF version 3.7.1 is used in this study (Skamarock et al. 2008). The WRF model can be implemented for both research and forecast activities. WRF is extensively used to dynamic downscaling purposes in South America (e.g. Spera et al. 2018; Trachte 2018; Posada-Marín et al. 2019; Saavedra et al. 2020; Junquas et al. 2022; Rosales et al. 2022; Dominguez et al. 2022) and to analyze deforestation impacts on the regional climate (e.g. Bagley et al. 2014; Eghdami and Barros 2019; Eiras-Barca et al. 2020; Sierra et al. 2021). This is a non-hydrostatic model with terrain-following vertical coordinates. In our configuration, the model presents 50 vertical levels (model top at 10 hPa), a 60s running time step and a horizontal resolution of 20 km x 20 km encompassing the South American continent (Figures 3.1a-b). Table 3.1 summarizes the general configuration of the model.

After different preliminary sensitivity tests (not shown), the physical parameterizations chosen in this work include the RRTMG radiation scheme (Iacono et al. 2008), the Morrison 2-moment scheme for cloud microphysics and dynamics of water species (Morrison et al. 2009), the Mellor Yamada MYNN level 2 scheme for the planetary boundary and surface layers (Nakanishi and Niino 2006) and the convection scheme Grell Freitas (Grell and Freitas 2014). To simulate the effects of land cover change on the interactions between soil/vegetation and the atmosphere, WRF is coupled with the land surface model ORCHIDEE (Krinner et al. 2005; Maignan et al. 2011). ORCHIDEE resolves the processes of the energy and water balances at the surface, as well as

the evolution of the vegetation and the carbon cycle. In this sense, it represents the vegetation mechanisms that control the carbon assimilation and determine vegetation state and its evaporative capacity. Table 3.2 summarizes the complete WRF's set-up.

Table 3.1 Characteristics of the WRF simulations

Model version	3.7.1
Horizontal resolution (km)	20
Number of vertical levels	50
Run time step (s)	60
Output time resolution (h)	3
Domain center coordinates	21° 6' 36" S 60° 17' 60" W

Table 3.2 Physical configuration of the WRF simulations

	Parameterizations	**References**
Radiation	Longwave-shortwave RRTMG radiation scheme	(Iacono et al. 2008)
Cumulus	Grell Freitas scheme	(Grell and Freitas 2014)
Planetary boundary layer	Mellor Yamada MYNN 2	(Nakanishi and Niino 2006)
Cloud microphysics	Morrison 2-moment scheme	(Morrison et al. 2009)
Surface layer	MYNN Scheme	(Nakanishi and Niino 2006)
Land surface	ORCHIDEE	(Krinner et al. 2005)

Boundary conditions are extracted from the fifth generation reanalysis of the European Centre for Medium-Range Weather Forecast (ECMWF) ERA5 (Hersbach et al. 2020). With a higher spatial and temporal resolution (31 km x 31 km horizontal grid size, 137 hybrid sigma-pressure levels and data each hour, respectively), ERA5 improves the representation of several atmospheric processes, including the vertical structure of winds and humidity, and more consistent soil moisture, evaporation and sea surface temperatures with respect to its predecessor ERA-Interim (Hoffmann et al. 2019; Hersbach et al. 2020). This data set is available at https://www.ecmwf.int/en/forecasts/datasets/reanalysis-datasets/era5 (last access July 2022). In order to constrain the large-scale meteorological conditions in WRF simulations toward the synoptic circulation at the domain boundaries, we use spectral nudging (von Storch et al. 2000) above the planetary boundary (at scales above 1200km) over horizontal winds and temperature (Miguez-Macho et al. 2004; Zhang et al. 2022). Omrani et al. (2015)

recognize that the horizontal wind is the most important variable to nudge in order to improve the representation of surface temperature, wind and precipitation.

In the present study, a 3-month spin-up time is used for the atmospheric component, spanning from 1st October 2000 to 31st December 2000. Due to the slow evolution of soil dynamics and the strong impact of land surface conditions on the performance of regional climate models, several studies suggest the use of an off-line spin-up for the land surface model (Smith et al. 1994; Cosgrove et al. 2003; de Goncalves et al. 2006; Sutton et al. 2006; Case et al. 2008). For this reason, we implement an off-line spin-up for ORCHIDEE based on 10 concatenated 1-year simulations where last restart of the previous run is used as initial condition of the following one, using as an atmospheric forcing WRF-alone 1-year simulation performed at the exact same domain.

3.2.2.2 Description of the experiments

In order to obtain a representative view of the long-term atmospheric intra-seasonal variability, we use 19 years of simulations covering the period 2001-2019. For this period, we perform two simulations sharing the same boundary forcing from ERA5 but with different land-use conditions. The control experiment (hereafter 'RegIPSL-Control' or 'RegIPSL-C') utilizes information of the annual evolution of land-use/cover from the European Space Agency Climate Change Initiative (ESA-CCI) land-cover maps (ESA 2017; Lamarche et al. 2017). This data set, originally covering the period 1992-2015, was recently extended until 2020 by the Copernicus Climate Change Service. It presents a 300 m x 300 m spatial resolution. The 22 land-cover ESA-CCI classes were reclassified into 13 Plant Functional Types (PFTs) required by the ORCHIDEE model (Bontemps et al. 2013).

On the other hand, the deforested experiment (hereafter 'RegIPSL-Deforested' or 'RegIPSL-D') is based on future projections of Amazonian deforestation developed by Soares-Filho et al. (2006). In the present study, the Business-As-Usual (BAU) scenario for the year 2050 was used (Figure 3.1b). This scenario is the result of an empirically-based modeling study where 1997-2002 deforestation rates derived from satellite imagery were projected (Soares-Filho et al. 2006). Additional assumptions include

paving all planned highways, the lack of new protected areas in the basin, and empirical relationships involving the forest loss probability and the proximity to roads, rivers and towns, as well as already deforested patches. This deforestation scenario is widely used for the assessment of the influence of land use changes on the hydrology and climate of the South American continent (Coe et al. 2009; Swann et al. 2015; Eiras-Barca et al. 2020; Sierra et al. 2021). This BAU data set has a 1 km x 1 km horizontal resolution and labels each pixel as forest, deforested or non-forest. Since the ORCHIDEE PFTs maps have a coarser resolution (20 km x 20 km), all BAU scenario pixels within each PFTs grid cell were used to calculate the forest/deforested ratio. Then, to each PFT pixel in the control experiment, we impose this calculated ratio to the existent proportion between the classes 'tropical broad-leaved evergreen' and 'C3 agriculture'. Our premise is that deforestation is a change from forest to agricultural crops. In this sense, we keep unaltered the areas of the rest of land cover classes and only modify the area covered by forest and crops. Modifications to the PFTs were made for each year in both control and deforested experiments.

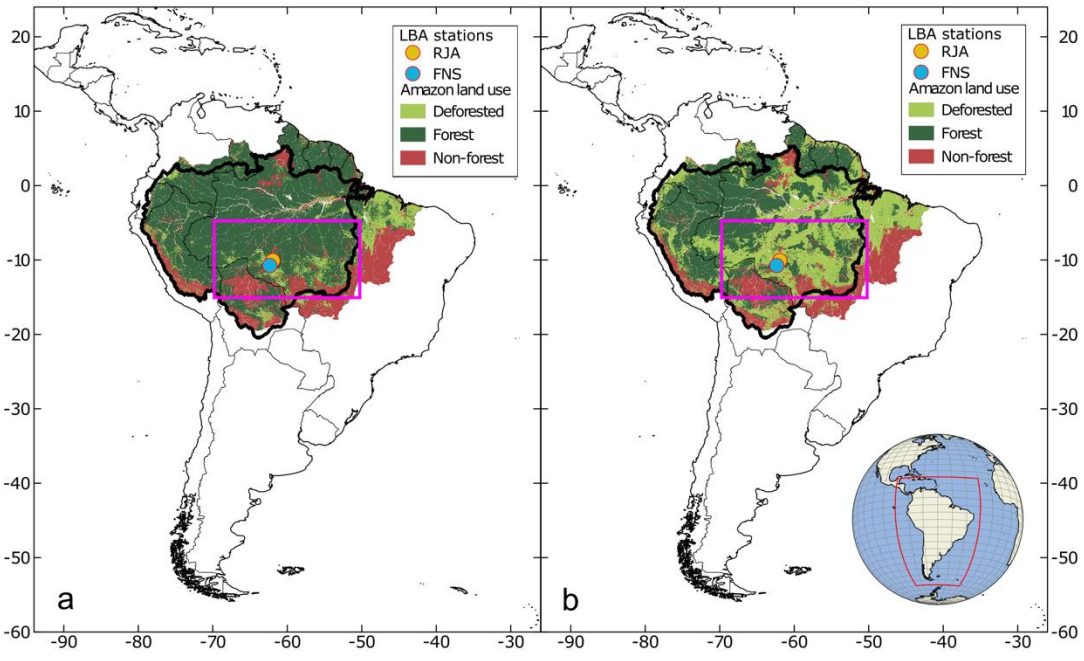

Fig. 3.1 Experiment scenarios: **a** Control and **b** Deforested. RegIPSL simulation domain is shown in the left bottom corner in panel **b**. Magenta box shows the southern Amazon region (5°S-15°S, 70°W-50°W) defined to compute the annual cycle in Figure 3.2. Blue and yellow circles in a and b show the location of the flux towers from the Large-Scale Biosphere–Atmosphere experiment in the Amazon.

3.2.2.3 Reference datasets

In order to assess the model performance, we use evapotranspiration and surface energy variables such as incoming/outgoing shortwave and longwave radiation, sensible/latent heat fluxes and surface net radiation obtained from ERA5-Land (Muñoz-Sabater et al. 2021). This data set is the product of numerical integrations of the ECMWF land surface model forced with the downscaled atmospheric forcing from ERA5 reanalysis. ERA5-Land has an enhanced horizontal resolution of ~9 km x 9 km at hourly scales, with data available from 1950 to present. ERA5-Land presents improvements in latent heat fluxes, Bowen ratio, skin temperature and soil moisture with respect to ERA5 (Muñoz-Sabater et al. 2021). To compare the model surface fluxes against in-situ measurements at a local scale, we use flux tower measurements from the Large-Scale Biosphere-Atmosphere Experiment in the Amazon (LBA) project (Saleska et al. 2013). The LBA project was an international project initiated in 1998 as a scientific effort to better understand, among other questions, the effects of land use changes in the Amazon on the regional climate. Two stations located inside our region of interest, the southern Amazon (5°S-15 °S, 70°W-50°W, magenta box in Figures 3.1a-b), were selected from the LBA data base. Located at 10.75° S, 62.35° W, and 306 m a.s.l., the station Fazenda Nossa Senhora de Aparecida (blue circle labeled as 'FNS' in Figure 3.1a-b), corresponds to a cattle ranch over a deforested area. Additionally, the station Rondonia Jaru Biological Reserve is located at 191 m a.s.l., 10.08° S, 61.93° W (yellow circle labeled as 'RJA' in Figure 3.1a-b). This station is located inside a natural reserve created by the Brazilian government in the 1960s. These stations present daily record of surface energy and water fluxes for the period 1999-2002. However, only the years 2001 and 2002 that overlap in time with our simulations are used. This dataset is available at https://daac.ornl.gov/LBA/guides/CD32_Brazil_Flux_Network.html (last access July 2022).

We use rainfall information from the Climate Hazards Group InfraRed Precipitation with Station data (CHIRPS) data set version 2 (Funk et al. 2015). Developed by the United States Geological Survey (USGS) and the Earth Resources Observation and Science (EROS), this data set is the result of a combination between satellite measurements, rain gauges data and interpolation techniques. Its high spatial and temporal resolutions (5 km x 5 km and daily data, respectively), as well as its long

record period from 1981 to 2020, makes this data set suitable to analyze the precipitation-atmospheric flow regime relationship at high temporal frequencies. When compared against rain gauges and in situ discharge measurements, CHIRPS exhibits a good representation of Amazon hydrology (Wongchuig Correa et al. 2017; Haghtalab et al. 2020). Therefore, this database is widely used to study the rainfall variability over tropical South America (e.g. Paccini et al. 2018; Cerón et al. 2020; Arias et al. 2020; Funatsu et al. 2021). The dataset is available at https://data.chc.ucsb.edu/products/CHIRPS-2.0/ (last access July 2022).

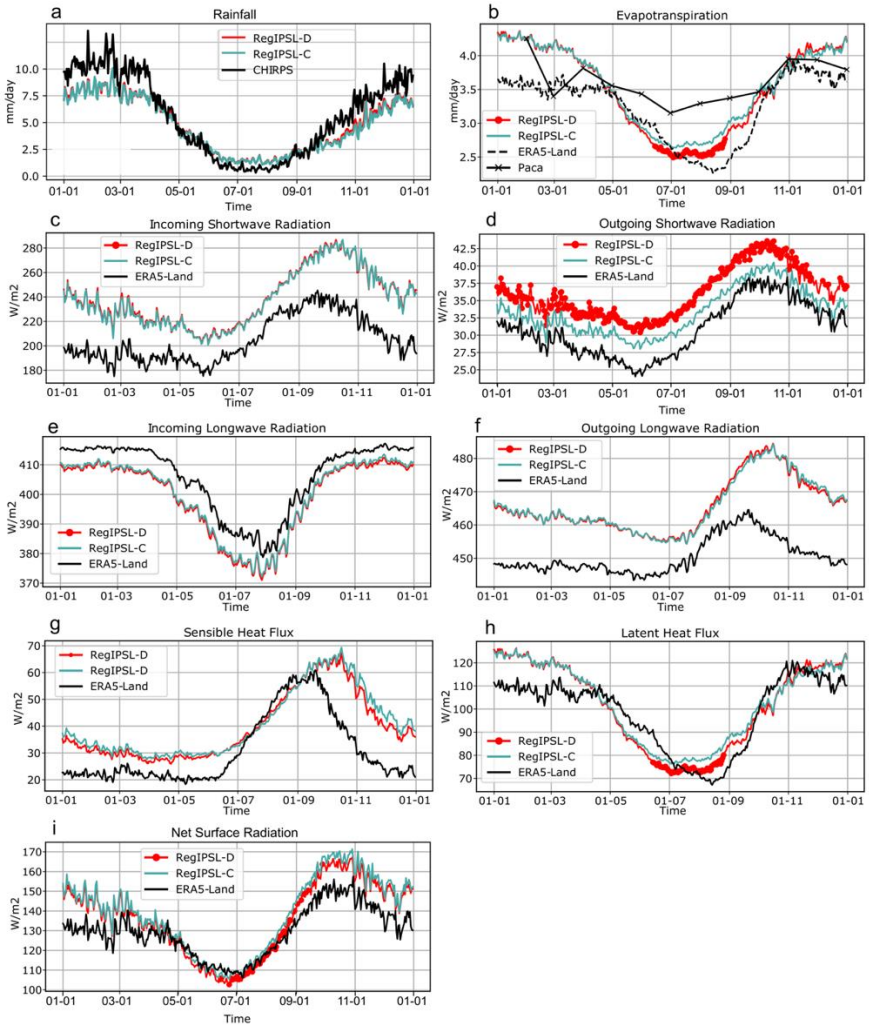

Fig. 3.2 Annual cycle in southern Amazon (see Figure 3.1) for: **a** rainfall and **b** evapotranspiration in mm day^{-1}, **c** incoming shortwave radiation, **d** outgoing shortwave radiation, **e** incoming longwave radiation, **f** outgoing longwave radiation, **g** sensible heat flux and **h** latent heat flux, and **i** net surface radiation (in W m^{-2}). Cyan and red lines represent RegIPSL-Control and RegIPSL-Deforested, respectively. Significant changes (t-test, $p<0.05$) between RegIPSL-Control and RegIPSL-Deforested are marked with red dots. Black lines represent reference datasets (CHIRPS and Paca in **a**-**b**, or reanalysis ERA5-Land in **c**-**i**).

In order to evaluate the actual evapotranspiration in the southern Amazon, we use the data base developed by Paca et al. (2019), hereafter called 'Paca'. By merging several global remote sensing evapotranspiration products, this data set presents a high resolution (250 m x 250 m) description of the spatial variability within the Amazon basin. Monthly values are provided for the 2003-2013 period and are available at www.wateraccounting.org (last access July 2022). Validated against flux tower measurements from the LBA project, this dataset captures the observed spatial and temporal evapotranspiration variability at monthly and inter-annual scales (Paca et al. 2019). Since there are significant discrepancies among evapotranspiration datasets that reflect the uncertainties in evapotranspiration estimations (Maeda et al. 2017; Sörensson and Ruscica 2018; Fassoni-Andrade et al. 2021), the use of a data based on different products is a way of dealing with the inter-product uncertainty. A more complete validation of the representation of evapotranspiration annual mean and annual cycle by RegIPSL model can be found in Wongchuig et al. (2022; submitted to Journal of Hydrology).

3.2.2.4 Definition of the large-scale circulation patterns (CPs)

The definition of the CPs is based on unfiltered daily meridional and zonal wind components at 850 hPa over the region 10°N-30°S, 90°W-30°W. Adding other variables in the CP's definition (such as temperature, rainfall or geopotential height) increases the computation cost and does not improve the classification of the atmospheric states related to precipitation (Espinoza et al. 2012). Horizontal winds at 850 hPa have proven to be suitable for the description of the main atmospheric circulation phenomena in tropical South America, such as the easterly winds, the southern regimes or 'cold surges', the South American Low-level Jet (SALLJ), among others (Paccini et al. 2018). In addition, winds at 850 hPa (around 1500 m of altitude) are most of the time located within the Planetary Boundary Layer (PBL) and, therefore, should not be affected by the imposed large-scale nudging in our model experiments. As a first step, horizontal winds are standardized using the long-term mean and standard deviation at each grid-cell so keeping all the time variations including the seasonal cycle. In order to accelerate computations and to retain only the main variability modes, we apply principal component analysis over standardized winds from ERA5, RegIPSL-Control and RegIPSL-Deforested independently. The principal

component approach has been used in previous studies to filter out the smallest spatial scales of the regional-scale atmosphere's phase space (Moron et al. 2008, 2015; Olmo et al. 2022). We use the 30 leading principal components, which explain 78% and 73% of the total variability for ERA5 and RegIPSL-Control/Deforested, respectively, to identify the CPs using the k-means methodology.

K-means is a dynamical clustering procedure that looks for classifying data into k clusters in an n-dimensional subspace, in this case, spanned by the 30 leading principal components. The *k* clusters are selected by recursive iterations that seek to minimize the sum of variance between points belonging to the same cluster (Diday and Simon 1976). Defining the number of groups or clusters to be used is a key question in clustering analysis. Different indices have been designed in order to find the optimal number of clusters, all of them sharing the basic principle: identifying the number of clusters with greatest similarity between the members of a cluster and with the highest inter-cluster difference (Calinski and Harabasz 1974; Michelangeli et al. 1995). Previous studies have demonstrated that a number of 9 CPs are appropriated to represent the main stages of the annual regional-scale circulation in northern South America (da Anunciação et al. 2014; Paccini et al. 2018; Espinoza et al. 2021). Following Espinoza et al. (2021), we define 9 clusters to summarize the regional atmospheric variability, considering all times scales from daily to decadal. In this sense, the 6935 days of our interest period 2001-2019 are classified in 9 groups or CPs. The assignment of each day to a particular CP is, up to a certain point, dependent to the *k*-means methodology, specifically to initial cluster centroids used for starting the classification or 'initialization' (Michelangeli et al. 1995). For this reason, 1000 reclassifications of the 6935-day time series were performed independently for ERA5, RegIPSL-Control and RegIPSL-Deforested using random initial seeds on each day-classification. For most of the analysis in the present work, we use a particular classification using a smart way to select the initial cluster centers in order to speed up the convergence (Pedregosa et al. 2011). However, for the assessment of changes in the CPs annual cycle frequency in section 4, we use the 1000 classifications in order to evaluate whether the signal induced by deforestation is consistent and independent of the statistical classification method. Finally, composite analysis of interest variables (such as rainfall or evapotranspiration) is carried out over the days belonging to each CP.

3.2.2.5 Definition of the wet season onset in the southern Amazon

The onset of the wet season is estimated based on the methodology developed in Li and Fu (2004). We first compute the spatial mean of daily rainfall over the southern Amazon. Then, pentad rainfall time series are estimated by temporally averaging over 5-day period in order to reduce the synoptic noise. According to Li and Fu (2004), the dry season end/wet season onset is established when 6 out of 8 preceding pentads are below the climatological rain rate annual mean and 6 out of 8 subsequent pentads are above it. However, in most of the years there are few consecutive pentads that meet these two conditions. Li and Fu (2004) define the wet season onset as the earliest date or the first of these pentads. Nevertheless, in order to assure that wet conditions begin to be dominant and well established, instead of using the earliest pentad we use the date of the latest pentad fulfilling these conditions as the date of the onset. This analysis is performed independently for CHIRPS and RegIPSL (using data during the same periods).

3.2.2.6 Evaluation framework

The assessment of the model's skill in representing the observed CPs, taking as a reference ERA5 for winds, and CHIRPS for precipitation, is performed through the analysis of the spatial patterns of CP composite means, as well as their climatological frequency of occurrence along the year.

The evaluation of the CP spatial pattern is addressed by comparing the mean composite fields from reference datasets and RegIPSL Control using Taylor diagrams. Taylor diagram is a graphical tool that summarizes the match between two spatial or temporal fields in terms of the Pearson correlation, the root-mean-square error and the ratio of their variances (Taylor 2001). This methodology is widely used in climate modeling studies (e.g. Voldoire et al. 2013; Sierra et al. 2015; Ortega et al. 2021; Olmo et al. 2022). For each CP we compare separately the spatial distribution of rainfall, zonal and meridional winds.

On the other hand, following Olmo et al. (2022), the representation of the CP frequencies of occurrence is analyzed with an error metric that quantifies the absolute difference between the climatological daily frequencies in the reanalysis and model outputs (Equation 3.1). This metric is computed for each CP and can be estimated as:

$$Error_{CP} = \frac{\sum_{i=1}^{D} \left| f\ ERA5_{CP_i} - f\ RegIPSL_{CP_i} \right|}{D} \qquad (3.1)$$

where D is the total number of days during the evaluated season. A special attention is paid to the dry-to-wet transition (July-November), D corresponds to 153 days. Then, i is an index for dates varying between July 1st and November 31st. $f\ ERA5_{CP_i}$ and $f\ RegIPSL_{CP_i}$ are the number of days corresponding to a specific CP for the date i in the whole 2001-2019 period for ERA5 and RegIPSL respectively. For example, for i corresponding to July 1st, and analyzing the representation of the CP T1, $f\ ERA5_{CP_i}$ represents the number of times that T1 is observed on this particular date in the whole 19-year period. A similar interpretation applies for $f\ RegIPSL_{CP_i}$.

3.2.3 Model validation

In this section, we show the validation of the RegIPSL-Control simulations in terms of the annual cycle of rainfall and surface fluxes in the southern Amazon. The dominant modes of the regional low-level circulation variability in tropical South America and the model's skill to reproduce the meteorological conditions for the onset of the wet season are also assessed. For this purpose, we use in-situ LBA measurements, satellite and reanalysis data.

3.2.3.1 Rainfall and surface fluxes in the southern Amazon

The seasonality of precipitation over the southern Amazon is well represented by RegIPSL-Control, with rainfall maxima during December-February according to observations as described in section 1 (cyan line in Figure 3.2a). During this season, the model underestimates the rainfall rates by about -20% (-2.4 mm day^{-1}) with respect to CHIRPS. On the contrary, precipitation minimum is simulated and observed in June-August, with an overestimation of about +120% (+0.46 mm day^{-1}) in this particular

season. As a consequence, the steep rainfall switch in both dry-to-wet and wet-to-dry transition periods is weaker in RegIPSL-Control than in CHIRPS. For example, during the dry-to-wet transition between September 1st and November 1st, mean rainfall increases at a rate of 2.50 mm d^{-1} per month in CHIRPS, and only about half of this value (1.21 mm d^{-1} per month) in the model. Nevertheless, since our study focuses on atmospheric circulation patterns for characterizing the wet season onset instead on rainfall, particular emphasis will be placed on biases on wind circulation of the model (Section 3.2.3.2).

The mean evapotranspiration annual cycle is well represented by RegIPSL-Control compared with Paca and ERA5-Land estimates, with maximum and minimum fluxes during the wet and dry seasons respectively (cyan line in Figure 3.2b). RegIPSL does not capture the bimodal regime observed in Paca et al. (2019), although it represents a small peak in October when maximum incoming solar and net surface radiation are simulated (Figures 3.2c and 3.2i). Additionally, the general amplitude of the seasonal cycle is higher in RegIPSL-Control, ranging between 2.67-4.27 mm day^{-1}, compared to Paca et al. (2019), with values between 3.15-4.25 mm day^{-1}. Similar to RegIPSL-Control, evapotranspiration in ERA5-Land varies between 2.34-3.85 mm day^{-1}. Differences among evapotranspiration data sets have been reported by previous works and reflect the uncertainty, the lack of data and the need of a better-understanding of the vegetation evaporative capacity in the Amazon basin and in the tropics in general (Maeda et al. 2017; Sörensson and Ruscica 2018; Fassoni-Andrade et al. 2021).

On the other hand, RegIPSL-Control shows a realistic representation of the seasonal cycle of incoming and reflected solar radiation fluxes (cyan line in Figures 3.2c-d). The incoming solar radiation is overestimated in about +30 W m^{-2} or +12% along the year. This error is probably caused by an underestimation of the cloud cover. Less clouds in the model outputs are also linked with a drier atmosphere which radiates less energy to the ground, causing an underestimation of the incoming longwave radiation (Figure 3.2e). A little lag in the peak of the incoming solar radiation is part of the model outputs. While maximum incoming solar radiation occurs in the middle of September in ERA5-Land, it is located in October in RegIPSL-Control. Since this is energy flux is the only energy input to the surface that exhibits a delay, we hypothesize that this bias is related

to the slightly lagged peak in outgoing longwave radiation and sensible heat (Figures 3.2f-g). The possible mechanism behind this bias could be related again to problems in the representation of clouds. Cloudiness could be larger in RegIPSL in September than in October, in contrast to ERA5, what can cause an underestimation (overestimation) of the incoming solar radiation during September (October). On the other hand, although more energy reaches the ground in terms of solar radiation, the underestimation of the incoming longwave radiation and the overestimation of the outgoing longwave flux help to balance the energy budget and, at the end, the net surface radiation is well represented in seasonality and magnitude. However, an overestimation by RegIPSL-Control is observed during the dry-to-wet and wet seasons in the net surface radiation (Figure 3.2i). The overestimation of surface energy fluxes, especially net surface radiation and sensible heat flux seem to be a systematic error in WRF over the Amazon basin regardless of the model configuration (Wang et al. 2021).

Although our main interest is the southern Amazonia as a whole region, the model validation up to now is strongly based on a model to model comparison. For this reason, we also analyze the representation of surface fluxes at a more local scale using the selected flux towers from the LBA project, located over one forested and one deforested site (Figures 3.1a-b). The distance between the two LBA stations is 87 km. Thereby, we use a surrounding area of 100 km x 100 km (5 x 5 grid cells) encompassing the measurements sites for surface fluxes from RegIPSL-Control outputs. Then, we select grids with forest or cropland fractional areas higher than 70%, in order to compare the model against the forested and deforested LBA sites for the years 2001-2002. The results of this analysis are shown in Figure A1 and reflect the same model biases observed at a regional scale described previously (except for rainfall). At local scale, RegIPSL-Control and observations present the same rainfall seasonality, with a wet season in December-May and a dry season in June-August. However, the model exhibits a strong rainfall overestimation during the wet season over forested and deforested areas (Figures A1a-b). Similar to the behavior exposed by Paca et al. (2019) at a more regional scale, evapotranspiration shows little seasonality with fluctuations around the 2.5 mm day^{-1} and 3 mm day^{-1} over the forest and pasture LBA sites, respectively (Figures A1c-d). Higher precipitation rates in RegIPSL-Control causes an evapotranspiration overestimation between January and

May. Evapotranspiration overestimation is higher over croplands in the model outputs. Nevertheless, the model is able to represent the weak seasonality of this surface water flux along the year. Most of the surface energy variables are realistically represented in terms of magnitude and seasonality (Figures A1e-n). However, RegIPSL-Control overestimates the incoming solar radiation between August to November, with a slightly higher bias over the forest site (Figure A1f). As a consequence, the model also overestimates the outgoing or reflected solar radiation over the forest site (Figure A1h). In addition, the model slightly underestimates (overestimates) the incoming (outgoing) longwave radiation flux along the year over both areas in a similar way to the regional analysis shown previously (Figures A1i-l). Nevertheless, in the same way that at regional scale, these errors compensate each other, and the net surface radiation is well represented by the model (Figures A1m-n).

3.2.3.2 Main circulation patterns (CPs) in tropical South America

In this sub-section, we show if the model is able to capture the dominant modes of the regional circulation variability over tropical South America. The regional atmospheric circulation variability is summarized through 9 CPs that can be understood as preferred states of the regional climatic system (Figures 3.3 and 3.4). As described by Espinoza et al. (2021), there is a clear seasonal cycle in the relative CPs frequency (Figure 3.3). We identify 3 CPs with major activity during austral summer, corresponding to the wet season in the southern Amazon, labeled as W1-W2-W3 (blue colors), 3 austral winter CPs with usual dry conditions and largest frequencies in June-August, labeled D1-D2-D3 (orange-red colors), and 3 transitional CPs characterizing mostly the dry-to-wet transition $T2_{DW}$ (dark green), the wet-to-dry shift $T3_{WD}$ (yellow) and a CP that occurs in both transitional periods T1 (green color). Table 3.3 summarizes the main features of the circulation and rainfall anomalies associated with each atmospheric state or CP. A more exhaustive description of the CPs low-level circulation and atmospheric mechanisms is presented by Espinoza et al. (2021).

As seen in Figure 3.3b, RegIPSL-Control is able to properly represent the relative CP's frequency along the year even if the classification is done independently from ERA5. Differences in the CP's frequency during the dry-to-wet transition period (July to November) between ERA5 and RegIPSL-Control are quite small and does not surpass

±1 day of mean error (Table A1). It is interesting to note that higher frequency errors are presented during the transition CPs T1 and $T2_{DW}$. Similar results were reported recently by Olmo et al. (2022) for the representation of the same transitional CPs by last generation global climate models.

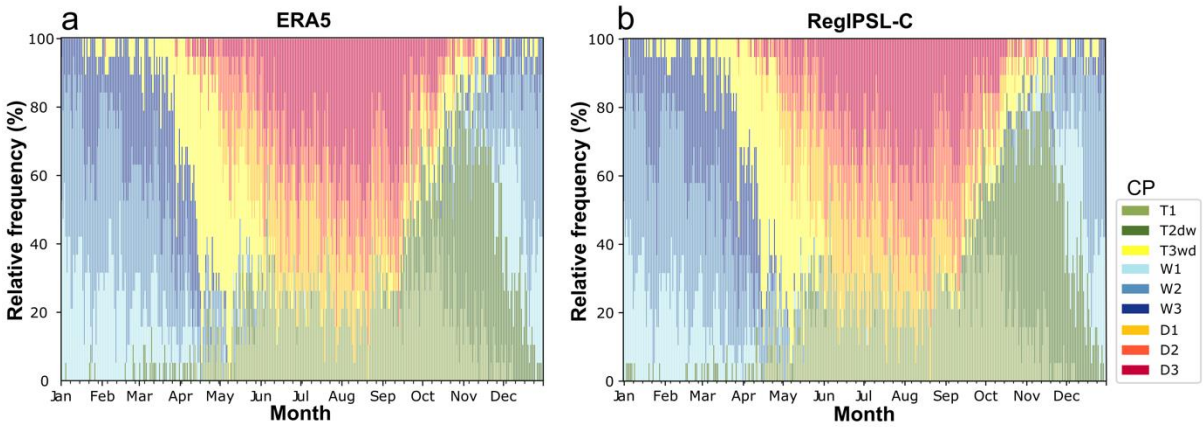

Fig. 3.3 Relative mean daily frequency of the 9 circulation patterns (CPs) defined from the k-means clustering analysis for: **a** ERA5, and **b** RegIPSL-Control (RegIPSL-C). The horizontal axis represents the days from January 1st to December 31st in the climatology during the period 2001-2019.

Table 3.3 Brief overview of the main features of the CPs explaining the atmospheric circulation variability in tropical South America identified by Espinoza et al. (2021). D1, D2, D3 (W1, W2, W3) correspond to dry (wet) season CPs. Transitional CPs are labeled T1, T2DW (transition from dry-to-wet conditions) and T2WD (transition from wet-to-dry conditions). See Figure S2 in supplementary material for rainfall and wind composites with ERA5/CHIRPS.

	Intra-seasonal variability			
Seasonality	**Dry season or austral winter CPs**	**D1**	**D2**	**D3**
		- Major frequency during the early dry season (June). - Positive (negative) rainfall anomalies over northern (southern) tropical South America. - Low-level wind divergence centered in the southwestern Amazon and related to southerly cross-equatorial wind.	- Major frequency during the core of the dry season (July-August). - Positive (negative) rainfall anomalies over northern (southern) tropical South America and the northwestern Amazon. - Anomalous southerly cross-equatorial regime coming from the subtropics linked to cold intrusions.	- Major frequency during the late dry season (August). - Positive (negative) rainfall anomalies over northern (southern) tropical South America. - Low-level wind divergence centered in the southwestern Amazon and related to southerly cross-equatorial wind. Development of a winter SALLJ.
		W1	**W2**	**W3**

	Wet season or austral summer CPs	- Major frequency during the early wet season (December). - Positive rainfall anomalies over the continental South Atlantic Convergence Zone (SACZ) and most of the tropical Andes. - Anomalous northerly cross-equatorial flow deviated eastward due to the encounter with southerly wind intrusion.	- Major frequency during the core of the wet season (December-February). - Positive rainfall anomalies in SESA, the Amazon-Andes rainfall hotspots and the Andes. - Anomalous northerly cross-equatorial winds reaching southern latitudes of tropical South America related to the summer SALLJ.	- Major frequency during the late wet season (February-March). - Positive rainfall anomalies over the Amazon basin and the tropical Andes. - Anomalous northerly cross-equatorial flow encountering southerly wind intrusion and generating convergence over the Amazon basin.
	Transitional CPs	**T1**	**$T2_{DW}$**	**$T3_{WD}$**
		- Major frequency during the wet-to-dry (May-June) and dry-to-wet (September-October) periods. - Positive rainfall anomalies over South Eastern South America (SESA) and negative anomalies over the southern Amazon and eastern Brazil. - Intensified South American Low-level Jet (SALLJ) below 14°S.	- Major frequency in the dry-to-wet transition (October-November). - Positive rainfall anomalies over the southern Amazon and southeastern Brazil. - Anomalous northerly cross-equatorial winds encountering a southerly wind incursion.	- Major frequency in the wet-to-dry transition (April-May). - Positive (negative) rainfall anomalies over the northern (southern) south America. - Anomalous southerly cross-equatorial winds from tropical south Atlantic.

Figure 3.4 shows low-level horizontal wind and rainfall anomalies (vs the annual mean) for each CP according to RegIPSL-Control. A direct comparison with ERA5/CHIRPS composites (Figure A2), as well as the Taylor diagrams analysis (Figure A3), allows us to conclude that RegIPSL-Control captures well the spatial structure of wind and rainfall patterns associated with all CPs. Indeed, spatial correlations for the CP composites with respect to reference datasets are significantly high (>0.78) as seen in the Taylor diagrams in Figure A3. Precipitation is the variable with the lowest spatial correlations, mainly during the transition CPs T1 and $T2_{DW}$ (0.79 and 0.81, respectively; Figure A3a). The spatial distribution of horizontal winds at 850 hPa is well represented by the model for all circulation patterns (spatial correlation > 0.95; Figures

A3b-c), except for the meridional component of D2. This particular CP presents a strong meridional component of the wind that characterizes the entry of the so called 'cold fronts' into tropical South America coming from the southern part of the continent (see Table 3.3). For this reason, this CP is more sensitive to the representation of the meridional wind. In order to better explore the biases in RegIPSL outputs, we compute the differences in low-level winds and rainfall with respect to ERA5 and CHIRPS as seen in Figure 3.5.

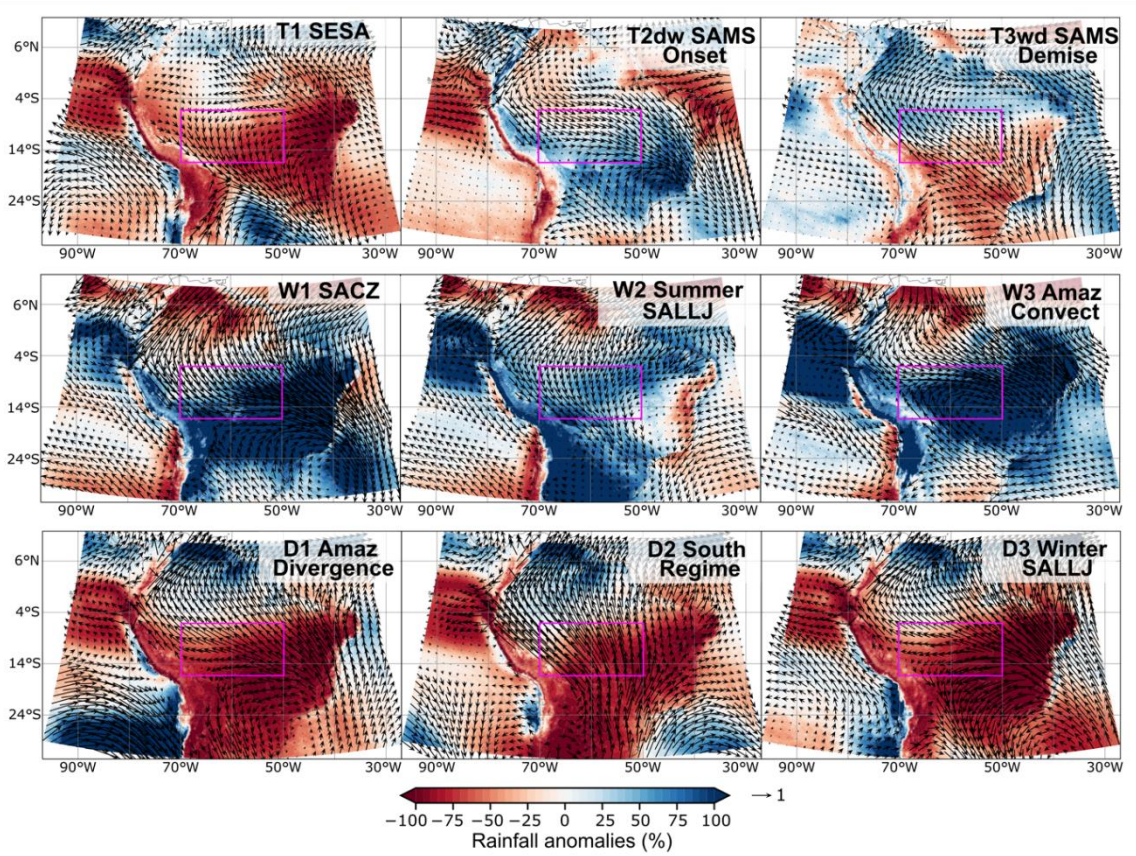

Fig. 3.4 Rainfall and 850 hPa horizontal wind anomalies (vs the annual mean) composites for the 9 circulation patterns (CPs) defined from the k-means clustering analysis using RegIPSL-Control outputs. Rainfall (shaded) is in percentage respect to the inter-annual mean and horizontal winds at 850 hPa (vectors) are adimensional. Magenta box shows the southern Amazon domain (5°S-15°S, 70°W-50°W).

In general, rainfall composite differences between RegIPSL-Control and CHIRPS are rather constant across the transitional and wet season CPs (Figure 3.5). The model exhibits lower precipitation rates over Colombia and Ecuador while overestimates it in northeastern Amazonia and northern Brazil (Figure 3.5). Rainfall is also underestimated by RegIPSL-Control over the South Eastern South America region (SESA, defined as the continental area east of the Andes below 23°S) during T1, W2

and D3 events. These circulation patterns are very related with the activity of the SALLJ (see Table 3.3) which suggests a bad representation of the link between rainfall and the SALLJ circulation in La Plata basin. Recent works demonstrate that adding the representation of floodplains to the RegIPSL model can result in a better representation of precipitation and the moisture transport by the SALLJ in La Plata basin (Schrapffer 2022). In the same way, precipitation biases are similar among the wet season CPs. While less rainfall is simulated over the central Amazon and the Guianas, higher rainfall is simulated over the eastern Brazil.

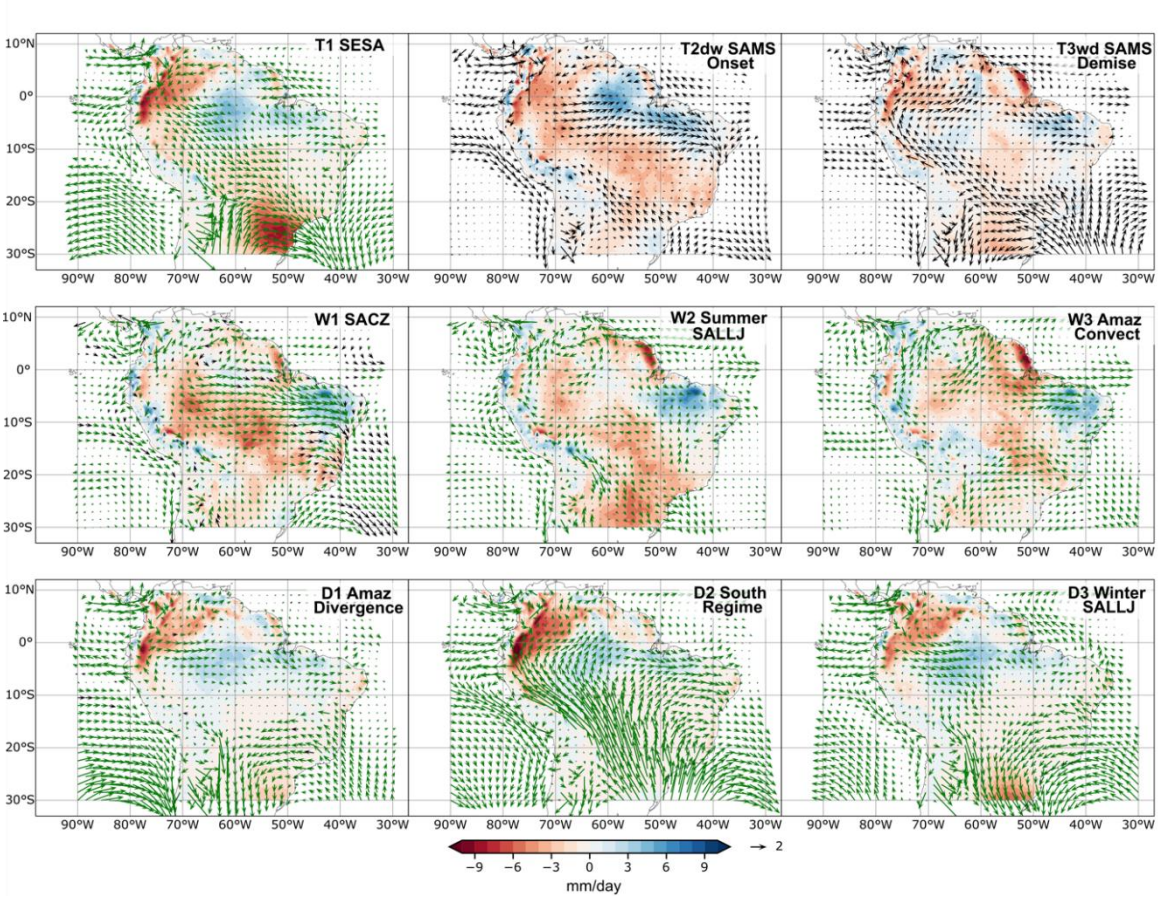

Fig. 3.5 Rainfall and 850 hPa horizontal wind anomalies composites differences RegISPL-Control minus ERA5/CHIRPS for the 9 circulation patterns (CPs) defined from the k-means clustering analysis. Rainfall differences (shaded) are in mm day^{-1} and horizontal winds at 850 hPa (vectors) are in m s^{-1}. Only significant rainfall differences are shown (t-test, $p<0.05$). Green vectors represent significant wind differences (t-test, $p<0.05$).

Wind differences between RegIPSL-Control and ERA5 in tropical South America are higher for the dry and transition season CPs (Figure 3.5). For CPs T1, T3$_{WD}$ and D2, the spatial distribution of wind differences between RegIPSL-Control and ERA5 are very similar to their mean patterns shown in Figure 3.4. This implies that the model

presents a stronger regional circulation and overestimates the 850 hPa winds over the entire region on these particular meteorological conditions. $T3_{WD}$ and $T2_{DW}$ present no statistically significant wind differences with respect to ERA5 despite their relatively high wind differences (Figure 3.5) which suggests a large low-level wind variability during these particular transitional atmospheric patterns. A stronger low-level circulation during the dry and dry-to-wet transition seasons in RegIPSL could be related to a high model sensitivity to the external synoptic signal from ERA5 boundary forcing. Indeed, D1 and D3 display stronger southward winds blowing from southwestern Amazon toward the La Plata basin in RegIPSL-Control. Contrary to winter CPs, summer CPs (W1-W2-W3) present little wind differences with respect to ERA5.

3.2.3.3 Wet season onset characteristics in terms of CPs

This subsection analyzes the conditions in the atmospheric circulation states, rainfall and evapotranspiration during the preceding and subsequent days of the wet season onset in reanalysis dataset and RegIPSL-Control.

Figure 3.6a shows the evolution of CP frequency throughout the development of the wet season onset (defined in section 3.2.2.5). Around 90 days before the onset, nearly 80% of the days are under winter or dry conditions (D1, D2 and D3), according to ERA5. Precipitation in southern Amazonia (see Figures 3.1a-b for the location) is almost zero before the day -90 (i.e. 90 days before the wet season onset), whereas evapotranspiration is near its minimum (Figures 3.6c-d). After the day -80, dry season CPs start to be less frequent and are replaced by T3WD and mainly by $T2_{DW}$ (Figure 3.6a). In this sense, by the day -75, dry season CPs occur 80% of the time while transitional regimes $T3_{WD}$ and $T2_{DW}$ are not observed. Nonetheless, after 25 days (by the day -50), dry season and transitional CPs occur 61% and 12% of the time, respectively. At the same time, rainfall and evapotranspiration begin to increase (Figures 3.6c-d). Consistent with our results, previous works locate the end of the dry and the beginning of the dry-to-wet transition season about 90 days before the onset, when the atmosphere starts to moisten and the lower troposphere begins to gain (reduce) available potential energy (the convective inhibition) (Fu et al. 1999; Li and Fu 2004; Wright et al. 2017). The incoming solar radiation increases rapidly until the

day -60, and then a slower increment is sustained until its maximum in the day -25 for ERA5-Land (not shown). It is precisely after the day -25 when the steep evapotranspiration increment flattens out slightly in ERA5-Land (Figure 3.6d). Thus, because of the combination of positive incoming solar radiation anomalies over the southern Amazon (related to a higher frequency of T1, $T2_{DW}$ and D3; not shown) and positive precipitation anomalies (linked to the presence of $T2_{DW}$ during this period; see Figure 3.4) there is a rapid evapotranspiration increase between days -60 and -25. The role of the solar radiation on the rainforest's response in terms of evapotranspiration during the transition from dry to wet season is reported in observational-based works (Myneni et al. 2007). On the other hand, precipitation presents a stronger increase between the days -60 and 0, when $T2_{DW}$ starts to be more frequent during this period. Wright et al. (2017) find a rainfall and evapotranspiration increase between 60 to 30 days before the onset in consistency with our results. A peak in the frequency of $T2_{DW}$ (64%) is observed precisely at the onset of the wet season (pentad 0; Figure 3.6a). Previous studies demonstrate the relationship between the variability of the Amazonian wet season onset and the frequency of $T2_{DW}$ (Espinoza et al. 2021). In fact, our $T2_{DW}$ looks very similar to circulation anomalies registered by early works during the wet season onset in the southeastern Amazon, with enhanced trade winds in the Atlantic, southern wind intrusion in the Amazon and more rainfall in central and southern parts of the basin (see Figures 10-11 of Marengo et al. 2001). According to Wright et al. (2017), the last 30 days before the onset mark a shift from shallow to deep convection. During this period, CP W1, W2 and W3 begin to appear and develop deep convection in the region (Figure 3.6a). Five days after the SAMS onset, summer or wet season CPs are observed during ~20% of the time and by the day +50, they occur 80% of the time (about 60% is occupied by the presence of the SACZ-SALLJ dipole corresponding to the W1-W2 co-existence).

The model shows a realistic development of the different characteristics of the wet season onset (Figures 3.6b-d). However, there are some differences in the simulated development of the wet season in RegIPSL-Control. The model exhibits an early retreat of the dry or winter circulation patterns around the day -105, and consequently, an early development of the transitional CP $T2_{DW}$. While in ERA5, around the day -95, dry season CPs (D1-D2-D3) account for 80% of total frequency, in the model these

atmospheric wintertime regimes account for only 62%. Likewise, at this time, the transitional CP $T2_{DW}$ is absent in the reanalysis but in the model, it is observed prematurely 8% of the time. Similarly, the evapotranspiration and rainfall start to increase around 20 days in RegIPSL-Control before the reference data sets (Figures 3.6c-d). Consistently, wet season circulation patterns W1-W2-W3 start to appear also 20 days early in the model simulation. However, similarly to ERA5, the model exhibits the major activity of CP T2DW around the onset date (day 0), with a 62% of frequency.

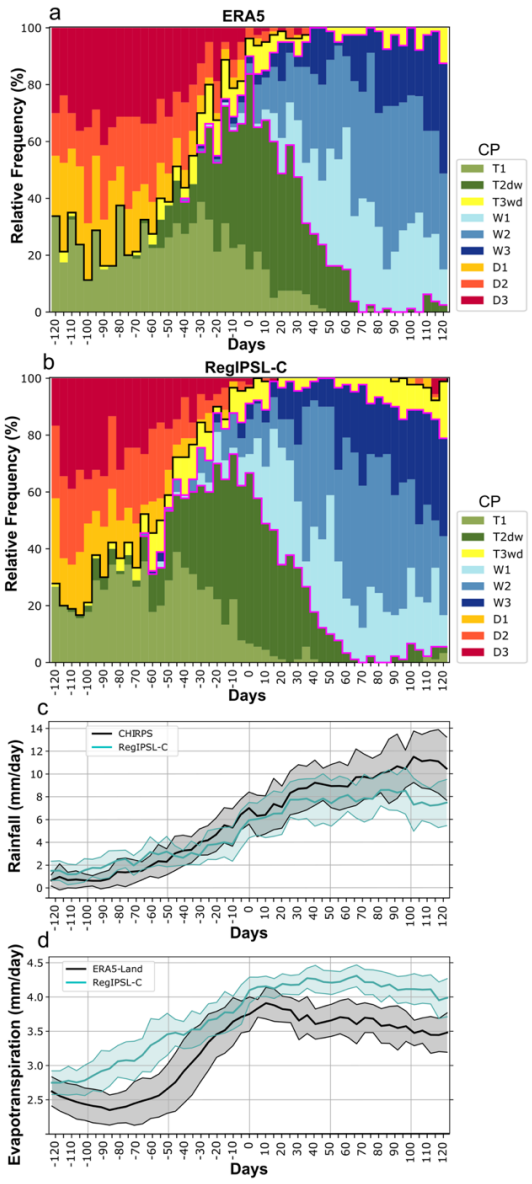

Fig. 3.6 Composite time series of: **a** and **b** relative frequency of circulation patterns from **a** ERA5 **b** RegIPSL-Control, taking as a reference the date of the wet season onset in southern Amazonia (day 0); **c** rainfall and **d** evapotranspiration for reference datasets in black solid lines (CHIRPS for rainfall, and ERA5-Land for evapotranspiration) and RegIPSL-Control (cyan solid lines) in mm day^{-1}. The x-axis represents the time, with negative (positive) values for days before (after) the onset. Gray and cyan envelopes represent the standard deviation at inter-annual scale for reference datasets and RegIPSL, respectively. Black and magenta lines in **a** and **b** enclose the dry and wet season CPs respectively.

One limitation of the previous rainfall and evapotranspiration analysis is the homogenization of meteorological variables through spatially averaging over a big area. The southern Amazon is characterized by the juxtaposition of rainforest trees and croplands/grasslands. These land surface heterogeneities are determinant for triggering mesoscale circulations and for defining the nature of convective activity, cloudiness and atmospheric stability in this particular region (Cutrim et al. 1995; Silva Dias and Regnie 1996; Souza et al. 2000; Wang et al. 2009). The land cover effect is particularly important during the dry and dry-to-wet transition seasons, when the extratropical cold surges are less frequent and the atmosphere is more stable (Siqueira and Toledo Machado 2004; Wang et al. 2009). Therefore, understanding the evolution of surface fluxes and atmospheric variables over the different land covers is crucial for disentangling their differentiated contribution on the beginning of the wet season onset.

3.2.3.4 Wet season onset characteristics over forest and croplands/grasslands

After a validation of the representation of atmospheric circulation states, rainfall and evapotranspiration along the development of the wet season by RegIPSL-Control (see section 3.2.3.3), in this section we evaluate the evolution of surface and atmospheric characteristics over different land covers in the region. To this end, we identify and select the areas within the southern Amazonia (see Figure 3.1a for location) where forest or croplands/grasslands are the dominant vegetation type. Pixels labeled as ‘forest’ present a fractional area higher than 60% covered by the ‘Tropical Broadleaf Evergreen’ category. Similarly, pixels labeled as ‘cropland/grassland’ correspond to a 60% or more of fractional area covered by the categories ‘Temperate Natural Grassland’, ‘Natural Grassland’ and ‘C3-C4 Crops’. We compute spatial averages for meteorological variables over forest and cropland/grassland areas separately, as well as composites for the preceding and subsequent days of the rainy season onset (Figures 3.7 and A4).

Although the general temporal evolution for most of the variables is similar between forest and crop/grass, there are significant differences in magnitude mainly before the onset of the rainy season. Since forest covers around 92% of the southern Amazon

total area, the magnitude and temporal pattern between averages over the forest area and over the total area (green and blue lines in Figure 3.7, respectively) are very similar for all the analyzed variables. Reduced precipitation is observed over croplands/grasslands during the whole period but only significant before the day -25 (Figure 3.7a), when wet season CPs W1-W2 start to occur in the model outputs (Figure 3.6b). In agreement with in-situ observations, evapotranspiration in the control experiment over forest areas is higher than croplands/grasslands during the dry season due to the greater access of forest roots to deep soil water (Wright et al. 1992; Sommer et al. 2002; von Randow et al. 2004). After the arrival of the first rainy events before the onset (between days -80 to -50), cropland/grassland evapotranspiration increases rapidly after the atmospheric water input (Figure 3.7b). This fast evapotranspiration response after rainy events has been described previously in in-situ measurements from the African Monsoon Multidisciplinary Analysis (Lohou et al. 2014). According to these authors, evapotranspiration speed response is dependent on the soil water content during the previous days in an inverse relation, where for drier soils there is a faster response (Lohou et al. 2014). However, after the beginning of the rainy season (day 0) and with the occurrence of wet season CPs, which present positive rainfall anomalies broadly in the region, we observe no difference in the evapotranspiration flux between forest and crop/grass (Figure 3.7b). Little difference between evapotranspiration rates over forested and non-forested areas was observed in the Brazilian state of Rondonia during the wet season using MODIS16 in agreement with our results (da Silva et al. 2019).

Sensible heat increases from days -120 to -30, reaching its maximum 30 days before the onset and decreasing later in both forest and croplands/grasslands (Figure 3.7c). However, croplands/grasslands exhibit significant higher values before the onset in about ~+25 W m2, what has been reported in observations and climate model simulations (Shukla et al. 1990; Polcher and Laval 1994; Gash and Nobre 1997; Fisch et al. 2004; von Randow et al. 2004; Eiras-Barca et al. 2020). Similarly, the net radiation peaks at the day -30 (Figure 3.7d) indistinctly for forests and croplands/grasslands, following the temporal evolution of the incoming solar radiation (Figure A4a). Nevertheless, crop/grass areas have a reduced net surface radiation (~-10 W m^{-2}) in the pre-onset period as a consequence of the enhanced loss of energy from the reflected solar radiation (albedo effect) and the decreased energy entry from

the incoming longwave radiation due to a drier atmosphere (Figures 3.7d and A4b-c). These deforestation induced alterations in the surface energy balance have been widely studied and described by previous works (Eltahir 1996; Gash and Nobre 1997; Claussen et al. 2001; Berbet and Costa 2003; von Randow et al. 2004; Figure 3.7b). Due to the increased sensible heat flux and the reduced evapotranspiration over crop/grass areas, the Bowen ratio (which corresponds to the ratio between sensible and latent heat fluxes) is higher than forest before the onset (Figure 3.7e). It is interesting to note that the Bowen ratio over forest is always less than 1, which reflects the dominant role of the latent heat flux in the surface energy partition during the entire period. Otherwise, croplands/grasslands present a Bowen ratio higher than 1 until the day -20, when rainfall and evapotranspiration increases reach their maximum rates and when wet season CPs start to be frequent (Figures 3.6b and 3.7a-e). At the rainy season onset, crop/grass and forest present a similar Bowen ratio (Figure 3.7e). Although the differences is not significant, the Planetary Boundary Layer (PBL) height is higher over croplands before the onset (Figure 3.7f) in response to the increased sensible heat flux and a warming of the low-level troposphere (Figure A4e-f; Fisch et al. 2004). Consistently with other variables, croplands/grasslands and forest present a similar PBL after the establishment of the wet season (Figure 3.7f).

During the first part of the pre-onset period (days -120 to -60), the vertically integrated moisture divergence is similar over croplands/grasslands and forests (not shown). Therefore, the low troposphere (below 800 hPa) is moister over forested areas (Figures 3.7g-h) due to the higher forest evapotranspiration rates shown in Figure 3.7b. After the day -50, the combined effect of increased evapotranspiration by croplands/grasslands and the beginning of the regional-scale atmospheric moisture convergence (not shown), which is related to less frequent dry season CPs D1-D2-D3 (Figure 3.6b), reduce the gap between forests and pastures in the atmospheric moisture content (Figure 3.7h). It is interesting to note the moister air observed over croplands/grasslands at 600-775 hPa for the entire period, with a peak around the day -30. At the local scale, this forest-crop/grass difference can be explained by the

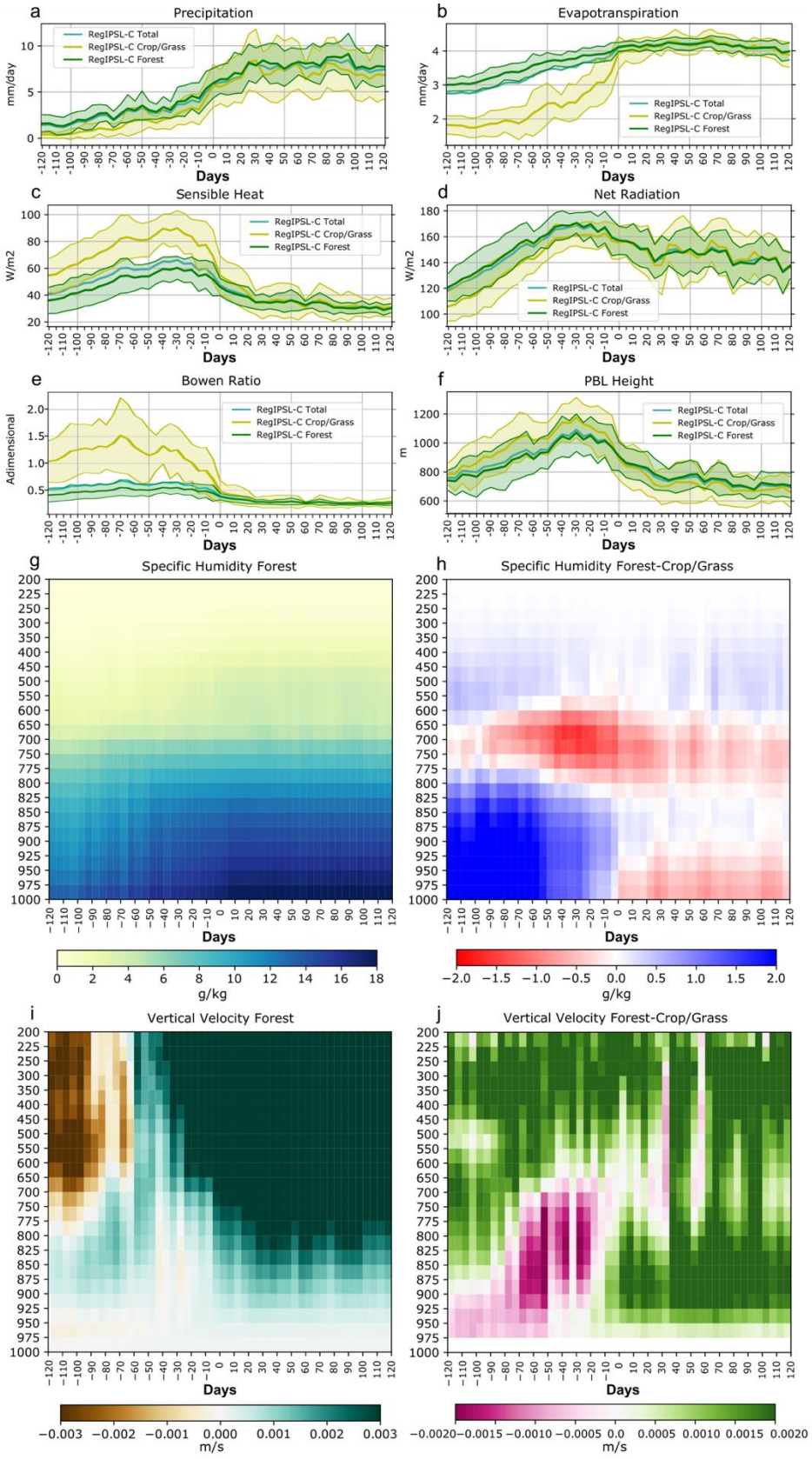

Fig. 3.7 Composite time series of: **a** precipitation (mm day^{-1}), **b** evapotranspiration (mm day^{-1}), **c** sensible heat flux (W m^{-2}), **d** net radiation (W m^{-2}), **e** Bowen ratio (adimensional), **f** Planetary Boundary Layer (PBL) height (m) over the total southern Amazon, forest and cropland areas (cyan, green and yellow lines, respectively) from RegIPSL-Control. Green and yellow envelopes represent the standard deviation for each land cover. Vertical cross-sections of: **g** specific humidity (g kg^{-1}) over forest areas

and **h** forest minus crop/grass specific humidity difference (g kg^{-1}), **i** vertical wind component over forest areas (m s^{-1}) and **j** forest minus crop/grass vertical wind component difference (m s^{-1}). The x-axis represents the time, with negative (positive) values for days before (after) the onset.

increased moisture removal linked to higher precipitation in forested areas, and by the vertical moisture advection from the surface to the mid-troposphere caused by the intensification of the vertical wind over crops (Figures 3.7i-j). However, horizontal moisture advection at these particular levels could also play a role in the forest-crop/grass atmospheric moisture difference.

A shallow ascending motion is simulated over croplands/grasslands by RegIPSL-Control between days -120 to -50 (Figures 3.7i-j). Weaker vertical upward wind is observed over forested areas but confined in the 900-700 hPa layer. This stronger surface ascending motion over croplands/grasslands seems to be related with the warming of the lower troposphere (Figures A4e-f), caused by higher sensible heat flux and the lower specific heat capacity of the drier air over these areas. A smaller Convective Inhibition Energy (CINE) over croplands/grasslands during the morning and noon also facilitates the air ascension (not shown). This enhanced ascending motion over croplands generates a higher mid-level cloudiness (between 440 hPa and 680 hPa) with respect to forest areas (Figure A.7). During the same period (days -120 to -50), it is also observed a strong subsidence above the 750 hPa linked to the dominant presence of the dry season CPs (Espinoza et al. 2021; Figures 3.6b and 3.7i). This large-scale circulation forcing inhibits the development of convective activity triggered by the local signal. Only until the day -50, the locally forced ascension can surpass the regional subsidence and generate deep convection, mainly over forest areas (Figures 3.7i-j). Although by this time, the vertical component of the wind is higher over croplands below the 700 hPa level, convection is stronger above this level over forested areas as a consequence of a higher Convective Available Potential Energy (CAPE) during the pre-onset period (not shown). Higher CAPE over forested areas is a consequence of a wetter atmosphere, which increases the equivalent potential temperature over the lower atmospheric levels and its vertical gradient (Figures A4g-h). Higher CAPE and conditional atmospheric instability have been observed over forest sites compared with pasture sites (Taylor and Ellis 2006; Wang et al. 2009). The development of convective systems depends not only on the

atmospheric instability, but also on trigger mechanisms allowing the release of the convective available potential energy (Adler et al. 2011). According to our results, we hypothesize that the thermally induced shallow ascending movement over croplands/grassland can be advected and propagated by the horizontal circulation toward forest neighboring areas, where it acts as a trigger mechanism for developing convection. A similar mechanism is described by Froidevaux et al. (2014) using an idealized cloud-resolving model. When the rainy season onset arrives (day 0), a reduction in the sensible heat flux over croplands/grasslands (Figure 3.7c) causes shallower PBL (Figure 3.7f), a descending air motion below 850 hPa (Figure 3.7j), and an increase in the specific humidity over the shallow troposphere (Figure 3.7h).

The land cover-differentiated analysis for the temporal evolution of meteorological variables along the development of the rainy season allow us to identify the following key messages: (i) the temporal variability is similar for croplands/grasslands and forest surfaces for all the analyzed variables and is controlled by regional-scale phenomena; (ii) the forest and crop/grass local scale response to the synoptic forcing is different in terms of the magnitude of the variables only before the onset of the rainy season. Therefore, land surface heterogeneities can have a stronger impact on the local circulation during the pre-onset period; (iii) with the rainy season onset, the establishment of wet season atmospheric regimes bring rainfall to the whole Amazon basin, which helps to eliminate the local differences associated to land-surface heterogeneities, and generates similar behavior between forests and croplands/grasslands for all the analyzed variables. For this reason, in the following sections we assess the impacts of Amazonian deforestation with an especial focus on the changes of circulation patterns and surface conditions before the onset of the wet season.

3.2.4 Deforestation impacts on the dry-to-wet transition season

In this subsection, we analyze the deforestation-induced changes in precipitation, evapotranspiration and low-level wind circulation of the CPs and the consequences of these disturbances on the development and onset of the rainy season. Finally, we determine the individual effect of changes in frequency and characteristic rainfall of

the CPs caused by deforestation for the total rainfall accumulated in the 120-day period prior to the onset.

3.2.4.1 Rainfall and surface fluxes seasonal cycles over the southern Amazon

The loss of tropical forest causes important changes in evapotranspiration and surface energy fluxes, while only little rainfall alterations are simulated over southern Amazonia (Figure 3.2). Although not significant, rainfall slightly increases between October and November in the deforested experiment (red line in Figure 3.2a). However, deforestation induces significant reductions in evapotranspiration and latent heat fluxes (red line in Figure 3.2d-h) of about ~-5 to -6% during the dry season in consistency with flux tower measurements, satellite and meteorological reanalysis estimates (von Randow et al. 2004; Khand et al. 2017; Baker and Spracklen 2019; Oliveira et al. 2019; Laipelt et al. 2020) and climate models (Nobre et al. 1991; Polcher and Laval 1994; Sud et al. 1996; Lean and Rowntree 1997; Perugini et al. 2017; Eiras-Barca et al. 2020). On the contrary, the sensible heat flux is slightly increased in the deforested scenario in the dry-to-wet transition in agreement with observations (Figure 3.2g; Gash et al. 1996; von Randow et al. 2004; Garcia-Carreras et al. 2010). Otherwise, important and significant changes in the reflected solar radiation are induced by the forest loss. Due to the higher cropland albedo, a general increase in the reflected solar radiation (~+2 W m^{-2} or +5.7%) occurs throughout the year in RegIPSL-Deforested (red line in Figure 3.2d) in agreement with measurements from the Anglo-Brazilian Amazonian Climate Observation Study (ABRACOS) project (Berbet and Costa 2003; von Randow et al. 2004). This energy loss, in conjunction with less incoming longwave radiation (-0.8 W m^{-2} or -0.17%) due to a drier atmosphere (Figures 3.2e-f; Eltahir 1996; Claussen et al. 2001), leads to a reduction in the net surface radiation of ~ -3 W m^{-2} (-2.5%) during the dry-to-wet transition season (Figure 3.2i). Reductions in the net surface radiation have been reported over cleared areas in the Amazon (Bastable et al. 1993).

3.2.4.2 CPs and associated regional composites

Figure 3.8 shows simulated changes in evapotranspiration for the different atmospheric states or CPs. Similarly, Figure 3.9 displays deforestation-induced changes in rainfall and 850 hPa horizontal wind for each CP. At the same time, we use the Taylor diagram for assessing the changes in the spatial patterns of rainfall and horizontal winds for each circulation pattern (Figure A5). In this case, instead of comparing a reference or 'observed' field with a modeled field as usual, we use the RegIPSL-Control as a reference dataset and evaluate the similarity with the CP spatial distributions in the deforested experiment (RegIPSL-Deforested).

In agreement with our previous results (section 3.2.4.1), evapotranspiration decreases over the deforested area mainly in dry and transition regimes (CPs D1, D2, D3, T1 and $T2_{DW}$), driven by reductions in the net surface radiation added to the effect of crop shorter roots (not shown). During these CPs, local weak changes in 850 hPa winds are also registered over the cleared area (Figures 3.9 and A6). D1, D2, D3 and T1 exhibit a wind acceleration over the deforested patch associated with a reduced surface roughness length. The stronger winds enhance the surface humidity transport toward central and southwestern Amazon and increase moisture convergence and precipitation in T1 and small patches of $T2_{DW}$ (Figures 3.7 and A6). Similar changes in moisture convergence for Amazon deforestation scenarios have been reported in modeling studies (Lean and Rowntree 1997; Eiras-Barca et al. 2020). The slight significant rainfall increases in T1 and $T2_{DW}$ explain the modest, but not significant, precipitation increment over the southern Amazon between October-November shown in previous subsections (see Figure 3.2a). On the contrary, a wind deceleration occurs in the deforestation scenario for $T2_{DW}$ over the deforested patch, which is related to a slight increase in moisture convergence (Figure A6). This is also observed by Ruiz-Vásquez et al. (2020), who identified a weaker southerly cross-equatorial flow during the dry and dry-to-wet transition seasons in association with deforestation over the Southern Amazon. It is important to remark that CP $T2_{DW}$ is an almost exclusive condition of the dry-to-wet transition season and is featured by the encounter of a northerly cross-equatorial flow with southerly wind incursions that generates low-level convergence and triggers precipitation in the southern Amazon and south eastern Brazil (Espinoza et al. 2021). However, a non-statistically significant weakening of the

southerly wind incursions below 10°S and between 70°W-50°W is observed with the rainforest loss. It is precisely in this area where cold fronts are frequent during the transition from dry to wet conditions (Machado et al. 2004). A weaker than usual extratropical cold front incursions are generally related to a delayed rainy season (Li et al. 2006). Compared with wet season CPs, dry season and transition regimes have almost zero rainfall and wind changes according to Figures 3.9 and A6. Minor changes in the regional-scale circulation during the dry season and the dry-to-wet transition period are expected due to the important role of the extratropical forcing in this time of the year (e.g. Jones and Simmonds 1993; Sinclair 1995; Espinoza et al. 2012). In addition, since our simulations are done with a regional climate model laterally forced by ERA5, the deforestation impacts on the atmospheric dynamics are limited to the modeling domain while any external forcing (such as the extratropical westerly Rossby waves) remains undisturbed (Sud et al. 1996; Gedney and Valdes 2000; Badger and Dirmeyer 2016).

During the wet season, the continental thermodynamics and the vegetation role are determinant to shape the regional-scale circulation (e.g. Gill 1980; Figueroa et al. 1995; Eltahir 1996; Gedney and Valdes 2000). Accordingly, deforestation generates profound alterations in the atmospheric circulation and rainfall during this season over the entire continent (Figure 3.9). It is in the wet season CPs when the differences in low-level circulation are highest. Thus, lower spatial correlations between RegIPSL-Control and RegIPSL-Deforested are observed for CPs W1-W2-W3 in Figures A5b-c. The first wet season circulation pattern W1 experiments a weakening of the characteristic circulation of the SACZ (see Table 3.3 and Figures 3.4). Southerly winds are diminished south of 10° S, which allows northerly winds to reach further south and decrease their eastward deviation over the southern Amazon. As a consequence, rainfall is reduced (increased) over the eastern (southern) part of the continent and over the southern Amazon (Figure 3.9). A weakened SACZ has been documented in tropical deforestation experiments by previous studies (Badger and Dirmeyer 2016). Similarly, there is a weakening of the northerly winds that feature the summer SALLJ in W2 (Figure 3.9). The weaker north-south moisture transport in the deforestation scenario prompts precipitation and moisture convergence increase (decrease) over northern (southern) tropical South America (Figure A6). As a component of the SAMS and the summer regional Hadley cell, a weakening of the SALLJ is consistent with

deforestation theoretical frameworks and with climate model experiments (Zhang et al. 1996; Eltahir 1996; Zeng and Neelin 1999; Badger and Dirmeyer 2016; Sierra et al. 2021). Finally, W3 displays an enhanced northerly and southerly winds, a stronger eastward deviation and moisture convergence, triggering more convection over southeastern Brazil (Figures 3.9 and A6). Changes in low-level winds for W3 are very similar to the normal conditions of W1 (Figures 3.4 and 3.9). In fact, we find that under the deforestation scenario, the days with W1 conditions tend to convert to CP W3 (not shown).

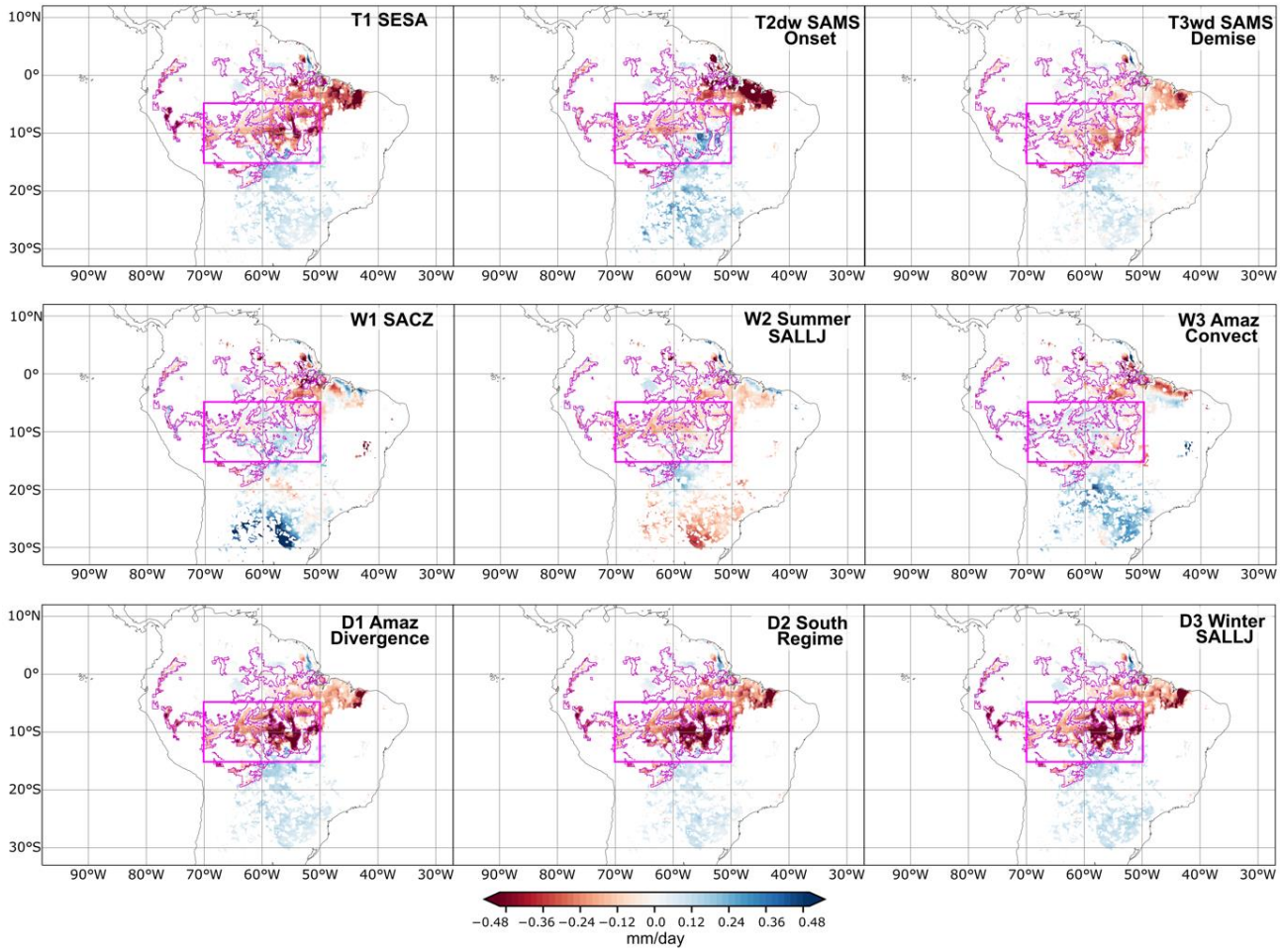

Fig. 3.8 Differences RegIPSL-Deforested minus RegIPSL-Control in evapotranspiration composites for the 9 circulation patterns (CPs) defined from the k-means clustering analysis. Differences are in mm day^{-1}. Only significant evapotranspiration differences are shown (t-test, $p<0.05$). Magenta box shows the southern Amazon domain (5°S-15°S, 70°W-50°W). The magenta line highlights the deforested area.

Alterations in the frequency of occurrence for the different CPs in the deforested experiment are shown in Figure 10. Each subpanel represents the annual cycle frequency for a specific atmospheric regime in RegIPSL-Control and RegIPSL-

Deforested (blue and red lines, respectively). In order to assess the statistical significance of the differences in CP frequencies between control and deforested experiments, we implement a bootstrap-like methodology. We split our complete time series for both experiments, using the selected day-to-day classification (see section 2.4), in 10-year running windows. For each time window we compute the frequency of occurrence of each CP in order to get the frequency variance in control and deforestation scenarios. Days with significant differences are highlighted with red dots (p-value <0.05, Figure 3.10).

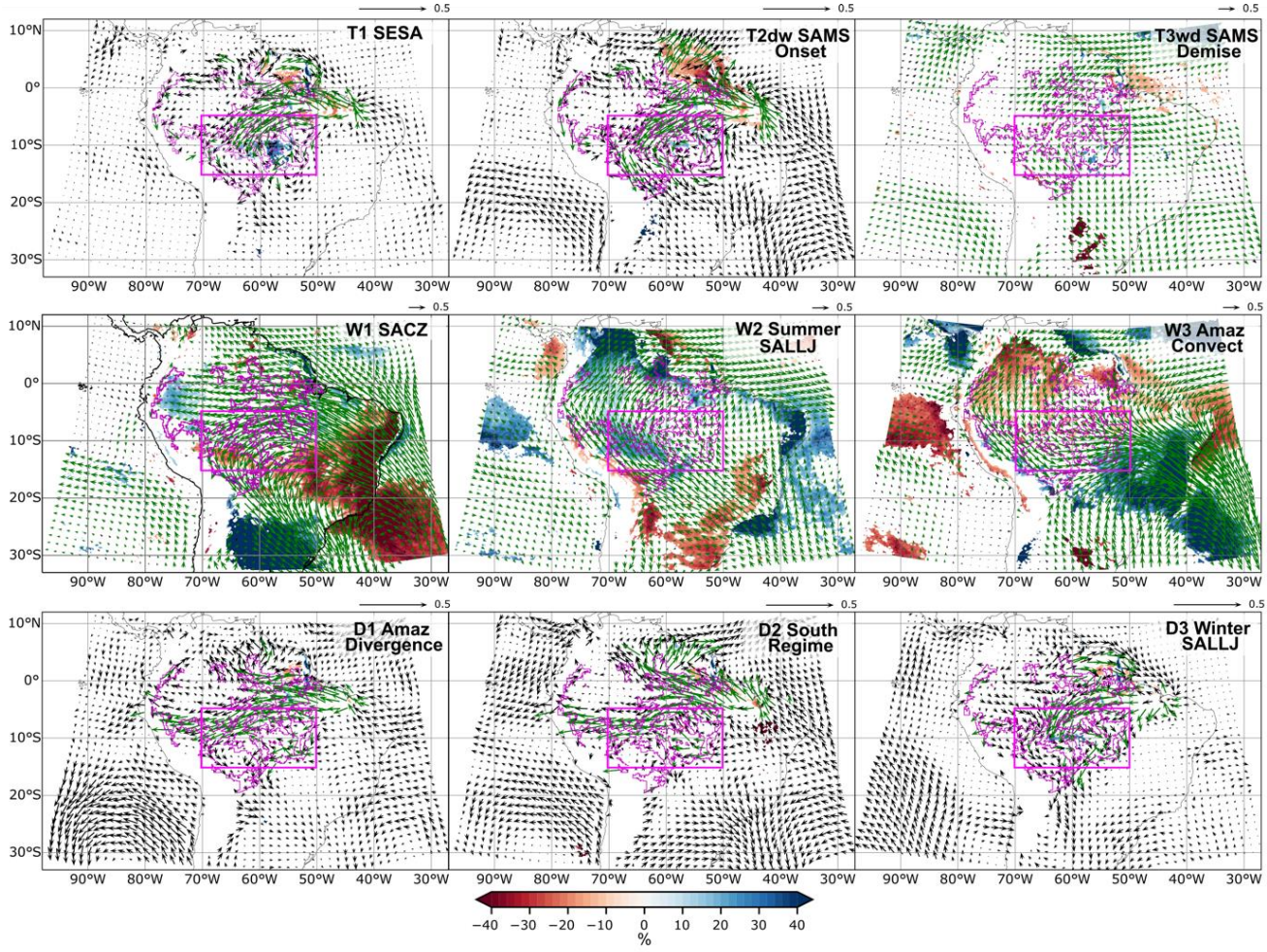

Fig. 3.9 Differences RegIPSL-Deforested minus RegIPSL-Control in 850 hPa horizontal winds and rainfall composites for the 9 circulation patterns (CPs) defined from the k-means clustering analysis. Rainfall differences (shaded) are in percentage respect to values in the control scenario. Horizontal winds at 850 hPa (vectors) are in m/s. Only significant rainfall differences are shown (t-test, p<0.05). Green vectors represent significant wind differences (t-test, p<0.05). Magenta box shows the southern Amazon domain (5°S-15°S, 70°W-50°W). The magenta line highlights the deforested area.

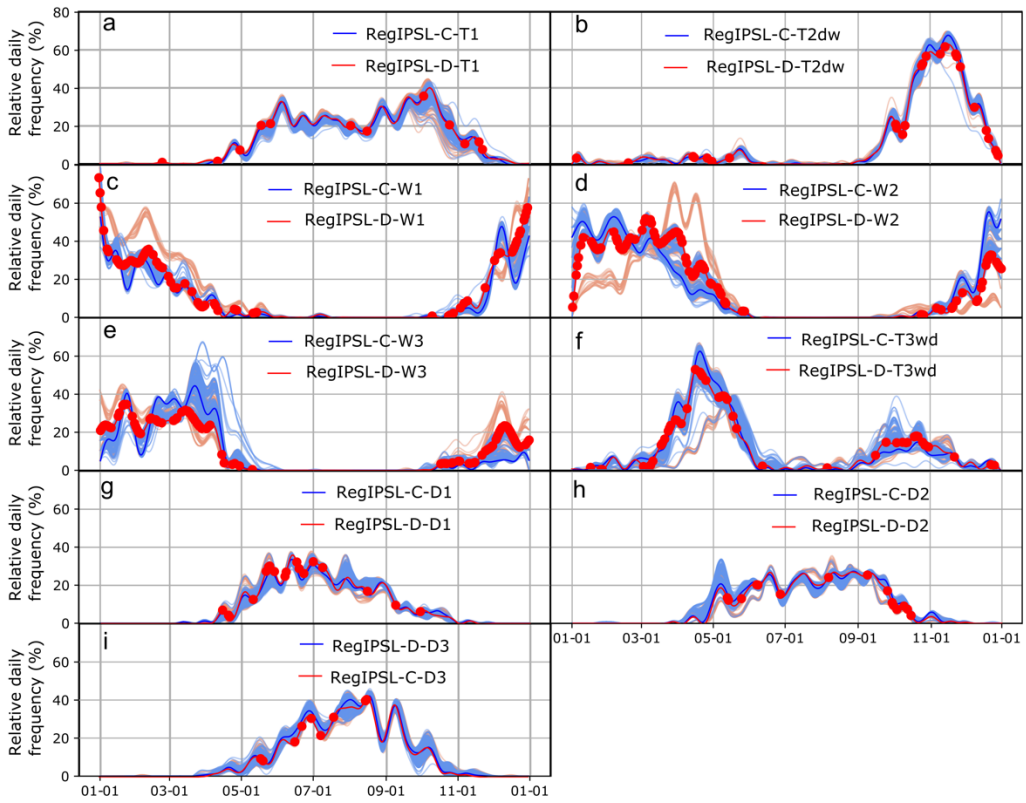

Fig. 3.10 Relative mean daily frequency of the 9 circulation patterns (CPs, a-i) defined from the k-means clustering analysis for RegIPSL-Control ('RegIPSL-C') and RegIPSL-Deforested ('RegIPSL-D'), blue and red lines, respectively. Light blue and red lines correspond to 1000 day-reclassifications with random cluster center initialization in control and deforested scenarios. Solid blue and red lines are the selected partitions for previous section analysis and correspond to a smart selection of initial centroids seeds for k-means. The horizontal axis represents the days from January 1st to December 31st in the climatology during the period 2001-2019. CP's annual cycles were smoothed using a temporal lowpass Butterworth filter retaining only frequencies lower than 1/30 cycles per day.

Consistent with our previous results discussed above, transitional CP T1 and dry season CPs D1-D2-D3 experience minor changes in frequency throughout the year with deforestation (Figures 10a and 3.10g-i). Nonetheless, during the dry-to-wet transition period (end of September and October) there is a reduction of -6% in the frequency of $T2_{DW}$ (Figure 3.10b). At the same time, $T3_{WD}$ increases its occurrence in the deforestation experiment by about +5% (Figure 3.10f). As we discussed before, the first atmospheric regime that appears during the wet season corresponds to the SACZ conditions (W1; Figure 3.10c). Deforestation induces a decrease in the frequency of W1 at the very beginning of the wet season (-17%) and an increase between December-February (+18%). The decrease in the activity of W1 during this month is linked to the increase in the frequency of W3, reflecting the W1-to-W3 switch discussed before. For the control run, the development of CP W1 is followed by the emergence of the SALLJ (CP W2), conforming the SACZ-SALLJ dipole. However,

forest loss alters the development of the SAMS and causes a delay in the W2 activity, with fewer events during November-February (between -10% to -20%, depending of the month) and more occurrences at the end of the wet season (March-April; +10% to +20% according to the month; Figure 10d). At the end of the rainy season, between March-April, W3 becomes less frequent and is replaced by W2 events. Similarly, as a consequence of the delayed activity of the SALLJ (W2), $T3_{WD}$ frequency is reduced during late April.

In summary, the changes in $T2_{DW}$, $T3_{WD}$, W1 and W2 points in the same direction: a later onset of the rainy season based on CPs under the deforested experiment. However, we did not find any change in the onset/end wet season dates using the rainfall-based criteria of Li and Fu (2004). A possible explanation for this is the dependence of this methodology on precipitation, and therefore on the convection parameterization. In agreement with our results, several modeling studies find a more frequent longer dry seasons with the Amazon forest removal (Costa and Pires 2010; Boisier et al. 2015; Nobre et al. 2016; Alves et al. 2017; Ruiz-Vásquez et al. 2020). Widespread deforestation generates a less heterogenous land cover over southern Amazonia, what can weaken the combined effect of warmer surface, reduced CINE and shallow ascending motion over croplands and the large CAPE available for exploiting these thermally driven vertical wind anomalies over forested areas, thus delaying the large-scale triggering of convection and the wet season onset.

3.2.4.3 Analysis of the isolated effect of the CP changes in frequency and characteristic rainfall

Precipitation during the dry-to-wet transition period is crucial for increasing the evapotranspiration, the atmospheric moisture and for triggering shallow convection during the early stages of the rainy season onset (see section 3.2.3.4; Wright et al. 2017). Deforestation can alter the rainfall and evapotranspiration during the pre-onset period, and, therefore, impact the whole development of the wet season (Li and Fu 2004). In the previous section we analyze the changes induced by the forest loss in the mean rainfall amount or characteristic rainfall of each circulation pattern, as well as changes on its frequency of occurrence separately. To complement these analyses, the question addressed in this subsection is how these alterations act together to

impact the pre-onset rainfall. Therefore, we estimate the relative importance of the changes in CP frequency versus alterations in CP characteristic rainfall induced by deforestation for the total accumulated pre-onset rainfall. Here, the pre-onset period is defined as the 120 days preceding the rainy season onset.

The accumulated rainfall at grid-cell j between the day -120 and the onset (day 0) P_j can be estimated through a decomposition of the characteristic rainfall $p_{j,k}$ associated to each k circulation pattern at location j, multiplied by its frequency of occurrence of during the day i, denoted as $n_{i,k}$, according to Equation 3.2.

$$P_j = \sum_{k=1}^{9} \sum_{i=-120}^{0} p_{j,k} n_{i,k} \qquad (3.2)$$

With this approximation, we assume that all the days with atmospheric conditions corresponding to each CP k will have the same associated rainfall, which corresponds to the CP's rainfall composite mean. A similar approach has been previously used for analyzing rainfall variability over different regions (Polcher 1995; Moron et al. 2008). In order to test our approximation, Figure 3.11 shows the comparison between the climatology of the accumulated precipitation during the pre-onset period in RegIPSL-Control, and the total rainfall estimation using Equation 3.2, labeled as 'reconstruction' (Figures 3.11a and 3.11b, respectively). The pre-onset period usually occurs between boreal summer and fall (July-September). For this reason, we observe high amounts of accumulated rainfall over northern South America and the Pacific and Atlantic Intertropical Convergence Zone (ITCZ; Figure 3.11a). The reconstruction of total rainfall is very close to the accumulated rainfall climatology in spatial structure and rainfall magnitude (Figure 3.11b). Precipitation is overestimated by the reconstruction over most of the area (Figure 3.11c). Rainfall distribution at daily time scale is usually skewed due to the presence of very frequent zero or non-rainfall values mainly during the dry and dry-to-wet seasons. However, Equation 3.2 uses the precipitation probability for each CP computed over the whole year. Therefore, the mean daily precipitation associated with each CP is influenced by precipitation during both rainy and dry seasons while our reconstruction is limited to a relatively dry period. Nevertheless, within our region of interest (southern Amazonia, magenta box in Figure

3.11c), the total rainfall overestimation is only about +70.25 mm (+22%) in the three-month period (Figure 3.11c). We also compute the reconstruction of the total pre-onset rainfall for the deforestation experiment using the same methodology, in order to evaluate the changes caused by the forest-loss.

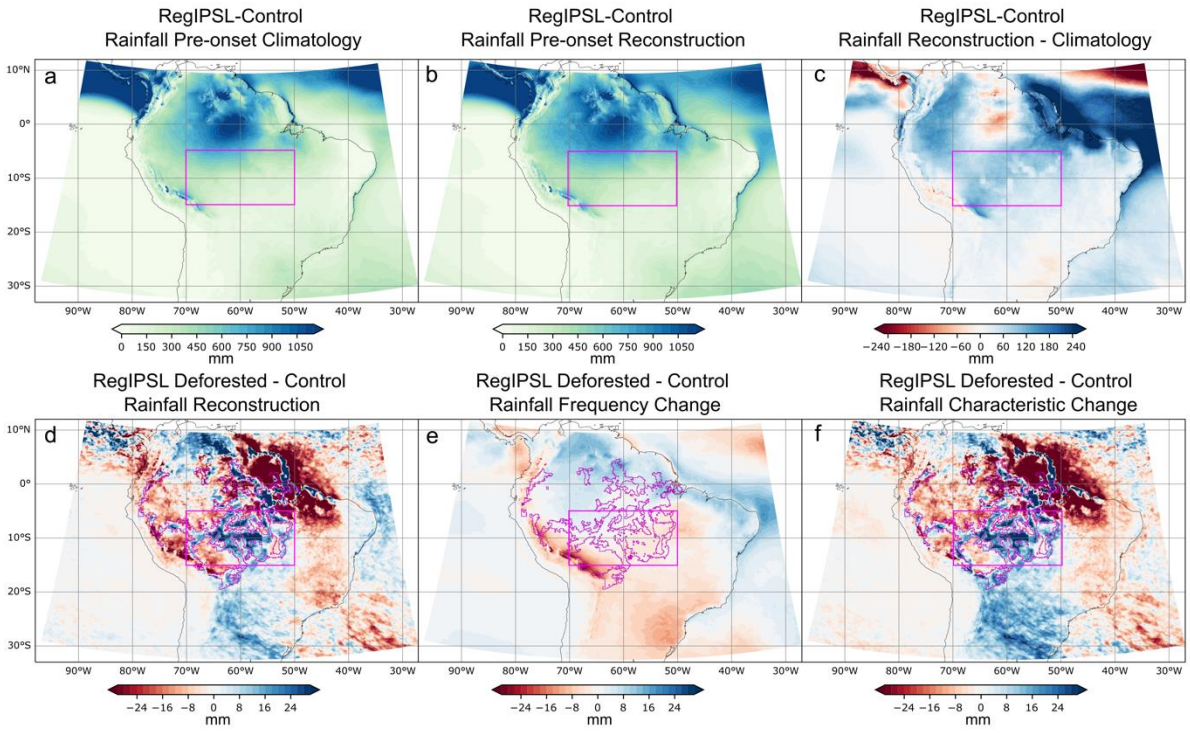

Fig. 3.11 Total accumulated rainfall for the pre-onset period (day -120 to day 0 or onset of the rainy season) for: **a** RegIPSL Control climatology and **b** rainfall reconstruction using Equation 2. **c** Differences in the total accumulated rainfall for the pre-onset period between RegIPSL-Control climatology minus RegIPSL reconstruction. **d** Differences in the total accumulated rainfall between reconstructions in the RegIPSL-Deforested minus RegIPSL-Control experiment. **e** Total accumulated rainfall changes induced by deforestation due to alterations in the frequency of the circulation patterns. **f** Total accumulated rainfall changes induced by deforestation due to alterations in the characteristic rainfall of the circulation patterns. Magenta box shows the southern Amazon domain (5°S-15°S, 70°W-50°W). The magenta line highlights the deforested area. All subplots are in mm.

Following Equation 3.2, we can analyze the deforestation-induced change in total accumulated pre-onset rainfall, as well as the individual effect of the changes in frequency and characteristic rainfall of the CPs. The change in the total pre-onset rainfall at grid-cell j between the deforestation and control experiments dP_j, can be divided in two different terms: (i) a first term representing the effect of changes only in the frequency of each circulation pattern k with deforestation during each day i in the pre-onset period ($dn_{i,k}$). The characteristic rainfall of CP k, $p_{j,k}$, remains unperturbed; (ii) a second term corresponding to the effect of changes in the characteristic rainfall

of each circulation pattern k, $dp_{j,k}$. This term uses the CP frequencies of occurrence of from the control experiment $n_{i,k}$ (Equation 3.3).

$$dP_i = \sum_{k=1}^{9} \sum_{i=-120}^{0} p_{j,k} dn_{i,k} + \sum_{k=1}^{9} \sum_{i=-120}^{0} n_{i,k} dp_{j,k} \qquad (3.3)$$

Figure 3.11d displays differences in the total pre-onset rainfall reconstructions between the deforested and control experiments. Deforestation increases rainfall over the northern part of the continent (Colombia and Venezuela), the southeastern South America (La Plata basin) and over the deforested areas of central and southern Amazon. On the other hand, rainfall decreases over the eastern flank of the Andes, the northeastern Atlantic coast, southeastern Brazil and over the surrounding areas of the deforested patches. Over the southern Amazon, rainfall increases on average by +2.98 mm. This rainfall increment is confined over the cleared areas (+12.17 mm), whereas over non-deforested areas rainfall decreases around -5.43 mm. This enhanced rainfall over deforested patches and its reduction over forested neighboring areas is a typical spatial structure of the observed local thermally-driven circulations induced by deforestation during the Amazonian dry season (Souza et al. 2000; Negri et al. 2004; Chagnon and Bras 2005; Wang et al. 2009).

Changes in the regional total pre-onset precipitation due to the alterations in the CPs frequency exhibit a very different spatial pattern. A latitudinal dipole with more (less) rainfall in the northern (southern) part of the continent is observed (Figure 3.11e). It is interesting to note that the local precipitation changes over the deforested patches observed in the differences between the total and the reconstructed pre-onset rainfall climatology are not explained by the alteration in the CPs frequency. Conversely, changes in the frequency of occurrence generate a regional-scale rainfall response. Precipitation reduction over the eastern flank of the Andes (Figure 11d) is almost completely explained by the alteration of CPs frequency. During the pre-onset period, the most frequent CPs are the dry season regimes D1-D2-D3 and transitional CPs T1 and $T2_{DW}$ (see section 3.2.3.3). However, deforestation affects mostly the frequency of CP $T2_{DW}$ (reduces its frequency in about -6%) while the rest of the weather regimes do not exhibit significant changes (see section 3.2.4.2). For this reason, the isolated

effect of CP frequency changes on the total pre-onset rainfall is very similar to a negative phase of the rainfall anomalies linked to the CP T2wd (see Figure 3.4). Under normal conditions, during this period of the year, the southern Amazon receives precipitation due to the activity of the CP $T2_{DW}$. Thus, it is expected that a reduction in the occurrence of $T2_{DW}$ generates a rainfall decrease of –2.48 mm over the southern Amazon. This rainfall reduction occurs over both deforested and non-deforested areas (-1.71 mm and -3.18 mm, respectively) as it is related to regional circulation changes.

Alterations in the CPs characteristic rainfall induced by deforestation dominate the total change in the accumulated pre-onset precipitation over most of the region (Figures 3.11d-f). The precipitation increase over the deforested areas and the decrease over the surroundings is fully explained by the changes in the CP's characteristic rainfall. In this way, the local effects of deforestation seem to influence the magnitude and spatial distribution of rainfall associated with each CP rather than its frequency. However, rainfall alterations over the SESA-SACZ region suggest that deforestation also generates a regional-scale effect outside the deforested area boundaries in the rainfall pattern linked with each CP. As our results were obtained using a regional climate model with imposed large-scale circulation at the boundaries of the spatial domain, the regional rainfall changes induced by alterations in the CP frequencies should be confirmed by using a global climate model which fully represents the non-local effects of the Amazonian forest loss (Zhang et al. 1996; Gedney and Valdes 2000). Conversely to the southern Amazon rainfall depletion linked to the changes in the CPs frequency, changes in the characteristic CPs rainfall cause a rainfall increase of +5.48 mm. This rainfall increase is observed over the deforested areas (+13.94 mm) as a local response to forest loss. At the same time, rainfall is decreased (-2.24 mm) over the neighboring non-cleared areas as a result of the development of mesoscale circulations supported by thermal contrast due to land surface heterogeneities (Souza et al. 2000; Wang et al. 2009; Wongchuig et al. 2022 submitted to Journal of Hydrology).

3.2.5 Summary and conclusions

Previous works suggest that tropical rainforest evapotranspiration is crucial moistening the lower troposphere, for triggering shallow convection and for initiating

the wet season onset (Li and Fu 2004; Wright et al. 2017). However, how deforestation can affect the initiation of the Amazon wet season is something that remains poorly understood. In this study, we assess the impacts of the Amazon forest-to-cropland conversion on the climatic conditions during the dry-to-wet transition period (August-September), as well as on the onset and development of the rainy season in the southern Amazon (5°S-15°S, 70°W-50°W). Using a weather typing approach, we decompose the atmospheric circulation variability in tropical South America in its dominant modes in order to analyze perturbations induced by deforestation in the evolution of the rainy season. To accomplish this, we use 19 years of simulations (2001-2019) with the regional climate model RegIPSL under two scenarios: (i) a control scenario and (ii) a deforestation scenario based on future projections of Amazonian forest loss developed by Soares-Filho et al. (2006).

The validation of the model is performed in three steps. First, the representation of the annual cycle in water and energy variables over the southern Amazon is evaluated. By comparing with satellite, in-situ measurements and reanalysis data, we find a well-represented seasonality of precipitation, evapotranspiration and surface energy fluxes by RegIPSL-Control. Using ERA5 horizontal winds at 850 hPa, the atmospheric low-level circulation variability is decomposed in 9 regimes that correspond to recurrent atmospheric states or circulation patterns (CPs). As previous works, we identify three dry season (D1-D2-D3), three wet season (W1-W2-W3) and three transitional (T1-$T2_{DW}$-$T3_{WD}$) regimes (Espinoza et al. 2021). Therefore, in the second validation step we assess the model's skill to properly represent the spatial structure and the relative frequency of each CP along the year. A direct comparison with ERA5/CHIRPS wind and rainfall anomalies shows that RegIPSL-Control reproduces broadly the main atmospheric circulations and its seasonality. Finally, we complement the validation analyzing the evolution in the atmospheric and surface conditions during the preceding and subsequent days of the wet season onset. Despite small differences, RegIPSL-Control is able to represent a realistic time evolution of the atmospheric circulation, rainfall and evapotranspiration in the preceding and subsequent days of the wet season onset, what enables the use of this model for exploring deforestation changes in the evolution of the dry-to-wet transition.

The southern Amazon is a region with land cover heterogeneity (mainly forest and cropland/grassland). Different vegetation types can play a distinct role in the development of the wet season onset. Thus, we use outputs from the control experiment to analyze the differential behavior of forest and croplands/grasslands along the preceding and subsequent days of the rainy season onset. The temporal evolution of surface and atmospheric variables is similar over crop/grass and forest areas and is controlled by large-scale phenomena. Nevertheless, the magnitude of the forest and croplands/grasslands response to the synoptic forcing is different before the onset of the rainy season. Less rainfall is simulated by RegIPSL-Control over croplands/grasslands until wet season CPs W1-W2 begin to occur. Although the forest areas exhibit higher evapotranspiration rates during the pre-onset period, crops respond rapidly to the first rainy events before the wet season onset, and by the onset date, crops and forest present similar evapotranspiration values. Due to the higher evapotranspiration rates, the atmospheric column above forest areas is moister and contain more convective available potential energy (CAPE) before the onset. However, crop/grass areas present a warmer low-level atmosphere as a consequence of higher sensible heat flux. Consequently, the lower troposphere is destabilized over croplands/grasslands developing a shallow ascending motion during the beginning of the wet-to-dry transition season. Crop/grass low-level ascending motion is suppressed by large-scale subsidence associated to dry season CPs until 50 days before the onset. By this time, the locally forced ascension overcomes the regional subsidence and generates deep convection in the region, mainly over rainforest areas, where the atmosphere presents higher potential for triggering convection. Finally, with the wet season onset, the different response of forest and croplands/grasslands to the synoptic forcing vanishes, and both vegetation type behaves similarly to the regional atmospheric conditions.

With respect to our analysis on the impact of deforestation over the southern Amazon, deforestation increases the reflected solar radiation, and decreases net surface radiation, evapotranspiration and latent heat flux during the dry and dry-to-wet seasons. Dry season atmospheric regimes D1-D2-D3 suffer very local changes in circulation, with a wind acceleration over the deforested areas linked to a reduction in the surface length. Additionally, deforestation does not affect the frequency of occurrence of dry season atmospheric regimes D1-D2-D3 or the transitional circulation

pattern T1. It is only by the end of the pre-onset period, when important changes in circulation and frequency of occurrence begin to be important. The CP $T2_{DW}$, which characterizes the atmospheric conditions during the onset of the rainy season over the southern Amazonia, decreases its frequency of occurrence in about -6% with deforestation suggesting a delayed wet season onset. Changes in the atmospheric circulation patterns linked to the SACZ and the SALLJ reinforce the idea of a deforestation-induced dry season lengthening in agreement with previous studies (Costa and Pires 2010; Boisier et al. 2015; Nobre et al. 2016; Alves et al. 2017; Ruiz-Vásquez et al. 2020; Douville et al. 2021). Additionally, the austral summer SALLJ experiments a weakening of the northerly winds that transport moisture toward southern South America in the deforestation scenario, which increases (decreases) precipitation in the northern (southern) part of the continent.

Finally, during the 120 days preceding the rainy season onset (pre-onset period), deforestation induces a rainfall increase over the northern and southeastern parts of the South American continent, as well as over the deforested patches of the central and southern Amazon (+12.17 mm). At the same time, precipitation is decreased over the eastern flank of the Andes, the northeastern Atlantic coast, and over the forested areas in the vicinity of the deforested patches (-5.43 mm). Through a decomposition of the individual attribution of changes in frequency and changes in the CP characteristic associated rainfall, we identify two opposite effects on the accumulated pre-onset rainfall: (i) a more regional deforestation-induced change linked to a rainfall decrease (increase) over the southern (northern) part of the continent and the eastern flank of the Andes. This change is caused solely by changes in the frequency of the CPs, mainly by the reduced occurrence of the T2dw; (ii) a combination of local and regional rainfall responses. The local signal explains the precipitation increase (decrease) over the deforested areas (the surroundings of the deforested areas), while the regional part is related with the rainfall rise over the southeastern South America.

Based on a weather typing approach, and therefore on the representation of the atmospheric circulation from daily to inter-decadal timescales, our results strengthen the link between the deforestation and the lengthening of the dry season over the southern Amazonia. At the same time, these results show how the impacts of deforestation are not limited to the wet season onset and affect the main features of

circulation patterns during the wet season. In fact, we conclude that the land-atmosphere interactions show differentiated changes through the year. Local alterations near the land surface dominate during the dry and dry-to-wet transition seasons, while regional-scale changes in the atmospheric circulation and precipitation are observed during the wet season. However, the physical mechanisms behind the changes in the frequency and spatial structure of wet season circulation patterns remain unexplored in the present work. As far as we know, this is the first time in analyzing the effect of deforestation on the evolution of the rainy season at intra-seasonal timescales instead of looking for seasonal changes. Understanding the progress of deforestation perturbations on the regional atmospheric circulation is crucial in order to better comprehend the forest role on the climate system at different timescales.

4

The effects of Amazonian forest loss on the wet season over the Amazon-Andes transition region

Contents

4.1 Introduction

In the previous chapter we explore the impacts of Amazonian deforestation on the principal atmospheric phenomena acting from daily to decadal timescales. In agreement with several previous works (e.g. Badger and Dirmeyer 2015; Alves et al. 2017), we find major changes in the regional circulation and rainfall during the austral summer (December-February). Precipitation during these months is important because it constitutes nearly 75% of the total annual rainfall over the south tropical Andes (Garreaud et al. 2003; Vuille and Keimig 2004) and around 50% over the southern Amazon (Espinoza et al. 2009b), it has a direct effect in snow accumulation in the mass balance of Peruvian and Bolivian glaciers (Sicart et al. 2005; Vuille et al. 2008; Rabatel et al. 2013), it feeds Amazonian groundwater reservoirs that allows rainforest evapotranspiration during dry months (Miguez-Macho and Fan 2012b). Therefore, in the present chapter we assess the possible impacts accompanying the Amazon forest loss on the hydro-climatology of the Amazon-Andes transition region (defined as the southwestern Amazon and the eastern flank of the Andes). This is an important and little explored question taking into account that over this particular region are located the rainfall and biodiversity hotspots, where precipitation recycling is the highest, and where most of the sediments that fertilizes the Amazon lowlands are produced (Chapters 1 and 2). The analysis performed on this chapter has been published in a scientific article entitled **'Deforestation impacts on Amazon-Andes hydroclimatic connectivity'** in the journal Climate Dynamics.

4.2 Deforestation impacts on Amazon-Andes hydroclimatic connectivity

Juan P. Sierra, Clementine Junquas, Jhan C. Espinoza, Hans Segura, Thomas Condom, Marcos Andrade, Jorge Molina-Carpio, Laura Ticona, Valeria Mardoñez, Luis Blaccutt, Jan Polcher, Antoine Rabatel, Jean Emmanuel Sicart

Article published in the journal Climate Dynamics on the 21th of October 2021

4.2.1 Introduction

The Amazon is the largest tropical rainforest in the world. It exchanges water, energy, and carbon with the atmosphere and is considered as an essential dynamic component of the climate system (Bonan 2008; Malhi et al. 2008). The Amazon ecosystem has been recognized as one of the major sources of evapotranspiration (Fisher et al. 2011), releasing large amounts of water vapor to the atmosphere and sustaining rainfall not only in the Amazon itself, but also in remote regions of the South American continent (Eltahir and Bras 1994; Van Der Ent et al. 2010; Martinez and Dominguez 2014; Zemp et al. 2014). In addition, the latent heat release linked to moisture recycling over the Amazon basin engines global and regional atmospheric circulation (Gill 1980; Eltahir 1996; Gedney and Valdes 2000). Therefore, understanding the impacts of continued deforestation on the regional and global hydroclimate has become an urgent and extensively explored scientific question.

The Amazonian forest has been intensively cleared since the 1970's (Fearnside 1993; Nepstad et al. 2009). After a slowdown of deforestation rates during the period 2004–2012, the small-scale forest loss rates increased again over the last decade (Kalamandeen et al. 2018; Eiras-Barca et al. 2020). Deforestation, as every effect of human activities on the climate system, disturbs the Earth's radiation budget and can be an important forcing for climate change (Hartmann et al. 2013; Mahowald et al. 2017). Indeed, when the rainforest is replaced by cropland or grassland, the energy balance is disturbed by: (i) a reduction in surface roughness and actual evapotranspiration, decreasing the surface energy loss from turbulent heat removal and latent heat flux (Gash and Nobre 1997; Lee et al. 2011; De Nob- let-Ducoudré et al. 2012); (ii) an increase in the incoming solar radiation at the surface linked to less clouds and less evapotranspiration rates (Salati and Vose 1984; Bala et al. 2007); (iii) a reduction in absorbed solar radiation due to an increased surface albedo (Berbet and Costa 2003; von Randow et al. 2004); and finally (iv) less incoming infrared radiation driven by drier air as a result of the reduced evapo- transpiration (Eltahir 1996; Claussen et al. 2001). In-situ measurements find a decrease in the surface net radiation over cleared areas (Bastable et al. 1993; von Randow et al. 2004). Although at the annual time scales an air temperature warming of the layer close to the surface follows the forest clearance (Gash and Nobre 1997), the reduction in the net surface

radiation generates a cooling of the upper atmosphere and a subsidence that weakens the regional circulation (Eltahir 1996). In this sense, perturbations that initially occur at the surface and within the lower part of the atmosphere modify the vertical transport of heat and moisture, altering convection and subsidence over extended regions and affecting large-scale features such as the Hadley and Walker cells (Zhang et al. 1996; Snyder 2010; Badger and Dirmeyer 2015).

Atmospheric circulation and Amazonian rainforest compound a coupled bio-geophysical balanced system. Perturbations in the vegetation state through deforestation can drive very different changes in atmospheric circulation depending on its spatial scale. Observations and theoretical works show small-scale deforestation (<10 km) triggering thermally driven land breeze resulting from differences in sensible heat fluxes between pastured and forested areas (Pielke 1984, 2001; Atkinson 1989; Wang et al. 1996; Souza et al. 2000; D'Almeida et al. 2007; Lawrence and Vandecar 2015). However, thermally driven circulations seem to be scale-dependent and can weaken as deforestation areas increase (Avissar and Schmidt 1998; Patton et al. 2005). At spatial scales larger than 100 km, land surface heterogeneities cannot produce enough surface gradient to sustain thermal circulation (Dalu and Pielke 1993). In fact, a recent study in Rondonia-Brazil demonstrates how when cleared areas grow, a shift occurs from a thermally convective regime towards a dynamically driven state where the roughness length reduction dominates and favors (inhibits) convection over areas in the downwind (upwind) direction of the deforested zone (Khanna et al. 2017). Since deforestation impacts on hydrological and atmospheric processes are complex and scale dependent, regional and global climate models stand out as useful tools to better understand the response of the climate system to land-use perturbations.

Numerical climate models have been extensively used for analyzing the impacts of deforestation over regional and global climate (Nobre et al. 2016 and references therein). Mesoscale models are able to represent the observed changes in circulation and clouds that follow small-scale deforestation (Chen and Avissar 1994; Wang et al. 2000; Saad et al. 2010). Furthermore, the thermal-to-dynamical shift regime caused by the rainforest loss reported over south-western Brazil is also reproduced by these models (Khanna et al. 2017). Under different deforestation scenarios, models project more frequent dry events and a lengthening of the Amazonian dry season (Nobre et

al. 1991; Costa and Pires 2010; Bagley et al. 2014; Alves et al. 2017; Ruiz-Vásquez et al. 2020). Although recent observational studies report similar changes in Amazonian dry season hydrology since 1979, the attribution of these alterations to deforestation is not straightforward and evidence suggest an additional influence of the tropical north Atlantic Ocean warming (Fu and Li 2004; Yoon and Zeng 2010; Butt et al. 2011; Marengo et al. 2011; Fu et al. 2013; Debortoli et al. 2017; Espinoza et al. 2019, 2021; Leite-Filho et al. 2020). It is important to remark that, taking into account the dependency of cli- mate response to the size of deforestation, the current spatial scale of Amazonian cleared area is not enough for predictions of extreme deforestation scenarios to be manifested or detected (D'Almeida et al. 2007; Nobre et al. 2016). On the other hand, under extensive deforestation scenarios climate models predict a reduction in precipitation recycling and rainfall in places downstream of the cleared areas caused by the shut off of forest transpiration (D'Almeida et al. 2007; Moore et al. 2007; Correia et al. 2008; Swann et al. 2015). At the same time, empirical estimates have found that south- western Amazon is particularly dependent on evapotranspiration from other parts of the basin (Zemp et al. 2017b; Staal et al. 2018). Hence, several simplified and regional climate models present a decrease in rainfall and moisture transport over this particular area (Sun and Barros 2015a; Boers et al. 2017; Zemp et al. 2017a; Ruiz-Vásquez et al. 2020). However, an opposite effect of intensified moisture transport towards south-western Amazon and south-eastern South America has been suggested by some modelling studies as the result of deforestation induced decreasing in surface roughness (Lean and Rowntree 1997; Eiras-Barca et al. 2020). These different responses to similar deforestation scenarios suggest the need to further assess the impacts of Amazon forest clearance over the regional climate.

In the Amazon-Andes transition region lies the rainiest and biologically richest area of the entire Amazon basin (Myers et al. 2000; Killeen et al. 2007; Hoorn et al. 2010; Espinoza et al. 2015). This region encompasses complex Andean topography, ranging between almost sea level in the Amazon lowlands to more than 6000 m a.s.l. over the Andean summits. This causes a strong orographic effect that interacts with regional atmospheric circulation to produce an exceptional spatial rainfall contrast (Chavez and Takahashi 2017; Junquas et al. 2018). There, high precipitation rates lead to large values of runoff per unit area (Moquet et al. 2011), providing most of the sediment load

to Amazon rivers (Vauchel et al. 2017; Armijos et al. 2020). Consequently, extreme hydrological events over this region can impact the whole basin downstream (Espinoza et al. 2014). Particularly, the Amazon-Andes transition region exhibits the largest precipitation recycling (portion of the precipitated water previously transpired by the Amazonian rainforest) of the Amazon catchment (Eltahir and Bras 1994; Dirmeyer and Brubaker 2007; Van Der Ent et al. 2010; Staal et al. 2018). Therefore, this region can potentially be highly sensitive to Amazon deforestation effects. Nevertheless, the surface- atmosphere coupling over this area has been poorly studied and most of the referent work has been focused over Brazilian Amazon or was based on coarse horizontal resolution modelling experiments insufficient to capture the required details of the topographical influence on local convection.

This study aims to better understand the deforestation effects on moisture transport and rainfall over the Amazon-Andes transition region during the heart of the wet season (December-January–February, DJF). During this season nearly 50% of total annual precipitation falls over the region (Espinoza et al. 2009). Since Amazonian groundwater recharge during wet periods can sustain forest transpiration rates during dry months (Miguez-Macho and Fan 2012), DJF alterations in rainfall patterns may have a profound impact in the watershed hydrology. The strong summer convection in the region is controlled by atmospheric processes that are part of the development of the South American Monsoon System (SAMS; Vera et al. 2006; see Sect. 3.1 for details) and which may be sensitive to impacts on surface energy/ water fluxes induced by land use change (Li and Fu 2004).

Taking into account the potential sensitivity of the Amazon-Andes transition region to deforestation and the need for high-resolution studies, the present work analyzes the deforestation land-use change impacts on regional energy and water budgets, as well as rainfall alterations at a local scale through the use of high-resolution simulations (up to 1 km horizontal grid size) with the regional climate model Weather Research and Forecasting Model (WRF). Model hourly outputs are compared with observational data from rain-gauges and satellites in order to elucidate the possible changes caused by Amazonian deforestation in the diurnal and nocturnal precipitation inside two typical Andean valleys during 2001–2011 austral summers. We describe the configuration of the model, the deforestation experiment and reference data used in Sect. 4.2.2. In

Sect. 4.2.3, we validate the model skill to reproduce the precipitation, general circulation and moisture transport at regional scale, as well as its ability to properly represent the deforestation signal in comparison with observations from the Large-Scale Bio- sphere–Atmosphere (LBA) project. The impacts of deforestation on moisture transport and rainfall at regional, meso and local scales are analyzed in Sect. 4.2.4. Finally, Sect. 4.2.5 summarizes and discusses the main results.

4.2.2 Data and methods

4.2.2.1 Model description

This study uses the regional climate model WRF version 4.1 (Skamarock et al. 2019). The model WRF was used in previous works to study the climatology of tropical South America and the Amazon basin (Bagley et al. 2014; Sun and Barros 2015b, a; Mourre et al. 2016; Junquas et al. 2018; Spera et al. 2018; Trachte 2018; Heredia et al. 2018; Yang and Dominguez 2019; Eiras-Barca et al. 2020; Saavedra et al. 2020). WRF is a non-hydrostatic model with terrain- following vertical levels (we use 49 vertical levels with higher level density near the surface). We employ three one- way nested modelling domains as shown in Fig. 4.1a. Table 4.1 summarizes the information of spatial and temporal resolution for each of the three domains used in this work. The first domain encompasses tropical South America and has a horizontal resolution of 15 km × 15 km with a time step of 90 s. The second and third domains have spatial resolutions of 5 km×5 km and 1 km×1 km, respectively and cover the south-western part of the basin. Time steps for these two domains are 30 s and 6 s, respectively. Domain 3 comprises the instrumented Andean valleys of Zongo and Huarinilla used for model validation (Fig. 4.1b). In order to analyze the diurnal and nocturnal atmospheric conditions we use an out- put time resolution of 3 h for domains 1 and 2, and 1 h for the finest domain.

Lateral boundary conditions from ERA5 reanalysis (Hersbach et al. 2020) are used. This reanalysis presents an enhanced horizontal resolution of 0.28° × 0.28° (31 km) with data available every 6 h (https://www.ecmwf.int/en/forecasts/datasets/reanalysis-datasets/era5). Significant improvements in the representation of several model

processes in this reanalysis are reflected in a better fit in winds, temperature and humidity in the troposphere compared against radiosonde data (Hersbach et al. 2020).

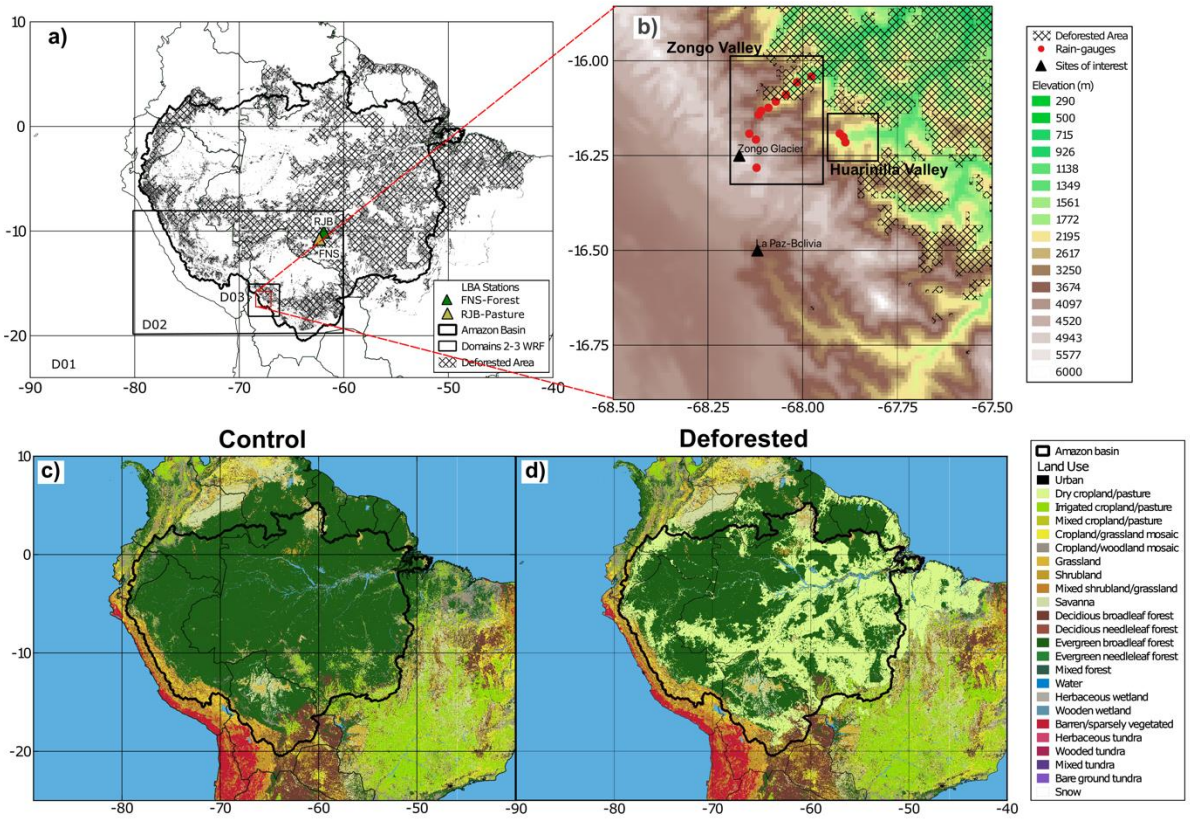

Fig. 4.1 **a** WRF simulation domains (black boxes labelled D01, D02, and D03 respectively), deforested area and locations of selected flux towers from the Large-Scale Biosphere–Atmosphere Experiment in the Amazon. Domains 1, 2 and 3 encompass the areas 24 °S–10 °N/90–40 °W, 20–8 °S/80–60 °W and 18–15 °S/69–66 °W respectively. Delineated area represents the boundary of the Amazon River basin (black). **b** D03 subregion (red square in a) and locations of rain-gauges stations over two Andean mountain valleys. Land-use category distributions for: **c** Control and **d** deforested scenarios.

Table 4.1 Characteristics of the domains used in WRF simulations

	WRF-D01	**WRF-D02**	**WRF-D03**
Horizontal resolution (km)	15	5	1
Domain	Tropical South America	South-western Amazon	Bolivian Andean valleys
Domain center coordinates	7° 30’ 00” S, 65° 00’ 00” W	13° 56’ 12” S, 70° 4’ 49” W	16° 35’ 49” S, 67° 38’ 56” W
Configuration	Regional simulation	One-way nesting	One-way nesting
Forcing	ERA5	WRF-D01	WRF-D02
Vertical resolution	49 hybrid vertical levels	49 hybrid vertical levels	49 hybrid vertical levels
Run time step (s)	90	30	6
Output time resolution (h)	3	1	1

Table 4.2 Physical parameterizations used in WRF simulations

	Parameterizations	**References**
Radiation	Longwave: rapid radiative transfer model (RRTM)	(Mlawer et al. 1997)
	Shortwave: Dudhia scheme	(Dudhia 1989)
Cumulus	Grell 3D	(Grell and Dévényi 2002)
Planetary boundary layer	Yonsei University scheme	(Hong et al. 2006)
Land surface	Noah land surface model	(Chen and Dudhia 2001)
Cloud microphysics	Lin scheme	(Lin et al. 1983)
Surface layer	MM5 similarity	(Paulson 1970)

Preliminary tests for different model configurations (not shown) allow selecting the parameterizations shown in Table 4.2. Summarizing, we use the Yonsei University scheme for representation of the boundary layer (Hong et al. 2006) with the wind topographic correction activated (Jiménez and Dudhia 2012). This wind correction takes into account the momentum sink term generated by the unresolved terrain at sub-grid scale in the model. It has shown improvements in the simulated wind field over complex terrains (Jiménez and Dudhia 2012) and has already been tested in the tropical Andes (Junquas et al. 2018). Lin's microphysics scheme is implemented (Lin et al. 1983) for phase change and precipitation. We also use Grell 3D parametrization for sub-grid scale convection over domains 1 and 2 (Grell and Dévényi 2002). Previous studies demonstrate convection parametrizations as one of the major uncertainties in the representation of rainfall diurnal cycle (Brockhaus et al. 2008; Hohenegger et al. 2008). Taking this into account and considering that a spatial resolution higher than 4 km is considered enough for non-hydrostatic models to explicitly solve convection (Weis- man et al. 1997; Ramos da Silva and Avissar 2006), we deactivate the cumulus parameterization over the finest domain. Additionally, we change the default WRF topography from the United States Geological Survey (USGS) to the Shuttle Radar Topography Mission (SRTM) product (Farr et al. 2007). This dataset presents a more realistic representation of the altitude of meteorological stations over the Peruvian Andes when compared with USGS and enhances the representation of rainfall and temperature in the same region with the model WRF (Saavedra et al. 2020). The SRTM dataset has a spatial resolution of 30 arc-second or approximately 1 km.

In order to obtain a climatological state of the south-western Amazon wet season, our simulations cover 10 years of austral summers for the time period 2001–2011. Each

simulation starts on November 1st and the first month is removed as a spin-up for the output analysis.

4.2.2.2 Description of the experiments

For each austral summer in the period 2001–2011, we con- duct two simulations with WRF sharing the same atmospheric lateral boundary conditions, but with different land- cover states. The control simulation ("Control" or "Con") corresponds to vegetation conditions for the year 2000 using the land cover map developed for South America by Eva et al. (2004) (Fig. 4.1c). This dataset was implemented in WRF by Saavedra et al. (2020) and exhibits a spatial resolution of 1 km × 1 km. For the deforested simulation ("Deforested" or "Def"), we use the deforested scenario 2050 business-as- usual from Soares-Filho et al. (2006; Fig. 4.1d). This scenario reaches 45% of forest lost and assumes the continuation of the 1997–2002 registered deforestation rates, no definition of new protected areas in the basin and the building of all planned highways (Soares-Filho et al. 2006). This scenario does not include the forest impoverishment through logging and fires. The implemented deforestation polygon is shown in Fig. 4.1a. Amazon deforestation involves the replacement of native forest by mixed crops (mainly soybean and corn), as well as pasture for cattle feeding. For this reason, within the deforested polygon natural vegetation (this includes all types of forest, shrublands, grasslands and savannas) grid points are replaced by cropland/grassland mosaics.

4.2.2.3 Data

In order to validate the model's ability to represent the rain- fall spatial distribution in the region, we use the product Tropical Rainfall Measuring Mission 3B42 (TRMM; https:// disc.gsfc.nasa.gov). This dataset, available from 1998, presents a 0.25° × 0.25° resolution and includes precipitation rates every 3 h (Huffman et al. 2007). However, previous studies have identified a strong rainfall underestimation by TRMM in the Amazon-Andes region (Espinoza et al. 2015; Zubieta et al. 2015; Chavez and Takahashi 2017). For this reason, we complement the model validation with daily information of 10 rain-gauge stations (Fig. 4.1b) from the Bolivian Electric Power Company (COBEE) and man- aged in collaboration with the Institute of Research for

the Development (IRD)—France. Additionally, three stations with hourly data were used from Schwabe et al. (2011). Table 4.3 presents the general information of each rain-gauge station according to official records of COBEE. We complement this information with location and altitude information of the stations from author's field campaigns (Table B1). The quality assessment of these rainfall stations was carried out by previous works (Molina-Carpio et al. 2019 and Laura Ticona, personal communication). The use of in-situ information also allows characterizing the model skill to capture the precipitation variability at small spatial scale in an Andean valley where local processes are important (Egger et al. 2005; Trachte et al. 2010; Junquas et al. 2018). Additionally, the representation of the regional atmospheric circulation and moisture transport are validated by a direct comparison between WRF outputs and ERA5 and NCEP- NCAR (Kalnay et al. 1996) data.

To test whether WRF responds realistically to the changes induced by land-use alterations, we use observations of energy surface fluxes, air temperature, precipitation and wind speed from the Large-Scale Biosphere–Atmosphere (LBA) project (Saleska et al. 2013). This dataset is avail- able at the website https://daac.ornl.gov/LBA/guides/ CD32_Brazil_Flux_Network.html. The LBA project was a large scientific effort carried out between 1996 and 2006 for assessing the influence of tropical forest conversion in carbon storage, nutrient dynamics and trace gas fluxes in the Amazon. Since the region of interest of this study is the Amazon-Andes transition region, we only use the closest stations from the LBA project that fits inside our second modelling domain (Fig. 4.1a). Because of their geographical location, these stations experience annual cycles of precipitation and temperature similar to the south-western Amazon variability. The first station, *Fazenda Nossa Senhora de Aparecida* (yellow triangle labeled as "FNS" in Fig. 4.1a), is a cattle ranch located at the center of a deforested area of about 50 km in radius cleared in 1977 for crop cultivation. The tower flux stands at 306 m a.s.l., 10.75° S, 62.35° W and presents daily data for the period 1999–2002. The second station corresponds to Rondonia Jaru Biological Reserve and is located at 191 m a.s.l., 10.08° S, 61.93° W (green triangle labeled as "RJB" in Fig. 4.1a). This is a natural reserve of the Brazilian Environmental Protection Agency covered by tropical dry forest with a mean tree height of 33 m that was established in the 1960s and expanded in 2006. The proximity of these stations (around 87 km) allows testing the impacts of land use change on

surface fluxes and the atmospheric bottom conditions. For validation we only use data for DJF 2001–2002 when WRF simulations and LBA data availability periods overlap in time.

Table 4.3 Name, geographic location, elevation, temporal range and annual rainfall of rain-gauge stations from the Bolivian Electric Power Company (COBEE) and Schawe et al. (2011). Annual and DJF rainfall means in the fifth column correspond to the period 2001-2011 except for the three last stations covering the period 2001-2002. Geographic location and elevation of rain-gauge stations recorded by author's field campaigns are shown in Supplementary material, Table B1

Name of station	**Location (latitude, longitude)**	**Elevation (m a.s.l.)**	**Temporal period (years)**	**Mean annual rainfall and standard deviation in mm/year (mean and standard deviation of DJF rainfall in mm/month)**
Plataforma	16° 16' 43.0" S, 68° 07' 24.0" W	4750	1971-2018	691 ± 221 (138 ± 23)
Tiquimani	16° 12' 27.1" S, 68° 07' 20.0" W	3900	1971-2018	918 ± 274 (196 ± 33)
Botijlaca	16° 11' 32.5" S, 68° 08' 26.0" W	3492	1971-2018	983 ± 128 (178 ± 35)
Cuticucho	16° 08' 34.5" S, 68° 06' 55.0" W	2697	1971-2018	2053 ± 180 (341 ± 50)
Santa Rosa	16° 07' 55.8" S, 68° 06' 29.5" W	2505	1971-2018	1748 ± 563 (317 ± 51)
Sainani	16° 07' 24.5" S, 68° 05' 21.5" W	2210	1971-2018	1975 ± 604 (358 ± 46)
Chururaqui	16° 06' 20.7" S, 68° 04' 05.5" W	1830	1971-2018	2086 ± 211 (334 ± 67)
Harca	16° 05' 20.2" S, 68° 02' 40.0" W	1480	1971-2018	2061 ± 678 (358 ± 73)
Cahua	16° 03' 21.6" S, 68° 00' 50.7" W	1195	1981-2018	2595 ± 394 (405 ± 76)
Huaji	16° 02' 28.4" S, 67° 58' 37.4" W	945	1999-2018	2676 ± 830 (454 ± 70)
Hornuni 1800	16.215° S, 67.887° W	1800	2001-2002	2310 (311)
Hornuni 2600	16.201° S, 67.892° W	2600	2001-2002	3970 (489)
Hornuni 3010	16.192° S, 67.902° W	3010	2001-2002	5150 (651)

4.2.2.4 Calculation of energy/water balances and atmospheric stability

The energy budget at the surface is described by Duveiller et al. (2018):

$$N_R = (S_{in} - S_{out}) + (L_{in} - L_{out}) = Sens_H + Lat_H + Gr_H \qquad (4.1)$$

Here, N_R corresponds to net radiation and is the summation of contributions from shortwave and longwave components: S_{in} is the incident shortwave or solar radiation, S_{out} is the reflected solar radiation, L_{in} is the incoming longwave component and L_{out} is the emitted longwave radiation flux. The net turbulent heat flux is later distributed in sensible heat flux ($Sens_H$), latent heat flux associated with evaporation from the surface (Lat_H) and molecular conduction flux from the ground (Gr_H). All the terms in Eq. (4.1) are in W m^{-2}. Land use change disturbances in the energy budget are assessed by computing the differences in DJF climatological means for each term of Eq. (4.1) between Deforested and Control scenarios.

The atmospheric water budget establishes how precipitation, evapotranspiration and net moisture transport entering/leaving an atmospheric column controls the temporal changes in the vertically integrated water content (Peixoto and Oort 1992). At seasonal timescales the temporal changes in atmospheric moisture are negligible and precipitation, evapotranspiration and column moisture convergence nearly balances each other (Brubaker et al. 1993; Li et al. 2013). Hence, the climatological changes induced by deforestation in the water balance can be expressed as follows:

$$\Delta\overline{P}_{Def-Con} = \Delta\overline{E}_{Def-Con} - \frac{1}{g}\Delta\overline{\nabla \cdot \int_{1000_{hPa}}^{200_{hPa}} q\,\vec{V}_H dp}_{Def-Con} \qquad (4.2)$$

In Eq. (4.2), P is precipitation, E is evapotranspiration, and $\nabla \cdot \int_{1000_{hPa}}^{200_{hPa}} q\,\vec{V}_H dp$ is the divergence field of vertically integrated moisture flux from 1000 hPa to 200 hPa. The bars denote climatological DJF means.

Finally, we evaluate the deforestation impacts on the atmospheric stability in tropical South America. Over the Amazon, the moistening of mid-tropospheric levels is associated with the development of deep convection in the region, which is related to the decreasing of atmospheric stability between middle and upper levels of the troposphere (Scala et al. 1990; Zhuang et al. 2017). For this reason, recent works use the difference of equivalent potential temperature (θ_e) between middle (500 hPa) and upper (200 hPa) troposphere ($\theta_{e_{200-500}}$) as an atmospheric stability index (Segura et

al. 2020). The equation of equivalent potential temperature can be written following Stull and Ahrens (2011):

$$\theta_e = \theta + \left(\frac{L_V \theta}{C_P T}\right) r \qquad (4.3)$$

where, θ corresponds to potential temperature, L_V is the latent heat of vaporization, C_P is the specific heat for air at constant pressure, T corresponds to the air absolute temperature and r is the air mixing ratio. The first term of this equation is related to dry adiabatic processes while the second one includes the effect of moisture in the net energy of an air parcel. Thus, the changes in the difference between mid and upper tropospheric equivalent potential temperature ($\theta_{e_{200-500}}$) allows separating the individual effects of dry and wet processes in the regional atmospheric stability. Again, climatological mean differences in each term of Eq. (4.3) between Deforested and Control scenarios allow evaluating the impact of deforestation in the regional atmospheric stability.

4.2.3 Model validation

4.2.3.1 Regional scale

The development of the SAMS establishes a northerly cross-equatorial flow (Wang and Fu 2002) and enhances convection over central Amazon (Vera et al. 2006; Fig. 4.2a, c). A cloudiness/rainfall band known as the South Atlantic Convergence Zone (SACZ) extends from southern Amazonia towards south-eastern Brazil and accompanies the mature phase of the SAMS (Kodama 1992; Figueroa et al. 1995; Zhou and Lau 1998; Fig. 4.2a). The diabatic heating released by the convective activity generates a large anticy- clonic circulation at the upper troposphere centered around 15 °S–65 °W known as the Bolivian High (Lenters and Cook 1997; Fig. 4.2e). Latent heat release over central Amazon also promotes a low-level continental-scale gyre that transports water vapor from the Atlantic Ocean inland towards Amazon and La Plata basins (Rodwell and Hoskins 2001; Vera et al. 2006; Fig. 4.2c). Over the eastern flank of the Andes, this circulation reaches its maximum wind velocities forming the South American Low-Level Jet (SALLJ). Over its trajectory, the transport of moisture through the SALLJ encounters the topographical barrier of the Andes triggering forced

convection in very localized places or rainy hotspots mainly in the Bolivian and Peruvian piedmonts (Espinoza Villar et al. 2009; Espinoza et al. 2015; Chavez and Takahashi 2017; Fig. 4.2a).

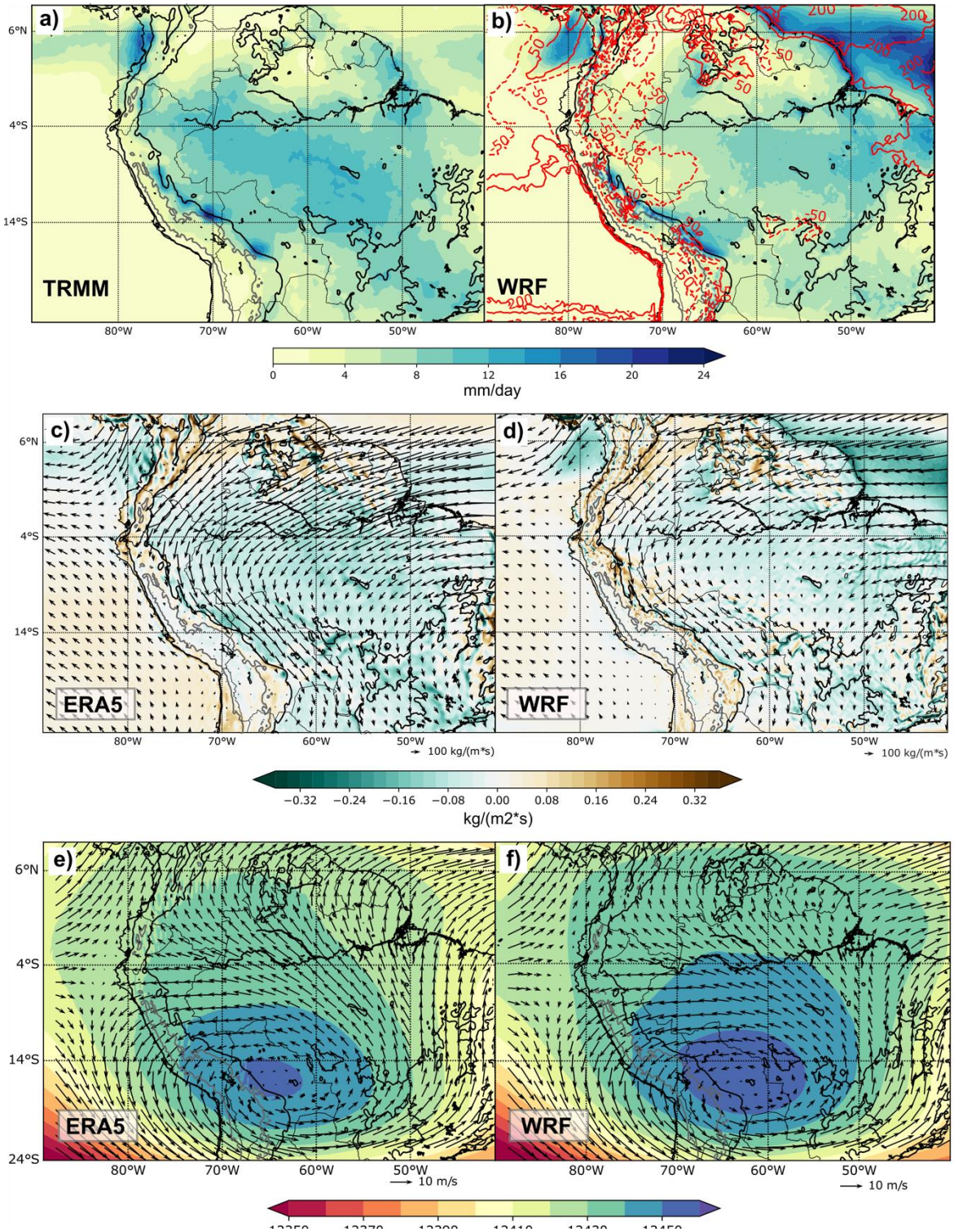

Fig. 4.2 DJF climatological means over the period 2001–2011 for: **a** and **b** precipitation from TRMM-3B42 (**a**) and WRF-Control (**b**) in mm/day. Red lines in **b** represent rainfall differences with respect to TRMM in percentage. **c** and **d** vertically integrated moisture flux (vectors, kg/m*s) and its divergence (shaded, kg/m2*s) from ERA5.

In general terms, the model is able to reproduce the main precipitation features during the austral summer (Fig. 4.2b). WRF-D01 represents the strong precipitation over central Amazon but with its maximum shifted eastward. The characteristic northwest-southeast rainfall band of the SACZ is present in WRF simulation. However, the model shows a considerable negative bias over the northern Peruvian low- lands (until −50% of dry bias when compared to TRMM; red contours in Fig. 4.2b). Rainfall Peruvian and Bolivian hotspots are also part of the model climatology. Nevertheless, WRF underestimates the former and overestimates the latter. The Atlantic ITCZ is strongly overestimated by WRF (up to +200% with respect to TRMM; red contours in Fig. 4.2b). This wet bias is related to a too strong vertically integrated moisture convergence in the model output (Fig. 4.2d). Finally, upper and lower atmospheric circulations are realistically represented by WRF (Fig. 4.2d, f). As in ERA5 outputs, WRF easterly low-level winds carry moisture from the Atlantic Ocean toward the continent (Fig. 4.2d). The moisture flow moves parallel to the Andes cordillera mechanically deviated exporting humidity toward southern latitudes both for ERA5 and WRF. At the altitude of 200 hPa, the model develops the anticyclonic circulation of the Bolivian High (Fig. 4.2f). Simi- lar features of vertically integrated moisture flux and upper level atmospheric circulation are found in NCEP-NCAR reanalysis (see Supplementary material, Fig. B1).

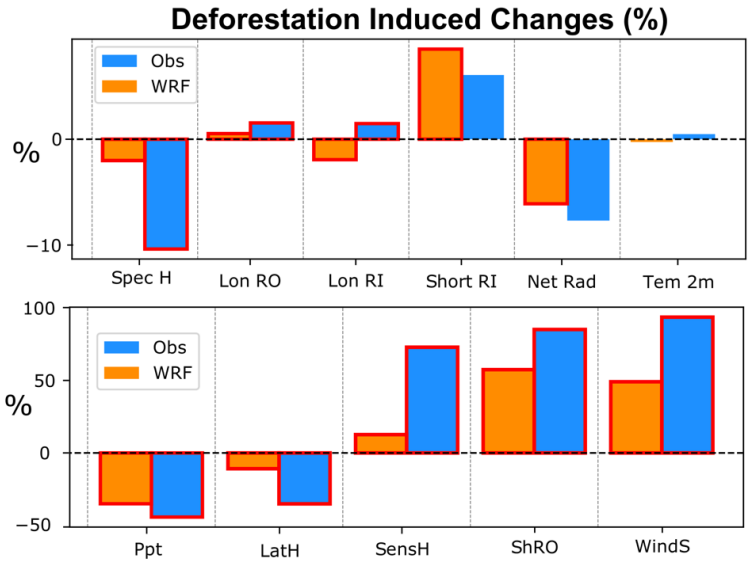

Fig. 4.3 Deforestation induced changes in surface atmospheric variables over LBA stations (blue bars) and WRF-D02 (orange bars) for DJF in the period 2001–2002. Significant differences are delineated in red (t-test, p<0.05). Abbreviations are as follows: Spec H-specific humidity at 2 m, Lon RO-longwave outgoing radiation, Lon RI-longwave incoming radiation, Short RO-shortwave outgoing radiation, Short

RI-shortwave incoming radiation, Net-Rad-net radiation, Tem2 2 m-air temperature at 2 m, LatH-latent heat flux, SensH-sensible heat flux, Ppt-precipitation, WindS—wind speed at 10 m.

4.2.3.2 Local scale

In order to validate if WRF reproduces the observed land use change impacts on surface fluxes and atmospheric variables at a local scale, we compare the selected LBA stations (Sect. 4.2.2.3) against the WRF-D02 Control simulation for DJF 2001–2002. We take the paired pasture/rainforest sites from the LBA project and compute the observed changes in surface variables in percentage respect to the forest values. Then, similarly, we take the coordinates of the LBA pasture and rainforest stations and extract information of atmospheric variables from model outputs in order to compute the percentage changes. For WRF outputs, we average variables of interest around each location inside a surrounding area of 15 km × 15 km (one grid-point-radius) but selecting only the grids corresponding to cropland/grassland or forest respectively and ignoring grid cells with a different land use category. Between a 15 km radius and a 50 km radius, no significant changes are found in the WRF deforestation response (not shown).

Figure 4.3 shows the simulated and observed (orange and blue bars, respectively) mean differences of surface variables due to deforestation. Significant differences are highlighted in red contour according to a t-test ($p< 0.05$). In general terms, WRF is able to properly represent the nature of most of the alterations in surface fluxes and atmospheric variables induced by the land use change. Land cover change is related to reduced precipitation by around −44% and −30% in observations and WRF, respectively. However, since precipitation is also related with non-local processes, it is difficult to establish a deforestation-rainfall causality relation. Consistently, significant reductions in surface specific humidity are observed but weakly simulated (around −11% and −1% in observations and WRF, respectively).

Accordingly, there is a significant decrease in latent heat flux for observations (−37%) with a weaker response by WRF (−14%). This implies that WRF underestimates the evapotranspiration response induced by deforestation. There is a significant increase in sensible heat flux and surface air temperature in LBA stations (68% and 1%, respectively). WRF strongly underestimates the sensible heat increase and even

slightly invert the temperature response to land use change (1.49% and −0.02% respectively). The effects of the increased sensible heat and temperature (only sensible heat in WRF) act to give an increase in the outgoing longwave radiation flux in LBA stations of 1.6% (0.7% in WRF). Since pastures and croplands are brighter than forest (Oguntoyinbo 1970; Bonan 2008), an increase in the albedo raises the out- going or reflected shortwave radiation by 86% for observations (Loarie et al. 2011). The albedo effect is overestimated by WRF, which presents an outgoing shortwave radiation pasture/forest difference of 104%. This overestimated energy loss can be related with the model underestimation of sensible heat flux increase. More incoming shortwave radiation reaches the surface in model and observations (4% and 7% respectively). This difference in WRF simulation is a consequence of cloud reduction over deforested areas (not shown). There is a disagreement between the modelled and observed changes in the incoming longwave radiation. While WRF exhibits a decrease in this variable (−1.64%), observations report an increase of about 1.38%. This difference is possibly explained by biases in the model representation of clouds or because of the drier WRF mid-upper tropo- sphere (not shown). At the end, driven by the incremented energy losses through longwave radiation fluxes and short- wave radiation reflection, there is a reduction in net radiation for WRF (−15%) and LBA stations (−8%). Finally, the enhanced surface wind speed at 2 m is a direct consequence of the deforestation induced roughness-length reduction in both model (53%) and observations (95%).

4.2.4 Results and discussion

This section is composed of two subsections, in the first part we evaluate the effects of deforestation in the energy and water balances, as well as the atmospheric stability at regional-scale (90°–60° W, 24° S–9° N). The second subsection is focused on the alterations in the hydro-climatology at meso and local scales, especially over the Amazon-Andes transition region and Andean valleys of Bolivia.

4.2.4.1 Regional changes in energy and water balances

Climatological alterations in the surface energy balance (Eq. 4.1) induced by deforestation are shown in Fig. 4.4, in which significant differences are highlighted with

black slashes. The last term in Eq. 4.1 corresponding to soil heat flux is omitted because it exhibits much smaller magnitudes with respect to the other terms (±1 W m^{-2}). Indeed, in situ measurements report low soil heat fluxes below tropical forest (Shuttleworth et al. 1984), but important values for crops (Oliver et al. 1987; Gash and Shuttleworth 1991).

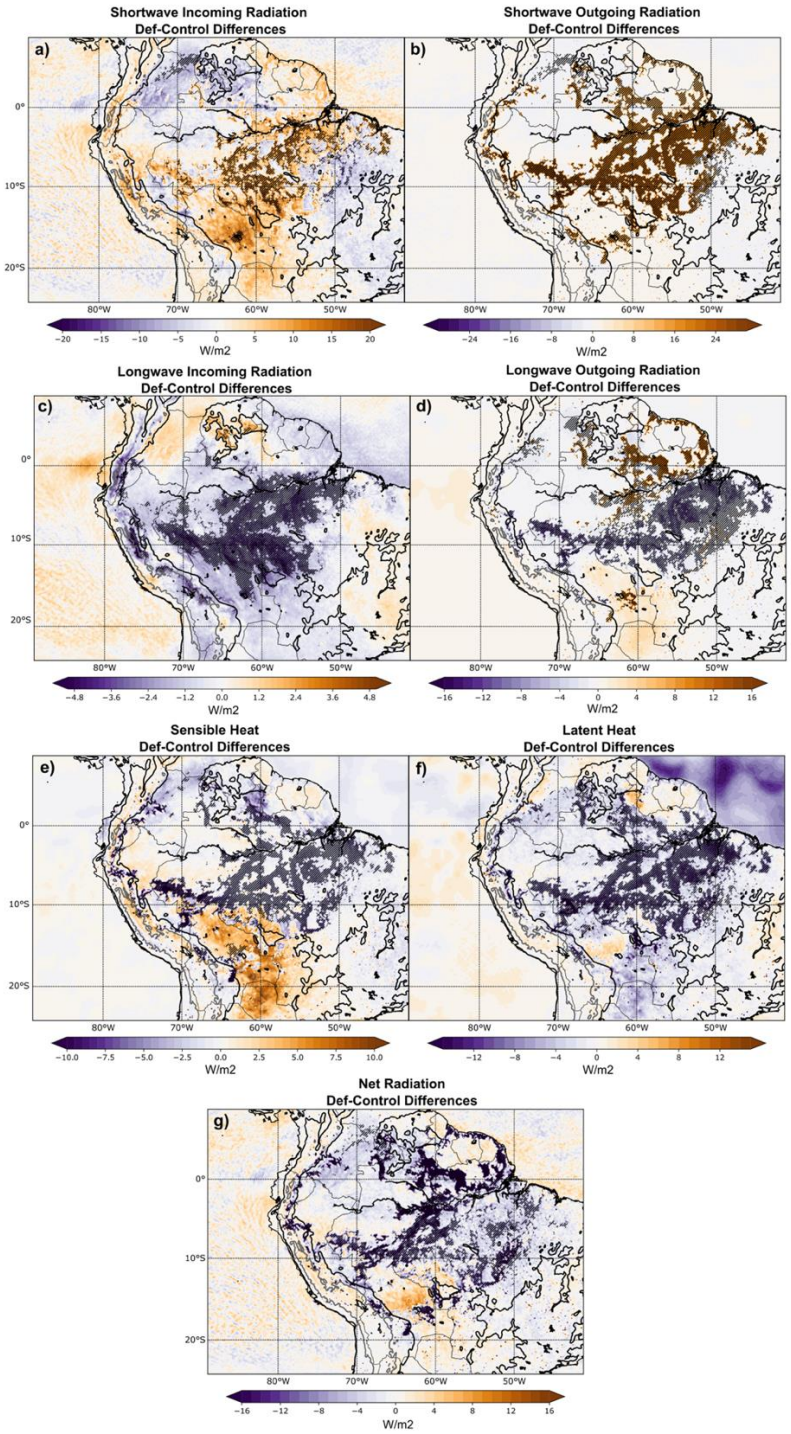

Fig. 4.4 *DJF seasonal climatological differences Deforested minus Control during 2001–2011 in surface energy balance variables:* ***a*** *Short-wave incoming radiation ($\Delta\overline{S_{in}}_{Def-Con}$).* ***b*** *Shortwave outgoing*

*radiation ($\Delta\overline{S_{out}}_{Def-Con}$). **c** Longwave incoming radiation ($\Delta\overline{L_{in}}_{Def-Con}$). **d** Longwave outgoing radiation ($\Delta\overline{L_{out}}_{Def-Con}$). **e** Sensible heat flux ($\Delta\overline{Sens_H}_{Def-Con}$). **f** Latent heat flux ($\Delta\overline{Lat_H}_{Def-Con}$). **g** Net radiation ($\Delta\overline{NR}_{Def-Con}$). All figures are in W m^{-2}. Significant changes (t-test, p< 0.05) are marked with black slashes. Orography elevation is shown at 500 and 3500 m a.s.l. as black and grey contours, respectively.*

Important changes in the incoming solar radiation are induced by the forest loss in the region (Fig. 4.4a). In general, more (less) incident solar radiation reaches the ground over places where reduction (rise) in precipitation and moisture convergence are located (see Fig. 4.5) such as in the central and south-western Amazon (north of South America and eastern Brazil). Hence, disturbances in incident solar radiation are closely linked with changes in clouds in WRF simulations as confirmed by analyzing top of the atmosphere (TOA) outgoing longwave flux and cloud water content (not shown). However, major changes in the energy balance occur in the outgoing shortwave radiation (Fig. 4.4b). A significant increase in about +20 W/m^{-2} occurs only over deforested areas which reflects the very local response induced by the higher cropland/grassland albedo. With a minor response, reductions in the longwave incoming radiation occur over most of the Amazonian watershed (Fig. 4.4c) as a result of a drier atmosphere and lower cloud cover in the deforested scenario (not shown). On the other hand, there is a meridional dipole in longwave outgoing radiation changes (Fig. 4.4d). Important disturbances in this variable take place mainly over deforested areas which implies the influence of very local processes. North of the Amazon river (<5°S) at the East of the basin, upward longwave radiation increases as a consequence of an increase in surface emissivity over this area (not shown). However, in the southern part of the basin, less outgoing longwave radiation is related to reductions in the air surface temperature. Sensible heat disturbances are linked to surface air temperature changes (not shown). Thereby, reductions (increments) in this turbulent flux are located over deforested areas (Fig. 4.4e) and are related to decreasing (increasing) surface temperature (not shown). Similarly, latent heat flux decreases over regions with evapotranspiration reductions (Figs. 4.4f, 4.5b). In the end, the enhanced energy loss through reflected shortwave radiation as well as the reduced incoming longwave radiation flux decrease the surface net radiation over the deforested and surrounding areas (Fig. 4.4g). This reduction in net radiation is very important for driving alterations in the regional moisture convergence as pointed out by Zeng and Neeling (1999). It is important to remark that the overestimation of the

albedo effect and the weaker model responses in sensible heat and longwave outgoing radiation fluxes, as well as roughness length and surface wind velocity (see Sect. 4.2.3.2) constrain our conclusions in the following sections.

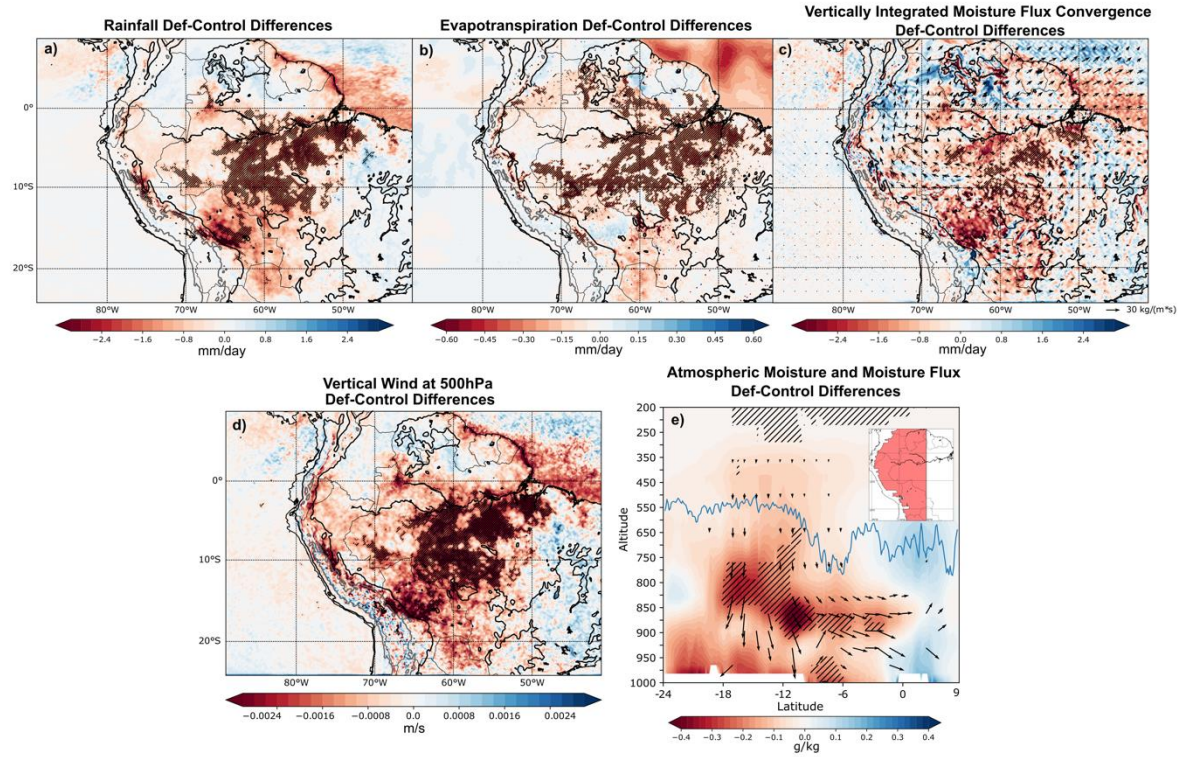

Fig. 4.5 DJF seasonal climatological differences Deforested minus Control during 2001-2011 in water balance variables: **a** Rainfall ($\Delta\overline{P}_{Def-Con}$). **b** Evapotranspiration ($\Delta\overline{E}_{Def-Con}$). **c** Vertically integrated moisture flux (vectors) and moisture flux convergence ($-\frac{1}{g}\Delta\nabla\cdot\overline{\int_{1000_{hPa}}^{200_{hPa}} q\,\vec{V}_H dp}_{Def-Con}$;shaded). **d** Vertical velocity at 500 hPa in m/s. **e** Meridional moisture (shaded, in g kg^{-1}) and moisture flux (vectors in g kg^{-1}*m s^{-1}) zonally averaged over the shaded region displayed at the upper right side. Only significant vectors are shown. Figures **a**-**c** are in mm day^{-1}. Significant changes (t-test, p<0.05) are marked with black slashes. Orography elevation is shown in **Figs. 4.5a**-**d** at 500 and 3500 m a.s.l. as black and grey contours, respectively. The blue line in **Fig. 4.5e** represents the Andes' profile calculated as the maximum topographic elevation inside the area displayed in red at the upper right side.

Figure 4.5 shows simulated changes in the water balance following Eq. (4.2). Significant reductions in the seasonal rainfall are found over central and south-western Amazon closely matching the deforestation area (Fig. 4.5a). To some extent, these precipitation changes are related to the local impact of the decreased evapotranspiration, especially over the center of Brazilian Amazon (Fig. 4.5b). Nevertheless, for analyzing the effect that evapotranspiration changes induced by deforestation have on rainfall, a quantification of precipitation recycling ratio should be assessed (e.g. Eiras-Barca et al. 2020). On the other hand, the drier conditions over

Bolivian Amazon are closely linked with changes in the regional atmospheric circulation, where increased moisture divergence is a response to deforestation (Fig. 4.5c). Here, the observed northwest-southeast (Fig. 4.2d) integrated moisture flux at the east of the Andes weakens in the deforested scenario (Fig. 4.5c). It is interesting to note that near the surface (10 m), an opposite change in the moisture flux enhances the water vapor transport toward the southern and eastern parts of the continent (not shown). This result suggests that in the western Amazon the changes in the vertically integrated moisture transport are not dominated by the surface conditions; instead, alterations in the integrated humidity trans- port are related to regional circulation changes such as the decrease in moisture convergence and vertical velocity over most of the Amazon (Fig. 4.5c, d), the rise in the atmospheric pressure at lower levels (not shown), and a weakening of the regional Hadley cell (Fig. 4.5e). These changes are in agreement with the theoretical frameworks laid out by Gill (1980) and Eltahir (1996), and with modelling studies (Zhang et al. 1996; Sun and Barros 2015a; Badger and Dirmeyer 2016). Opposite to the forcing in Gill (1980), Amazon deforestation induces a lack of diabatic heating as a result of a drier atmosphere and less convection in the region (Eltahir 1996; Badger and Dirmeyer 2016). This feature is observed in Fig. 5e as a drier troposphere below 650 hPa over 10–18°S and as an enhanced subsidence over the same latitudinal band. These changes are also associated with slightly stronger westerlies at the upper troposphere and a small weakening of the Boliv- ian High (not shown). Similar changes in the regional circulation and in the regional Hadley cell have been reported by previous modelling and theoretical studies (Zhang et al. 1996; Eltahir 1996; Zeng and Neelin 1999; Badger and Dirmeyer 2016). In the linear model developed by Eltahir (1996), the tropical subsidence is a consequence of a reduction in the boundary layer entropy that follows large-scale deforestation. On the other hand, according to Zeng and Neelin (1999) and in agreement with Fig. 4.4, reductions in rainfall and moisture convergence over the Amazon basin induced by tropical deforestation can be partially initiated by the enhanced energy loss due to the albedo effect.

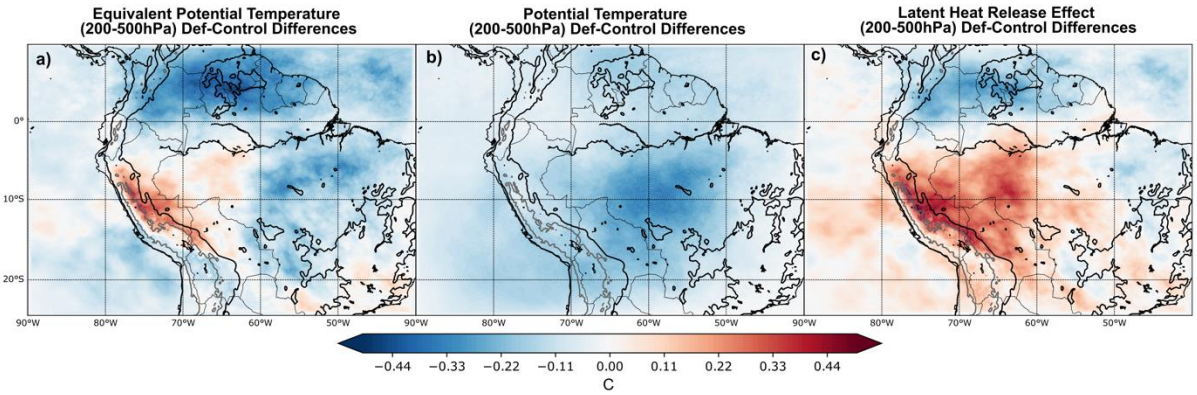

Fig. 4.6 DJF seasonal climatological differences Deforested minus Control during 2001-2011 in atmospheric stability index $\theta_{e_{(200-500)}}$: a Equivalent potential temperature 200-500 hPa ($\Delta\overline{\theta_{e}}_{200-500_{Def-Con}}$). b Potential temperature 200-500 hPa ($\Delta\overline{\theta}_{200-500_{Def-Con}}$). c Latent heat release effect 200-500 hPa ($\Delta\overline{\frac{L_V\theta}{C_PT}r}_{200-500_{Def-Con}}$). All figures are in °C. Orography elevation is shown at 500 and 3500 m a.s.l. as black and grey contours, respectively.

On the other hand, Fig. 4.6 shows the differences between Deforested and Control scenarios for the DJF climatology of the atmospheric stability index, as well as its adiabatic dry and diabatic moist process components following Eq. (4.3). An increment in the equivalent potential temperature and the other terms of the equation (red colors in Fig. 4.6) indicates an increase in the atmospheric stability and an inhibition tendency of the convective activity. Conversely, a decrease in each term of Eq. (4.3) (blue colors in Fig. 4.6) implies a reduction trend in atmospheric stability favoring convection development. A first evident result is that dry adiabatic processes exhibit the tendency to reduce the atmospheric stability over the whole region (Fig. 4.6b). Although with deforestation the troposphere cools at all levels (not shown), the upper levels exhibit a stronger cooling than middle levels, generating the decrease in potential temperature shown in Fig. 4.6b. This effect is more pronounced over the center of the Brazilian Amazon, near the deforested area. On the contrary, changes in wet processes and latent heat release lead to an increase in the atmospheric stability over the central and western Amazon, including the south- ern Andes and its eastern foothills (Fig. 4.6c). It is interesting to highlight that these areas have been recognized to be very sensitive to evapotranspiration upstream of the Amazon basin (Zemp et al. 2017b; Staal et al. 2018). Over the northern and eastern parts of the continent, a decrease in atmospheric stability is related to the enhancement in precipitation and moisture convergence (Fig. 4.5). Since WRF exhibits an underestimated response in evapotranspiration and latent heat flux to deforestation (Sect. 4.2.3.2), the effects in atmospheric stability due to

moist diabatic processes could be stronger. Similarly, earlier studies suggested two competing mechanisms as a response of tropical deforestation: (i) a dry atmosphere response linked to warmer surface that increases convergence; (ii) an enhanced divergence leaded by reductions in rainfall and latent heat release (Gill 1980; Lindzen and Nigam 1987; Eltahir and Bras 1993; Eltahir 1996). In summary, our results suggest that the com- bination of both dry adiabatic and moist (latent heat release) processes produces more stable atmospheric conditions and inhibits precipitation over the western part of the Amazonian basin and the eastern flank of the tropical Andes below the Equator (Fig. 4.6a). Colombia, Venezuela, Guyana and eastern Brazilian Amazon experience a net reduction in stability and more favorable conditions for convection in the deforested scenario. These alterations are more regional and not limited to deforested areas. Although changes in atmospheric stability are not statistically significant, the 10-year-period analyzed in this work might not be enough for identifying significant differences.

4.2.4.2 Mesoscale and local changes in daily scale precipitation

The previous section displays how deforestation reduces precipitation and moisture transport, as well as increases the atmospheric stability and inhibits convective activity over the western Amazon and the eastern Andes flank. We analyze the deforestation effect at meso and local scales for daytime and nighttime conditions over the Amazon-Andes transition region, with a particular focus on the Andean valleys of Huarinilla and Zongo in Bolivia (see Fig. 4.1 for precise location).

Daytime and nighttime rainfall patterns are shown in Fig. 4.7 for observations and WRF-D02. During the day, TRMM exhibits high precipitation values over the western part of the Altiplano and Andes highlands (Fig. 4.7a). Most tropical mountains display this daytime precipitation max- imum over summits partially as a result of the thermally driven upslope winds (Garreaud and Wallace 1997; Garreaud 1999; Kikuchi and Wang 2008; Zardi and Whiteman 2013). There are also significant precipitation rates East of the Andes and over Amazonian lowlands during the day as afternoon convection develops (Machado 2002; Romatschke and Houze 2010; Chavez and Takahashi 2017; Fig. 4.7a). During the night, observed rainfall peaks are located over the eastern Andean piedmonts associated with the so-called rainfall hotspots (Killeen et al. 2007;

Halladay et al. 2012; Espinoza et al. 2015; Fig. 4.7b). This nocturnal convective activity is driven by the convergence of downslope winds from the top of the Andes with the SALLJ nocturnal enhancement (Killeen et al. 2007; Romatschke and Houze 2010; Chavez and Takahashi 2017; Junquas et al. 2018).

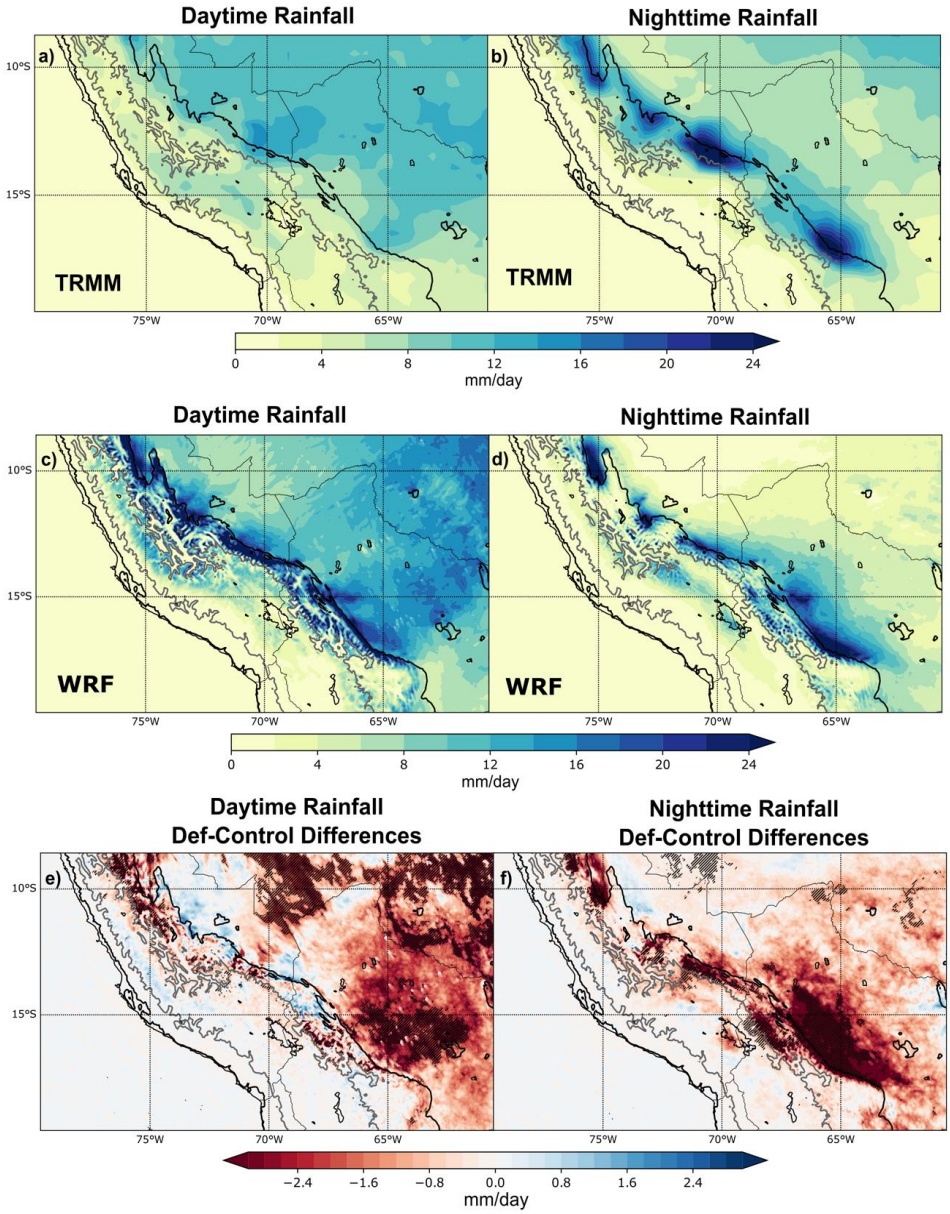

Fig. 4.7 DJF climatological means (2001-2011) for daytime and nighttime precipitation from: **a-b** TRMM-3B42. **c-d** WRF-D02. **e-f** WRF-D02 Deforested minus Control differences. All figures are in mm day^{-1}. Significant changes (t-test, p<0.05) are marked with black slashes. Orography elevation is shown at 500 and 3500 m a.s.l. as black and grey contours, respectively.

In general, WRF-D02 is able to represent the main features of diurnal and nocturnal rainfall variability in the region when compared to TRMM. Rainfall peaks above the 3500 m a.s.l. and over the central Peruvian Altiplano are simulated during the day by

WRF as shown in Fig. 4.7c. Daytime convection over Amazon lowlands below 500 m is also present in WRF outputs in agreement with TRMM. However, the model strongly overestimates daytime precipitation over the Bolivian Amazon plains and over the eastern Andes slopes. Nevertheless, dry biases have been identified by several studies in TRMM outputs over tropical Andes, which makes it difficult to properly quantify the model biases (Condom et al. 2011; Scheel et al. 2011; Rasmussen et al. 2013; Espinoza et al. 2015). During nighttime, WRF realistically represents the rainfall hotspots but exhibits a positive (negative) bias over the Peruvian Andes highlands (Brazilian Amazon lowlands) (Fig. 4.7d).

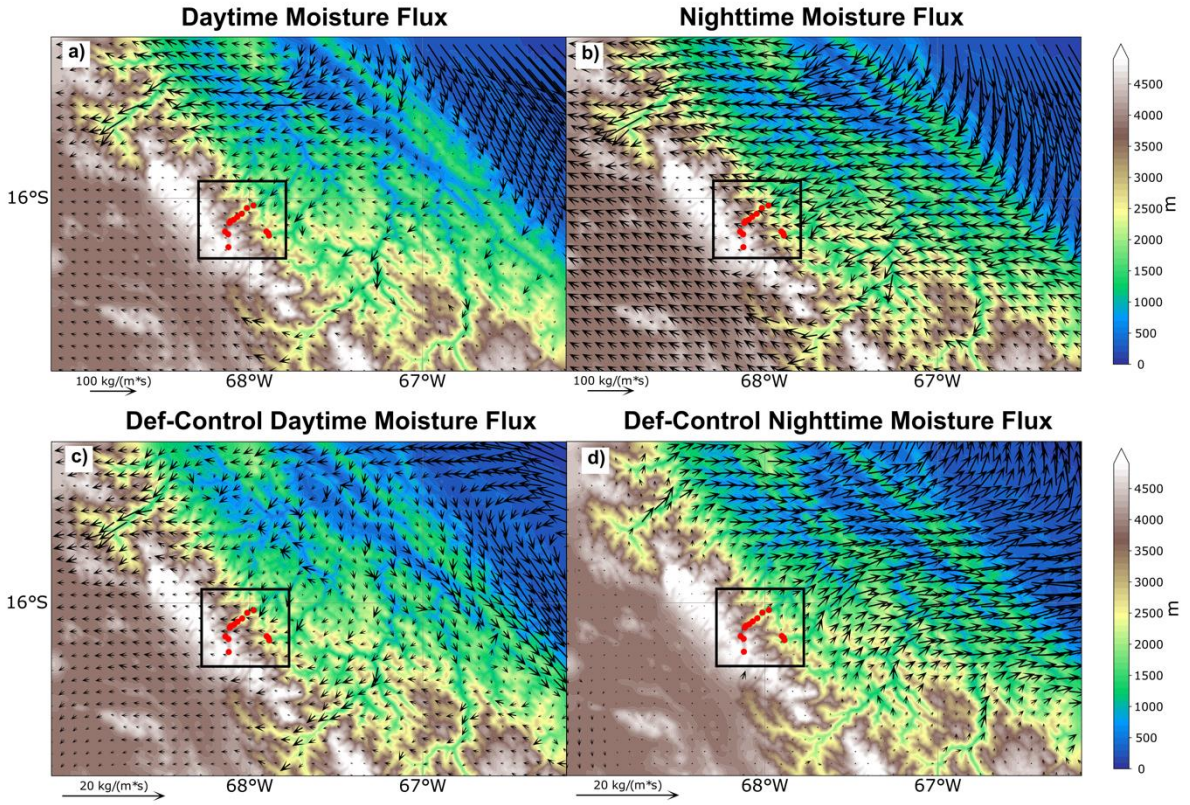

Fig. 4.8 DJF climatological means (2001-2011) for daytime and nighttime vertically-integrated moisture flux from WRF-D03: **a-b** Control and **c-d** Deforested minus Control differences. Terrain elevation in m (shaded) and rain-gauge stations (red dots). The black square shows the area where the Andean valleys of Huarinilla and Zongo are located.

Deforestation causes a general rainfall reduction in day- time and nighttime conditions but with different spatial distributions (Fig. 4.7e, f). During the day, significant precipitation reductions occur over the Amazon plains following the deforested area (between 10 and 20%), but no significant changes occurs over the tropical Andes above 3500 m a.s.l. On the eastern Andean slope between 500 and 3500 m a.s.l., significant changes are found, like in the central Andean- Amazon valleys of Peru near

the 10° S and 75° W (Fig. 4.7e). On the other hand, nighttime convection decrease (between 20 and 30%) is concentrated over the eastern flank of the Andes and particularly over the Bolivian piedmont (Fig. 4.7f). Taking into account that nighttime convection is responsible for nearly the 70–80% of the daily precipitation on the eastern tropical Andes slopes during austral summer (Perry et al. 2014; Chavez and Takahashi 2017), this nocturnal rainfall reduction can have a profound impact in the hydrology of the region. Since nocturnal precipitation over the eastern Andes slopes (including over rainfall hotspots) is closely related to the presence of the SALLJ, in Fig. 4.8 we evaluate the changes induced by deforestation in the vertically integrated moisture flux over the Bolivian piedmont inside our third modelling domain (Fig. 4.1). A northwesterly moisture transport is present in both daytime and nighttime conditions during DJF in the Control scenario associated with the SALLJ activity (Fig. 4.8; e.g. Marengo et al. 2004). This moisture transport is more parallel to the Andes during the day and is stronger and more perpendicular to the slopes during the night in agreement with previous works (Vernekar et al. 2003; Marengo 2004; Junquas et al. 2018; Fig. 4.8a, b). The humidity flux transported from Amazon toward the Andes is channelized both during day and night over the steepest valleys as modelling and observational works reported in the region (Zängl and Egger 2005; Perry et al. 2014; Junquas et al. 2018; Fig. 4.8a, b). The Andes act as a blocking barrier to this moisture laden winds coming from the Amazon lowlands, triggering forced convection mainly during nighttime when the trajectory is more perpendicular to the topography. This mechanism was hypothesized by Espinoza et al. (2015) based on in-situ stations and supported by modelling studies (Junquas et al. 2018).

In the Deforestation scenario, the daytime upslope moisture flux is enhanced over the major valleys (Fig. 4.8c). However, inside of our region of interest covering Zongo and Huarinilla valleys (black square in Fig. 4.8) this flux exhibits little changes during the day. Conversely, during the night there is a strong reduction in the humidity transport from the Amazon lowlands towards the Andes highlands over the entire region (Fig. 4.8d) in agreement with nocturnal rainfall reductions over eastern Andes slopes and Bolivian hotspots shown in Fig. 4.7f.

During nighttime, we hypothesize that the precipitation and moisture flux depletion in the region is caused by the following process: (i) the atmosphere dries up in the

Deforestation scenario over the whole Amazon basin and the northerly moisture flux weakens (Fig. 4.5); (ii) precipitation decreases over the western Amazon causing less latent heat released to the atmosphere over the region; (iii) there is a reduction in the local upslope moisture flux over the eastern flank of the Bolivian Andes. By suppressing the condensation latent heating due to rainfall in the Peruvian and Bolivian Andean slopes in a modelling experiment, Junquas et al. (2018) found a positive feedback with the reduction in the entrance of the upslope moisture flux coming from Amazon plains. Since latent heating is more important for sustaining circulation during the night (e.g. Souza et al. 2000), major impacts of such processes happen on nocturnal rainfall. Similarly, by preventing the energy influx into the atmosphere from latent heat fluxes over the eastern flank of the Andes in high resolution climate simulations, Sun and Barros (2015a, b) found a strong reduction in the energy available for moist convection, a decrease in rainfall, moisture convergence and cloudiness in the region, and a weakened upslope flow as a consequence of increased static stability. Our results points towards the same direction: the crucial role of moist processes for sustaining the atmospheric circulation and hydrological condition over the Amazon-Andes transition region.

In order to evaluate the potential impacts of Amazon forest loss on the hydro-climatology at local scales, our analysis is centered in two instrumented valleys located at the eastern flank of the Bolivian Andes: Huarinilla and Zongo valleys (Fig. 4.9a). The spatial distribution of rain-gauges within the two valleys allows analyzing how precipitation varies with orography and altitude in two opposite directions with respect to the Andean Cordillera. Stations inside the Zongo Valley are located from north-east to south-west in a perpendicular direction to the Andes (Fig. 4.9a). Conversely, stations located in the Huarinilla Valley are disposed parallel to the mountain chain. Following the rain stations from highlands to lowlands, two cross-sections were defined as shown in black solid lines of Fig. 4.9a. A third cross-section is analyzed in a perpendicular direct ion of the Zongo valley (northwest-southeast direction) in order to complement the understanding of local circulation alterations (black dashed line in Fig. 4.9a). The climatological relationship between precipitation and elevation is shown in Fig. 4.9b, c. There is an opposite relation between rainfall and terrain elevation in the two transects. For the Zongo Valley cross-section, precipitation generally

decreases with elevation, reaching minimum values above 3000 m a.s.l. and rainfall peaks near the 1000 m a.s.l. (Fig. 4.9b). This rainfall behavior was previously reported

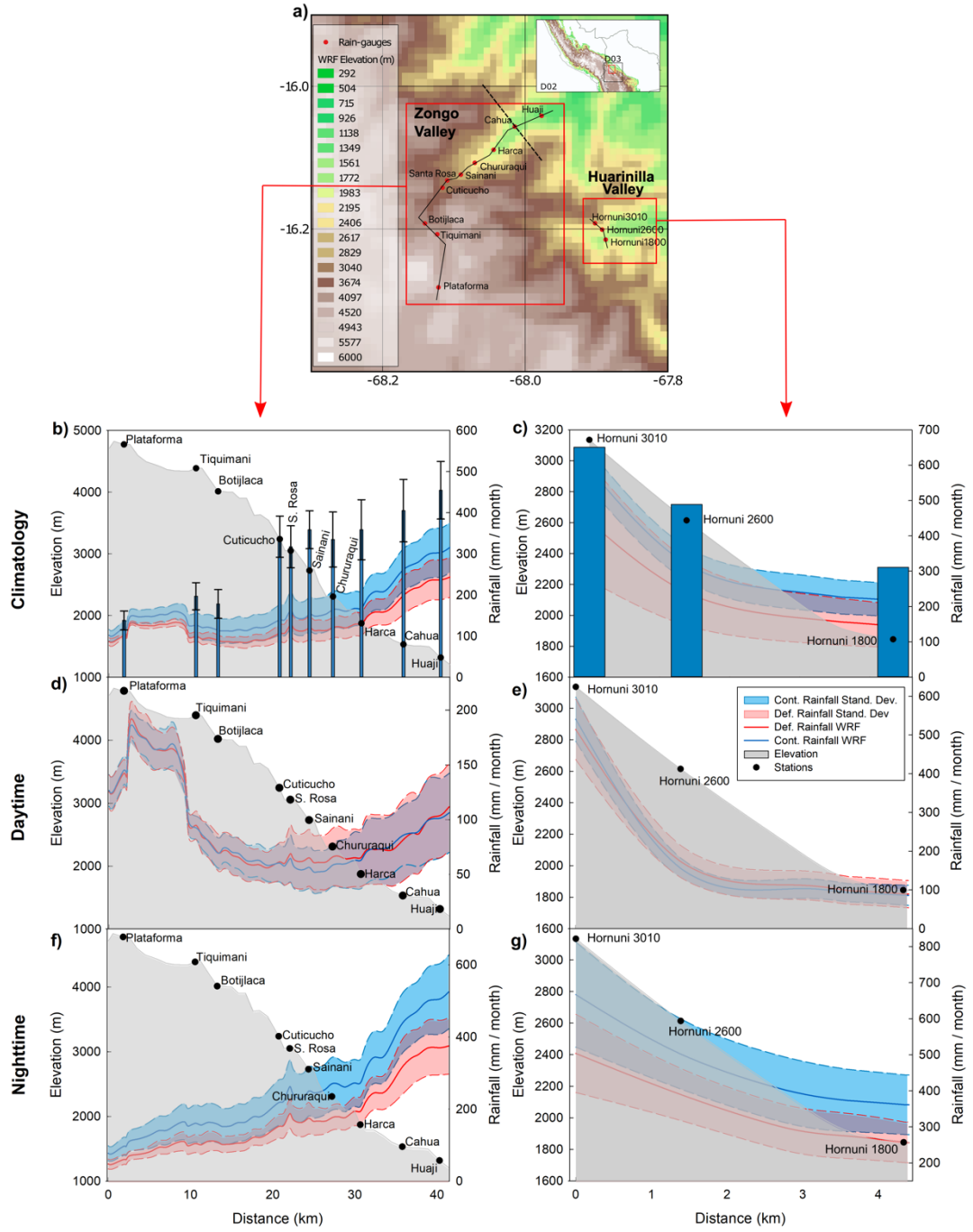

Fig. 4.9 **a** Map of the subregion inside D03 with terrain elevation (shaded) in m and rain-gauge stations (red dots). Two selected cross-sections are indicated in black solid lines. A perpendicular cross-section in Zongo Valley shown in Figure 10 is indicated as a dashed black line. **b-c** Cross-sections for **b** Zongo Valley and **c** Huarinilla Valley. Topographic profiles are displayed as a gray line (in m). Observed rain-gauge rainfall is presented as blue bars. Climatological means for Zongo and Huarinilla valleys corresponds to the periods 2001-2011 and 2001-2002 respectively. WRF-D03 Control and Deforested rainfall 2001-2011 DJF climatological means are shown as blue and red lines and are labeled as Cont. and Def., respectively. **d-g** Same as Fig. 4.9**b-c** but for daytime and nighttime conditions. Rainfall is in mm month^{-1}. The x axis represents the horizontal distance in km along the cross-sections. Blue and red

envelopes represent model standard deviation for each scenario. Black dots represent rain-gauge stations.

by Espinoza et al. (2015). Chavez and Takahashi (2017) demonstrated how the rainfall change with elevation along cross-sections transversal to the Andes in the region follows the profile of the horizontal moisture flux carried by the SALLJ. In this sense, the rainfall-elevation relation in the first transect seems to be more related with synoptic processes such as the SALLJ and less with local upslope processes in accordance with previous studies (Romatschke and Houze 2010). An opposite behavior is observed in the Huarinilla Valley, where maximum rainfalls are located at high elevations around 3000 m a.s.l. (Fig. 4.9c). Here, daytime thermally-driven anabatic winds are responsible for trans- porting moisture transpired inside the valley in the upslope direction and generates a rainfall peak in the afternoon (Molina-Carpio et al. 2019).

WRF exhibits a realistic representation of the rainfall-elevation relationship for both cross-sections. The model reproduces the observed rainfall increases over very local orographic elevations such as the rain-gauges of Tiquimani, Santa Rosa and Sainani. However, a rainfall underestimation (around −30%) occurs in all the stations inside the Zongo Valley and is higher below the 3000 m a.s.l. The model also presents problems in the representation of the steep precipitation decrease that occurs between Cuticucho and Tiquimani and instead exhibits an almost linear rainfall reduction from Huaji to Plataforma. However, this issues in the local variation of precipitation in the Zongo Valley could be related with problems in the representation of local topography. By comparing Table 4.3 values with Fig. 4.9, it is easy to identify that for the Zongo Valley, WRF overestimates the real altitude of the stations (from 20 m at Plataforma to 476 m at Sainani). Major differences occur on stations located in places with very high slopes (such as Sainani or Botijlaca). Although our simulations use an enhanced digital elevation model instead of the default dataset in WRF, the complex and steep topography in the region is still poorly represented. This misrepresentation in the local topography can cause issues in the representation of moisture transport, surface circulation and can also affect rainfall and surface air temperature (e.g. Saavedra et al. 2020). On the other hand, taking into account that precipitation is very related to the SALLJ moisture transport in this valley, WRF rainfall underestimation could be

related to the weaker SALLJ moisture flux present in the model simulation (not shown). Daytime and nighttime rainfall conditions for both transects are shown in Fig. 4.9d–g according to WRF outputs. In Zongo Valley, diurnal precipitation is much less than nocturnal values confirming that the dominant mechanism in this valley is the regional moisture transport of the SALLJ (Fig. 4.9d–f). At this time, precipitation falls mainly over highlands for both transects as shown in Figs. 4.9d, e. At the bottom of the Zongo Valley there is a secondary rainfall peak as a consequence of convective activity related with the solar heating over Amazonian plains (Romatsche and Houze 2013). However, in terms of percentage of the summer climatological mean at each station, daytime lowlands rainfall is lower than in the highland. Nighttime rainfall is concentrated mainly at lowlands in agreement with the mechanism described before (Fig. 4.9f). It is interesting to note that for the Huarinilla Valley, similar precipitation magnitudes are simulated for day-time and nighttime conditions (Fig. 4.9f, g). This suggests that local and synoptic mechanisms are equally important in this valley as reported from previous works (Molina-Carpio et al. 2019).

Amazon deforestation induces significant reductions in the climatological rainfall mean over both Zongo and Huarinilla cross-sections but increases its interannual variability only in Huarinilla Valley (Fig. 4.9b, c). Major precipitation drop is located over areas below 2000 m a.s.l. in the Zongo Valley (Fig. 4.9b). For this cross-section, daytime precipitation presents little changes in its mean value (Fig. 4.9d). Conversely, during the night precipitation decreases, especially at lowlands, and no change in the variability occurs (Fig. 4.9f). This result confirms our hypothesis that rainfall depletion in this valley is mainly related with the decreased entry of SALLJ moist winds from Amazon towards the Andes highlands. On the other hand, the Huarinilla Valley cross-section does not present significant changes in daytime rainfall but increases its interannual variability (Fig. 4.9e). However, decreased rainfall take place during nighttime especially over highlands in agreement with the regional alterations in the SALLJ related moisture flux (Fig. 4.9g).

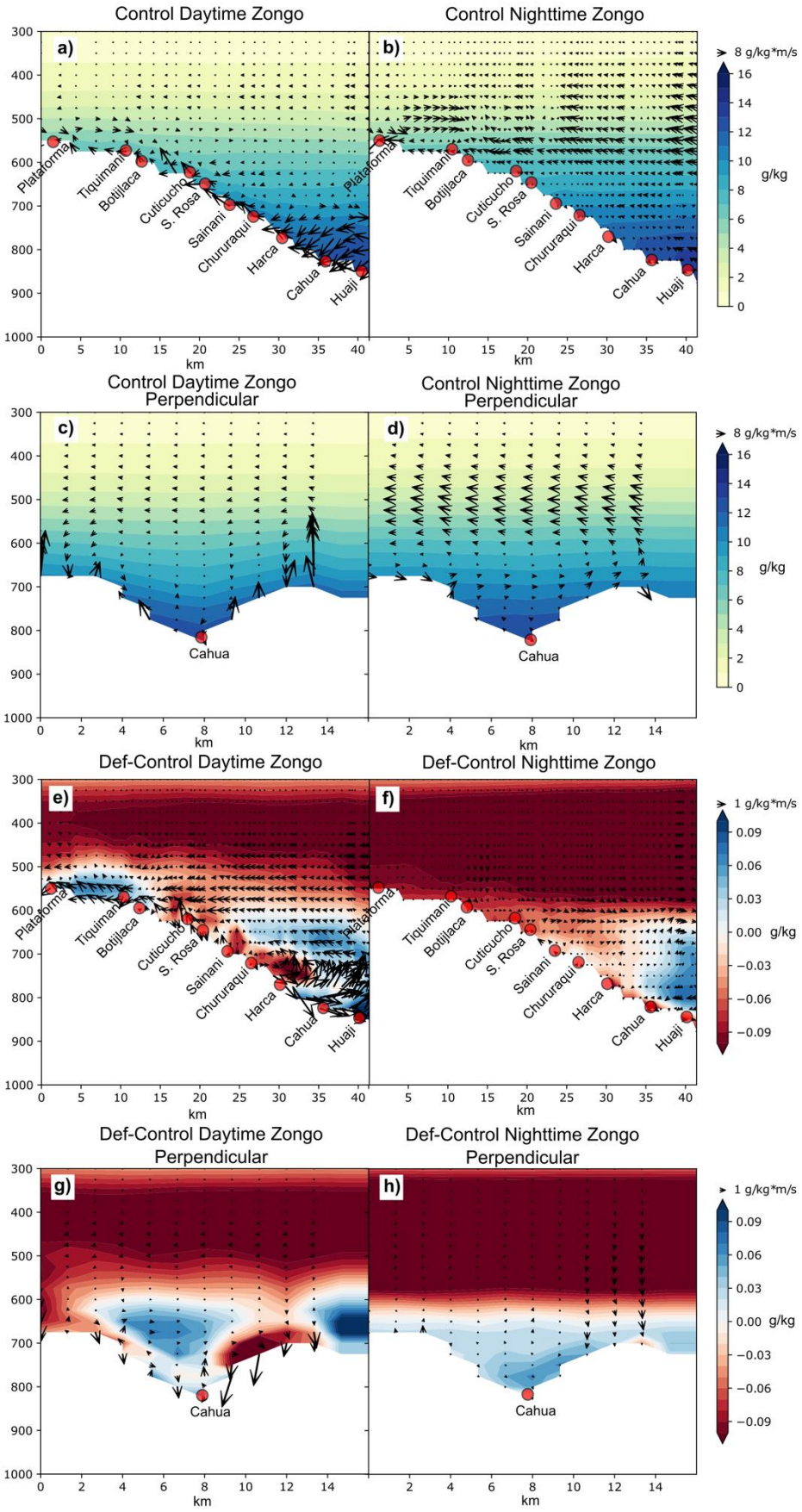

Fig. 4.10 Vertical cross-section for daytime and nighttime DJF climatological means (2001-2011) in atmospheric moisture (shaded, g kg^{-1}) and moisture flux (vectors, g kg^{-1}*m s^{-1}) for the Zongo Valley in

two opposite directions: parallel to the transect (see black solid line in Fig. 4.9a) and perpendicular to the transect (see black dashed line in Fig. 4.9a). Daytime (**a**) and nighttime (**b**) WRF-Control conditions for the transect parallel to the Zongo Valley. Daytime (**c**) and nighttime (**d**) WRF-Control conditions for the transect perpendicular to the Zongo Valley. Daytime (**e**) and nighttime (**f**) Deforested minus Control differences in the transect parallel to the Zongo Valley. Daytime (**g**) and nighttime (**h**) Deforested minus Control differences in the transect perpendicular to the Zongo Valley. Red dots represent rain-gauge stations. Vertical component of the moisture flux is exaggerated by a factor of ten.

Aiming to complement the previous analysis, Fig. 4.10 displays the atmospheric humidity and moisture flux in the vertical cross-section along parallel (black solid line in Fig. 4.9a) and perpendicular (black dashed line in Fig. 4.9a) directions of the Zongo Valley. Similar results are found for the Huarinilla Valley (not shown). During daytime, upslope moisture flux (Fig. 4.10a) causes the rainfall peaks over summits described in Fig. 4.9d. Similar anabatic winds are present in the perpendicular direction of the Zongo Valley (Fig. 4.10c). During nighttime, surface moisture flux weakens, and light katabatic winds develops in the Zongo Valley (Fig. 4.10b–d). At the same time, the mid-tropospheric moisture coming from the Amazon plains is strengthened mainly in the perpendicular direction of the Zongo Valley (Fig. 4.8a, b, 4.10b–d). Another interesting feature of the nocturnal circulation in the perpendicular direction is the development of a moisture flux around 700 hPa in the opposite direction (northwest-southeast) of the main mid-tropospheric flow (Fig. 4.10d). This returning flow seems to be a consequence of the ascending motion over lowlands summits to satisfy continuity.

Deforestation induces a weakening of the daytime upslope flow over both directions of the Zongo Valley (Fig. 4.10e–g). A reduction in the intensity of the daytime circulation increases the atmospheric moisture near the surface at the bottom of the valley (Fig. 4.10e, g). Based on the thermodynamics of heat engines, Souza et al. (2000) explain the physical mechanism behind the observed circulation over areas with different surface conditions in sloping terrains. According to this work, the intensity of the circulation depends on the absorption of sensible and latent heat by a parcel that moves along a closed streamline. They also recognize the hydrostatic pressure and non-adiabatic expansion/compression as important effects. Following this argument, we assess the surface energy balance along the Zongo Valley for the Control and Deforestation scenarios. We focus on daytime conditions, when local surface heterogeneities play an important role (Fig. 4.11). However, night- time

changes were also analyzed and are not significant (not shown). Small changes in the incoming shortwave radiation are induced by deforestation in the Zongo Valley and are linked with differences in clouds (Fig. 4.11a). On the contrary, a strong increment in the reflected shortwave radiation causes a loss of around −50 W m^{-2} at the bottom of the valley where deforestation occurs (Fig. 4.11b). The longwave components of the energy balance remain almost unaltered (Fig. 4.11c, d). Due to the increase in the outgoing shortwave energy loss, the surface net radiation decreases at lowlands below Harca rain-gauge (Fig. 4.11e). This net radiation reduction generates a decrease in the altitude of the planetary boundary layer (PBL) (Fig. 4.11f) and is distributed in reductions in latent heat but mainly in sensible heat flux over low- lands (Fig. 4.11g, h). These fluxes are essential in the triggering and development of upslope flows (e.g., Junquas et al 2018). The reductions in the sensible and latent heat fluxes explain the weakening of the upslope surface circulation during daytime described in Fig. 4.10. However, these results have to be taken with caution taking into account that WRF strongly underestimates (overestimates) the impact of forest loss on the sensible heat flux (reflected incoming radiation) (Sect. 4.2.3.2).

On the other hand, nighttime differences in circulation mainly occur at regional scale through mid-tropospheric moisture flux reduction in the deforested scenario (Figs. 4.8d, 4.10f–h). This moisture transport is very important for developing the nocturnal convection and its decrease causes less rainfall over the entire region (Fig. 4.9f, g). The nighttime conditions are also characterized by a strong reduction in atmospheric humidity above the 600 hPa as a consequence of deforestation (Fig. 4.10f, h).

Rainfall reductions and increased rainfall variability over Huarinilla and Zongo valleys can impact the wet ecosystems of local humid-montane forest and its endemic biological species (Ibisch et al. 2001; Mueller et al. 2002; Kessler and Kluge 2008). Additionally, the area encompasses part of the Cordillera Real-Bolivia and the Huayna Potosi Massif where several glaciers (e.g. Zongo Glacier) are located (Francou et al. 1995). The glacier surface mass balance variability of the tropical glaciers is strongly controlled by the precipitation amount and temporal distribution that determine the glacier surface albedo and therefore the surface energy balance

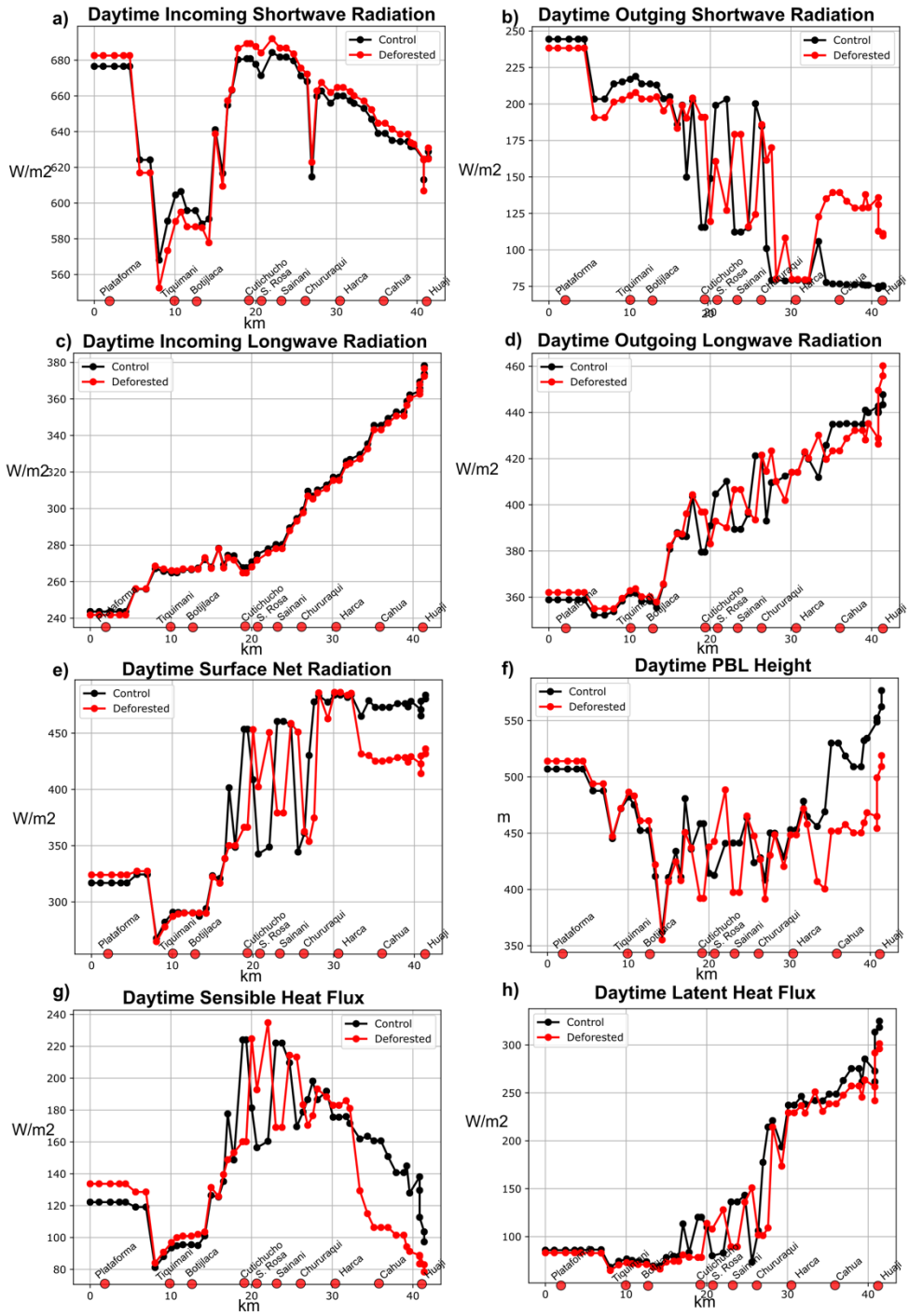

Fig. 4.11 WRF-D03 daytime mean variation along the Zongo Valley transect in Control and Deforested scenarios (black and red lines, respectively) for: **a** Shortwave incoming radiation. **b** Shortwave outgoing radiation. **c** Longwave incoming radiation. **d** Longwave outgoing radiation. **e** Surface net radiation. **f** Planetary boundary layer (PBL) height. **g** Sensible heat flux. **h** Latent heat flux. Red dots represent rain-gauge stations.

(e.g. Sicart et al. 2005; Rabatel et al. 2013), as well as regional atmospheric circulation (Favier et al. 2004; Sicart et al. 2016). Our results state that Amazonian large-scale deforestation can have an important effect in the regional circulation and precipitation. This means that retreat of the tropical Andes glacier documented since the early 1980s

and linked to climate change (e.g. Ramírez et al. 2001; Francou et al. 2003; Rabatel et al. 2013) is likely to be further increased as extensive Amazonian deforestation can also have an impact on precipitation and therefore on the surface mass balance of tropical glaciers.

It is important to remark that wide-spread deforestation can have strong nonlocal atmospheric responses (Avissar and Werth 2005; Hasler et al. 2009). Thus, the use of a regional model where both control and deforested scenarios present the same lateral boundary conditions generates a bias where these nonlocal effects are not included (Medvigy et al. 2011). In this sense, the results discussed above do not include the possible remote responses of deforestation in the boundary conditions of our analysis domain. On the other hand, a strong perturbation in the land surface conditions (such as the implementation of a deforestation scenario) can require a long spin-up period for a regional climate model to reach a physical equilibrium state. Surface hydrological variables such as evapotranspiration and soil moisture require long spin-up periods ranging from several months to several years (Christensen 1999; Cos- grove et al. 2003). Since these variables are crucial for surface energy and water budgets, the evaluation of the spin-up window influence in deforestation scenarios is a relevant topic to be evaluated by future studies. Nevertheless, the atmospheric component (which is the main interest in the present study) responds faster to dynamical/ thermo-dynamical forcings (de Ela et al. 2002; Cholette et al. 2015; Jerez et al. 2020).

4.2.5 Summary and conclusions

This study aims to evaluate the impacts of Amazonian deforestation on the hydro-climatic connectivity between Amazon and eastern tropical Andes during the austral summer in terms of hydrological and energetic balances. To this end, we use 10-year December–January–February high-resolution simulations (2001–2011) with the regional climate model WRF. Two scenarios are used: (i) a control simulation corresponding to vegetation conditions for the year 2000; (ii) a business-as-usual deforested scenario (45% of forest lost) designed by Soares-Filho et al. (2006).

By comparing with reanalysis (ERA5 and NCEP-NCAR) and precipitation satellite outputs (TRMM), we find a realistic representation of the main atmospheric circulation

(e.g. SALLJ, the Bolivian High) and rainfall features (e.g. SACZ, Amazon convection) during austral summer by WRF at a regional scale. The model is also able to reproduce the daytime and nighttime rainfall conditions over the Amazon-Andes transition region and the rainfall-elevation relation at a local-scales inside instrumented Andean valleys. However, at local scale, in regions with high orography, day and night rainfall conditions were only compared with rain-gauge estimations for a very short period (1 year) in Huarinilla valley. The lack of observations at intra-diurnal time scale in the region is an important limitation for assessing the high-resolution model representation of local atmospheric mechanisms and its interaction with mesoscale features. We complement the validation by assessing the model skill to reproduce the observed land use change impacts on surface fluxes and atmospheric variables at a local scale against LBA stations. We find a realistic model response to deforestation for most of the surface atmospheric variables in Amazon lowlands. However, WRF overestimates the effect of the albedo on the reflected shortwave radiation and strongly underestimates the sensible heat flux and evaporation/latent heat response to forest loss. These model biases constrain our conclusions about the impacts of deforestation on the regional climate. How these errors interact with each other is something that remains unexplored in this work.

At a regional scale, the energy balance is profoundly disrupted by the forest loss. The combined effect of enhanced energy losses through shortwave radiation reflection, longwave incoming and outgoing radiation fluxes leads to a decrease in the surface net radiation over most of the basin. According to the deforestation theory developed by Zeng and Neeling (1998), this reduction in surface net radiation may lead to alterations in the regional moisture convergence. Accordingly, deforestation reduces precipitation almost over the entire Amazonian basin (~20%). Rainfall depletion is related with the very local response of decreased evapotranspiration over cleared areas. The drier atmosphere seems to present a decrease in latent heat release that weakens moisture convergence and causes an anomalous winds subsidence in the region in agreement with early theoretical frameworks. In agreement with these theoretical works, deforestation induces a slight weakening of the Bolivian High and decreases (increases) the 200 hPa geopotential height (surface pressure) over the southwestern Amazon. These alterations in the regional precipitation and atmospheric circulation are summarized in Fig. 4.12a, b. Regarding the regional atmospheric

stability, our analysis suggests the rise of two competing mechanisms for tropical deforestation: (i) an adiabatic response decreases atmospheric stability and enhances convective activity over the continental area; (ii) conversely, reductions in the latent heat release increase atmospheric stability and disfavor convection mainly over western Amazon, and the eastern sides of tropical Andes. Although the effects of deforestation in atmospheric stability are relatively small and non-significant, the underestimated WRF response in latent heat flux to forest loss implies that this effect could be stronger.

Over the Amazon-Andes transition region, deforestation causes a general rainfall reduction in both daytime and nighttime conditions but with a clearly spatial differentiation. Daytime precipitation reductions occur over the Amazon plains following the deforested area (between 10 and 20%). Conversely, nighttime convection decreases between 20 and 30% mainly over the eastern flank of the Andes and over the Bolivian piedmont. Since nighttime convection is responsible for nearly 70–80% of the daily precipitation on the eastern tropical Andes slopes during austral summer, this rainfall reduction can seriously impact the hydrology of the region. The decrease in nocturnal rainfall over eastern Andean hillside is caused by a reduction in the humidity transport from the Amazon lowlands towards the Andean highlands during nighttime in agreement with previous modelling studies.

Finally, at a local scale, Amazon deforestation induces significant reductions in the climatological rainfall mean over both Zongo and Huarinilla valleys (−25%) and increases its interannual variability. For the Zongo Valley, major precipitation drop occurs over areas below 2000 m a.s.l. In this valley, daytime precipitation presents little changes in its mean value. However, during the night precipitation decreases, especially at lowlands. The rainfall depletion in this valley seems to be mainly related with the decreased entry of SALLJ moist winds from Amazon towards the Andean highlands (Fig. 4.12d–f). Similarly, the Huarinilla Valley does not present significant changes in daytime rainfall but exhibits decreased precipitation especially over highlands during nighttime. However, as a result of numerical modelling these conclusions have to be taken with caution as they are partially dependent on the model configuration. More efforts have to be done to understand the sensitivity and robustness of these results to model parametrizations. Finally, this work and most of

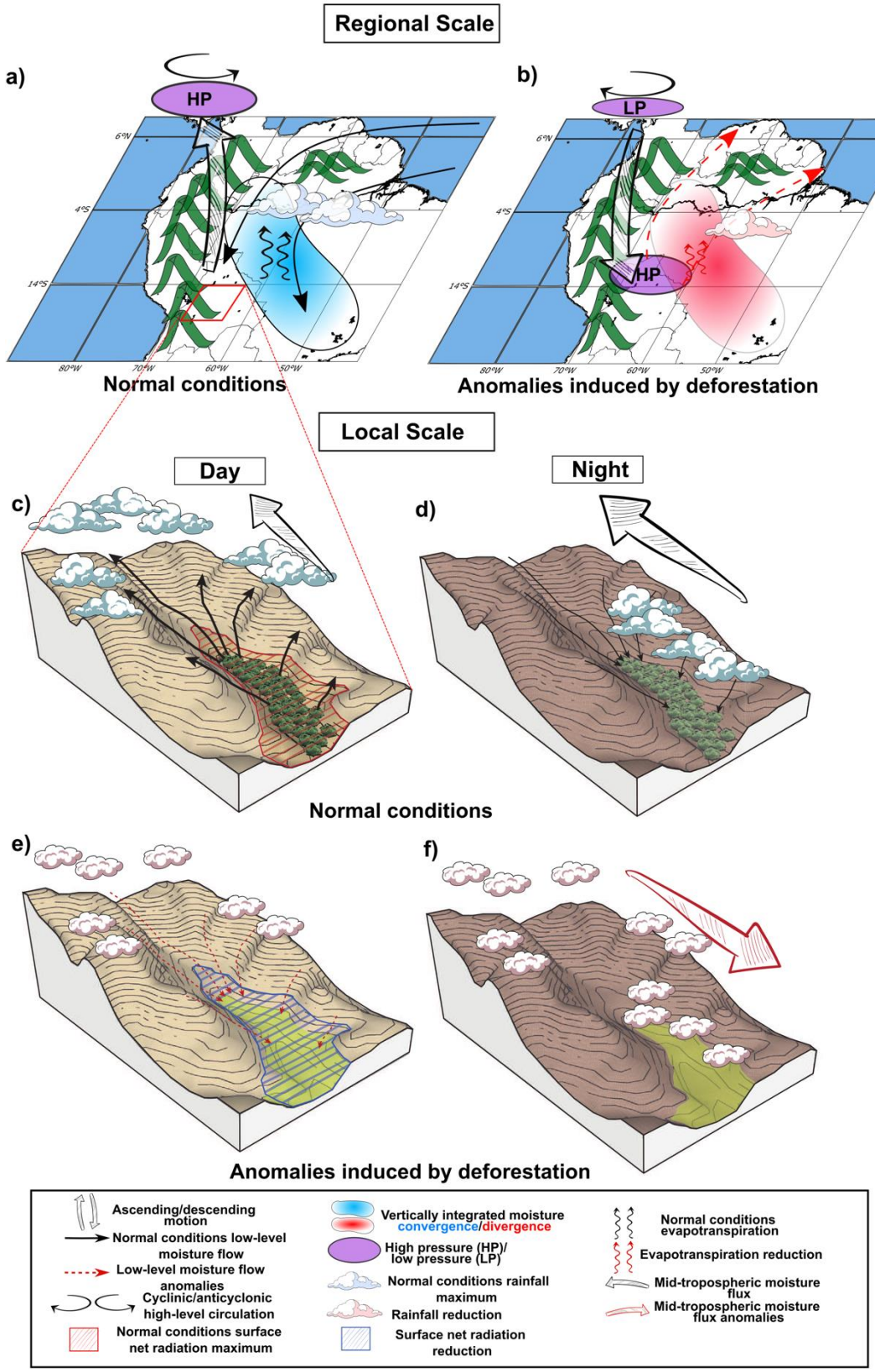

Fig. 4.12 Schematic representation of DJF climatological atmospheric conditions at regional (**a-b**) and local scales (**c-f**) for normal conditions (**a-c-d**) and deforestation induced anomalies (**b-e-f**) in WRF simulations. The red square in a indicates the approximated location of the Zongo Valley sketched in **c-f**. Black solid (red dashed) thin arrows represent surface moisture transport under normal conditions (deforestation anomalies). Black (red) thick arrows represent mid-tropospheric moisture flux under

normal conditions (deforestation anomalies). Vertical thick arrows represent ascending and descending motions. Black (red) curved arrows represent evapotranspiration under normal conditions (deforestation anomalies). Blue and red shaded areas indicate vertically integrated moisture convergence and divergence, respectively. Purple areas indicate pressure changes. Blue and red clouds indicate rainfall maximum and rainfall reductions under normal and deforested conditions, respectively. Red (blue) hatched area in **c** (**e**) indicates surface net radiation maximum (reduction) under normal (deforestation) conditions.

deforestation modelling studies are focused on forest loss impacts on atmospheric processes at climatological time scales. How deforestation can alter rainfall distribution and the atmospheric circulation patterns that drive moisture advection at synoptic intra-seasonal time scale is a question that should be addressed to better understand the deforestation disturbances at longer time scales.

5

The southern tropical Andes and the effects of Amazonian forest loss

Contents

5.1 Introduction

The Andes, the longest mountain chain in the world, is a determinant factor for the atmospheric circulation and climate at continental scale (Garreaud 2009; Espinoza et al. 2020). The tropical Andes (20◦ S - 11◦ N) hold high species-rich ecosystems (Myers et al. 2000; Borsdorf and Stadel 2015; Chapter 2), host nearly 99% of all tropical glaciers (Kaser 1999) and house numerous population centers (Figure 5.1 and Chapter 1). The water supply for nearly 75 million people relies on water resources originated from the tropical Andes (Vergara et al. 2007; Poveda et al. 2020; Segura 2021). Over the southern part of the tropical Andes (20◦ S - 12◦ S 80◦W - 64◦W, magenta box in Figure 5.1 a-b) most of the total annual rainfall (>70%) is concentrated in the austral summer (Aceituno and Garreaud 1995; Minvielle and Garreaud 2011; Figure 5.1 d). Between December and February, deep convection in the Amazon allows diabatic heating in the mid and upper troposphere developing an anticyclonic circulation at upper tropospheric levels known as the Bolivian High (Lenters and Cook 1997). Centered at 18 S◦ – 62◦ W and at the 200 hPa level (Figure 5.2 a), the easterly winds associated with the Bolivian High carry moist air from the Amazon toward the southern tropical Andes feeding convection in the region (Garreaud 1999; Falvey and Garreaud 2005). This mechanism acts also at inter-annual time scales. Therefore, year-to-year fluctuations in the intensity and position of the Bolivian High are closely linked to precipitation variability in the Andean highlands (Vuille et al. 2000; Garreaud and Aceituno 2001; Garreaud et al. 2003; Vuille and Keimig 2004). However, recent changes in the Walker circulation related to the warming of the tropical North Atlantic seem to be related to a shift in the controlling process of the southern tropical Andean rainfall (Segura et al. 2020). Segura et al. (2020) find a weakening of the well-known correlation between southern tropical Andes rainfall and the easterly winds at the upper troposphere since the 2000's. After 2002, a different dominant mode leads the rainfall inter-annual variability over the south tropical Andean summits. An enhanced ascending motion over the western Amazon caused by the strengthening of the Walker circulation (Wang et al. 2018; Barichivich et al. 2018; Espinoza et al. 2019a, 2021) has moistened the mid-troposphere in the western part of tropical South America leading to an increase in the atmospheric instability over the southern tropical Andes (Segura et al. 2020). Taking into account that one of the possible factors for the sustained warming of the tropical North Atlantic, and therefore for the recent changes

in the regional Walker cell, is the anthropogenic influence through an increase in greenhouse gases and aerosol emissions (Du and Xie 2008; Booth et al. 2012; Dong et al. 2014; Servain et al. 2014; Li et al. 2016), it is crucial to investigate the consequences of the current human large-scale pressures over the water resources of the tropical Andes.

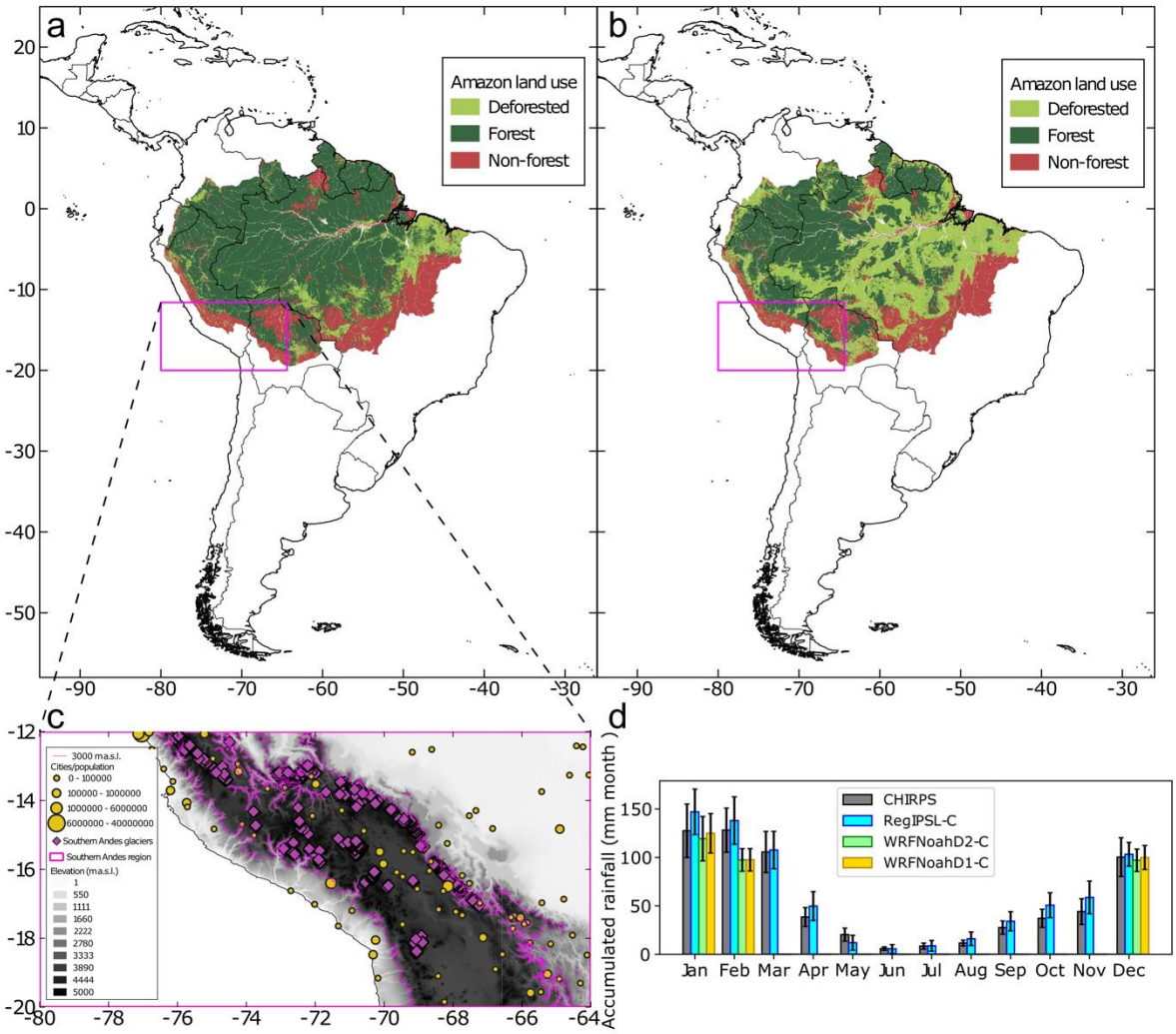

Fig. 5.1 Experiment scenarios: **a** Control and **b** Deforested. Magenta box shows the southern tropical Andes region (20°S-12°S, 80°W-64°W). **c** Elevation (shaded; in m a.s.l.), location of cities (yellow dots) and tropical glaciers (magenta diamond) over the southern tropical Andes. The magenta line highlights the 3000 m elevation contour. **d** annual cycle of rainfall spatially averaged above the 3000 m level for CHIRPS, RegIPSL-Control, WRF-Noah over the first ('WRFNoahD1') and second domains ('WRFNoahD1') (gray, blue, yellow and orange bars, respectively). Whiskers represent the ± 1 standard deviation. Data source for the digital elevation model is the USGS 30 ARC-second Global Elevation Data, GTOPO30. Population dataset comes from https://simplemaps.com/data/world-cities. Glacier dataset is obtained from the Randolph Glacier Inventory (available at https://nsidc.org/data/nsidc-0770/versions/6#anchor-1).

For more than a decade, global circulation models have predicted a warmer future climate, with warming increasing with altitude in the lower troposphere (Bradley et al.

2004, 2006; Urrutia and Vuille 2009; Pepin et al. 2015). This model-based projection has been confirmed with instrumental observations in the tropical Andes (Beniston et al. 1997; Vuille et al. 2003). As a consequence, glacier retreat has been observed over all Andean countries in the recent decades (Kaser and Osmaston 2002; Francou et al. 2003, 2005; Ceballos et al. 2006; Braun and Bezada 2013; Veettil et al. 2014), disrupting the hydrological cycle and threatening mountain ecosystems and human water resources. As an additional concern, future warming-scenario projections also suggest drier conditions over the southern tropical Andes caused by an increased upper-tropospheric westerly flow entering from the Pacific Ocean (Thibeault et al. 2010, 2012; Marengo et al. 2010; Minvielle and Garreaud 2011). At the same time, other studies suggest the moisture transport from the Amazon basin toward the Andes may be reduced under greenhouse gases emission scenarios (Marengo and Espinoza 2016).

The Amazon rainforest is more than a source of moisture for the tropical Andes, it is crucial for the establishment of the wet season circulation features such as the Bolivian High (Gill 1980; Eltahir 1996; Gedney and Valdes 2000; Rodwell and Hoskins 2001; Costa et al. 2021). Therefore, the Amazon and the Andes are tightly linked through atmospheric and surface processes conforming a coupled bio-geophysical system (Poveda et al. 2006; Builes-Jaramillo and Poveda 2018; Espinoza et al. 2020). Thus, the loss of the rainforest in the Amazon could have an impact on precipitation over the southern tropical Andes (Aide et al. 2019). This chapter explores the possible impacts of Amazonian deforestation on the mechanisms driving wet season precipitation over the tropical southern Andes. To this, we use two sets of model simulations forced with the same deforestation scenario but using different model configurations, geographical domains, horizontal resolutions and different time periods. The first is a 19-year simulation (2000-2019) with the Regional Earth System Model of the Institute Pierre Simone Laplace (RegIPSL). See Chapter 3 for the model configuration details. It is worth remembering that these simulations have a spatial resolution of 20 km and that they use the spectral nudging technique on temperature and winds, which restricts the response of our model to the deforestation signal over the upper troposphere. In addition, RegIPSL uses the complex surface model ORCHIDEE developed by the Institut Pierre Simon Laplace. On the other hand, we also implement simulations with the Weather Research and Forecasting Model coupled to the land surface model

NOAH, a simple land surface model developed by National Centers for Environmental Prediction (NCEP) in collaboration with other institutes. WRF-NOAH presents three one-way nested domains with horizontal grid sizes of 15 km, 5 km and 1 km (see Chapter 4 for details). However, in this chapter we only use model outputs form the two biggest domains.

This chapter is structured as follows. The reference datasets used and methods as well as the are described in section 5.2. Section 5.3 is addressed to model validation in terms of the representation of precipitation over the southern tropical Andes annual cycle and the dominant modes controlling the austral summer rainfall. In section 5.4, we evaluate the impacts of Amazonian deforestation on the southern Andes precipitation. Finally, section 5.5 presents a brief summary and discussion the main results.

5.2 Reference data and methods

5.2.1 Reference datasets

Mountain regions, especially the tropical Andes, present a low density of *in-situ* meteorological stations. For this reason, satellite estimations are commonly used in order to obtain a description of the spatial and temporal variability of precipitation in these areas. In the present study, we use precipitation from the Climate Hazard group Infrared Precipitation with Stations (CHIRPS) version 2 (Funk et al. 2015). This dataset mixes information from satellite measurements and rain gauges, and presents a spatial and temporal resolution of 5 km and 1 day, respectively (Funk et al. 2015). CHIRPS information is available from 1981 to near-present at https://data.chc.ucsb.edu/products/CHIRPS-2.0/ (last access August 2022). Many previous works have assessed the quality of CHIRPS estimations against terrestrial observations over the Amazon region (Wongchuig Correa et al. 2017; Haghtalab et al. 2020), and over the tropical Andes (Paccini et al. 2018; Segura et al. 2019, 2020).

As a reference information for atmospheric data we use reanalysis of the European Centre for Medium-Range Weather Forecast (ECMWF) ERA5 (Hersbach et al. 2020). This reanalysis presents a spatial resolution of 31 km, hourly information outputs and

137 hybrid sigma-pressure levels. Comparisons against radiosonde data have demonstrated significant improvements in the representation of the vertical moisture and wind distributions (Hoffmann et al. 2019; Hersbach et al. 2020). This data set is available at https://www.ecmwf.int/en/forec asts/datasets/reanalysis-datasets/era5 (last access August 2022).

5.2.2 Empirical orthogonal function

Previous studies demonstrated the inter-annual variability of the austral summer precipitation over the entire southern tropical Andes is controlled by the same mechanisms (Segura et al. 2019, 2020). For this reason, following Segura et al. (2020) we use the empirical orthogonal function (EOF) over normalized precipitation data from CHIRPS, RegIPSL-Control, RegIPSL-Deforested, WRF-Noah Control and WRF-Noah Deforested experiments independently in order to obtain the leading mode of the spatio-temporal rainfall variability during the austral summer (December-February, hereafter DJF). The normalization of precipitation is done over each grid-cell by subtracting the inter-annual mean and dividing by the inter-annual standard deviation of the DJF mean rainfall. Normalization allow us to avoid spurious influence of the strong west-east precipitation gradient on the EOF analysis. Hereafter we denote as PC1-Andes the first principal component of the DJF precipitation over the southern tropical Andes.

5.3 Results

5.3.1 Model validation

5.3.1.1 Precipitation annual cycle over the southern tropical Andes

Previous studies showed the highlands of the southern tropical Andes (above 3000 m) exhibit a similar precipitation variability at seasonal and inter-annual time scales (Segura et al. 2019). For this reason, we compute spatial averages of precipitation in the region. As described in the Introduction, according to CHIRPS, precipitation at the upper-elevation southern tropical Andes exhibits a strong seasonality. Of the 655 mm rainfall per year falling in average in the region, nearly 70%, or 461 mm fall between December and March (gray bars in Figure 5.1d). RegIPSL-Control overestimates

precipitation almost the entire year (in average about ~+22 mm or +12% per month), mainly between October and November (with an overestimation of +13 mm and 14 mm or +36% and 33%, respectively). However, the model properly represents the seasonality of rainfall in the region. In the model outputs, nearly 68% of the annual rainfall occur in the December-March period in agreement with satellite data (blue bars in Figure 5.1d). WRF-Noah shows a better representation of the rainfall magnitude in the region, with a slight underestimation (-23% or -30 mm for both model domains) during February. There are no significant differences in the average rainfall from domains 1 and 2. The magnitude of the inter-annual monthly rainfall variability is also well represented by the model as is evidenced by a direct comparison in the whiskers for CHIRPS and models outputs. WRF-Noah underestimates the variability what could be related with the shorter time period used in this model simulations.

5.3.1.2 Main drivers of DJF rainfall over the southern tropical Andes

In order to evaluate the representation of the main drivers of DJF rainfall in the southern tropical Andes, we analyze the model skill in reproducing the Bolivian High and the upward motion over the central and western Amazon (Figure 5.2). ERA5 reanalysis displays the anticyclonic circulation of the Bolivian High centered at 62◦W and 18◦S as described before. North of the anticyclonic center, easterly winds carry moisture toward the Andes mountains. In agreement with early theoretical works (Gill 1980; Silva-Dias et al. 1983), at the northeast of the Bolivian High center, over the central Amazonia, strong air masses ascension is observed at 500 hPa linked to deep convection (blue colors in Figure 5.2a). At lower levels, easterly winds enter to the continent from the Atlantic Ocean as part of the South American Monsoon System (SAMS) (Virji 1981; Rodwell and Hoskins 2001; Vera et al. 2006b; Figure 5.2b). It is thanks to the moisture transported by the low-level easterlies, in conjunction with water vapor from Amazonian evapotranspiration, that deep convection and heavy rainfall is sustained in the Amazon (Gibbs 1970; Rao et al. 1996; Vera et al. 2006b; Martinez and Dominguez 2014; Poveda et al. 2014; Ruiz-Vásquez et al. 2020). As a consequence of the Sverdrup vorticity balance, a northerly cross-equatorial flow is developed at the east of the Andes and favors the condensational heating and the upward air motion in the central Amazon (Rodwell and Hoskins 2001; Figure 5.2 b-c). This north-south cross-equatorial flow increases the moisture transport from the

Atlantic Ocean and enhances net moisture convergence in the region (Wang and Fu 2002; Li and Fu 2004).

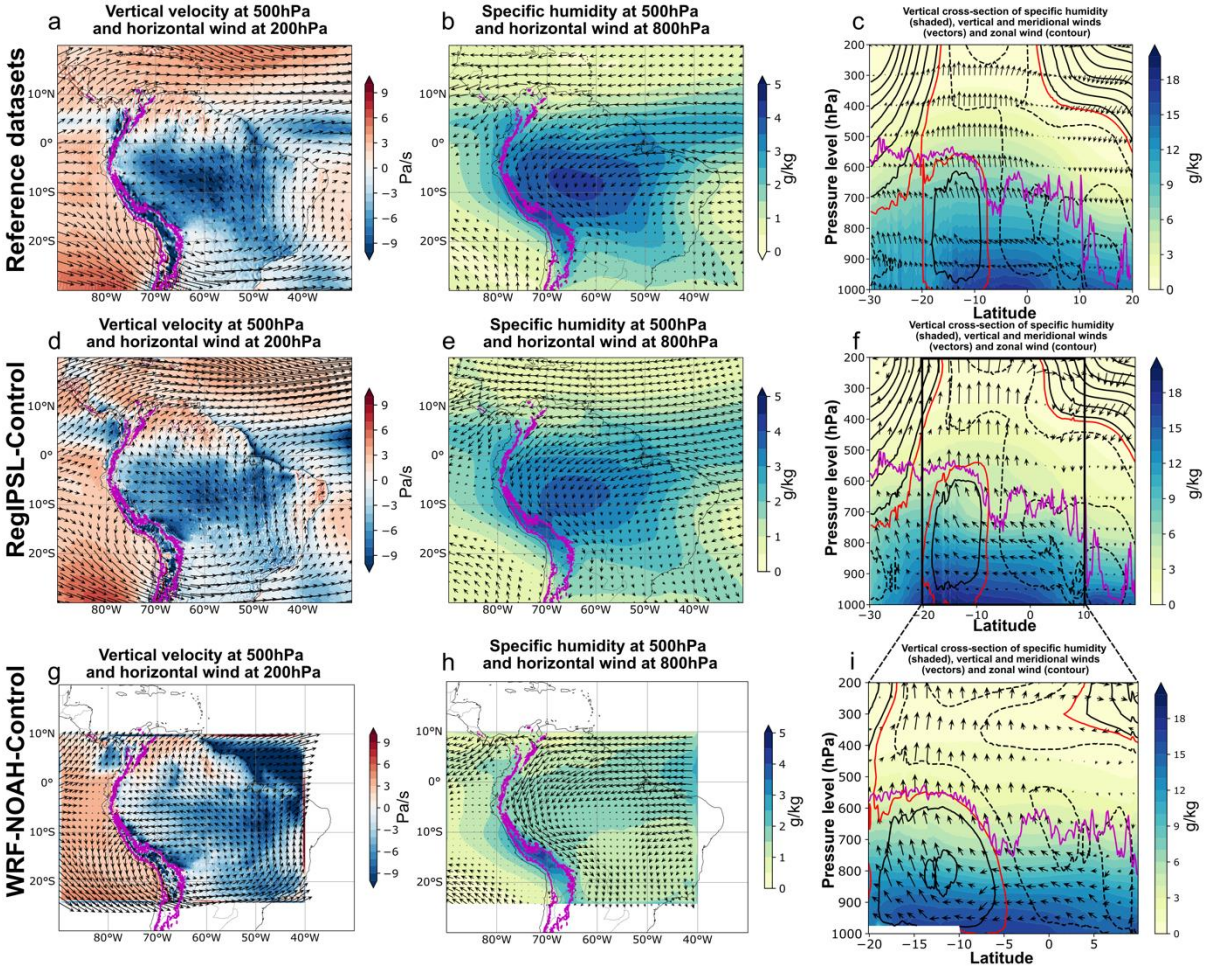

Fig. 5.2 December-February climatology of: **a-d-g** 500 hPa vertical velocity (shaded, units in Pa s^{-1}) multiplied by a factor of 100 and 200 hPa horizontal winds (vectors, units in m s^{-1}); **b-e-h** 500 hPa specific humidity (shaded, units in g kg^{-1}) and 800 hPa horizontal winds (vectors, in m s^{-1}); **c-f-i** Pressure-latitude cross-section of the zonally-mean meridional circulation in the tropical North Atlantic and western South America. Zonal-Mean is calculated over a region encompassing the easternmost side of the 3000 m elevation contour and the 60◦W. Meridional and vertical (multiplied by a factor of 100) components of the winds for vectors (in m s^{-1} and Pa s^{-1}, respectively), specific humidity (shaded, units in g kg^{-1}) and zonal wind in contour (solid lines represent positive/westerly winds and dashed lines represent negative/easterly winds; the red line shows the 0 m s^{-1} contour). Figures **a-b-c** correspond to ERA5 reference dataset, **d-e-f** depict atmospheric circulation for RegIPSL-Control outputs, and **g-h-i** shows outputs from WRF-Noah D1. Magenta line in Figures a-b-d-e represents the elevation contour at 3000 m a.s.l. Magenta line in Figures c-f shows the Andes' profile calculated as maximum orographic elevation in the Andes axis.

RegIPSL-Control is able to represent realistically the basic features of the SAMS. The location, magnitude and spatial structure of the Bolivian High is well displayed in the model simulation as expected taking into account the spectral nudging applied to horizontal winds at the upper troposphere (Figures 5.2d-f). Nevertheless, the anticyclonic circulation of the Bolivian High is slightly shifted westward in the model

outputs (Figure 5.2d). The spatial distribution of the vertical wind component is captured by the model, with strong ascending (descending) motion over the central Amazon, over the Andean summits, and over the eastern flank of the Andes in the Peruvian and Bolivian rainfall hotspots (northern South America and the western tropical South Atlantic Ocean). However, the ascension of air masses over the central Amazon is lightly underestimated by RegIPSL-Control. The low-level atmospheric circulation is reproduced by RegIPSL-Control, with easterly winds entering from the Atlantic Ocean and deviated southwards by the effect of the Andes barrier (Figure 5.2e). Maximum atmospheric moisture values are located over the central and western Amazon for both reanalysis and model data (Figures 5.2b-e). High specific humidity is also observed over the southern tropical Andes summits in both datasets as a result of the moisture transported by the upper-level easterlies. However, RegIPSL-Control underestimates the mid-tropospheric moisture of about -1 g kg^{-1} over the central and southern Amazon as displayed in Figure 5.2e. Finally, the latitudinal cross-section shows a well-represented structure of the regional Hadley cell, with strong convection and ascending motion between 0◦-20◦S. The solid and dashed contours exhibit also a good representation of the zonal circulation, with easterly winds north of 8◦S and westerly winds between 10◦S-20◦S. Nonetheless, there are issues in the vertical distribution of the specific humidity in RegIPSL-Control. In this dataset, maximum atmospheric moisture values are simulated far south around the 15◦S. At the same time, moisture is more restricted to the lower layers of the troposphere (Figure 5f).

WRF-NOAH, on the other hand, adequately represents the position and intensity of the winds associated with the Bolivian High (Figure 5g). Although the model represents the observed upwelling of air in the western Amazon basin, over the Amazon basin in general and over southeastern South America, it presents an overestimated (underestimated) ascending motion in eastern (western) Brazil. The model presents very strong ascending motion over the Atlantic Ocean linked to an overestimated moisture convergence and precipitation in the Atlantic ITCZ (see Chapter 4). At lower levels, WRF-NOAH properly reproduce the easterly winds entering from the tropical Atlantic, but it exhibits a too strong low-level convergence in central Brazil (Figure 5h). The mid-tropospheric moisture is heavily underestimated (~-2.5 g/kg) over the entire Amazon region. It is interesting to remark that over the southern tropical Andes region, the model is able to produce a humid air similar to

ERA5. This implies that WRF-NOAH is also able to represent the Bolivian High easterly wind mechanism which brings moisture from the Amazon region to this area. The regional Hadley cell is present in WRF-NOAH simulations, with a well-represented vertical structure of both the meridional and zonal winds. Similar to RegIPSL results, WRF-NOAH also keeps the atmospheric moisture in the shallower levels in comparison with ERA5 (Figure 5i), what could suggest this as a systematic bias in the WRF atmospheric model.

5.3.1.3 Inter-annual variability of precipitation over the southern tropical Andes

In order to assess the capacity of the model in reproducing the inter-annual rainfall variability over the southern tropical Andes, Figure 5.3 shows the time series of DJF rainfall and its first principal component according to CHIRPS and RegIPSL-Control. There is a high correlation (0.99) between southern tropical Andes rainfall and its first principal component in the satellite dataset as described before by previous works (Segura et al. 2019, 2020). For CHIRPS, around 57% of the variance is explained by the PC1-Andes. It is easy to note that for some years under the warm (cold) phase of El Niño Southern Oscillation such as 2002-2003, 2004-2005, 2006-2007, 2008-2009, 2014-2015 (2011-2012), negative (positive) rainfall anomalies are observed over the Andean region. The strong influence of the Pacific Ocean on the rainfall variability over the tropical Andes has been widely studied in the past (Aceituno and Garreaud 1995; Ronchail 1995; Lagos et al. 2008; Lavado-Casimiro et al. 2013; Imfeld et al. 2019). In general, more (less) precipitation is registered over the southern tropical Andes during La Niña (El Niño) years (Garreaud and Aceituno 2001; Vuille and Keimig 2004; Sulca et al. 2018).

RegIPSL-Control presents an adequate representation of the upper-Andean inter-annual rainfall variability, with a Pearson correlation of 0.76 between CHIRPS and the model time series (black lines in Figure 5.3a-b). The PC1-Andes and the rainfall over the southern tropical Andes are closely related in the model outputs with a Pearson correlation coefficient of 0.88 as in observations. Figure 5.4 presents the same analysis but for WRF-NOAH using rainfall simulated with 15 km grid size for domain 1 and 5 km grid size for domain 2. The correlations between CHIRPS (using the same time period of WRF-NOAH) and WRF-NOAH over the domains 1 and 2 are relatively

low (0.32 and 0.12, respectively). Nevertheless, the variance of the spatially averaged precipitation over the southern tropical Andes is highly correlated with the PC1 (0.80 and 0.70 for domains 1 and 2, respectively). For this reason, in the next analysis we use PC1-Andes in both model and reference data to summarize the rainfall variability at inter-annual timescales.

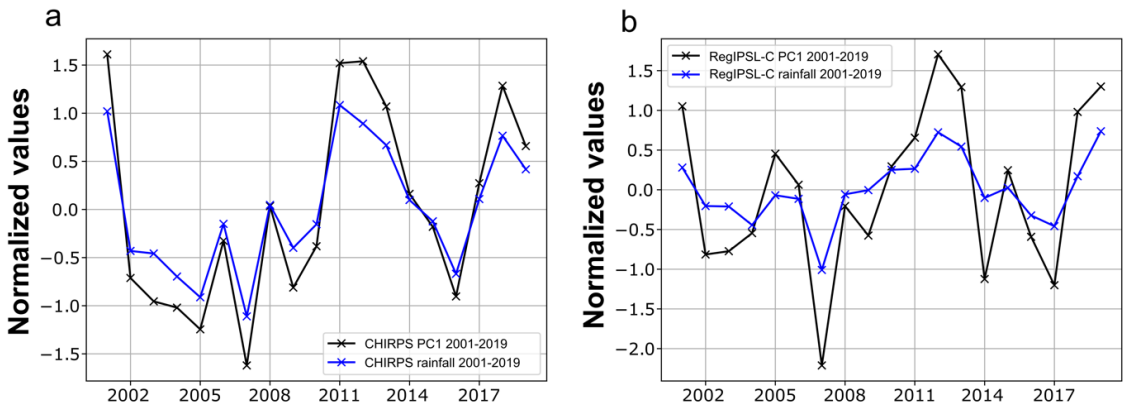

Fig. 5.3 First principal component (labeled as PC1-Andes) of the December-February precipitation spatially averaged over the southern tropical Andes (black line) and the mean normalized December-February precipitation spatially averaged over the southern tropical Andes (blue line) for: **a** CHIRPS and **b** RegIPSL-Control.

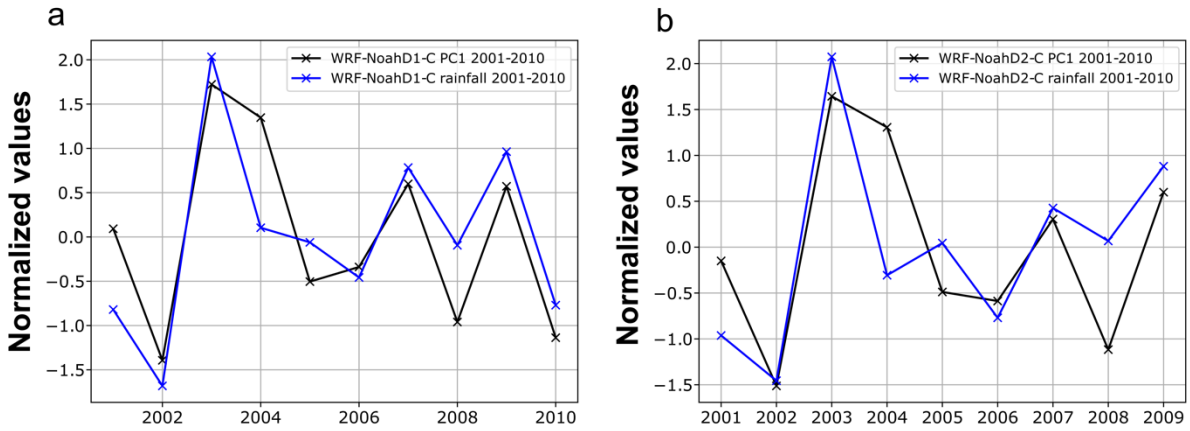

Fig. 5.4 First principal component (labeled as PC1-Andes) of the December-February precipitation spatially averaged over the southern tropical Andes (black line) and the mean normalized December-February precipitation spatially averaged over the southern tropical Andes (blue line) for WRF-NOAH rainfall from domain 1 (**a)** and domain 2 (**b**).

The validation of the model is completed with an evaluation of the relation between DJF precipitation and zonal winds at 200 hPa, as well as vertical wind at 500 hPa, which are considered the main atmospheric phenomena leading the inter-annual fluctuations of precipitation in the interest region (see Section 5.1). CHIRPS/ERA5

exhibits a slight significant negative correlation (~-0.5) between the zonal winds and the rainfall PC1-Andes over the western coast of northern Chile and southern Peru (Figure 5.5a). Stronger westerly (positive zonal winds) winds coming from the Pacific Ocean are therefore linked to negative rainfall anomalies over the southern tropical Andes. However, as discussed before, this relationship has weakened since the year 2000, what explains the low correlation values. Stronger correlations are observed between the vertical component of the wind and PC1-Andes (Figure 5.5b). Negative correlations of about -0.7 and -0.8 are recorded by CHIRPS/ERA5 over the western Amazon, meaning that a stronger ascending motion (negative values of vertical velocity) is related with increased precipitation over the tropical Andes.

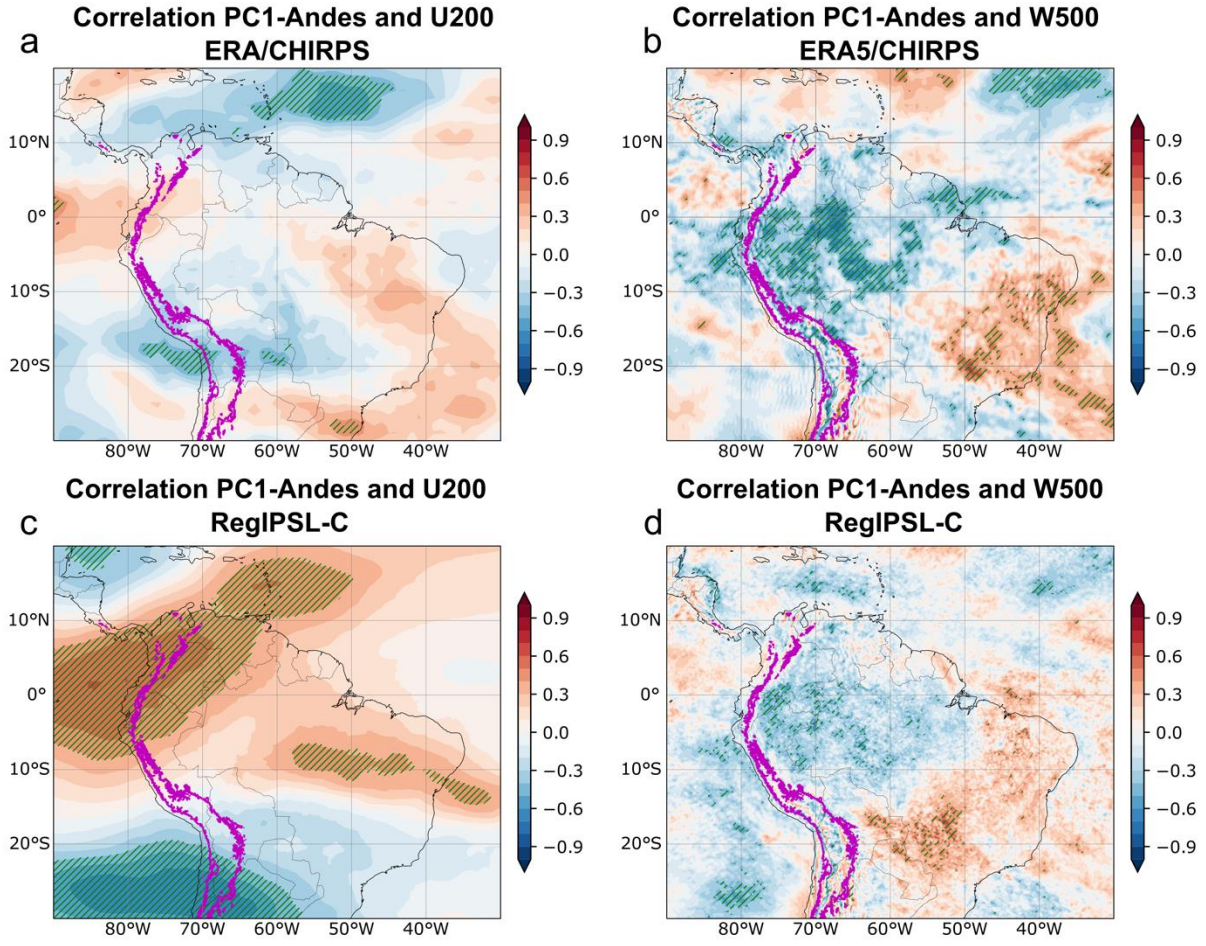

Fig. 5.5 Correlation maps between the first principal component (PC1-Andes) of the December-February precipitation spatially averaged over the southern tropical Andes and: **a-c** DJF zonal winds at 200 hPa (U200); **b-d** DJF vertical component of the wind at 500 hPa (W500) for CHIRPS/ERA5 (**a-b**) and RegIPSL-Control (**c-d**) during the period 2001-2019. Magenta line represents the elevation contour at 3000 m a.s.l. Green slashes show significant correlations at the 90% confidence-level.

RegIPSL-Control exhibits a completely different correlation field between PC1-Andes and the upper-level zonal winds, with positive (negative) correlation coefficient over the northern South America (south of 20◦S over western South America; Figure 5.5c). Nevertheless, this mechanism has lost prominence since the 2000's (Segura et al. 2020). Thus, we will focus on the second and more important process, the relationship between vertical wind and Andean precipitation. RegIPSL-Control displays a realistic spatial correlation distribution between PC1-Andes and the vertical component of the wind at the mid-troposphere, with negative (positive) values over the northwestern and central Amazon (south eastern South America and eastern Brazil; Figure 5.db). Significant, although underestimated, correlations are located over the western Amazon as observed in reference datasets.

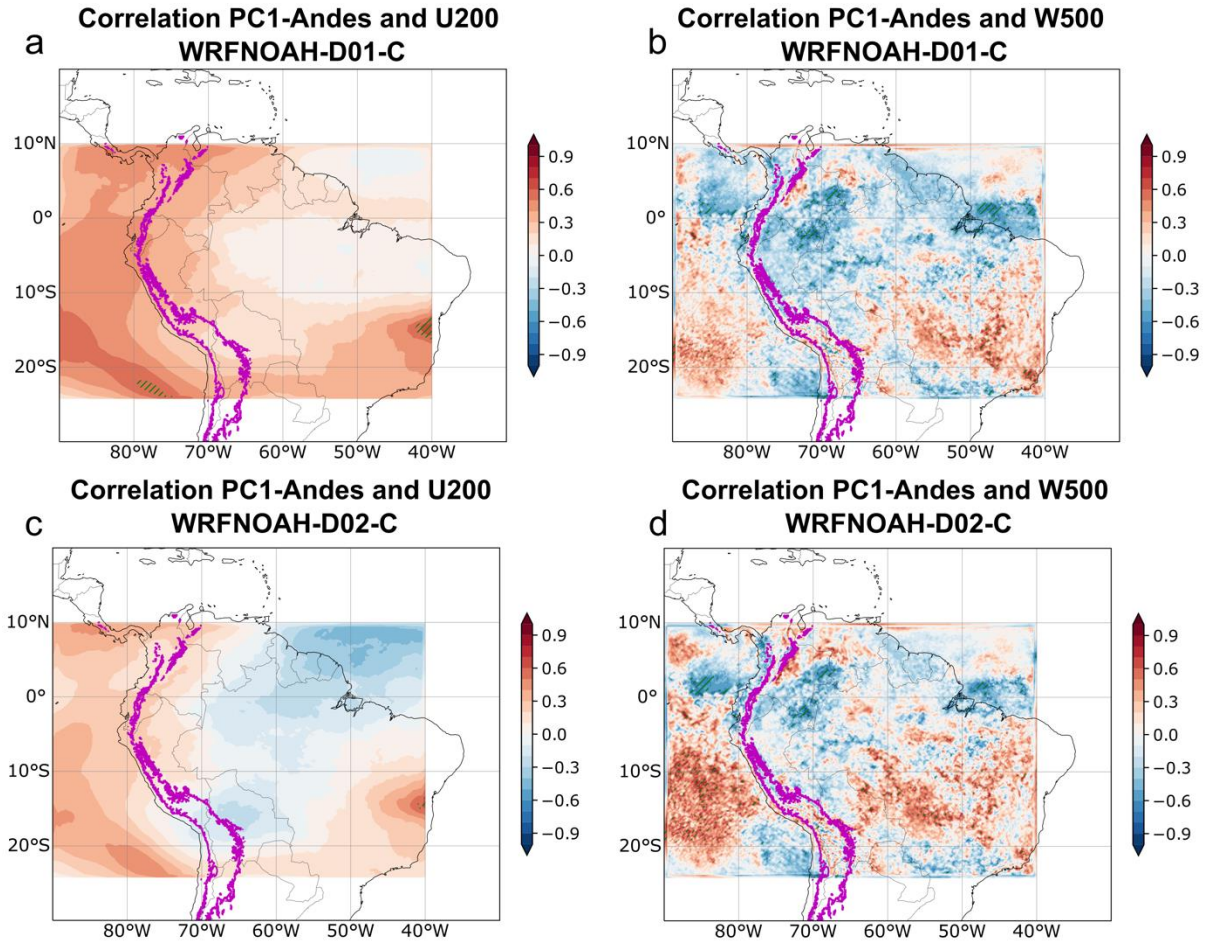

Fig. 5.6 Correlation maps between the first principal component (PC1-Andes) of the December-February precipitation spatially averaged over the southern tropical Andes and: **a-c** DJF zonal winds at 200 hPa (U200); **b-d** DJF vertical component of the wind at 500 hPa (W500) for WRF-NOAH domain 1 (**a-b**) and WRF-NOAH domain 2 (**c-d**) during the period 2001-2011. Magenta line represents the elevation contour at 3000 m a.s.l. Green slashes show significant correlations at the 90% confidence-level.

Figure 5.6 shows the simulated relationship between the first principal component of the southern Andes rainfall and horizontal winds at 200hPa and the vertical component of the wind at 500hPa but for the model WRF-NOAH using rainfall outputs from domains 1 (Figures 5.6a-b) and 2 (Figures 5.6c-d). WRF-NOAH D1 is not able to represent the covariance of the rainfall and the Bolivian High easterly winds. However, it is very interesting to note that, when resolution is enhanced in domain 2, WRF-NOAH properly captures a signal of negative correlation between these two variables similar to ERA5 and CHIRPS over the Altiplano and the northeastern part of tropical South America (Figures 5.6a-c). The correlation between mid-tropospheric ascending motion in the western and central Amazon with rainfall in the southern tropical Andes is equally well represented by WRF-NOAH over the two domains, with statistically significant values even the short time period analyzed. Summarizing, both RegIPSL and WRF-NOAH are capable of reproducing the inter-annual covariance between DJF Andean precipitation and the ascending motion of airmasses over the western Amazon.

5.3.2 Effects of Amazonian deforestation on the southern tropical Andes rainfall

Under normal conditions, the total austral summer rainfall exhibits a north-south dipole with more (less) precipitation over the Peruvian (Bolivian) Andes in both reference datasets (CHIRPS) and models (RegIPSL-Control, WRF-NOAH-D1 and WRF-NOAH-D2) (Figures 5.7a-b-c-d). While RegIPSL overestimates DJF rainfall over almost the entire Peruvian Andes, WRF-NOAH underestimates this variable un the southern and western parts of the interest region. Different studies have demonstrated climate models present a better representation of the physical mechanisms leading precipitation than the precipitation itself (Leung and Qian 2009; Gutowski et al. 2010; Glisan and Gutowski 2014). Consequently, although we analyze changes in rainfall, we focus mainly on changes in the underlying physical mechanisms in the deforested scenario. Deforestation alters the spatial pattern of the DJF precipitation over the southern tropical Andes in different manners for both models. For RegIPSL, a rainfall decrease is observed over the northwestern side of the south tropical Peruvian Andes and increasing it over the southern and eastern parts of the region (Figure 5.7e). The western flank of the southern tropical Andes is a region particularly sensitive to

changes in the austral summer precipitation (Buytaert and De Bièvre 2012; Schoolmeester et al. 2018). An opposite deforestation change in austral summer is present in WRF-NOAH with more (less) rainfall in the western (eastern) Andean flank. Although these changes are not statistically significant, this spatial gradient in the rainfall alterations demonstrates that there is not a homogenous effect of Amazonian deforestation in the precipitation of the region.

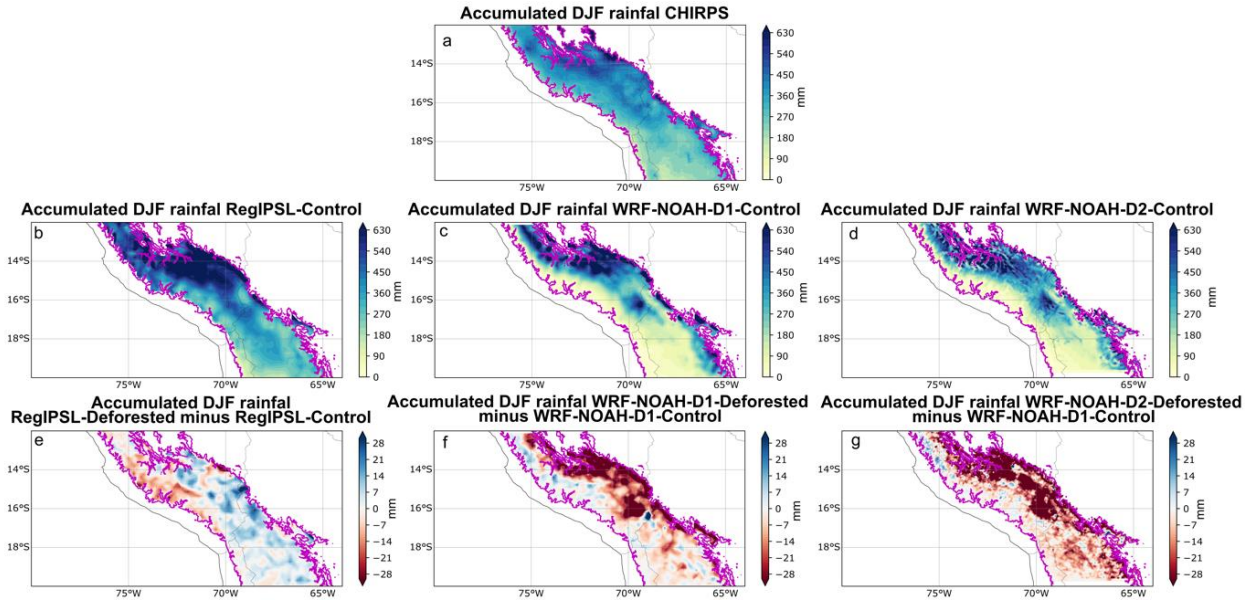

Fig. 5.7 DJF total rainfall climatology over the southern tropical Andes for: **a** CHIRPS, **b** RegIPSL-Control, **c** WRF-NOAH-D1-Control (over domain 1) and **d** WRF-NOAH-D2-Control (over domain 2). DJF total rainfall climatology differences deforested minus control experiment for: **e** RegIPSL, **f** WRF-NOAH-D1 and **g** WRF-NOAH-D2. The magenta line highlights the 3000 m elevation contour. Precipitation values are in mm.

Figure 5.8 shows the simulated changes in the main atmospheric drivers for the southern tropical Andes DJF rainfall. No significant perturbations are simulated for the Bolivian High circulation under the deforestation scenario (vectors in Figure 5.8a) by RegIPSL. Nevertheless, since our control and deforested experiments are forced with a spectral nudging over the upper-level horizontal wind field, it is expected to have no significant changes in this variable at the upper troposphere for RegIPSL. WRF-NOAH exhibits important changes in the upper level circulation that can be understood as a weakening of the Bolivian High (Figure 5.8b). North of 10◦S, a westerly anomaly is observed in the deforested scenario what suggest lower easterly winds coming from the Amazon toward the southern tropical Andes highlands. As demonstrated in Chapter 4, this weakening of the Bolivian High anticyclonic circulation is caused by a

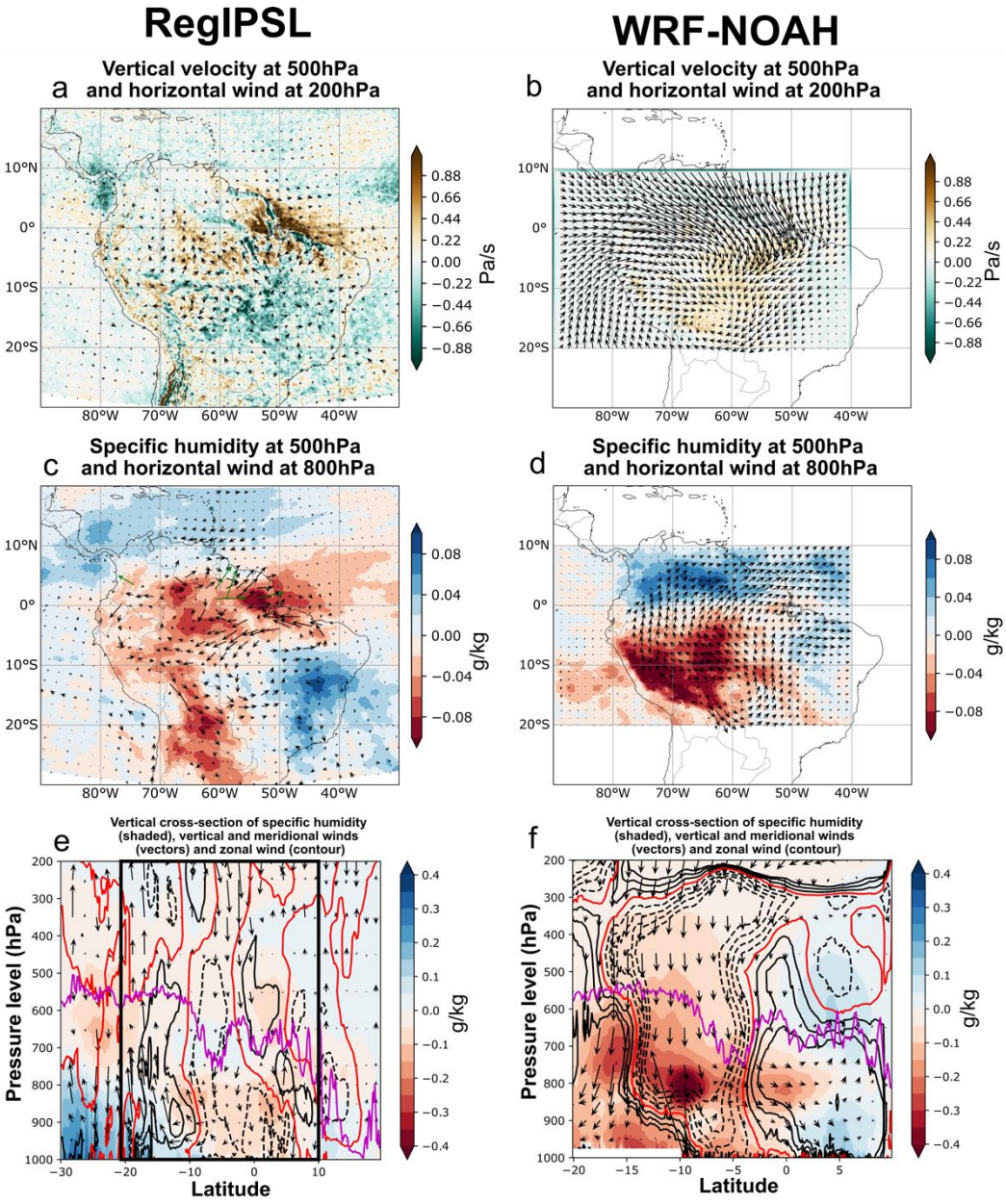

Fig. 5.8 December-February climatological differences Deforested minus Control for RegIPSL (**a-c-e**) and WRF-NOAH (**b-d-f**) in: **a-b** 500 hPa (vertical velocity shaded, units in Pa s^{-1}) multiplied by a factor of 100 and 200 hPa horizontal winds (vectors, units in m s^{-1}), **c-d** 500 hPa specific humidity (shaded, units in g kg^{-1}) and 800 hPa horizontal winds (vectors, in m s^{-1}), **d-e** pressure-latitude cross-section of the zonally-mean meridional circulation in the tropical North Atlantic and western South America. Zonal-Mean is calculated over a region encompassing the easternmost side of the 3000 m elevation contour and the 60◦W. Meridional and vertical (multiplied by a factor of 100) components of the winds for vectors (in m s^{-1} and Pa s^{-1}, respectively), specific humidity (shaded, units in g kg^{-1}) and zonal wind in contour (solid lines represent positive/westerly winds and dashed lines represent negative/easterly winds; the red line shows the 0 m s^{-1} contour). Magenta line in **e-f** shows the Andes' profile calculated as maximum orographic elevation in the Andes axis. The black rectangle in **e** represents the area shown in **f.**

loss of energy in the surface caused by deforestation and is in agreement with theoretical works (Gill 1980; Eltahir 1996). On the other hand, important changes in

the mid-tropospheric vertical component of the wind are induced by the Amazonian deforestation for both models (shaded values in Figures 5.8a-b). In general, deforestation decreases the ascending motion over the central and western Amazon and increases the vertical velocity in the southern Amazon basin and southeastern Brazil in RegIPSL simulations. WRF-NOAH displays a similar result, with a reduction (increasing) in the vertical velocity over the central and western Amazon (southeastern Brazil) generates a drying (moistening) of the mid-troposphere in the deforestation experiment as evidenced in Figures 5.8c-d. At the same time, a reduction in the vertical wind could also imply a decrease in precipitation over the southern tropical Andes for both model results (Segura et al. 2020).

At lower levels, the easterly winds entering to the continent from the Atlantic Ocean north of the equator deaccelerate in the deforestation experiment for both models (Figures 5.8c-d). However, the reduction in the surface roughness length caused by the forest lost generates a low-level wind acceleration in the deforestation scenario over the cleared areas south of the equator in RegIPSL (vectors in Figure 5.8c). WRF and RegIPSL agree that below the equator, moisture from the South Atlantic is trapped over eastern Brazil due to wind deacceleration. Similarly, in these models the north-south flow below 10◦S accelerates but apparently related to different causes in both simulations. While RegIPSL presents enhanced easterly winds over the deforested areas that that subsequently are blocked by the Andes barrier and are deviated southward increasing the north-south flow (Figures 5.8c-e), in WRF-NOAH there is a large-scale subsidence over the Amazon region what generates a positive pressure anomaly (not shown) in the lower atmosphere and wind divergence over the southwestern Amazon (15◦S-65◦W) driving north-south flow (Figures 5.8d-f). These enhanced easterly winds over the deforested patches are also visible in the pressure-latitude cross-section over the eastern flank of the Andes as more negative zonal winds (dashed contours) between 10◦S and the equator in both models (Figures 5.8e-f). Since the enhanced southward flow in RegIPSL comes from the winds entering the continent from the Atlantic Ocean, these winds transport moisture from the Amazon toward southern latitudes. Thus, a moister low troposphere is simulated by RegIPSL-Deforested below the 800 hPa level and south of 10◦S (Figure 5.8e). A similar alteration in the low-level circulation under deforestation experiments has been reported in several previous works (Eiras-Barca et al. 2020; Ruiz-Vásquez et al. 2020).

Conversely, since the southerly anomalous flow in the WRF-NOAH deforested experiment parts from the southern Amazon, these winds don't carry moisture toward the southern latitudes (Figure 5.8f). It is interesting to note that RegIPSL, like WRF-NOAH, also presents a weakening of the ascending motion of air masses over the central and western Amazon what is observed as a subsidence between 10◦S and the equator in Figure 5.8e. However, between 15◦S-20◦S, vertical wind is strengthened by the enhanced north-south flow in the deforestation simulation.

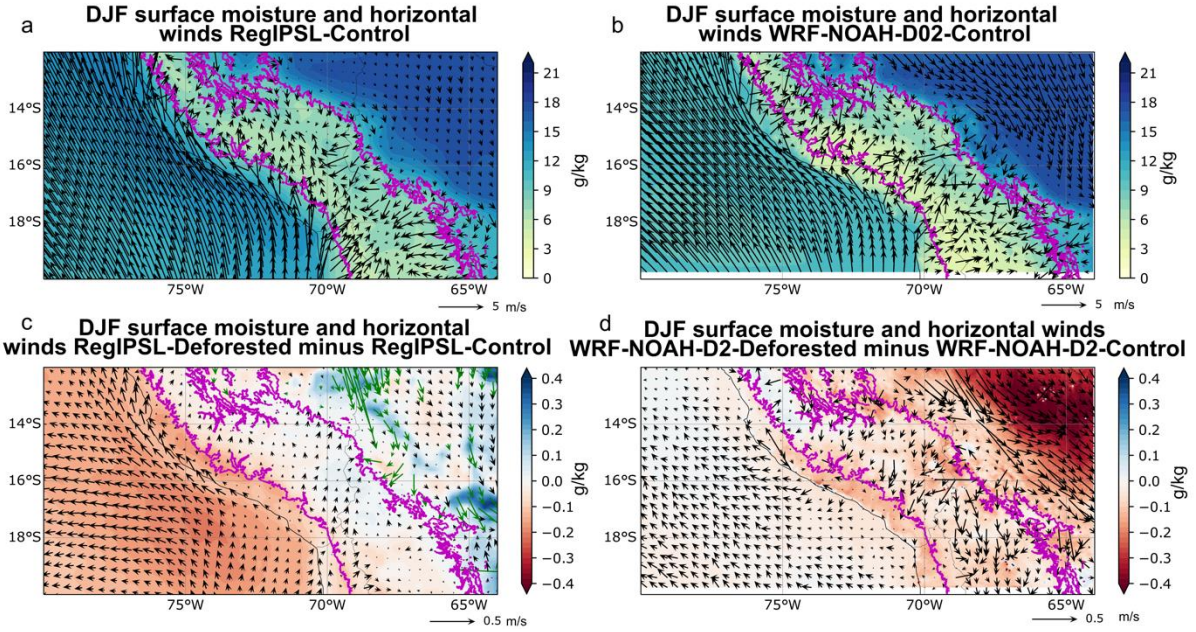

Fig. 5.9 December-February climatological specific humidity at 2m and horizontal winds at 10m for **a** RegIPSL-Control and **b** WRF-NOAH-D2-Control. Differences **c** RegIPSL-Deforested minus RegIPSL-Control and **d** WRF-NOAH-D2-Deforested minus WRF-NOAH-D2-Control in specific humidity at 2m and horizontal winds at 10m. Specific humidity (shaded) has units in g kg^{-1} and horizontal winds (vectors) has units in m s^{-1}. Significant changes in horizontal winds are marked as green vectors (plevel <0.05). The magenta line highlights the 3000 m elevation contour.

Precipitation over the upper part of the southern tropical Andes is also influenced by local processes such as mechanical channelization (Egger et al. 2005; Junquas et al. 2018). This mechanically driven circulation transport moisture from the humid Amazon lowlands to the Andes highlands (Figures 5.9a-b). The stronger northerly flow over the eastern flank of the Andes in the deforestation scenario boosts the upslope circulation in some passes of the eastern Andean valleys, increasing the surface moisture transport toward the Andean summits in RegIPSL (Figure 5.9c). Conversely, for WRF-NOAH, deforestation increases the northwest-southeast flow over the eastern side of the Andes, but this circulation doesn't enter toward the Andes valleys (Figure 5.9d).

The strengthening channelization in RegIPSL occurs mainly near the Peruvian-Bolivian border and over the Bolivian Andes where precipitation slightly increases in RegIPSL-Deforested simulations (Figure 5.7e).

During the austral summer, the moistening of the middle troposphere increases the equivalent potential temperature and decreases the stability between the mid and upper troposphere. This thermodynamic process enhances deep convection in the Amazon (Scala et al. 1990; Fu et al. 1999; Zhuang et al. 2017; Segura et al. 2020). Since the upward motion over the western Amazon is closely linked with precipitation in the southern tropical Andes (Segura et al. 2020), we assess the changes induced by deforestation in the regional mid-tropospheric stability. Following the methodology described by (Sierra et al. 2021; see Chapter 4), we separate the individual impact of temperature and moisture deforestation-induced changes on the atmospheric stability index.

In RegIPSL outputs, deforestation increases the atmospheric stability in the central and northern Amazon, the eastern flank of the Andes and over the tropical Andes with the exception of the Altiplano plateau near the 18◦S-72◦W (Figure 5.10a). As a consequence, in these areas, the development of deep convection is constrained under the deforestation experiment. Perturbations in the regional atmospheric stability are related to the increase in precipitation (Figure S1) and mid tropospheric ascending motion (Figure 5.8a) induced by deforestation over the eastern Brazil, as well as with the precipitation and vertical velocity decrease over the central Amazon. It is interesting to note that atmospheric stability also increases east of the Andes for all latitudes (Figure 5.10a). Nevertheless, precipitation slightly increase over most of this area (Figure C1) probably due to the enhanced low-level moisture transport from the Atlantic Ocean caused by the reduction in the surface roughness length (Figure 5.8c).

The main contributor to the higher stability and reduced tendency to develop deep convection in the 5◦S -10◦S band and over the eastern Andean side is the drier mid-troposphere as is evidenced in Figure 5.10b. Changes in the potential temperature in the deforestation experiment play a minor role in the stabilization of the middle and upper troposphere. In general, these alterations inhibit (enhance) convection over the Amazon and the northern part of South America (southeastern South America, the

southern 20◦S-30◦S Andean summits and the south eastern Brazil) (Figure 5.10c). The potential temperature stabilization increase over the Amazon region is caused by a deforestation-induced cooling in the mid-troposphere and a warming at the 200 hPa level (not shown).

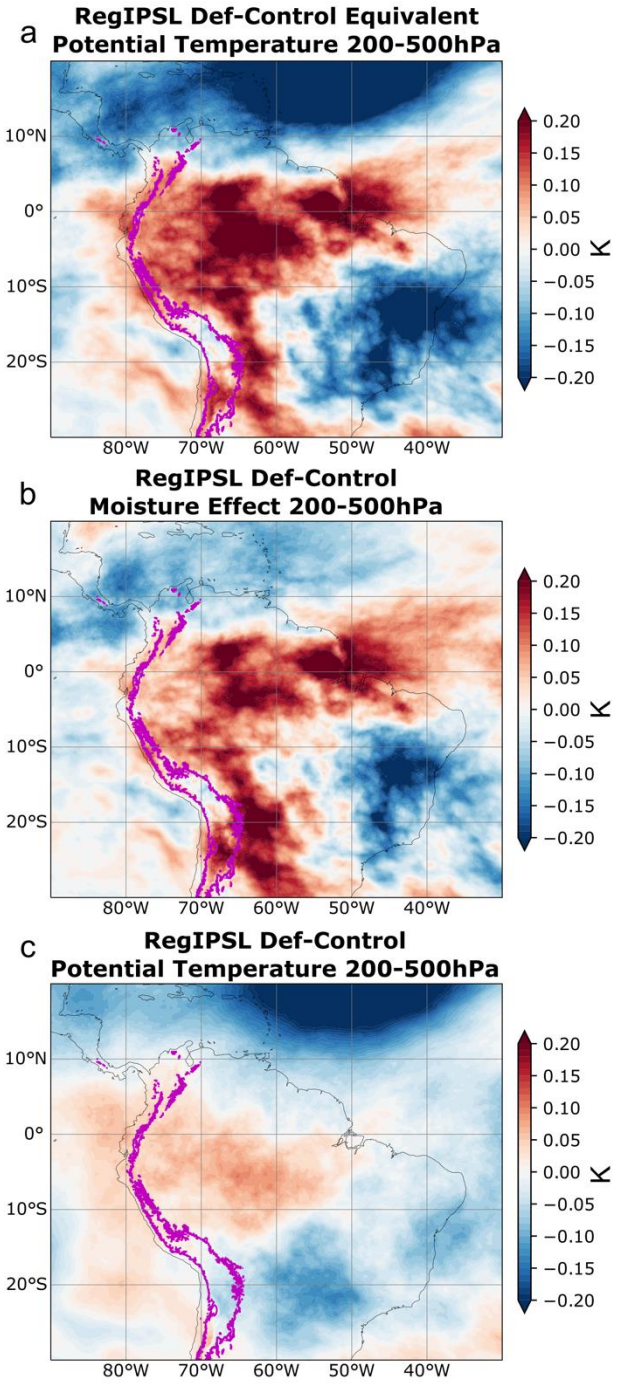

Fig. 5.10 December-February climatological differences Deforested minus Control in the atmospheric stability index: **a** Equivalent potential temperature 200-500 hPa; **b** moisture effect 200-500 hPa component; **c** potential temperature at 200 hPa minus potential temperature at 500 hPa component. All figures are in K. The magenta line highlights the 3000 m elevation contour.

WRF-NOAH exhibits different changes in the atmospheric stability with a more stable mid-troposphere over the western Amazon and the tropical Andes in the 5◦S-15◦S latitudinal band (see Figure 4.6 in Chapter 4). Contrary to RegIPSL, the adiabatic effect of changes in potential temperature destabilizes the atmosphere over the entire region due to increased atmospheric cooling in the upper troposphere (Figure 4.6b in Chapter 4). However, for RegIPSL, the effect of deforestation is to stabilize the troposphere thanks to a generalized cooling (Figure 5.10c). The loss of moisture in the troposphere under the deforested scenario generates greater stability in both models, mainly in the western Amazon. This result is related to the subsidence anomalies presented by both models over this particular area.

Summarizing, according to different model configurations, deforestation generates two different and opposite effects on the precipitation over the southern tropical Andes. First, WRF-NOAH and RegIPSL agree that deforestation induces important changes in the upward wind motion, mid-tropospheric moisture and atmospheric stability in the region. The combination of a drier and cooler mid-troposphere generates more stable conditions in the whole Amazon basin. A decrease in the ascending motion over the western and central Amazon could suggest a decrease in rainfall over the southern tropical Andes in both models. Indeed, over the tropical Andes, deforestation increases the stability except over the Andean Altiplano in RegIPSL, where the atmospheric stability is decreased favoring the convective activity. Secondly, the reduction in the surface roughness length over the deforested areas generates an acceleration of the low-level easterly winds entering to the continent from the Atlantic Ocean. As a result, an enhanced surface moisture transport toward the eastern side of the Andes and toward the southern latitudes is simulated only by RegIPSL-Deforested. Mechanical channelization of this moisture flow from the Amazon lowlands toward the Andes highlands is strengthened only in a specific latitudinal range of the southern tropical Andes, particularly between 15◦S-20◦S. It is precisely over this latitudinal band where the atmospheric stability is reduced favoring the development of convection. These atmospheric mechanisms are not independent and act together, what makes difficult to find out the causal relation between them. Through modelling experiments, it has been suggested that although the main mechanism for generating precipitation in the southern tropical Andes highlands is the thermally driven circulation, the latent heat release strengthens the convective activity in the

region (Junquas et al. 2018). For this reason, an increase in precipitation in this part of the tropical Andes implies more diabatic heating and could enhance the moisture transport from the lowlands and enhance the channelization effect.

5.4 Conclusions

The present chapter evaluates the potential impacts of Amazonian deforestation on the austral summer precipitation over the southern tropical Andes. This goal is addressed through 19-year climate simulations (2001-2019) with the Earth system regional climate model RegIPSL and 10-year simulations (2001-2011) with WRF-NOAH coupled model for a control and a deforested experiment. The annual cycle, spatial distribution of DJF precipitation and the inter-annual variability of rainfall over the southern tropical Andes are compared to CHIRPS data in order to validate the models. Both RegIPSL and WRF-NOAH exhibit a good representation of all the characteristics of precipitation in the interest region. However, RegIPSL (WRF-NOAH) overestimates (underestimates) rainfall during most of the year, particularly during January-February and October-November (December). Using wind information from ERA5 reanalysis, in conjunction with rainfall information from CHIRPS, we also evaluate the model skill to reproduce the inter-annual covariance between rainfall-upper easterly winds, and rainfall-western Amazon mid-tropospheric ascending motion. Although RegIPSL fails in capturing the relation between rainfall and the upper easterly flow part of the Bolivian High, recent works demonstrated that this mechanism have lost importance in leading the rainfall inter-annual variability of the southern tropical Andes. WRF-NOAH presents a realistic representation of the upper easterlies and rainfall covariance mainly using rainfall simulated over the 5 km gridsize domain. Year-to-year fluctuations of precipitation over the southern tropical Andes are dominated by the ascension of air masses over the western and central Amazon since the 2000's (Segura et al. 2020). Both models properly represent this last mechanism, although underestimate the strength of the correlation between rainfall and the vertical component of the wind.

Deforestation weakens the convection over central and western Amazon while enhances it over the south eastern Brazil for both models. Although less ascending motion over the Amazon would imply a reduction in the southern tropical Andes region,

we find reductions in this region only in WRF-NOAH and in the northwestern part of the interest region for RegIPSL. Thanks to its dry conditions and its strong dependence on austral summer rainfall, this region is particularly sensitive to deforestation induced changes. We find two mechanisms that could partially explain these alterations in the DJF precipitation. At a regional scale, the decrease in the mid-tropospheric vertical wind over central and western Amazon dries and cools the troposphere for the two analyzed models. As a consequence, atmospheric stability increases in most of the continent (except in the south eastern Brazil) and particularly in the western Amazon and the Andean summits with an exception of the Andean Altiplano. Over the southern tropical Andes, there is a disagreement between the two climate models in the precipitation changes. In the RegIPSL deforestation scenario, the low-level easterly winds coming from the Atlantic Ocean accelerates thanks to the less surface roughness length induced by the forest-to-crop conversion. The surface moisture transport towards the eastern flank of the Andes and the southern parts of tropical South America is stronger in the deforested scenario generating a strengthening in the mechanically driven channelization over the eastern Andean valleys and causing a slightly increase in precipitation and surface moisture over the southern and eastern parts of the interest region. Increased moisture there seems to lead to reduction in the atmospheric stability. Hence, both mechanisms could be related but further analysis should be carried out in order to identify causal effects. On the other hand, WRF-NOAH displays a strong reduction in precipitation over the southern Andes due to a weakening in the vertical component of the wind in the western Amazon and in the Bolivian High easterlies. The discrepancy between the two models on the changes in the mechanical channeling of superficial winds over the valleys of the eastern Andes appears to be related to the sensitivity of the models' response to parameters such as albedo and surface roughness. Sensitivity analyses on these parameters should be performed to gain an understanding of the possible impacts of deforestation in the area.

6

Conclusions and perspectives

Contents

6.1 Conclusions

The principal scientific question of this work is: *How can Amazonian deforestation impact the Amazon-Andes hydro-climatic connectivity?*

The potential effects that Amazonian deforestation can have on the climate at continental and global scales is a widely explored research topic since the late 1980's as a response to the intense forest loss during the 1970's decade. Despite more than 3 decades of research, there are still many questions that remain unanswered. It is well known in the scientific literature that there is a strong connection between the Amazon rainforest and the tropical Andes in terms of water, energy and nutrients exchange. However, it has been poorly explored the alterations that Amazon forest loss can impinge on this bio-geophysical system. The following questions arise from this issue:

- What is the impact of Amazonian deforestation on the synoptic and recurrent atmospheric circulations in the tropical South America?
- How the Amazon rainforest loss can affect the onset and development of the southern Amazon wet season?
- Is there a differential role between forest and croplands/grasslands in the onset and development of the wet season in the southern Amazon? If yes, what is the particular contribution of croplands/grasslands to the onset and development of the wet season in the southern Amazon?
- How Amazonian forest clearance can impact the rainfall over the Amazon-Andes transition region (particularly over the eastern flank of the Andes and the Peruvian and Bolivian rain/biodiversity hotspots)?
- What could be the possible effects of Amazonian logging on the austral summer precipitation over the highlands of the southern tropical Andes?

After the introduction and discussion about the motivation of this work (Chapter 1 and Chapter 2), in the first part of the thesis (Chapter 3), we investigated the impacts of Amazon deforestation on the dominant modes of the regional atmospheric circulation (a.k.a. circulation patterns or 'CPs'). We use this CPs and its deforestation-induced

changes as a tool to assess the perturbations in the initiation and evolution of the rainy season in the southern Amazon. To this end, we implement simulations with a control and a deforestation scenario with the Regional Earth System Model from the Institute Pierre Simone Laplace (RegIPSL). The projected forest-to-cropland conversion over the Amazon is not a forcing strong enough to create a completely new atmospheric circulation regime specific to the deforested conditions. Instead of this, deforestation modifies the wind and precipitation fields of the existent circulation patterns. Although the major changes occur during the austral summer (December-January-February, DJF), as a weakening of the South Atlantic Convergence Zone (SACZ) and the South American Low-level Jet (SALLJ) circulations, slighter but equally important perturbations take place during the dry-to-wet transition season. The conjunction of DJF changes and alterations in the frequency of occurrence and low-level spatial wind distribution of the characteristic wet season onset circulation pattern suggest a delayed wet season onset under the deforestation experiment.

Forest and crops over the southern Amazon present different contributions to the rainy season onset in the region. While croplands/grasslands exhibit a stronger shallow convection, forced by higher surface temperatures, the still remaining dry season large-scale subsidence inhibits convection over most of the area with the exception of forested areas where the atmosphere presents more convective potential energy. Our results suggest that the thermally induced upward vertical wind anomalies over crop areas can be transported by the large-scale base flow toward forested areas where they can grow and trigger deep convection, establishing the wet season onset. Extensive deforestation causes a less heterogenous land cover over southern Amazonia, what reduce this cropland-forest complementary effect to develops convection in the early stage of the wet season and could explain the late onset under deforested conditions.

Precipitation diminishes over the eastern flank of the Andes during the dry-to-wet transition period as a consequence of modifications in the regional atmospheric circulation. This region (a.k.a. Amazon-Andes transition region) is particularly sensitive to forest loss due to its high percentage of recycled precipitation and to its great biological species richness (Eltahir and Bras 1994; Myers et al. 2000; Dirmeyer and Brubaker 2007; Killeen et al. 2007b; Hoorn et al. 2010; Espinoza et al. 2015; Staal et

al. 2018). Therefore, the second part of this thesis is intended to assess the consequences of Amazonian rainforest loss on the hydro-climatic connectivity between the Amazon and the eastern tropical Andes.

The second stage of the present work (Chapter 4) is based on convective-permitting climate simulations with the Weather Research and Forecasting Model (WRF). The use of high-resolution climate simulations allows us to study the evolution of deforestation impacts from the synoptic and regional scale to the local scale in two instrumented Andean valleys in Bolivia (Zongo and Huarinilla valleys). We conclude that Amazonian deforestation generates profound alterations in the surface energy balance and the atmospheric circulation during the austral summer at regional scale. The forest loss reduces the net surface energy due to the effect of increased albedo. This energy depletion, together with a decrease in evapotranspiration, results in less moisture convergence and precipitation over the Amazon basin. As a result, deforestation dries and cools the troposphere, generating a subsidence in the central Amazon and a weakening of the regional Hadley circulation in agreement with early theoretical works (Gill 1980; Eltahir 1996; Zeng and Neelin 1999). Consequently, the characteristic austral summer north-to-south moisture flow weakens. Over the eastern Andean piedmonts, deforestation reduces precipitation during nighttime in about -20% to -30% due to a decreased moisture transport from the Amazon lowlands toward the Andean summits by the SALLJ circulation. Since nocturnal rainfall in the region accounts for 70-80% of summer precipitation (Perry et al. 2014; Chavez and Takahashi 2017), this rainfall depletion seriously threats the regional hydrology, the endemic mountainous ecosystems and the tropical glaciers. Through high resolution simulations (up to 1 km grid size) we evaluate the effects of local deforestation inside the Zongo Andean valley, in addition to the regional scale signal of the widespread deforestation. Local deforestation affects the upslope daytime circulation thanks to an energy loss at the bottom of the valley over the deforested area. However, this diurnal circulation alteration does not have any impact on the local rainfall. Instead, nocturnal rainfall depletion occurs in both analyzed Andean valleys due to the decreased entry of SALLJ moist winds from Amazon towards the Andes highlands.

After having addressed the effects of deforestation in the early stages of the wet season in the southern and southwestern Amazon, as well as the impacts it generates

on the eastern flank of the Andes, we finish this work by an evaluation of the potential modifications on the mechanisms driving summer precipitation over the southern tropical Andes highlands (Chapter 5). Since the 2000's, summer precipitation variability at inter-annual scales is strongly related to the upward motion over the western Amazon and it is less related to the upper easterlies of the Bolivian High (Segura et al. 2020). Logging in the Amazon basin leads to a reduction in the ascending motion of air masses over the western part of the Amazon region and a general drier mid-troposphere according to two different climate models. Although this result suggests a reduction in summer precipitation over the southern tropical Andes according to the experimental wind-rainfall relation reported by Segura et al. (2020), this only occurs in one of the analyzed models. The second regional climate model presents a spatially differentiated rainfall response with a slight decrease (increase) in the northwestern (eastern and southern) part of the southern tropical Andes. Precipitation reduction over the western tropical Andes during the austral summer are important because most of the water resources of the region depend on rain falling in the December-March period. A different mechanism in this particular model drives the precipitation increment in the eastern and southern parts of the Andes highlands. The forest-to-cropland conversion causes a decrease in the surface roughness length over an extensive area of the Amazon basin, generating an acceleration of the low-level winds entering to the continent from the Atlantic Ocean. As a result, the mechanic channelization over the eastern Andes valleys that brings moisture from the Amazon lowlands toward the upper Andes is stronger with deforested conditions. However, this is a preliminary conclusion and further analysis will be addressed in the near future to complement and enrich this section.

6.2 Perspectives

Although our results have shed light on the impacts that Amazonian deforestation may have on the climate connection between the Amazon region and the tropical Andes, many questions remain and can be the base for future works. We classify these potential research topics in five main categories: i) the improvement of the robustness of modelling-based results, ii) the assessment of the conjoint effect of Amazon deforestation plus the climate change and the projected global warming signal, iii) Amazon forest loss impacts extended with hydrological models, iv) cold front

incursions under deforestation experiments, v) Amazon deforestation and the Walker circulation.

6.2.1 Improvement of the robustness of model-based conclusions

Considering that all the conclusions presented in this thesis are derived from the use of regional climate models, there are technical restrictions that limit our conclusions and should be further studied in the future. Regional climate models have inherent uncertainties, among these, the so-called 'structural uncertainty'. Different regional or global climate models have different representation of the physical and dynamical processes and, as a consequence, they respond differently to the same external forcing as the land-use change (Caya and Biner 2004; Giorgi and Gutowski 2015). To deal with this type of uncertainty, it is common to assess the range of possible climate responses using different climate models forced by the same boundary and lateral conditions (Chen et al. 2021). For this reason, we use a set of simulations using different regional climate models in Chapter 5 sharing the same deforestation scenario. However, these two simulations are not completely comparable because they differ in the spatial and temporal domains, the land surface model used and the atmospheric model configurations. In order to quantify the spectrum of different climate responses associated with the structural uncertainty a set of more homogeneous simulations should be performed.

A strong limitation of using regional climate models is that these models by definition are limited to a specific geographic area. Many different theoretical, observational and modelling studies describe how deep convection in the tropics, and particularly in the Amazon region, is dependent and can affect the climatic conditions in remote regions (Gill 1980; Silva-Dias et al. 1983; Kiladis and Wheeler 1995; Figueroa et al. 1995; Zhang et al. 1996; Gedney and Valdes 2000; Hasler et al. 2009; Badger and Dirmeyer 2016). For instance, deforestation decreases the vertical ascent what generates, by mass continuity, a reduction in descent elsewhere (Henderson-Sellers et al. 1993; McGuffie et al. 1995; Zhang et al. 1996; Jonko et al. 2010; Badger and Dirmeyer 2016). These perturbations over distant regions can alter the moisture/energy entry to the originally deforested area generating positive or negative feedbacks. However, the

use of a regional climate model with imposed observed boundary conditions inhibits to take into account the feedback response. To overcome this issue, deforestation climate simulations could be performed with a global climate model with or without variable resolution. Another solution is to implement simulations running a global and a regional climate model concurrently, allowing the information exchange in both directions, a technique known as two-way-nesting.

Despite the fact that we have taken advantage of the added value of high-resolution simulations in some parts of our work (Chapter 4), the high computational cost involved in this type of simulations has limited its use. However, some parts of our analysis would benefit from the use of a finer horizontal resolution. Typically, finer horizontal grid cells can lead to a better model representation over areas where local forcings modulate the climate signal, such as regions with complex topography (as the southern tropical Andes region analyzed in Chapter 5) or regions with land surface heterogeneity (such as the southern Amazon analyzed in Chapter 3)(Di Luca et al. 2012; Giorgi and Gutowski 2015; Rosales et al. 2022).

For the evaluation of a model, it is essential to have observations at a spatial and temporal resolution sufficient to analyze the physical processes of interest. In the case of the present work, we take advantage of daily precipitation data taken along the Zongo and Huarinilla valleys in the Bolivian Andes provided by the Bolivian Electric Power Company (COBEE) and managed in collaboration with the Institute of Research for the Development (IRD)-France. This dataset allows us to analyze the model performance in representing daily-scale processes such as anabatic and katabatic winds, and the spatial rainfall variability along a small Andean valley. The use of these data, crucial to our work, was derived from IRD collaborations with researchers in Bolivia. Therefore, collaborations such as this can help the development of future work in the region and should be promoted in other places. Currently potential collaborations with the ANDEX project could help in this direction. ANDEX is a Regional Hydroclimate Project part of the GEWEX Hydro climatology Panel which looks for improving our understanding of the climate and hydrology along the Andes mountain chain.

6.2.2 Assessment of the conjoint effect of Amazon deforestation and the climate change signal

As described in Chapter 1, the Amazon is currently suffering strong and concurrent anthropic pressures mainly thanks to deforestation and global warming (Nepstad et al. 2008; Nobre and Borma 2009). The majority of studies in the scientific literature focus on analyzing each of these forcings individually and few works have analyzed the simultaneous effect of tropical forest loss and the greenhouse gases forcing (e.g. Franchito et al. 2012; Devaraju et al. 2015; Guimberteau et al. 2017). This is a very complex problem due to the numerous atmosphere-biosphere feedbacks and interactions act together in the system, many of which are not adequately represented in current climate and surface models (Coe et al. 2013). For instance, an increase in the atmospheric CO_2 can accelerate the forest growth rates (Norby et al. 2001, 2005) raising the area/density of rainforest, and consequently evapotranspiration in the Amazon basin. At the same time, an CO_2-enriched atmosphere causes a stomatal closure in plants what reduces the evapotranspiration rates and can impact precipitation in the region (de Boer et al. 2011; Lammertsma et al. 2011). However, even with current climate models little is known about how deforestation may amplify or attenuate the global warming signal in the South American region. An amplification of the synergic effects of deforestation, global warming and other anthropogenic drivers such as wildfires has been predicted by computational models and suggested by observational evidence. This conjoint effect could lead to a collapse of the rainforest and to a rainforest-to-savannah transformation (Nobre et al. 2016 and referenches therein). Nonetheless, further analysis should be done in this area to gain a better understanding of the interaction between these anthropogenic forcings.

6.2.3 Amazon forest loss impacts extended with hydrological models

In Chapter 4 our results indicate the possible rainfall reduction associated to deforestation over the eastern flank of the Andes. Over this particular region, large runoff rates erode the Andean rocks and produce most of the sediment and nutrient loads for downstream in the Amazon basin (Moquet et al. 2011; Pepin et al. 2013; Vauchel et al. 2017; Armijos et al. 2020b). Therefore, it would be interesting to couple

the outputs from our regional climate model with a hydrological model in order to assess the effects of the tropical forest loss on the sediment production and fertilization over the Amazon lowlands. A limited number of studies perform this kind of analysis in the scientific literature (e.g. Guimberteau et al. 2017). On the other hand, Chapter 4 evidences the decrease in the atmospheric moisture transport from the Amazon lowlands toward the Bolivian Andes highlands. This region encompasses several glaciers which can be affected by these deforestation-induced circulation perturbations. How extensive Amazon deforestation could affect the mass balance of the Bolivian glaciers is a very interesting question to be developed in future works through an integration of regional climate simulations with hydrological models.

6.2.4 Cold fronts in South America and Amazonian deforestation

The intrusion of cold air masses from higher latitudes is an important phenomenon that affects the Amazon basin and the tropical Andes in several ways that include the agricultural crop damage for cold and freeze extreme events (Marengo et al. 1997 and references therein), the enhancement of snow accumulation in tropical glaciers (Sicart et al. 2016) and the destabilization of the atmosphere that helps the rainy season onset in the Amazon (Li and Fu 2006; Espinoza et al. 2013b, 2021). In Chapter 3 we show that deforestation could decrease the southerly wind incursions of the cold fronts. However, this result was not analyzed in depth and it deserves a further evaluation. Considering that southern cold incursions occur on an intra-seasonal scale (the same time scale at which operational weather forecasts are performed), and taking into account the potential predictability of these kind of events (Krishnamurti et al. 1999), assessing the effects of Amazon deforestation on cold fronts is a promising topic for future collaborations with weather forecasting agencies.

6.2.5 Amazon deforestation and the Walker circulation

According to our model experiments in Chapter 4 and Chapter 5, the loss of Amazon rainforest can generate significant impacts in the regional Hadley cell as well as in the low-level winds entering to the South American continent from the Atlantic Ocean, what could be related to perturbation on the Walker circulation. Due to the inherent spatial limitation of our regional simulations, our analyses of the impacts of

deforestation on Walker's circulation were limited. Both previous modeling and theoretical work have pointed to the possible effects of deforestation on large-scale circulation (Zhang et al. 1996; Gedney and Valdes 2000; Hasler et al. 2009; Snyder 2010b; Badger and Dirmeyer 2016; Ruiz-Vásquez et al. 2020). For example, (Badger and Dirmeyer 2016) find a decrease in the upper-tropospheric convergence over the central tropical Pacific Ocean and less divergence over northern South America. This implies changes in the Walker circulation that could impact the central Pacific sea surface temperature. However, an in-depth analysis of the changes in Walker circulation associated with deforestation in the Amazon is, to our knowledge, an unexplored topic in the literature.

Bibliography

Aceituno P (1988) On the Functioning of the Southern Oscillation in the South American Sector. Part I: Surface Climate. Mon Weather Rev 116:505–524. https://doi.org/10.1175/1520-0493(1988)116<0505:OTFOTS>2.0.CO;2

Aceituno P, Garreaud R (1995) Impacto de los fenónemos el Niño y la Niña en regímenes fluviométricos andinos. Rev Chil Ing Hidraul

Adler B, Kalthoff N, Gantner L (2011) Initiation of deep convection caused by land-surface inhomogeneities in West Africa: a modelled case study. Meteorol Atmos Phys 112:15–27. https://doi.org/10.1007/s00703-011-0131-2

Agudelo J, Arias PA, Vieira SC, Martínez JA (2019) Influence of longer dry seasons in the Southern Amazon on patterns of water vapor transport over northern South America and the Caribbean. Clim Dyn 52:2647–2665. https://doi.org/10.1007/s00382-018-4285-1

Aguiar APD, Câmara G, Escada MIS (2007) Spatial statistical analysis of land-use determinants in the Brazilian Amazonia: Exploring intra-regional heterogeneity. Ecol Modell 209:169–188. https://doi.org/10.1016/j.ecolmodel.2007.06.019

Aide TM, Grau HR, Graesser J, et al (2019) Woody vegetation dynamics in the tropical and subtropical Andes from 2001 to 2014: Satellite image interpretation and expert validation. Glob Chang Biol 25:2112–2126. https://doi.org/10.1111/gcb.14618

Akkermans T, Thiery W, Van Lipzig NPM (2014) The Regional Climate Impact of a Realistic Future Deforestation Scenario in the Congo Basin. J Clim 27:2714–2734. https://doi.org/10.1175/JCLI-D-13-00361.1

Alencar AA, Brando PM, Asner GP, Putz FE (2015) Landscape fragmentation, severe drought, and the new Amazon forest fire regime. Ecol Appl 25:1493–1505. https://doi.org/10.1890/14-1528.1.

Alves LM, Marengo JA, Fu R, Bombardi RJ (2017) Sensitivity of Amazon Regional Climate to Deforestation. Am J Clim Chang. https://doi.org/10.4236/ajcc.2017.61005

Amigo I (2020) When will the Amazon hit a tipping point? Nature 578:505–507. https://doi.org/10.1038/d41586-020-00508-4

Ampuero A, Stríkis NM, Apaéstegui J, et al (2020) The Forest Effects on the Isotopic Composition of Rainfall in the Northwestern Amazon Basin. J Geophys Res

Atmos 125:. https://doi.org/10.1029/2019JD031445

Anderegg WRL, Berry JA, Smith DD, et al (2012) The roles of hydraulic and carbon stress in a widespread climate-induced forest die-off. Proc Natl Acad Sci 109:233–237. https://doi.org/10.1073/pnas.1107891109

Aragão LEOC, Anderson LO, Fonseca MG, et al (2018) 21st Century drought-related fires counteract the decline of Amazon deforestation carbon emissions. Nat Commun 9:1–12. https://doi.org/10.1038/s41467-017-02771-y

Arias P, Bellouin N, Coppola E, et al (2021) Climate Change 2021: The Physical Science Basis. Contribution of Working Group14 I to the Sixth Assessment Report of the Intergovernmental Panel on Climate Change; Technical Summary. Cambridge University Press

Arias PA, Fu R, Vera C, Rojas M (2015) A correlated shortening of the North and South American monsoon seasons in the past few decades. Clim Dyn 45:3183–3203. https://doi.org/10.1007/s00382-015-2533-1

Arias PA, Martínez JA, Mejía JD, et al (2020) Changes in Normalized Difference Vegetation Index in the Orinoco and Amazon River Basins: Links to Tropical Atlantic Surface Temperatures. J Clim 33:8537–8559. https://doi.org/10.1175/JCLI-D-19-0696.1

Armenteras D, Cabrera E, Rodríguez N, Retana J (2013) National and regional determinants of tropical deforestation in Colombia. Reg Environ Chang 13:1181–1193. https://doi.org/10.1007/s10113-013-0433-7

Armijos E, Crave A, Espinoza JC, et al (2020a) Rainfall control on Amazon sediment flux: synthesis from 20 years of monitoring. Environ Res Commun 2:051008. https://doi.org/10.1088/2515-7620/ab9003

Armijos E, Crave A, Espinoza JC, et al (2020b) Rainfall control on Amazon sediment flux: synthesis from 20 years of monitoring. Environ Res Commun 2:051008. https://doi.org/10.1088/2515-7620/ab9003

Arraut JM, Nobre C, Barbosa HMJ, et al (2012) Aerial Rivers and Lakes: Looking at Large-Scale Moisture Transport and Its Relation to Amazonia and to Subtropical Rainfall in South America. J Clim 25:543–556. https://doi.org/10.1175/2011JCLI4189.1

Asner GP (2009) Tropical forest carbon assessment: integrating satellite and airborne mapping approaches. Environ Res Lett 4:034009. https://doi.org/10.1088/1748-9326/4/3/034009

Asner GP, Llactayo W, Tupayachi R, Luna ER (2013) Elevated rates of gold mining in the Amazon revealed through high-resolution monitoring. Proc Natl Acad Sci 110:18454–18459. https://doi.org/10.1073/pnas.1318271110

Assunção J, Gandour C, Rocha R (2015) Deforestation slowdown in the Brazilian Amazon: prices or policies? Environ Dev Econ 20:697–722. https://doi.org/10.1017/S1355770X15000078

Avissar R (2002) The Large-Scale Biosphere-Atmosphere Experiment in Amazonia (LBA): Insights and future research needs. J Geophys Res 107:8086. https://doi.org/10.1029/2002JD002704

Avissar R, Pielke RA (1989) A Parameterization of Heterogeneous Land Surfaces for Atmospheric Numerical Models and Its Impact on Regional Meteorology. Mon Weather Rev 117:2113–2136. https://doi.org/10.1175/1520-0493(1989)117<2113:APOHLS>2.0.CO;2

Badger AM, Dirmeyer PA (2015) Climate response to Amazon forest replacement by heterogeneous crop cover. Hydrol Earth Syst Sci 19:4547–4557. https://doi.org/10.5194/hess-19-4547-2015

Badger AM, Dirmeyer PA (2016) Remote tropical and sub-tropical responses to Amazon deforestation. Clim Dyn 46:3057–3066. https://doi.org/10.1007/s00382-015-2752-5

Bagley JE, Desai AR, Harding KJ, et al (2014) Drought and deforestation: Has land cover change influenced recent precipitation extremes in the Amazon? J Clim 27:345–361. https://doi.org/10.1175/JCLI-D-12-00369.1

Baidya Roy S, R. A (2002) Impact of land use/land cover change on regional hydrometeorology in Amazonia. J Geophys Res 107:8037. https://doi.org/10.1029/2000JD000266

Baker JCA, Spracklen D V. (2019) Climate Benefits of Intact Amazon Forests and the Biophysical Consequences of Disturbance. Front For Glob Chang 2:. https://doi.org/10.3389/ffgc.2019.00047

Ballantyne AP, Alden CB, Miller JB, et al (2012) Increase in observed net carbon dioxide uptake by land and oceans during the past 50 years. Nature 488:70–72. https://doi.org/10.1038/nature11299

Ban N, Caillaud C, Coppola E, et al (2021) The first multi-model ensemble of regional climate simulations at kilometer-scale resolution, part I: evaluation of precipitation. Clim Dyn 57:275–302. https://doi.org/10.1007/s00382-021-05708-w

Barichivich J, Gloor E, Peylin P, et al (2018) Recent intensification of Amazon flooding extremes driven by strengthened Walker circulation. Sci Adv 4:. https://doi.org/10.1126/sciadv.aat8785

Barthem RB, Charvet-Almeida P, Montag LFA, Lanna AE (2004) Global international waters assessment Amazon Basin, GIWA regional assessment 40 b.

Bastable HG, Shuttleworth WJ, Dallarosa RLG, et al (1993) Observations of climate, albedo, and surface radiation over cleared and undisturbed amazonian forest. Int J Climatol. https://doi.org/10.1002/joc.3370130706

Becker BK (2005) Geopolítica da amazônia. Estud avançados 19:71–86

Beniston M, Diaz HF, Bradley RS (1997) CLIMATIC CHANGE AT HIGH ELEVATION SITES: AN OVERVIEW. Clim Change 36:233–251. https://doi.org/10.1023/A:1005380714349

Berbet MLC, Costa MH (2003) Climate Change after Tropical Deforestation: Seasonal Variability of Surface Albedo and Its Effects on Precipitation Change. J Clim 16:2099–2104. https://doi.org/10.1175/1520-0442(2003)016<2099:CCATDS>2.0.CO;2

Berri GJ, Inzunza JB (1993) The effect of the low-level jet on the poleward water vapour transport in the central region of South America. Atmos Environ Part A Gen Top 27:335–341. https://doi.org/10.1016/0960-1686(93)90107-A

Betts AK, Silva Dias MAF (2010) Progress in understanding land-surface-atmosphere coupling from LBA research. J Adv Model Earth Syst 2:6. https://doi.org/10.3894/JAMES.2010.2.6

Boisier JP, Ciais P, Ducharne A, Guimberteau M (2015) Projected strengthening of Amazonian dry season by constrained climate model simulations. Nat Clim Chang 5:656–660. https://doi.org/10.1038/nclimate2658

Bonan G (2015) Ecological Climatology. Cambridge University Press

Bonan GB (2008a) Forests and Climate Change: Forcings, Feedbacks, and the Climate Benefits of Forests. Science (80-) 320:1444–1449. https://doi.org/10.1126/science.1155121

Bonan GB (2008b) Forests and climate change: Forcings, feedbacks, and the climate benefits of forests. Science (80-.).

Bontemps S, Defourny P, Radoux J, et al (2013) Consistent Global Land Cover Maps For Climate Modelling Communities: Current Achievements Of The ESA Land Cover CCI. In: Proceedings of the ESA living planet symposium. Edimburgh, pp

9–13

Booth BBB, Dunstone NJ, Halloran PR, et al (2012) Aerosols implicated as a prime driver of twentieth-century North Atlantic climate variability. Nature 484:228–232. https://doi.org/10.1038/nature10946

Borsdorf A, Stadel C (2015) The Andes. Springer International Publishing, Cham

Bradley RS, Keimig FT, Diaz HF (2004) Projected temperature changes along the American cordillera and the planned GCOS network. Geophys Res Lett 31:L16210. https://doi.org/10.1029/2004GL020229

Bradley RS, Vuille M, Diaz HF, Vergara W (2006) Threats to Water Supplies in the Tropical Andes. Science (80-) 312:1755–1756. https://doi.org/10.1126/science.1128087

Brando PM (2014) Abrupt increases in Amazonian tree mortality due to drought fire interactions. Proc Natl Acad Sci 111:6347–6352. https://doi.org/10.1073/pnas.1305499111.

Braun C, Bezada M (2013) The History and Disappearance of Glaciers in Venezuela. J Lat Am Geogr 12:85–124. https://doi.org/10.1353/lag.2013.0016

Brienen RJW, Phillips OL, Feldpausch TR, et al (2015) Long-term decline of the Amazon carbon sink. Nature 519:344–348. https://doi.org/10.1038/nature14283

Builes-Jaramillo A, Poveda G (2018) Conjoint Analysis of Surface and Atmospheric Water Balances in the Andes-Amazon System. Water Resour Res 54:3472–3489. https://doi.org/10.1029/2017WR021338

Bustamante MMC, Keller M, Silva DA (2009) Sources and sinks of trace gases in Amazonia and the Cerrado. In: Amazonia and global change. Geophysical Monograph Series., Washington, pp 337–354

Butt N, De Oliveira PA, Costa MH (2011) Evidence that deforestation affects the onset of the rainy season in Rondonia, Brazil. J Geophys Res Atmos. https://doi.org/10.1029/2010JD015174

Buytaert W, De Bièvre B (2012) Water for cities: The impact of climate change and demographic growth in the tropical Andes. Water Resour Res 48:. https://doi.org/10.1029/2011WR011755

Cadena CD, Cuervo AM, Céspedes LN, et al (2021) Systematics, biogeography, and diversification of Scytalopus tapaculos (Rhinocryptidae), an enigmatic radiation of Neotropical montane birds. Auk 138:. https://doi.org/10.1093/auk/ukaa024

Cai W, McPhaden MJ, Grimm AM, et al (2020) Climate impacts of the El Niño–

Southern Oscillation on South America. Nat Rev Earth Environ 1:215–231. https://doi.org/10.1038/s43017-020-0040-3

Caioni C, Silvério DV, Macedo MN, et al (2020) Droughts Amplify Differences Between the Energy Balance Components of Amazon Forests and Croplands. Remote Sens 12:525. https://doi.org/10.3390/rs12030525

Calinski T, Harabasz J (1974) A dendrite method for cluster analysis. Commun Stat - Theory Methods 3:1–27. https://doi.org/10.1080/03610927408827101

Callède J, Cochonneau G, Alves F V., et al (2010) The River Amazon water contribution to the Atlantic Ocean. Rev Des Sci l'eau 23:247–273

Cameron JGD (2018) A Forgotten Century of Brazilwood: The Brazilwood Trade from the Mid-Sixteenth to Mid-Seventeenth Century. J Port Hist

Case JL, Crosson WL, Kumar S V., et al (2008) Impacts of High-Resolution Land Surface Initialization on Regional Sensible Weather Forecasts from the WRF Model. J Hydrometeorol 9:1249–1266. https://doi.org/10.1175/2008JHM990.1

Caya D, Biner S (2004) Internal variability of RCM simulations over an annual cycle. Clim Dyn 22:33–46. https://doi.org/10.1007/s00382-003-0360-2

Ceballos G, Ehrlich PR (2006) Global mammal distributions, biodiversity hotspots, and conservation. Proc Natl Acad Sci 103:19374–19379. https://doi.org/10.1073/pnas.0609334103

Ceballos JL, Euscátegui C, Ramírez J, et al (2006) Fast shrinkage of tropical glaciers in Colombia. Ann Glaciol 43:194–201. https://doi.org/10.3189/172756406781812429

Cerón WL, Molina-Carpio J, Ayes Rivera I, et al (2020) A principal component analysis approach to assess CHIRPS precipitation dataset for the study of climate variability of the La Plata Basin, Southern South America. Nat Hazards 103:767–783. https://doi.org/10.1007/s11069-020-04011-x

Chagnon FJF, Bras RL (2005) Contemporary climate change in the Amazon. Geophys Res Lett 32:L13703. https://doi.org/10.1029/2005GL022722

Chagnon FJF, Bras RL, Wang J (2004) Climatic shift in patterns of shallow clouds over the Amazon. Geophys Res Lett 31:L24212. https://doi.org/10.1029/2004GL021188

Chavez SP, Takahashi K (2017) Orographic rainfall hot spots in the Andes-Amazon transition according to the TRMM precipitation radar and in situ data. J Geophys Res. https://doi.org/10.1002/2016JD026282

Chen D, Rojas M, Samset BH, et al (2021) Framing, Context, and Methods. In: Climate Change 2021: The Physical Science Basis. Contribution of Working Group I to the Sixth Assessment Report of the Intergovernmental Panel on Climate Change. University Press, Cambridge, United Kingdom and New York, NY, USA, pp 147–286

Chen F, Avissar R (1994) Impact of Land-Surface Moisture Variability on Local Shallow Convective Cumulus and Precipitation in Large-Scale Models. J Appl Meteorol 33:1382–1401. https://doi.org/10.1175/1520-0450(1994)033<1382:IOLSMV>2.0.CO;2

Chen F, Dudhia J (2001) Coupling an Advanced Land Surface–Hydrology Model with the Penn State–NCAR MM5 Modeling System. Part I: Model Implementation and Sensitivity. Mon Weather Rev 129:569–585. https://doi.org/10.1175/1520-0493(2001)129<0569:CAALSH>2.0.CO;2

Chen Y, Randerson JT, Morton DC, et al (2011) Forecasting Fire Season Severity in South America Using Sea Surface Temperature Anomalies. Science (80-) 334:787–791. https://doi.org/10.1126/science.1209472

Claussen M, Brovkin V, Ganopolski A (2001) Biophysical versus biogeochemical feedbacks of large-scale land cover change. Geophys Res Lett. https://doi.org/10.1029/2000GL012471

Cochrane MA, Alencar A, Schulze MD, et al (1999) Positive Feedbacks in the Fire Dynamic of Closed Canopy Tropical Forests. Science (80-) 284:1832–1835. https://doi.org/10.1126/science.284.5421.1832

Coe MT, Costa MH, Soares-Filho BS (2009) The influence of historical and potential future deforestation on the stream flow of the Amazon River – Land surface processes and atmospheric feedbacks. J Hydrol 369:165–174. https://doi.org/10.1016/j.jhydrol.2009.02.043

Coe MT, Marthews TR, Costa MH, et al (2013) Deforestation and climate feedbacks threaten the ecological integrity of south–southeastern Amazonia. Philos Trans R Soc B Biol Sci 368:20120155. https://doi.org/10.1098/rstb.2012.0155

Correa IC, Arias PA, Rojas M (2021) Evaluation of multiple indices of the South American monsoon. Int J Climatol 41:. https://doi.org/10.1002/joc.6880

Cosgrove BA, Lohmann D, Mitchell KE, et al (2003) Land surface model spin-up behavior in the North American Land Data Assimilation System (NLDAS). J Geophys Res Atmos 108:2002JD003316. https://doi.org/10.1029/2002JD003316

Costa MH, Borma LS, Espinoza JC, et al (2021) The physical hydroclimate system of the Amazon

Costa MH, Foley JA (2000) Combined effects of deforestation and doubled atmospheric CO2 concentrations on the climate of Amazonia. J Clim 13:18–34. https://doi.org/10.1175/1520-0442(2000)013<0018:CEODAD>2.0.CO;2

Costa MH, Pires GF (2010) Effects of Amazon and Central Brazil deforestation scenarios on the duration of the dry season in the arc of deforestation. Int J Climatol 30:1970–1979. https://doi.org/10.1002/joc.2048

Cox PM, Harris PP, Huntingford C, et al (2008) Increasing risk of Amazonian drought due to decreasing aerosol pollution. Nature 453:212–215. https://doi.org/10.1038/nature06960

Cuevas E, Medina E (1988) Nutrient dynamics within amazonian forests. Oecologia 76:222–235. https://doi.org/10.1007/BF00379956

Culf AD, Esteves JL, Marques Filho O, Rocha HR (1996) Radiation, temperature and humidity over forest and pasture in Amazonia. In: Amazonian Deforestation and Climate. John Wiley and Sons, Chichester

Culf AD, Fisch G, Hodnett MG (1995) The Albedo of Amazonian Forest and Ranch Land. J Clim 8:1544–1554. https://doi.org/10.1175/1520-0442(1995)008<1544:TAOAFA>2.0.CO;2

Cutrim E, Martin DW, Rabin R (1995) Enhancement of Cumulus Clouds over Deforested Lands in Amazonia. Bull Am Meteorol Soc 76:1801–1805. https://doi.org/10.1175/1520-0477(1995)076<1801:EOCCOD>2.0.CO;2

D'Almeida C, Vörösmarty CJ, Hurtt GC, et al (2007) The effects of deforestation on the hydrological cycle in Amazonia: A review on scale and resolution. Int. J. Climatol.

da Anunciação YMT, Walde DH-G, da Rocha RP (2014) Observed summer weather regimes and associated extreme precipitation over Distrito Federal, west-central Brazil. Environ Earth Sci 72:4835–4848. https://doi.org/10.1007/s12665-014-3607-9

da Costa WM (1988) O Estado e as políticas territoriais no Brasil. Ed Context

da Rocha HR, Goulden ML, Miller SD, et al (2004) SEASONALITY OF WATER AND HEAT FLUXES OVER A TROPICAL FOREST IN EASTERN AMAZONIA. Ecol Appl 14:22–32. https://doi.org/10.1890/02-6001

da Silva HJF, Gonçalves WA, Bezerra BG (2019) Comparative analyzes and use of

evapotranspiration obtained through remote sensing to identify deforested areas in the Amazon. Int J Appl Earth Obs Geoinf 78:163–174. https://doi.org/10.1016/j.jag.2019.01.015

Da Silveira Lobo Sternberg L (2001) Savanna-forest hysteresis in the tropics. Glob Ecol Biogeogr 10:369–378. https://doi.org/10.1046/j.1466-822X.2001.00243.x

Dai A (2006) Precipitation Characteristics in Eighteen Coupled Climate Models. J Clim 19:4605–4630. https://doi.org/10.1175/JCLI3884.1

Davidson EA, de Araújo AC, Artaxo P, et al (2012) The Amazon basin in transition. Nature 481:321–328. https://doi.org/10.1038/nature10717

Davidson EA, Reis de Carvalho CJ, Vieira ICG, et al (2004) NITROGEN AND PHOSPHORUS LIMITATION OF BIOMASS GROWTH IN A TROPICAL SECONDARY FOREST. Ecol Appl 14:150–163. https://doi.org/10.1890/01-6006

de Boer HJ, Lammertsma EI, Wagner-Cremer F, et al (2011) Climate forcing due to optimization of maximal leaf conductance in subtropical vegetation under rising CO 2. Proc Natl Acad Sci 108:4041–4046. https://doi.org/10.1073/pnas.1100555108

de Goncalves LGG, Shuttleworth WJ, Chou SC, et al (2006) Impact of different initial soil moisture fields on Eta model weather forecasts for South America. J Geophys Res 111:D17102. https://doi.org/10.1029/2005JD006309

Debortoli NS, Dubreuil V, Funatsu B, et al (2015) Rainfall patterns in the Southern Amazon: a chronological perspective (1971–2010). Clim Change 132:251–264. https://doi.org/10.1007/s10584-015-1415-1

Devaraju N, Bala G, Nemani R (2015) Modelling the influence of land-use changes on biophysical and biochemical interactions at regional and global scales. Plant Cell Environ 38:1931–1946. https://doi.org/10.1111/pce.12488

Di Luca A, de Elía R, Laprise R (2012) Potential for added value in precipitation simulated by high-resolution nested Regional Climate Models and observations. Clim Dyn 38:1229–1247. https://doi.org/10.1007/s00382-011-1068-3

Dias MAFS, Regnier P (1996) Simulation of meso-scale circulations in a deforested area of Rondonia in the dry season. In: Amazonian deforestation and climate. John Wiley and Sons, Chichester

Dickinson RE, Kennedy P (1992) Impacts on regional climate of Amazon deforestation. Geophys Res Lett 19:1947–1950. https://doi.org/10.1029/92GL01905

Diday E, Simon JC (1976) Clustering analysis, Digital Pattern recognition. Commun Cybern 10:47–94

Diniz CG, Souza AA de A, Santos DC, et al (2015) DETER-B: The New Amazon Near Real-Time Deforestation Detection System. IEEE J Sel Top Appl Earth Obs Remote Sens 8:3619–3628. https://doi.org/10.1109/JSTARS.2015.2437075

Dirmeyer PA, Brubaker KL (2007) Characterization of the global hydrologic cycle from a back-trajectory analysis of atmospheric water vapor. J Hydrometeorol. https://doi.org/10.1175/JHM557.1

Dirmeyer PA, Brubaker KL, DelSole T (2009) Import and export of atmospheric water vapor between nations. J Hydrol 365:11–22. https://doi.org/10.1016/j.jhydrol.2008.11.016

Dirzo R, Raven PH (2003) Global State of Biodiversity and Loss. Annu Rev Environ Resour 28:137–167. https://doi.org/10.1146/annurev.energy.28.050302.105532

Dolman AJ, Silva Dias MA, Calvet J-C, et al (1999) Meso-scale effects of tropical deforestation in Amazonia: preparatory LBA modelling studies. Ann Geophys 17:1095–1110. https://doi.org/10.1007/s00585-999-1095-0

Dominguez F, Eiras-Barca J, Yang Z, et al (2022) Amazonian Moisture Recycling Revisited Using WRF With Water Vapor Tracers. J Geophys Res Atmos 127:. https://doi.org/10.1029/2021JD035259

Dong L, Zhou T, Wu B (2014) Indian Ocean warming during 1958–2004 simulated by a climate system model and its mechanism. Clim Dyn 42:203–217. https://doi.org/10.1007/s00382-013-1722-z

Douville H, Raghavan K, Renwick J, et al (2021) Water Cycle Changes. In Climate Change 2021: The Physical Science Basis. Contribution of Working Group I to the Sixth Assessment Report of the Intergovernmental Panel on Climate Change [Masson-Delmotte, V., P. Zhai, A. Pirani, S.L. Connors, C. Péan, S. Cambridge University Press, Cambridge, United Kingdom and New York, NY, USA,

Du Y, Xie S-P (2008) Role of atmospheric adjustments in the tropical Indian Ocean warming during the 20th century in climate models. Geophys Res Lett 35:L08712. https://doi.org/10.1029/2008GL033631

Dubreuil V, Debortoli N, Funatsu B, et al (2012) Impact of land-cover change in the southern Amazonia climate: A case study for the region of Alta Floresta, Mato Grosso, Brazil. Env Monit Assess 184(2):877–891

Dudhia J (1989) Numerical Study of Convection Observed during the Winter Monsoon

Experiment Using a Mesoscale Two-Dimensional Model. J Atmos Sci 46:3077–3107. https://doi.org/10.1175/1520-0469(1989)046<3077:NSOCOD>2.0.CO;2

Egger J, Blacutt L, Ghezzi F, et al (2005) Diurnal Circulation of the Bolivian Altiplano. Part I: Observations. Mon Weather Rev 133:911–924. https://doi.org/10.1175/MWR2894.1

Eghdami M, Barros AP (2020) Deforestation Impacts on Orographic Precipitation in the Tropical Andes. Front Environ Sci 8:. https://doi.org/10.3389/fenvs.2020.580159

Eghdami M, Barros AP (2019) Extreme orographic rainfall in the eastern Andes tied to cold air intrusions. Front Environ Sci 7:. https://doi.org/10.3389/fenvs.2019.00101

Eiras-Barca J, Dominguez F, Yang Z, et al (2020) Changes in South American hydroclimate under projected Amazonian deforestation. Ann N Y Acad Sci. https://doi.org/10.1111/nyas.14364

Eltahir EAB (1996) Role of vegetation in sustaining large-scale atmospheric circulations in the tropics. J Geophys Res Atmos 101:4255–4268. https://doi.org/10.1029/95JD03632

Eltahir EAB, Bras RL (1994) Precipitation recycling in the Amazon basin. Q J R Meteorol Soc. https://doi.org/10.1002/qj.49712051806

ESA (2017) Land Cover CCI Product User Guide Version 2.

Espinoza J-C, Marengo JA, Schongart J, Jimenez JC (2022) The new historical flood of 2021 in the Amazon River compared to major floods of the 21st century: Atmospheric features in the context of the intensification of floods. Weather Clim Extrem 35:100406. https://doi.org/10.1016/j.wace.2021.100406

Espinoza JC, Chavez S, Ronchail J, et al (2015) Rainfall hotspots over the southern tropical Andes: Spatial distribution, rainfall intensity, and relations with large-scale atmospheric circulation. Water Resour Res. https://doi.org/10.1002/2014WR016273

Espinoza JC, Garreaud R, Poveda G, et al (2020) Hydroclimate of the Andes Part I: Main Climatic Features. Front Earth Sci 8:1–20. https://doi.org/10.3389/feart.2020.00064

Espinoza JC, Guyot JL, Ronchail J, et al (2009a) Contrasting regional discharge evolutions in the Amazon basin (1974-2004). J Hydrol 375:297–311. https://doi.org/10.1016/j.jhydrol.2009.03.004

Espinoza JC, Lengaigne M, Ronchail J, Janicot S (2012) Large-scale circulation patterns and related rainfall in the Amazon Basin: a neuronal networks approach. Clim Dyn 38:121–140. https://doi.org/10.1007/s00382-011-1010-8

Espinoza JC, PA A, V M, et al (2021) Recent changes in the atmospheric circulation patterns during the dry-to wet transition season in south tropical South America (1979-2020): Impacts on precipitation and fire season. J Clim. https://doi.org/10.1175/JCLI-D-21-0303.1

Espinoza JC, Ronchail J, Frappart F, et al (2013a) The Major Floods in the Amazonas River and Tributaries (Western Amazon Basin) during the 1970–2012 Period: A Focus on the 2012 Flood*. J Hydrometeorol 14:1000–1008. https://doi.org/10.1175/JHM-D-12-0100.1

Espinoza JC, Ronchail J, Guyot JL, et al (2009b) Spatio-temporal rainfall variability in the Amazon basin countries (Brazil, Peru, Bolivia, Colombia, and Ecuador). Int J Climatol 29:1574–1594. https://doi.org/10.1002/joc.1791

Espinoza JC, Ronchail J, Lengaigne M, et al (2013b) Revisiting wintertime cold air intrusions at the east of the Andes: propagating features from subtropical Argentina to Peruvian Amazon and relationship with large-scale circulation patterns. Clim Dyn 41:1983–2002. https://doi.org/10.1007/s00382-012-1639-y

Espinoza JC, Ronchail J, Marengo JA, Segura H (2019a) Contrasting North–South changes in Amazon wet-day and dry-day frequency and related atmospheric features (1981–2017). Clim Dyn. https://doi.org/10.1007/s00382-018-4462-2

Espinoza JC, Segura H, Ronchail J, et al (2016) Evolution of wet-day and dry-day frequency in the western Amazon basin: Relationship with atmospheric circulation and impacts on vegetation. Water Resour Res 52:8546–8560. https://doi.org/10.1002/2016WR019305

Espinoza JC, Sörensson AA, Ronchail J, et al (2019b) Regional hydro-climatic changes in the Southern Amazon Basin (Upper Madeira Basin) during the 1982–2017 period. J Hydrol Reg Stud 26:100637. https://doi.org/10.1016/j.ejrh.2019.100637

Etter A, Mc Alpine C, Possingham H (2008) A historical analysis of the spatial and temporal drivers of landscape change in Colombia since 1500. Ann Am Assoc Geogr 08:2–23

Falvey M, Garreaud RD (2005) Moisture variability over the South American Altiplano during the South American Low Level Jet Experiment (SALLJEX) observing

season. J Geophys Res 110:D22105. https://doi.org/10.1029/2005JD006152

Fassoni-Andrade AC, Fleischmann AS, Papa F, et al (2021) Amazon Hydrology From Space: Scientific Advances and Future Challenges. Rev Geophys 59:. https://doi.org/10.1029/2020RG000728

Fearnside PM (1993) Deforestation in Brazilian Amazonia: The effect of population and land tenure. Ambio. https://doi.org/10.1016/0006-3207(94)90222-4

Fearnside PM (2005) Deforestation in Brazilian Amazonia: History, Rates, and Consequences. Conserv Biol 19:680–688. https://doi.org/10.1111/j.1523-1739.2005.00697.x

Feldpausch TR, Lloyd J, Lewis SL, et al (2012) Tree height integrated into pantropical forest biomass estimates. Biogeosciences 9:3381–3403. https://doi.org/10.5194/bg-9-3381-2012

Field CB, Behrenfeld MJ, Randerson JT, Falkowski P (1998) Primary Production of the Biosphere: Integrating Terrestrial and Oceanic Components. Science (80-) 281:237–240. https://doi.org/10.1126/science.281.5374.237

Figueiredo V, Enrich-Prast A, Rütting T (2019) Evolution of nitrogen cycling in regrowing Amazonian rainforest. Sci Rep 9:8538. https://doi.org/10.1038/s41598-019-43963-4

Figueroa SN, Nobre CA (1990) Precipitation distribution over central and western tropical South America. Climanálise 5(6):36–45

Figueroa SN, Satyamurty P, Da Silva Dias PL (1995) Simulations of the Summer Circulation over the South American Region with an Eta Coordinate Model. J Atmos Sci 52:1573–1584. https://doi.org/10.1175/1520-0469(1995)052<1573:SOTSCO>2.0.CO;2

Fillion M, Passos CJS, Lemire M, et al (2009) Quality of Life and Health Perceptions Among Fish-Eating Communities of the Brazilian Amazon: An Ecosystem Approach to Well-Being. Ecohealth 6:121–134. https://doi.org/10.1007/s10393-009-0235-z

Fisch G, Tota J, Machado LAT, et al (2004) The convective boundary layer over pasture and forest in Amazonia. Theor Appl Climatol 78:47–59. https://doi.org/10.1007/s00704-004-0043-x

Fisher JB, Whittaker RJ, Malhi Y (2011) ET come home: Potential evapotranspiration in geographical ecology. Glob. Ecol. Biogeogr.

Flato G, Marotzke J, Abiodun B, et al (2013) : Evaluation of Climate Models. In: Climate

Change 2013: The Physical Science Basis. Contribution of Working Group I to the Fifth Assessment Report of the Intergovernmental Panel on Climate Change

Formenti P, Andreae MO, Lange L, et al (2001) Saharan dust in Brazil and Suriname during the Large-Scale Biosphere-Atmosphere Experiment in Amazonia (LBA) - Cooperative LBA Regional Experiment (CLAIRE) in March 1998. J Geophys Res Atmos 106:14919–14934. https://doi.org/10.1029/2000JD900827

Fosser G, Khodayar S, Berg P (2015) Benefit of convection permitting climate model simulations in the representation of convective precipitation. Clim Dyn 44:45–60. https://doi.org/10.1007/s00382-014-2242-1

Franchito SH, Rao VB, Fernandez JPR (2012) Tropical land savannization: Impact of global warming. Theor Appl Climatol 109:73–79. https://doi.org/10.1007/s00704-011-0560-3

Francou B, Coudrain A, Kundzewicz ZW (2005) Glacier shrinkage in the Andes and consequences for water resources. Hydrol Sci Journa 50:925–932

Francou B, Vuille M, Wagnon P, et al (2003) Tropical climate change recorded by a glacier in the central Andes during the last decades of the twentieth century: Chacaltaya, Bolivia, 16°S. J Geophys Res 108:4154. https://doi.org/10.1029/2002JD002959

Froidevaux P, Schlemmer L, Schmidli J, et al (2014) Influence of the Background Wind on the Local Soil Moisture–Precipitation Feedback. J Atmos Sci 71:782–799. https://doi.org/10.1175/JAS-D-13-0180.1

Fu R, Li W (2004) The influence of the land surface on the transition from dry to wet season in Amazonia. Theor Appl Climatol. https://doi.org/10.1007/s00704-004-0046-7

Fu R, Yin L, Li W, et al (2013) Increased dry-season length over southern Amazonia in recent decades and its implication for future climate projection. Proc Natl Acad Sci U S A. https://doi.org/10.1073/pnas.1302584110

Fu R, Zhu B, Dickinson RE (1999) How Do Atmosphere and Land Surface Influence Seasonal Changes of Convection in the Tropical Amazon? J Clim 1306–1321

Funatsu BM, Le Roux R, Arvor D, et al (2021) Assessing precipitation extremes (1981–2018) and deep convective activity (2002–2018) in the Amazon region with CHIRPS and AMSU data. Clim Dyn 57:827–849. https://doi.org/10.1007/s00382-021-05742-8

Funk C, Peterson P, Landsfeld M, et al (2015) The climate hazards infrared

precipitation with stations—a new environmental record for monitoring extremes. Sci Data 2:150066. https://doi.org/10.1038/sdata.2015.66

Gan MA, Kousky VE, Ropelewski CF (2004) The South America Monsoon Circulation and Its Relationship to Rainfall over West-Central Brazil. J Clim 17:47–66. https://doi.org/10.1175/1520-0442(2004)017<0047:TSAMCA>2.0.CO;2

Garcia-Carreras L, Parker DJ, Taylor CM, et al (2010) Impact of mesoscale vegetation heterogeneities on the dynamical and thermodynamic properties of the planetary boundary layer. J Geophys Res 115:D03102. https://doi.org/10.1029/2009JD012811

Garreaud R (1999) Multiscale Analysis of the Summertime Precipitation over the Central Andes. Mon Weather Rev 127:901–921. https://doi.org/10.1175/1520-0493(1999)127<0901:MAOTSP>2.0.CO;2

Garreaud R, Aceituno P (2001) Interannual Rainfall Variability over the South American Altiplano. J Clim 14:2779–2789. https://doi.org/10.1175/1520-0442(2001)014<2779:IRVOTS>2.0.CO;2

Garreaud R, Vuille M, Clement AC (2003) The climate of the Altiplano: observed current conditions and mechanisms of past changes. Palaeogeogr Palaeoclimatol Palaeoecol 194:5–22. https://doi.org/10.1016/S0031-0182(03)00269-4

Garreaud RD (2009) The Andes climate and weather. Adv Geosci 22:3–11. https://doi.org/10.5194/adgeo-22-3-2009

Gash JHC, Nobre CA (1997) Climatic Effects of Amazonian Deforestation: Some Results from ABRACOS. Bull Am Meteorol Soc 78:823–830. https://doi.org/10.1175/1520-0477(1997)078<0823:CEOADS>2.0.CO;2

Gash JHC, Nobre CA, Roberts JM, Victoria RL (1996) Amazonian deforestation and climate. John Wiley, Chichester, New York

Gedney N, Valdes PJ (2000) The effect of Amazonian deforestation on the northern hemisphere circulation and climate. Geophys Res Lett. https://doi.org/10.1029/2000GL011794

Gibbs RJ (1970) Mechanisms Controlling World Water Chemistry. Science (80-) 170:1088–1090. https://doi.org/10.1126/science.170.3962.108

Gill AE (1980) Some simple solutions for heat-induced tropical circulation. Q. J. R. Meteorol. Soc. 106:447–462

Giorgi F, Gutowski WJ (2015) Regional Dynamical Downscaling and the CORDEX Initiative. Annu Rev Environ Resour 40:467–490.

https://doi.org/10.1146/annurev-environ-102014-021217

Glisan JM, Gutowski WJ (2014) WRF summer extreme daily precipitation over the CORDEX Arctic. J Geophys Res Atmos 119:1720–1732. https://doi.org/10.1002/2013JD020697

Gloor M, Brienen RJW, Galbraith D, et al (2013) Intensification of the Amazon hydrological cycle over the last two decades. Geophys Res Lett 40:1729–1733. https://doi.org/10.1002/grl.50377

Greco S, Swap R, Garstang M, et al (1990) Rainfall and surface kinematic conditions over central Amazonia during ABLE 2B. J Geophys Res 95:17001. https://doi.org/10.1029/JD095iD10p17001

Grell GA, Dévényi D (2002) A generalized approach to parameterizing convection combining ensemble and data assimilation techniques. Geophys Res Lett 29:38-1-38–4. https://doi.org/10.1029/2002GL015311

Grell GA, Freitas SR (2014) A scale and aerosol aware stochastic convective parameterization for weather and air quality modeling. Atmos Chem Phys 14:5233–5250. https://doi.org/10.5194/acp-14-5233-2014

Guan K, Pan M, Li H, et al (2015) Photosynthetic seasonality of global tropical forests constrained by hydroclimate. Nat Geosci 8:284–289. https://doi.org/10.1038/ngeo2382

Guimberteau M, Ciais P, Ducharne A, et al (2017) Impacts of future deforestation and climate change on the hydrology of the Amazon Basin: a multi-model analysis with a new set of land-cover change scenarios. Hydrol Earth Syst Sci 21:1455–1475. https://doi.org/10.5194/hess-21-1455-2017

Guimberteau M, Drapeau G, Ronchail J, et al (2012) Discharge simulation in the sub-basins of the Amazon using ORCHIDEE forced by new datasets. Hydrol Earth Syst Sci 16:911–935. https://doi.org/10.5194/hess-16-911-2012

Gulev SK, Thorne PW, Ahn J, et al (2021) Changing State of the Climate System. In Climate Change 2021: The Physical Science Basis. Contribution of Working Group I to the Sixth Assessment Report of the Intergovernmental Panel on Climate Change. Cambridge, United Kingdom and New York, NY, USA,

Gutierrez-Cori O, Espinoza JC, Li LZX, et al (2021) On the Hydroclimate-Vegetation Relationship in the Southwestern Amazon During the 2000–2019 Period. Front Water 3:. https://doi.org/10.3389/frwa.2021.648499

Gutowski WJ, Arritt RW, Kawazoe S, et al (2010) Regional Extreme Monthly

Precipitation Simulated by NARCCAP RCMs. J Hydrometeorol 11:1373–1379. https://doi.org/10.1175/2010JHM1297.1

Haghtalab N, Moore N, Heerspink BP, Hyndman DW (2020) Evaluating spatial patterns in precipitation trends across the Amazon basin driven by land cover and global scale forcings. Theor Appl Climatol 140:411–427. https://doi.org/10.1007/s00704-019-03085-3

Hartmann DL, Klein Tank AMG, Rusticucci M, et al (2013) Observations: Atmosphere and surface. In: Climate Change 2013 the Physical Science Basis: Working Group I Contribution to the Fifth Assessment Report of the Intergovernmental Panel on Climate Change

Hasler N, Avissar R (2007) What Controls Evapotranspiration in the Amazon Basin? J Hydrometeorol 8:380–395. https://doi.org/10.1175/JHM587.1

Hasler N, Werth D, Avissar R (2009) Effects of tropical deforestation on global hydroclimate: A multimodel ensemble analysis. J Clim 22:1124–1141. https://doi.org/10.1175/2008JCLI2157.1

Hecht SB (2005) Soybeans, Development and Conservation on the Amazon Frontier. Dev Change 36:375–404. https://doi.org/10.1111/j.0012-155X.2005.00415.x

Heerspink BP, Kendall AD, Coe MT, Hyndman DW (2020) Trends in streamflow, evapotranspiration, and groundwater storage across the Amazon Basin linked to changing precipitation and land cover. J Hydrol Reg Stud 32:100755. https://doi.org/10.1016/j.ejrh.2020.100755

Henderson-Sellers A, Dickinson RE, Durbidge TB, et al (1993) Tropical deforestation: Modeling local- to regional-scale climate change. J Geophys Res Atmos 98:7289–7315. https://doi.org/10.1029/92JD02830

Hersbach H, Bell B, Berrisford P, et al (2020) The ERA5 global reanalysis. Q J R Meteorol Soc 146:1999–2049. https://doi.org/10.1002/qj.3803

Hirota M, Holmgren M, Van Nes EH, Scheffer M (2011) Global Resilience of Tropical Forest and Savanna to Critical Transitions. Science (80-) 334:232–235. https://doi.org/10.1126/science.1210657

Hoffmann L, Günther G, Li D, et al (2019) From ERA-Interim to ERA5: the considerable impact of ECMWF's next-generation reanalysis on Lagrangian transport simulations. Atmos Chem Phys 19:3097–3124. https://doi.org/10.5194/acp-19-3097-2019

Hong S-Y, Noh Y, Dudhia J (2006) A New Vertical Diffusion Package with an Explicit

Treatment of Entrainment Processes. Mon Weather Rev 134:2318–2341. https://doi.org/10.1175/MWR3199.1

Hoorn C, Wesselingh FP, Ter Steege H, et al (2010) Amazonia through time: Andean uplift, climate change, landscape evolution, and biodiversity. Science (80-) 330:927–931. https://doi.org/10.1126/science.1194585

Horel JD, Hahmann AN, Geisler JE (1989) An investigation of the Annual Cycle of Convective Activity over the Tropical Americas. J Clim 2:1388–1403. https://doi.org/10.1175/1520-0442(1989)002<1388:AIOTAC>2.0.CO;2

Hutyra LR, Munger JW, Nobre CA, et al (2005) Climatic variability and vegetation vulnerability in Amazônia. Geophys Res Lett 32:L24712. https://doi.org/10.1029/2005GL024981

Iacono MJ, Delamere JS, Mlawer EJ, et al (2008) Radiative forcing by long-lived greenhouse gases: Calculations with the AER radiative transfer models. J Geophys Res 113:D13103. https://doi.org/10.1029/2008JD009944

Imfeld N, Barreto Schuler C, Correa Marrou KM, et al (2019) Summertime precipitation deficits in the southern Peruvian highlands since 1964. Int J Climatol 39:4497–4513. https://doi.org/10.1002/joc.6087

Instituto Nacional De Pesquisas Espaciais (2014) (2014) Monitoramento da Floresta Amazônica Brasileira por Satélite: 2014

Jasechko S, Sharp ZD, Gibson JJ, et al (2013) Terrestrial water fluxes dominated by transpiration. Nature 496:347–350. https://doi.org/10.1038/nature11983

Jenkins CN, Pimm SL, Joppa LN (2013) Global patterns of terrestrial vertebrate diversity and conservation. Proc Natl Acad Sci 110:. https://doi.org/10.1073/pnas.1302251110

Jiang Y, Wang G, Liu W, et al (2021) Modeled Response of South American Climate to Three Decades of Deforestation. J Clim 34:2189–2203. https://doi.org/10.1175/JCLI-D-20-0380.1

Jiménez-Muñoz JC, Sobrino JA, Mattar C, Malhi Y (2013) Spatial and temporal patterns of the recent warming of the Amazon forest. J Geophys Res Atmos 118:5204–5215. https://doi.org/10.1002/jgrd.50456

Jiménez PA, Dudhia J (2012) Improving the Representation of Resolved and Unresolved Topographic Effects on Surface Wind in the WRF Model. J Appl Meteorol Climatol 51:300–316. https://doi.org/10.1175/JAMC-D-11-084.1

Jones DA, Simmonds I (1993) A climatology of Southern Hemisphere extratropical

cyclones. Clim Dyn 9:131–145. https://doi.org/10.1007/BF00209750

Jonko AK, Hense A, Feddema JJ (2010) Effects of land cover change on the tropical circulation in a GCM. Clim Dyn 35:635–649. https://doi.org/10.1007/s00382-009-0684-7

Juárez RIN, Hodnett MG, Fu R, et al (2007) Control of Dry Season Evapotranspiration over the Amazonian Forest as Inferred from Observations at a Southern Amazon Forest Site. J Clim 20:2827–2839. https://doi.org/10.1175/JCLI4184.1

Junquas C, Heredia MB, Condom T, et al (2022) Regional climate modeling of the diurnal cycle of precipitation and associated atmospheric circulation patterns over an Andean glacier region (Antisana, Ecuador). Clim Dyn. https://doi.org/10.1007/s00382-021-06079-y

Junquas C, Takahashi K, Condom T, et al (2018) Understanding the influence of orography on the precipitation diurnal cycle and the associated atmospheric processes in the central Andes. Clim Dyn. https://doi.org/10.1007/s00382-017-3858-8

Kahn J, Freitas C, Petrere M (2014) False Shades of Green: The Case of Brazilian Amazonian Hydropower. Energies 7:6063–6082. https://doi.org/10.3390/en7096063

Kalamandeen M, Gloor E, Mitchard E, et al (2018) Pervasive Rise of Small-scale Deforestation in Amazonia. Sci Rep. https://doi.org/10.1038/s41598-018-19358-2

Kaser G (1999) A review of the modern fluctuations of tropical glaciers. Glob Planet Change 22:93–103. https://doi.org/10.1016/S0921-8181(99)00028-4

Kaser G, Osmaston H (2002) Tropical glaciers. Cambridge University Press

Kendon EJ, Roberts NM, Senior CA, Roberts MJ (2012) Realism of Rainfall in a Very High-Resolution Regional Climate Model. J Clim 25:5791–5806. https://doi.org/10.1175/JCLI-D-11-00562.1

Khand K, Numata I, Kjaersgaard J, Vourlitis G (2017) Dry Season Evapotranspiration Dynamics over Human-Impacted Landscapes in the Southern Amazon Using the Landsat-Based METRIC Model. Remote Sens 9:706. https://doi.org/10.3390/rs9070706

Khanna J, Medvigy D, Fueglistaler S, Walko R (2017) Regional dry-season climate changes due to three decades of Amazonian deforestation. Nat Clim Chang 7:200–204. https://doi.org/10.1038/nclimate3226

Kiladis GN, Wheeler M (1995) Horizontal and vertical structure of observed tropospheric equatorial Rossby waves. J Geophys Res 100:22981. https://doi.org/10.1029/95JD02415

Killeen TJ, Calderon V, Soria L, et al (2007a) Thirty Years of Land-cover Change in Bolivia. J Hum Environ 36:600–606

Killeen TJ, Douglas M, Consiglio T, et al (2007b) Dry spots and wet spots in the Andean hotspot. In: Journal of Biogeography

Kleidon A, Heimann M (2000) Assessing the role of deep rooted vegetation in the climate system with model simulations: mechanism, comparison to observations and implications for Amazonian deforestation. Clim Dyn 16:183–199. https://doi.org/10.1007/s003820050012

Kodama Y (1992) Large-Scale Common Features of Subtropical Precipitation Zones (the Baiu Frontal Zone, the SPCZ, and the SACZ) Part I: Characteristics of Subtropical Frontal Zones. J Meteorol Soc Japan Ser II 70:813–836. https://doi.org/10.2151/jmsj1965.70.4_813

Kousky VE, Kagano MT, Cavalcanti IFA (1984) A review of the Southern Oscillation: oceanic-atmospheric circulation changes and related rainfall anomalies. Tellus A 36A:490–504. https://doi.org/10.1111/j.1600-0870.1984.tb00264.x

Krinner G, Viovy N, de Noblet-Ducoudré N, et al (2005) A dynamic global vegetation model for studies of the coupled atmosphere-biosphere system. Global Biogeochem Cycles 19:. https://doi.org/10.1029/2003GB002199

Krishnamurti TN, Tewari M, Chakraborty DR, et al (1999) Downstream Amplification: A Possible Precursor to Major Freeze Events over Southeastern Brazil. Weather Forecast 14:242–270. https://doi.org/10.1175/1520-0434(1999)014<0242:DAAPPT>2.0.CO;2

Lagos P, Silva Y, Nickl E, Mosquera K (2008) El Niño – related precipitation variability in Perú. Adv Geosci 14:231–237. https://doi.org/10.5194/adgeo-14-231-2008

Laipelt L, Ruhoff AL, Fleischmann AS, et al (2020) Assessment of an Automated Calibration of the SEBAL Algorithm to Estimate Dry-Season Surface-Energy Partitioning in a Forest–Savanna Transition in Brazil. Remote Sens 12:1108. https://doi.org/10.3390/rs12071108

Lamarche C, Santoro M, Bontemps S, et al (2017) Compilation and Validation of SAR and Optical Data Products for a Complete and Global Map of Inland/Ocean Water Tailored to the Climate Modeling Community. Remote Sens 9:36.

https://doi.org/10.3390/rs9010036

Lammertsma EI, Boer HJ de, Dekker SC, et al (2011) Global CO 2 rise leads to reduced maximum stomatal conductance in Florida vegetation. Proc Natl Acad Sci 108:4035–4040. https://doi.org/10.1073/pnas.1100371108

Latrubesse EM, Arima EY, Dunne T, et al (2017) Damming the rivers of the Amazon basin. Nature 546:363–369. https://doi.org/10.1038/nature22333

Laurent H (2002) Characteristics of the Amazonian mesoscale convective systems observed from satellite and radar during the WETAMC/LBA experiment. J Geophys Res 107:8054. https://doi.org/10.1029/2001JD000337

Lavado-Casimiro WS, Felipe O, Silvestre E, Bourrel L (2013) ENSO impact on hydrology in Peru. Adv Geosci 33:33–39. https://doi.org/10.5194/adgeo-33-33-2013

Lawrence D, Vandecar K (2015) Effects of tropical deforestation on climate and agriculture. Nat Clim Chang 5:27–36. https://doi.org/10.1038/nclimate2430

Le Quéré C, Andres RJ, Boden T, et al (2013) The global carbon budget 1959–2011. Earth Syst Sci Data 5:165–185. https://doi.org/10.5194/essd-5-165-2013

Lean J, Rowntree PR (1997) Understanding the Sensitivity of a GCM Simulation of Amazonian Deforestation to the Specification of Vegetation and Soil Characteristics. J Clim 10:1216–1235. https://doi.org/10.1175/1520-0442(1997)010<1216:UTSOAG>2.0.CO;2

Lean J, Warrilow DA (1989) Simulation of the regional climatic impact of Amazon deforestation. Nature 342:411–413. https://doi.org/10.1038/342411a0

Lee J-E, Lintner BR, Boyce CK, Lawrence PJ (2011) Land use change exacerbates tropical South American drought by sea surface temperature variability. Geophys Res Lett 38:n/a-n/a. https://doi.org/10.1029/2011GL049066

Leite CC, Costa MH, de Lima CA, et al (2011) Historical reconstruction of land use in the Brazilian Amazon (1940–1995). J Land Use Sci 6:33–52. https://doi.org/10.1080/1747423X.2010.501157

Lejeune Q, Davin EL, Guillod BP, Seneviratne SI (2015) Influence of Amazonian deforestation on the future evolution of regional surface fluxes, circulation, surface temperature and precipitation. Clim Dyn 44:2769–2786. https://doi.org/10.1007/s00382-014-2203-8

Lenters JD, Cook KH (1997) On the Origin of the Bolivian High and Related Circulation Features of the South American Climate. J Atmos Sci 54:656–678.

https://doi.org/10.1175/1520-0469(1997)054<0656:OTOOTB>2.0.CO;2

Lenton TM, Held H, Kriegler E, et al (2008) Tipping elements in the Earth's climate system. Proc Natl Acad Sci 105:1786–1793. https://doi.org/10.1073/pnas.0705414105

Leung LR, Qian Y (2009) Atmospheric rivers induced heavy precipitation and flooding in the western U.S. simulated by the WRF regional climate model. Geophys Res Lett 36:n/a-n/a. https://doi.org/10.1029/2008GL036445

Lewis SL, Brando PM, Phillips OL, et al (2011) The 2010 Amazon Drought. Science (80-) 331:554–554. https://doi.org/10.1126/science.1200807

Li W, Fu R (2004) Transition of the large-scale atmospheric and land surface conditions from the dry to the wet season over Amazonia as diagnosed by the ECMWF re-analysis. J Clim 17:2637–2651. https://doi.org/10.1175/1520-0442(2004)017<2637:TOTLAA>2.0.CO;2

Li W, Fu R (2006) Influence of Cold Air Intrusions on the Wet Season Onset over Amazonia. J Clim 19:257–275. https://doi.org/10.1175/JCLI3614.1

Li W, Fu R, Dickinson RE (2006) Rainfall and its seasonality over the Amazon in the 21st century as assessed by the coupled models for the IPCC AR4. J Geophys Res Atmos 111:

Li X, Xie S-P, Gille ST, Yoo C (2016) Atlantic-induced pan-tropical climate change over the past three decades. Nat Clim Chang 6:275–279. https://doi.org/10.1038/nclimate2840

Liebmann B, Marengo J (2001) Interannual Variability of the Rainy Season and Rainfall in the Brazilian Amazon Basin. J Clim 14:4308–4318. https://doi.org/10.1175/1520-0442(2001)014<4308:IVOTRS>2.0.CO;2

Lin Y-L, Farley RD, Orville HD (1983) Bulk Parameterization of the Snow Field in a Cloud Model. J Clim Appl Meteorol 22:1065–1092. https://doi.org/10.1175/1520-0450(1983)022<1065:BPOTSF>2.0.CO;2

Lohou F, Kergoat L, Guichard F, et al (2014) Surface response to rain events throughout the West African monsoon. Atmos Chem Phys 14:3883–3898. https://doi.org/10.5194/acp-14-3883-2014

Lovejoy TE, Nobre C (2019) Amazon tipping point: Last chance for action. Sci Adv 5:. https://doi.org/10.1126/sciadv.aba2949

M Silva GA, Ambrizzi T, Marengo JA (2009) Observational evidences on the modulation of the South American Low Level Jet east of the Andes according the

ENSO variability. Ann Geophys 27:645–657. https://doi.org/10.5194/angeo-27-645-2009

Machado LAT, Laurent H, Dessay N, Miranda I (2004) Seasonal and diurnal variability of convection over the Amazonia: A comparison of different vegetation types and large scale forcing. Theor Appl Climatol 78:. https://doi.org/10.1007/s00704-004-0044-9

Machado LO (1998) A fronteira agrícola na Amazonia. Geogr e meio Ambient no Bras 181–217

Madec G, Delecluse P, Imbard M, Levy C (1998) Opa 8 ocean general circulation model—reference manual.

Maeda EE, Ma X, Wagner FH, et al (2017) Evapotranspiration seasonality across the Amazon Basin. Earth Syst Dyn 8:439–454. https://doi.org/10.5194/esd-8-439-2017

Mahar DJ (1979) Frontier development policy in Brazil: a study of Amazonia., Praeger. New York

Mahowald NM, Ward DS, Doney SC, et al (2017) Are the impacts of land use on warming underestimated in climate policy? Environ Res Lett 12:. https://doi.org/10.1088/1748-9326/aa836d

Maignan F, Bréon F-M, Chevallier F, et al (2011) Evaluation of a Global Vegetation Model using time series of satellite vegetation indices. Geosci Model Dev 4:1103–1114. https://doi.org/10.5194/gmd-4-1103-2011

Malhi Y, Grace J (2000) Tropical forests and atmospheric carbon dioxide. Trends Ecol Evol 15:332–337. https://doi.org/10.1016/S0169-5347(00)01906-6

Malhi Y, Roberts JT, Betts RA, et al (2008a) Climate change, deforestation, and the fate of the Amazon. Science (80-) 319:169–172. https://doi.org/10.1126/science.1146961

Malhi Y, Roberts JT, Betts RA, et al (2008b) Climate change, deforestation, and the fate of the Amazon. Science (80-.).

Malhi Y, Wood D, Baker TR, et al (2006) The regional variation of aboveground live biomass in old-growth Amazonian forests. Glob Chang Biol 12:1107–1138. https://doi.org/10.1111/j.1365-2486.2006.01120.x

Malhi Y, Wright J (2004) Spatial patterns and recent trends in the climate of tropical rainforest regions. Philos Trans R Soc London Ser B Biol Sci 359:311–329. https://doi.org/10.1098/rstb.2003.1433

Marengo J, Cornejo A, Satyamurty P, et al (1997) Cold Surges in Tropical and Extratropical South America: The Strong Event in June 1994. Mon Weather Rev 125:2759–2786. https://doi.org/10.1175/1520-0493(1997)125<2759:CSITAE>2.0.CO;2

Marengo JA (2005) Characteristics and spatio-temporal variability of the Amazon River Basin Water Budget. Clim Dyn 24:11–22. https://doi.org/10.1007/s00382-004-0461-6

Marengo JA (1992) Interannual variability of surface climate in the Amazon basin. Int J Climatol 12:853–863. https://doi.org/10.1002/joc.3370120808

Marengo JA, Ambrizzi T, da Rocha RP, et al (2010) Future change of climate in South America in the late twenty-first century: intercomparison of scenarios from three regional climate models. Clim Dyn 35:1073–1097. https://doi.org/10.1007/s00382-009-0721-6

Marengo JA, Espinoza JC (2016) Extreme seasonal droughts and floods in Amazonia: causes, trends and impacts. Int J Climatol 36:1033–1050. https://doi.org/10.1002/joc.4420

Marengo JA, Fisch GF, Alves LM, et al (2017) Meteorological context of the onset and end of the rainy season in Central Amazonia during the GoAmazon2014/5. Atmos Chem Phys 17:7671–7681. https://doi.org/10.5194/acp-17-7671-2017

Marengo JA, Hastenrath S (1993) Case Studies of Extreme Climatic Events in the Amazon Basin. J Clim 6:617–627. https://doi.org/10.1175/1520-0442(1993)006<0617:CSOECE>2.0.CO;2

Marengo JA, Liebmann B, Kousky VE, et al (2001) Onset and End of the Rainy Season in the Brazilian Amazon Basin. J Clim 14:833–852. https://doi.org/10.1175/1520-0442(2001)014<0833:OAEOTR>2.0.CO;2

Marengo JA, Soares WR, Saulo C, Nicolini M (2004) Climatology of the Low-Level Jet East of the Andes as Derived from the NCEP–NCAR Reanalyses: Characteristics and Temporal Variability. J Clim 17:2261–2280. https://doi.org/10.1175/1520-0442(2004)017<2261:COTLJE>2.0.CO;2

Marengo JA, Tomasella J, Soares WR, et al (2012) Extreme climatic events in the Amazon basin. Theor Appl Climatol 107:73–85. https://doi.org/10.1007/s00704-011-0465-1

Markewitz D, Davidson E, Moutinho P, Nepstad D (2004) NUTRIENT LOSS AND REDISTRIBUTION AFTER FOREST CLEARING ON A HIGHLY WEATHERED

SOIL IN AMAZONIA. Ecol Appl 14:177–199. https://doi.org/10.1890/01-6016

Martinez JA, Dominguez F (2014) Sources of atmospheric moisture for the La Plata River Basin. J Clim. https://doi.org/10.1175/JCLI-D-14-00022.1

Maslin M, Malhi Y, Phillips O, Cowling S (2005) New views on an old forest: assessing the longevity, resilience and future of the Amazon rainforest. Trans Inst Br Geogr 30:477–499. https://doi.org/10.1111/j.1475-5661.2005.00181.x

Mather AS (1990) Global forest resources. Belhaven Press

McGregor S, Timmermann A, Stuecker MF, et al (2014) Recent Walker circulation strengthening and Pacific cooling amplified by Atlantic warming. Nat Clim Chang 4:888–892. https://doi.org/10.1038/nclimate2330

McGuffie K, Henderson-Sellers A, Zhang H, et al (1995) Global climate sensitivity to tropical deforestation. Glob Planet Change 10:97–128. https://doi.org/10.1016/0921-8181(94)00022-6

Medvigy D, Walko RL, Avissar R (2011) Effects of Deforestation on Spatiotemporal Distributions of Precipitation in South America. J Clim 24:2147–2163. https://doi.org/10.1175/2010JCLI3882.1

Melack JM, Basso LS, Fleischmann AS, et al (2022) Challenges Regionalizing Methane Emissions Using Aquatic Environments in the Amazon Basin as Examples. Front Environ Sci 10:. https://doi.org/10.3389/fenvs.2022.866082

Michelangeli P-A, Vautard R, Legras B (1995) Weather Regimes: Recurrence and Quasi Stationarity. J Atmos Sci 52:1237–1256. https://doi.org/10.1175/1520-0469(1995)052<1237:WRRAQS>2.0.CO;2

Miguez-Macho G, Fan Y (2012a) The role of groundwater in the Amazon water cycle: 2. Influence on seasonal soil moisture and evapotranspiration. J Geophys Res Atmos 117:n/a-n/a. https://doi.org/10.1029/2012JD017540

Miguez-Macho G, Fan Y (2012b) The role of groundwater in the Amazon water cycle: 1. Influence on seasonal streamflow, flooding and wetlands. J Geophys Res Atmos 117:n/a-n/a. https://doi.org/10.1029/2012JD017539

Miguez-Macho G, Stenchikov GL, Robock A (2004) Spectral nudging to eliminate the effects of domain position and geometry in regional climate model simulations. J Geophys Res Atmos 109:n/a-n/a. https://doi.org/10.1029/2003JD004495

Minvielle M, Garreaud RD (2011) Projecting rainfall changes over the South American Altiplano. J Clim 24:4577–4583. https://doi.org/10.1175/JCLI-D-11-00051.1

Mlawer EJ, Taubman SJ, Brown PD, et al (1997) Radiative transfer for

inhomogeneous atmospheres: RRTM, a validated correlated-k model for the longwave. J Geophys Res Atmos 102:16663–16682. https://doi.org/10.1029/97JD00237

Molina-Carpio J, Espinoza JC, Vauchel P, et al (2017) Hydroclimatology of the Upper Madeira River basin: spatio-temporal variability and trends. Hydrol Sci J 62:911–927. https://doi.org/10.1080/02626667.2016.1267861

Moquet JS, Crave A, Viers J, et al (2011) Chemical weathering and atmospheric/soil CO2 uptake in the Andean and Foreland Amazon basins. Chem Geol. https://doi.org/10.1016/j.chemgeo.2011.01.005

Moron V, Robertson AW, Qian J-H, Ghil M (2015) Weather types across the Maritime Continent: from the diurnal cycle to interannual variations. Front Environ Sci 2:. https://doi.org/10.3389/fenvs.2014.00065

Moron V, Robertson AW, Ward MN, Ndiaye O (2008) Weather Types and Rainfall over Senegal. Part I: Observational Analysis. J Clim 21:266–287. https://doi.org/10.1175/2007JCLI1601.1

Morrison H, Thompson G, Tatarskii V (2009) Impact of Cloud Microphysics on the Development of Trailing Stratiform Precipitation in a Simulated Squall Line: Comparison of One- and Two-Moment Schemes. Mon Weather Rev 137:991–1007. https://doi.org/10.1175/2008MWR2556.1

Muñoz-Sabater J, Dutra E, Agustí-Panareda A, et al (2021) ERA5-Land: a state-of-the-art global reanalysis dataset for land applications. Earth Syst Sci Data 13:4349–4383. https://doi.org/10.5194/essd-13-4349-2021

Myers N, Mittermeler RA, Mittermeler CG, et al (2000) Biodiversity hotspots for conservation priorities. Nature. https://doi.org/10.1038/35002501

Myneni RB, Yang W, Nemani RR, et al (2007) Large seasonal swings in leaf area of Amazon rainforests. Proc Natl Acad Sci 104:4820–4823. https://doi.org/10.1073/pnas.0611338104

Nakanishi M, Niino H (2006) An Improved Mellor–Yamada Level-3 Model: Its Numerical Stability and Application to a Regional Prediction of Advection Fog. Boundary-Layer Meteorol 119:397–407. https://doi.org/10.1007/s10546-005-9030-8

Negri AJ, Adler RF, Xu L, Surratt J (2004) The Impact of Amazonian Deforestation on Dry Season Rainfall. J Clim 17:1306–1319. https://doi.org/10.1175/1520-0442(2004)017<1306:TIOADO>2.0.CO;2

Neill C, Coe MT, Riskin SH, et al (2013) Watershed responses to Amazon soya bean cropland expansion and intensification. Philos Trans R Soc B Biol Sci 368:20120425. https://doi.org/10.1098/rstb.2012.0425

Nepstad D, McGrath D, Stickler C, et al (2014) Slowing Amazon deforestation through public policy and interventions in beef and soy supply chains. Science (80-) 344:1118–1123. https://doi.org/10.1126/science.1248525

Nepstad DC, de Carvalho CR, Davidson EA, et al (1994) The role of deep roots in the hydrological and carbon cycles of Amazonian forests and pastures. Nature 372:666–669. https://doi.org/10.1038/372666a0

Nepstad DC, Stickler CM, Ameida OT (2006) Globalization of the Amazon Soy and Beef Industries: Opportunities for Conservation. Conserv Biol 20:1595–1603. https://doi.org/10.1111/j.1523-1739.2006.00510.x

Nepstad DC, Stickler CM, Soares-Filho B, Merry F (2008) Interactions among Amazon land use, forests and climate: Prospects for a near-term forest tipping point. Philos Trans R Soc B Biol Sci 363:1737–1746. https://doi.org/10.1098/rstb.2007.0036

Nobre CA, Borma LDS (2009) 'Tipping points' for the Amazon forest. Curr Opin Environ Sustain 1:28–36. https://doi.org/10.1016/j.cosust.2009.07.003

Nobre CA, Sampaio G, Borma LS, et al (2016) Land-use and climate change risks in the amazon and the need of a novel sustainable development paradigm. Proc Natl Acad Sci U S A 113:10759–10768. https://doi.org/10.1073/pnas.1605516113

Nobre CA, Sellers PJ, Shukla J (1991) Amazonian Deforestation and Regional Climate Change. J Clim. https://doi.org/10.1175/1520-0442(1991)004<0957:adarcc>2.0.co;2

Nobre P, Malagutti M, Urbano DF, et al (2009) Amazon Deforestation and Climate Change in a Coupled Model Simulation. J Clim 22:5686–5697. https://doi.org/10.1175/2009JCLI2757.1

Norby RJ, DeLucia EH, Gielen B, et al (2005) Forest response to elevated CO 2 is conserved across a broad range of productivity. Proc Natl Acad Sci 102:18052–18056. https://doi.org/10.1073/pnas.0509478102

Norby RJ, Kobayashi K, Kimball BA (2001) Rising CO 2. Future Ecosystems. New Phytol 150:215–221

Oliveira G, Brunsell NA, Moraes EC, et al (2019) Effects of land-cover changes on the partitioning of surface energy and water fluxes in <scp>Amazonia</scp> using high-resolution satellite imagery. Ecohydrology 12:.

https://doi.org/10.1002/eco.2126

Olmo ME, Espinoza J -C., Bettolli ML, et al (2022) Circulation Patterns and Associated Rainfall Over South Tropical South America: GCMs Evaluation During the Dry-To-Wet Transition Season. J Geophys Res Atmos 127:. https://doi.org/10.1029/2022JD036468

Omrani H, Drobinski P, Dubos T (2015) Using nudging to improve global-regional dynamic consistency in limited-area climate modeling: What should we nudge? Clim Dyn 44:1627–1644. https://doi.org/10.1007/s00382-014-2453-5

Ortega G, Arias PA, Villegas JC, et al (2021) Present-day and future climate over central and South America according to <scp>CMIP5</scp> / <scp>CMIP6</scp> models. Int J Climatol 41:6713–6735. https://doi.org/10.1002/joc.7221

Pabón-Caicedo JD, Arias PA, Carril AF, et al (2020) Observed and Projected Hydroclimate Changes in the Andes. Front Earth Sci 8:. https://doi.org/10.3389/feart.2020.00061

Paca VH da M, Espinoza-Dávalos GE, Hessels TM, et al (2019) The spatial variability of actual evapotranspiration across the Amazon River Basin based on remote sensing products validated with flux towers. Ecol Process 8:6. https://doi.org/10.1186/s13717-019-0158-8

Paccini L, Espinoza JC, Ronchail J, Segura H (2018) Intra-seasonal rainfall variability in the Amazon basin related to large-scale circulation patterns: a focus on western Amazon–Andes transition region. Int J Climatol 38:2386–2399. https://doi.org/10.1002/joc.5341

Pan Y, Birdsey RA, Fang J, et al (2011) A Large and Persistent Carbon Sink in the World's Forests. Science (80-) 333:988–993. https://doi.org/10.1126/science.1201609

Paulson CA (1970) The Mathematical Representation of Wind Speed and Temperature Profiles in the Unstable Atmospheric Surface Layer. J Appl Meteorol 9:857–861. https://doi.org/10.1175/1520-0450(1970)009<0857:TMROWS>2.0.CO;2

Pedregosa F, Varoquaux G, Gramfort A, et al (2011) Scikit-learn: Machine Learning in Python. J Mach Learn Res 12:2825–2830

Pepin E, Guyot JL, Armijos E, et al (2013) Climatic control on eastern Andean

denudation rates (Central Cordillera from Ecuador to Bolivia). J South Am Earth Sci 44:85–93. https://doi.org/10.1016/j.jsames.2012.12.010

Pepin N, Bradley RS, Diaz HF, et al (2015) Elevation-dependent warming in mountain regions of the world. Nat Clim Chang 5:424–430. https://doi.org/10.1038/nclimate2563

Perry LB, Seimon A, Kelly GM (2014) Precipitation delivery in the tropical high Andes of southern Peru: new findings and paleoclimatic implications. Int J Climatol 34:197–215. https://doi.org/10.1002/joc.3679

Perugini L, Caporaso L, Marconi S, et al (2017) Biophysical effects on temperature and precipitation due to land cover change. Environ Res Lett 12:. https://doi.org/10.1088/1748-9326/aa6b3f

Phillips OL, Aragão LEOC, Lewis SL, et al (2009) Drought Sensitivity of the Amazon Rainforest. Science (80-) 323:1344–1347. https://doi.org/10.1126/science.1164033

Pichelli E, Coppola E, Sobolowski S, et al (2021) The first multi-model ensemble of regional climate simulations at kilometer-scale resolution part 2: historical and future simulations of precipitation. Clim Dyn 56:3581–3602. https://doi.org/10.1007/s00382-021-05657-4

Pielke RA (2001) Influence of the spatial distribution of vegetation and soils on the prediction of cumulus Convective rainfall. Rev Geophys 39:151–177. https://doi.org/10.1029/1999RG000072

Pielke RA, Pitman A, Niyogi D, et al (2011) Land use/land cover changes and climate: modeling analysis and observational evidence. WIREs Clim Chang 2:828–850. https://doi.org/10.1002/wcc.144

Pöhlker ML, Ditas F, Saturno J, et al (2018) Long-term observations of cloud condensation nuclei over the Amazon rain forest – Part 2: Variability and characteristics of biomass burning, long-range transport, and pristine rain forest aerosols. Atmos Chem Phys 18:10289–10331. https://doi.org/10.5194/acp-18-10289-2018

Polcher J (1995) Sensitivity of Tropical Convection to Land Surface Processes. J Atmos Sci 52:3143–3161. https://doi.org/10.1175/1520-0469(1995)052<3143:SOTCTL>2.0.CO;2

Polcher J, Laval K (1994) The impact of African and Amazonian deforestation on tropical climate. J Hydrol 155:389–405. https://doi.org/10.1016/0022-

1694(94)90179-1

Posada-Marín JA, Rendón AM, Salazar JF, et al (2019) WRF downscaling improves ERA-Interim representation of precipitation around a tropical Andean valley during El Niño: implications for GCM-scale simulation of precipitation over complex terrain. Clim Dyn 52:3609–3629. https://doi.org/10.1007/s00382-018-4403-0

Pöschl U, Martin ST, Sinha B, et al (2010) Rainforest Aerosols as Biogenic Nuclei of Clouds and Precipitation in the Amazon. Science (80-) 329:1513–1516. https://doi.org/10.1126/science.1191056

Poveda G, Espinoza JC, Zuluaga MD, et al (2020) High Impact Weather Events in the Andes. Front Earth Sci 8:. https://doi.org/10.3389/feart.2020.00162

Poveda G, Jaramillo L, Vallejo LF (2014) Seasonal precipitation patterns along pathways of South American low-level jets and aerial rivers. Water Resour Res. https://doi.org/10.1002/2013WR014087

Poveda G, Waylen PR, Pulwarty RS (2006) Annual and inter-annual variability of the present climate in northern South America and southern Mesoamerica. Palaeogeogr Palaeoclimatol Palaeoecol 234:3–27. https://doi.org/10.1016/j.palaeo.2005.10.031

Rabatel A, Francou B, Soruco A, et al (2013) Current state of glaciers in the tropical Andes: a multi-century perspective on glacier evolution and climate change. Cryosph 7:81–102. https://doi.org/10.5194/tc-7-81-2013

Ramos da Silva R, Werth D, Avissar R (2008) Regional Impacts of Future Land-Cover Changes on the Amazon Basin Wet-Season Climate. J Clim 21:1153–1170. https://doi.org/10.1175/2007JCLI1304.1

Rangel TF, Edwards NR, Holden PB, et al (2018) Modeling the ecology and evolution of biodiversity: Biogeographical cradles, museums, and graves. Science (80-) 361:. https://doi.org/10.1126/science.aar5452

Rao VB, Cavalcanti IF, Hada K (1996) Annual variation of rainfall over Brazil and water vapor characteristics over South America. J Geophys Res Atmos 101:26539–26551. https://doi.org/10.1029/96JD01936

Raven PH, Gereau RE, Phillipson PB, et al (2020) The distribution of biodiversity richness in the tropics. Sci Adv 6:. https://doi.org/10.1126/sciadv.abc6228

Richey JE, Nobre C, Deser C (1989) Amazon River Discharge and Climate Variability: 1903 to 1985. Science (80-) 246:101–103.

https://doi.org/10.1126/science.246.4926.101

Rizzolo JA, Barbosa CGG, Borillo GC, et al (2017) Soluble iron nutrients in Saharan dust over the central Amazon rainforest. Atmos Chem Phys 17:2673–2687. https://doi.org/10.5194/acp-17-2673-2017

Rodwell MJ, Hoskins BJ (2001) Subtropical Anticyclones and Summer Monsoons. J Clim 14:3192–3211. https://doi.org/10.1175/1520-0442(2001)014<3192:SAASM>2.0.CO;2

Ronchail J (1995) Variabilidad interanual de las precipitaciones en Bolivia. Bull l'Institut Français d'Études Andin 24:

Rosales AG, Junquas C, da Rocha RP, et al (2022) Valley–Mountain Circulation Associated with the Diurnal Cycle of Precipitation in the Tropical Andes (Santa River Basin, Peru). Atmosphere (Basel) 13:344. https://doi.org/10.3390/atmos13020344

Ruiz-Vásquez M, Arias PA, Martínez JA, Espinoza JC (2020) Effects of Amazon basin deforestation on regional atmospheric circulation and water vapor transport towards tropical South America. Clim Dyn 54:4169–4189. https://doi.org/10.1007/s00382-020-05223-4

Saavedra M, Junquas C, Espinoza JC, Silva Y (2020) Impacts of topography and land use changes on the air surface temperature and precipitation over the central Peruvian Andes. Atmos Res 234:104711. https://doi.org/10.1016/j.atmosres.2019.104711

Sagredo EA, Lowell TV (2012) Climatology of Andean glaciers: A framework to understand glacier response to climate change. Glob Planet Change 86–87:101–109. https://doi.org/10.1016/j.gloplacha.2012.02.010

Salati E, Dall'Olio A, Matsui E, Gat JR (1979) Recycling of water in the Amazon Basin: An isotopic study. Water Resour Res 15:1250–1258. https://doi.org/10.1029/WR015i005p01250

Salati E, Vose PB (1984) Amazon Basin: A System in Equilibrium. Science (80-) 225:129–138. https://doi.org/10.1126/science.225.4658.129

Salazar LF, Nobre CA, Oyama MD (2007) Climate change consequences on the biome distribution in tropical South America. Geophys Res Lett 34:. https://doi.org/10.1029/2007GL029695

Saleska SR, da Rocha HR, Huete AR, et al (2013) LBA-ECO CD-32 Flux Tower Network Data Compilation, Brazilian Amazon: 1999-2006.

https://doi.org///dx.doi.org/10.3334/ORNLDAAC/1174

Sampaio G, Nobre C, Costa MH, et al (2007) Regional climate change over eastern Amazonia caused by pasture and soybean cropland expansion. Geophys Res Lett. https://doi.org/10.1029/2007GL030612

Sastry A, Barua D (2017) Leaf thermotolerance in tropical trees from a seasonally dry climate varies along the slow-fast resource acquisition spectrum. Sci Rep 7:11246. https://doi.org/10.1038/s41598-017-11343-5

Satyamurty P, da Costa CPW, Manzi AO (2013) Moisture source for the Amazon Basin: a study of contrasting years. Theor Appl Climatol 111:195–209. https://doi.org/10.1007/s00704-012-0637-7

Scala JR, Garstang M, Tao W, et al (1990) Cloud draft structure and trace gas transport. J Geophys Res 95:17015. https://doi.org/10.1029/JD095iD10p17015

Schawe M, Gerold G, Bach K, et al Hydrometeorological patterns in relation to montane forest types along an elevational gradient in the Yungas of Bolivia. In: Tropical Montane Cloud Forests. Cambridge University Press, Cambridge, pp 199–207

Schmink M, Wood CH (1992) Contested frontiers in Amazonia. Columbia University Press

Schneider EK, Fan M, Kirtman BP, Dirmeyer PA (2006) Potential effects of Amazon deforestation on tropical climate. Center for Ocean-Land-Atmosphere Studies.

Schoolmeester T, Johansen KS, Alfthan B, et al (2018) The Andean Glacier and Water Atlas. UNESCO and GRID-Arendal

Schrapffer A (2022) High-resolution numerical analysis of land-river-floodplains-atmosphere interaction in La Plata Basin. Institut Polytechnique de Paris; Universidad de Buenos Aires

Segura H (2021) New insights into the atmospheric mechanisms associated with precipitation variability in the southern tropical Andes over a range of time scales. Université Grenoble Alpes

Segura H, Espinoza JC, Junquas C, et al (2020) Recent changes in the precipitation-driving processes over the southern tropical Andes/western Amazon. Clim Dyn 54:2613–2631. https://doi.org/10.1007/s00382-020-05132-6

Segura H, Junquas C, Espinoza JC, et al (2019) New insights into the rainfall variability in the tropical Andes on seasonal and interannual time scales. Clim Dyn 53:405–426. https://doi.org/10.1007/s00382-018-4590-8

Servain J, Caniaux G, Kouadio YK, et al (2014) Recent climatic trends in the tropical Atlantic. Clim Dyn 43:3071–3089. https://doi.org/10.1007/s00382-014-2168-7

Shukla J, Nobre C, Sellers P (1990) Amazon Deforestation and Climate Change. Science (80-) 247:1322–1325. https://doi.org/10.1126/science.247.4948.1322

Shukla PR, Skeg J, Buendia EC, et al (2019) Climate Change and Land: an IPCC special report on climate change, desertification, land degradation, sustainable land management, food security, and greenhouse gas fluxes in terrestrial ecosystems.

Shuttleworth WJ (1988) Evaporation from Amazonian rainforest. Proc R Soc London Ser B Biol Sci 233:321–346. https://doi.org/10.1098/rspb.1988.0024

Sicart JE, Espinoza JC, Quéno L, Medina M (2016) Radiative properties of clouds over a tropical Bolivian glacier: seasonal variations and relationship with regional atmospheric circulation. Int J Climatol 36:3116–3128. https://doi.org/10.1002/joc.4540

Sicart JE, Wagnon P, Pierre Ribstein (2005) Atmospheric controls of the heat balance of Zongo Glacier (16°S, Bolivia). J Geophys Res 110:D12106. https://doi.org/10.1029/2004JD005732

Sierra JP, Arias PA, Vieira SC (2015) Precipitation over Northern South America and Its Seasonal Variability as Simulated by the CMIP5 Models. Adv Meteorol 2015:1–22. https://doi.org/10.1155/2015/634720

Sierra JP, Junquas C, Espinoza JC, et al (2021) Deforestation impacts on Amazon-Andes hydroclimatic connectivity. Clim Dyn. https://doi.org/10.1007/s00382-021-06025-y

Silva-Dias P, Schubert WH, DeMaria M (1983) Large-scale response of the tropical atmosphere to transient convection. J Atmos Sci 40 (11):2689–2707. https://doi.org/10.1175/1520- 0469(1983)040%3c2689:LSROTT%3e2.0.CO;2

Silva Dias MAF, Regnie P (1996) Simulation of mesoscale circulations in a deforested area of Rondonia in the dry season. In: Gash JHC (ed) Amazonian Deforestation and Climate. Oxford University Press, pp 531–547

Silva Dias MAF, Regnier P (1996) Simulation of Mesoscale Circulations in a Deforested Area of Rondonia in the Dry Season. In: Gash J, Nobre C, Roberts J, Victoria R (eds) Amazon Deforestation Climate. Willey, pp 531–547

Silva Junior CHL, Pessôa ACM, Carvalho NS, et al (2021) The Brazilian Amazon deforestation rate in 2020 is the greatest of the decade. Nat Ecol Evol 5:144–145.

https://doi.org/10.1038/s41559-020-01368-x

Sinclair MR (1995) A Climatology of Cyclogenesis for the Southern Hemisphere. Mon Weather Rev 123:1601–1619. https://doi.org/10.1175/1520-0493(1995)123<1601:ACOCFT>2.0.CO;2

Siqueira JR, Toledo Machado LA (2004) Influence of the Frontal Systems on the Day-to-Day Convection Variability over South America. J Clim 17:1754–1766. https://doi.org/10.1175/1520-0442(2004)017<1754:IOTFSO>2.0.CO;2

Skamarock WC, Klemp JB, Dudhia J, et al (2008) A description of the advanced research wrf version 3.

Skamarock WC, Klemp JB, Dudhia J, et al (2019) A Description of the Advanced Research WRF Model Version 4 (No. NCAR/TN-556+STR). https://doi.org/10.5065/1dfh-6p97

Smith CB, Lakhtakia MN, Capehart WJ, Carlson TN (1994) Initialization of Soil-Water Content in Regional-Scale Atmospheric Prediction Models. Bull Am Meteorol Soc 75:585–593. https://doi.org/10.1175/1520-0477(1994)075<0585:IOSWCI>2.0.CO;2

Snyder PK (2010a) The influence of tropical deforestation on the Northern Hemisphere climate by atmospheric teleconnections. Earth Interact. https://doi.org/10.1175/2010EI280.1

Snyder PK (2010b) The Influence of Tropical Deforestation on the Northern Hemisphere Climate by Atmospheric Teleconnections. Earth Interact 14:1–34. https://doi.org/10.1175/2010EI280.1

Soares-Filho BS, Nepstad DC, Curran LM, et al (2006) Modelling conservation in the Amazon basin. Nature 440:520–523. https://doi.org/10.1038/nature04389

Sombroek W (2001) Spatial and Temporal Patterns of Amazon Rainfall. AMBIO A J Hum Environ 30:388–396. https://doi.org/10.1579/0044-7447-30.7.388

Sommer R, Sá TD d. A, Vielhauer K, et al (2002) Transpiration and canopy conductance of secondary vegetation in the eastern Amazon. Agric For Meteorol 112:103–121. https://doi.org/10.1016/S0168-1923(02)00044-8

Sörensson AA, Ruscica RC (2018) Intercomparison and Uncertainty Assessment of Nine Evapotranspiration Estimates Over South America. Water Resour Res 54:2891–2908. https://doi.org/10.1002/2017WR021682

Souza EP, Renno NO, Dias MAFS (2000) Convective circulations induced by surface heterogeneities. J Atmos Sci 57:2915–2922. https://doi.org/10.1175/1520-

0469(2000)057<2915:CCIBSH>2.0.CO;2

Spera SA, Winter JM, Chipman JW (2018) Evaluation of Agricultural Land Cover Representations on Regional Climate Model Simulations in the Brazilian Cerrado. J Geophys Res Atmos 123:5163–5176. https://doi.org/10.1029/2017JD027989

Spracklen DV, Baker JCA, Garcia-Carreras L, Marsham JH (2018) The Effects of Tropical Vegetation on Rainfall. Annu Rev Environ Resour 43:193–218. https://doi.org/10.1146/annurev-environ-102017-030136

Spracklen D V., Arnold SR, Taylor CM (2012) Observations of increased tropical rainfall preceded by air passage over forests. Nature 489:282–285. https://doi.org/10.1038/nature11390

Staal A, Tuinenburg OA, Bosmans JHC, et al (2018) Forest-rainfall cascades buffer against drought across the Amazon. Nat Clim Chang 8:539–543. https://doi.org/10.1038/s41558-018-0177-y

Staver AC, Archibald S, Levin SA (2011) The Global Extent and Determinants of Savanna and Forest as Alternative Biome States. Science (80-) 334:230–232. https://doi.org/10.1126/science.1210465

Stork NE (2018) How Many Species of Insects and Other Terrestrial Arthropods Are There on Earth? Annu Rev Entomol 63:31–45. https://doi.org/10.1146/annurev-ento-020117-043348

Stull RB, Ahrens CD (2011) Meteorology for scientists and engineers., 3th editio

Sud YC, Lau WK-M, Walker GK, et al (1996) Biogeophysical Consequences of a Tropical Deforestation Scenario: A GCM Simulation Study. J Clim 9:3225–3247. https://doi.org/10.1175/1520-0442(1996)009<3225:BCOATD>2.0.CO;2

Sulca J, Takahashi K, Espinoza J-C, et al (2018) Impacts of different ENSO flavors and tropical Pacific convection variability (ITCZ, SPCZ) on austral summer rainfall in South America, with a focus on Peru. Int J Climatol 38:420–435. https://doi.org/10.1002/joc.5185

Sutton C, Hamill TM, Warner TT (2006) Will Perturbing Soil Moisture Improve Warm-Season Ensemble Forecasts? A Proof of Concept. Mon Weather Rev 134:3174–3189. https://doi.org/10.1175/MWR3248.1

Swann ALS, Longo M, Knox RG, et al (2015) Future deforestation in the Amazon and consequences for South American climate. Agric For Meteorol 214–215:12–24. https://doi.org/10.1016/j.agrformet.2015.07.006

Swap R, Gsarstang M, Greco S, et al (1992) Saharan dust in the Amazon Basin. Tellus

B 44:133–149. https://doi.org/10.1034/j.1600-0889.1992.t01-1-00005.x

Tai S, Feng Z, Ma P, et al (2021) Representations of Precipitation Diurnal Cycle in the Amazon as Simulated by Observationally Constrained Cloud-System Resolving and Global Climate Models. J Adv Model Earth Syst 13:. https://doi.org/10.1029/2021MS002586

Taylor CM, Ellis RJ (2006) Satellite detection of soil moisture impacts on convection at the mesoscale. Geophys Res Lett 33:L03404. https://doi.org/10.1029/2005GL025252

Taylor KE (2001) Summarizing multiple aspects of model performance in a single diagram. J Geophys Res Atmos 106:7183–7192. https://doi.org/10.1029/2000JD900719

Thibeault J, Seth A, Wang G (2012) Mechanisms of summertime precipitation variability in the Bolivian Altiplano: present and future. Int J Climatol 32:2033–2041. https://doi.org/10.1002/joc.2424

Thibeault JM, Seth A, Garcia M (2010) Changing climate in the Bolivian Altiplano: CMIP3 projections for temperature and precipitation extremes. J Geophys Res 115:D08103. https://doi.org/10.1029/2009JD012718

Tian H, Melillo JM, Kicklighter DW, et al (2000) Climatic and biotic controls on annual carbon storage in Amazonian ecosystems. Glob Ecol Biogeogr 9:315–335. https://doi.org/10.1046/j.1365-2699.2000.00198.x

Toomey M, Roberts DA, Still C, et al (2011) Remotely sensed heat anomalies linked with Amazonian forest biomass declines. Geophys Res Lett 38:n/a-n/a. https://doi.org/10.1029/2011GL049041

Trachte K (2018) Atmospheric Moisture Pathways to the Highlands of the Tropical Andes: Analyzing the Effects of Spectral Nudging on Different Driving Fields for Regional Climate Modeling. Atmosphere (Basel) 9:456. https://doi.org/10.3390/atmos9110456

Trenberth KE (1999) Atmospheric Moisture Recycling: Role of Advection and Local Evaporation. J Clim 12:1368–1381. https://doi.org/10.1175/1520-0442(1999)012<1368:AMRROA>2.0.CO;2

Trenberth KE, Fasullo JT, Mackaro J (2011) Atmospheric Moisture Transports from Ocean to Land and Global Energy Flows in Reanalyses. J Clim 24:4907–4924. https://doi.org/10.1175/2011JCLI4171.1

Urrutia R, Vuille M (2009) Climate change projections for the tropical Andes using a

regional climate model: Temperature and precipitation simulations for the end of the 21st century. J Geophys Res 114:D02108. https://doi.org/10.1029/2008JD011021

Van Der Ent RJ, Savenije HHG, Schaefli B, Steele-Dunne SC (2010) Origin and fate of atmospheric moisture over continents. Water Resour Res. https://doi.org/10.1029/2010WR009127

Vauchel P, Santini W, Guyot JL, et al (2017) A reassessment of the suspended sediment load in the Madeira River basin from the Andes of Peru and Bolivia to the Amazon River in Brazil, based on 10 years of data from the HYBAM monitoring programme. J Hydrol. https://doi.org/10.1016/j.jhydrol.2017.07.018

Veettil BK, Leandro Bayer Maier É, Bremer UF, de Souza SF (2014) Combined influence of PDO and ENSO on northern Andean glaciers: a case study on the Cotopaxi ice-covered volcano, Ecuador. Clim Dyn 43:3439–3448. https://doi.org/10.1007/s00382-014-2114-8

Vera C, Baez J, Douglas M, et al (2006a) The South American Low-Level Jet Experiment. Bull Am Meteorol Soc 87:63–78. https://doi.org/10.1175/BAMS-87-1-63

Vera C, Higgins W, Amador J, et al (2006b) Toward a Unified View of the American Monsoon Systems. J Clim 19:4977–5000. https://doi.org/10.1175/JCLI3896.1

Vergara W, Deeb A, Valencia A, et al (2007) Economic impacts of rapid glacier retreat in the Andes. Eos, Trans Am Geophys Union 88:261–264. https://doi.org/10.1029/2007EO250001

Victoria RL, Martinelli LA, Moraes JM, et al (1998) Surface Air Temperature Variations in the Amazon Region and Its Borders during This Century. J Clim 11:1105–1110. https://doi.org/10.1175/1520-0442(1998)011<1105:SATVIT>2.0.CO;2

Virji H (1981) A Preliminary Study of Summertime Tropospheric Circulation Patterns over South America Estimated from Cloud Winds. Mon Weather Rev 109:599–610. https://doi.org/10.1175/1520-0493(1981)109<0599:APSOST>2.0.CO;2

Voldoire A, Royer J-F (2005) Climate sensitivity to tropical land surface changes with coupled versus prescribed SSTs. Clim Dyn 24:843–862. https://doi.org/10.1007/s00382-005-0014-7

Voldoire A, Royer JF (2004) Tropical deforestation and climate variability. Clim Dyn 22:857–874. https://doi.org/10.1007/s00382-004-0423-z

Voldoire A, Sanchez-Gomez E, Salas y Mélia D, et al (2013) The CNRM-CM5.1 global

climate model: description and basic evaluation. Clim Dyn 40:2091–2121. https://doi.org/10.1007/s00382-011-1259-y

von Randow C, Manzi AO, Kruijt B, et al (2004) Comparative measurements and seasonal variations in energy and carbon exchange over forest and pasture in South West Amazonia. Theor Appl Climatol 78:5–26. https://doi.org/10.1007/s00704-004-0041-z

von Randow R de CS, Tomasella J, von Randow C, et al (2020) Evapotranspiration and gross primary productivity of secondary vegetation in Amazonia inferred by eddy covariance. Agric For Meteorol 294:108141. https://doi.org/10.1016/j.agrformet.2020.108141

von Storch H, Langenberg H, Feser F (2000) A Spectral Nudging Technique for Dynamical Downscaling Purposes. Mon Weather Rev 128:3664–3673. https://doi.org/10.1175/1520-0493(2000)128<3664:ASNTFD>2.0.CO;2

Vourlitis GL, Filho NP, Hayashi MMS, et al (2002) Seasonal variations in the evapotranspiration of a transitional tropical forest of Mato Grosso, Brazil. Water Resour Res 38:30-1-30–11. https://doi.org/10.1029/2000WR000122

Vuille M, Bradley RS, Keimig F (2000) Interannual climate variability in the Central Andes and its relation to tropical Pacific and Atlantic forcing. J Geophys Res Atmos 105:12447–12460. https://doi.org/10.1029/2000JD900134

Vuille M, Bradley RS, Werner M, Keimig F (2003) 20th Century Climate Change in the Tropical Andes: Observations and Model Results. pp 75–99

Vuille M, Kaser G, Juen I (2008) Glacier mass balance variability in the Cordillera Blanca, Peru and its relationship with climate and the large-scale circulation. Glob Planet Change 62:14–28. https://doi.org/10.1016/j.gloplacha.2007.11.003

Vuille M, Keimig F (2004) Interannual Variability of Summertime Convective Cloudiness and Precipitation in the Central Andes Derived from ISCCP-B3 Data. J Clim 17:3334–3348. https://doi.org/10.1175/1520-0442(2004)017<3334:IVOSCC>2.0.CO;2

Walker R, Moore NJ, Arima E, et al (2009) Protecting the Amazon with protected areas. Proc Natl Acad Sci 106:10582–10586. https://doi.org/10.1073/pnas.0806059106

Wang C, Qian Y, Duan Q, et al (2021) Quantifying physical parameterization uncertainties associated with land-atmosphere interactions in the WRF model over Amazon. Atmos Res 262:105761.

https://doi.org/10.1016/j.atmosres.2021.105761

Wang H, Fu R (2002) Cross-Equatorial Flow and Seasonal Cycle of Precipitation over South America. J Clim 15:1591–1608. https://doi.org/10.1175/1520-0442(2002)015<1591:CEFASC>2.0.CO;2

Wang J, Bars RL, Eltahir EAB (1996) A Stochastic Linear Theory of Mesoscale Circulation Induced by the Thermal Heterogeneity of the Land Surface. J Atmos Sci 53:3349–3366. https://doi.org/10.1175/1520-0469(1996)053<3349:ASLTOM>2.0.CO;2

Wang J, Chagnon FJF, Williams ER, et al (2009) Impact of deforestation in the Amazon basin on cloud climatology. Proc Natl Acad Sci U S A. https://doi.org/10.1073/pnas.0810156106

Wang XY, Li X, Zhu J, Tanajura CAS (2018) The strengthening of Amazonian precipitation during the wet season driven by tropical sea surface temperature forcing. Env Res Lett 13(9):094015

Werth D, Avissar R (2002) The local and global effects of Amazon deforestation. J Geophys Res 107:8087. https://doi.org/10.1029/2001JD000717

Williams M (2000) Dark ages and dark areas: global deforestation in the deep past. J Hist Geogr 26:28–46. https://doi.org/10.1006/jhge.1999.0189

Wongchuig Correa S, Paiva RCD de, Espinoza JC, Collischonn W (2017) Multi-decadal Hydrological Retrospective: Case study of Amazon floods and droughts. J Hydrol 549:667–684. https://doi.org/10.1016/j.jhydrol.2017.04.019

Wongchuig S, Espinoza JC, Condom T, et al (2021) A regional view of the linkages between hydro-climatic changes and deforestation in the Southern Amazon. Int J Climatol. https://doi.org/10.1002/joc.7443

Wright IR, Gash JHC, Da Rocha HR, et al (1992) Dry Season Micrometeorology of Central Amazonian Ranchland. Q J R Meteorol Soc 118:1083–1099. https://doi.org/10.1002/qj.49711850804

Wright IR, Manzi AO, da Rocha HR (1995) Surface conductance of Amazonian pasture: model application and calibration for canopy climate. Agric For Meteorol 75:51–70. https://doi.org/10.1016/0168-1923(94)02203-V

Wright JS, Fu R, Worden JR, et al (2017) Rainforest-initiated wet season onset over the southern Amazon. Proc Natl Acad Sci 114:8481–8486. https://doi.org/10.1073/pnas.1621516114

Yin L, Fu R, Zhang Y-F, et al (2014) What controls the interannual variation of the wet

season onsets over the Amazon? J Geophys Res Atmos 119:2314–2328. https://doi.org/10.1002/2013JD021349

Yoon J-H, Zeng N (2010a) An Atlantic influence on Amazon rainfall. Clim Dyn 34:249–264. https://doi.org/10.1007/s00382-009-0551-6

Yoon JH, Zeng N (2010b) An Atlantic influence on Amazon rainfall. Clim Dyn. https://doi.org/10.1007/s00382-009-0551-6

Zemp DC, Schleussner CF, Barbosa HMJ, et al (2014) On the importance of cascading moisture recycling in South America. Atmos Chem Phys. https://doi.org/10.5194/acp-14-13337-2014

Zeng N, Neelin JD (1999) A Land–Atmosphere Interaction Theory for the Tropical Deforestation Problem. J Clim 12:857–872. https://doi.org/10.1175/1520-0442(1999)012<0857:ALAITF>2.0.CO;2

Zhang H, McGuffie K, Henderson-Sellers A (1996) Impacts of tropical deforestation. Part II: The role of large-scale dynamics. J Clim. https://doi.org/10.1175/1520-0442(1996)009<2498:IOTDPI>2.0.CO;2

Zhang L, Dawes WR, Walker GR (2001) Response of mean annual evapotranspiration to vegetation changes at catchment scale. Water Resour Res 37:701–708. https://doi.org/10.1029/2000WR900325

Zhang S, Zhang K, Wan H, Sun J (2022) Further improvement and evaluation of nudging in the E3SM Atmosphere Model version 1 (EAMv1). Geosci Model Dev Discuss. https://doi.org///doi.org/10.5194/gmd-2022-10

Zhuang Y, Fu R, Marengo JA, Wang H (2017) Seasonal variation of shallow-to-deep convection transition and its link to the environmental conditions over the Central Amazon. J Geophys Res Atmos 122:2649–2666. https://doi.org/10.1002/2016JD025993

A. Appendix: Chapter 3

Abstract, figures and tables from Chapter 3

A.1. Impacts of land-surface heterogeneities and Amazonian deforestation on the wet season onset in southern Amazon

Juan P. Sierra, Jhan C. Espinoza, Clementine Junquas, Sly Wongchuig, Jan Polcher, Vincent Moron, Lluís Fita, Paola A. Arias, Anthony Schrapffer, Romain Pennel

Article submitted to the journal Climate Dynamics on the 2nd of August 2022

A.1.1. Abstract

Continued Amazonian deforestation perturbs the surface turbulent fluxes which are important for building the conditions for the wet season onset in the southern Amazon. This work evaluates the impacts of tropical deforestation on the onset and development of the Amazonian rainy season using a weather typing approach. We use 19-year simulations (2001-2019) with the Regional Earth System Model from the Institute Pierre Simone Laplace (RegIPSL) with twin control/deforestation experiments. RegIPSL represents the dominant modes or the atmospheric circulation patterns (CPs) of the daily-to-decadal circulation variability in tropical South America, and the evolution of atmospheric and surface conditions along the dry-to-wet transition period. According to RegIPSL, forests and crops contribute differently to the onset. During the dry-to-wet transition period, croplands/grasslands present a stronger shallow convection driven by a higher atmospheric temperature. Large-scale subsidence suppresses low-level convection in the region and deep convection only persist over forests where the atmosphere presents more convective potential energy. After the onset and the establishment of large-scale rainfall structures, both land covers behave similarly in terms of surface fluxes. Deforestation decreases the frequency of the CP typically linked to the onset. Changes in the spatial structure and frequency of the wet season CPs reinforce the hypothesis of a deforestation-induced dry season lengthening. Variations in the CP frequency and characteristic rainfall have opposite effects on accumulated rainfall during the dry-to-wet transition period. Whereas alterations in frequency are associated with a regional circulation response, changes in the CP characteristic rainfall correspond to a local response to deforestation.

A.1.2. Figures

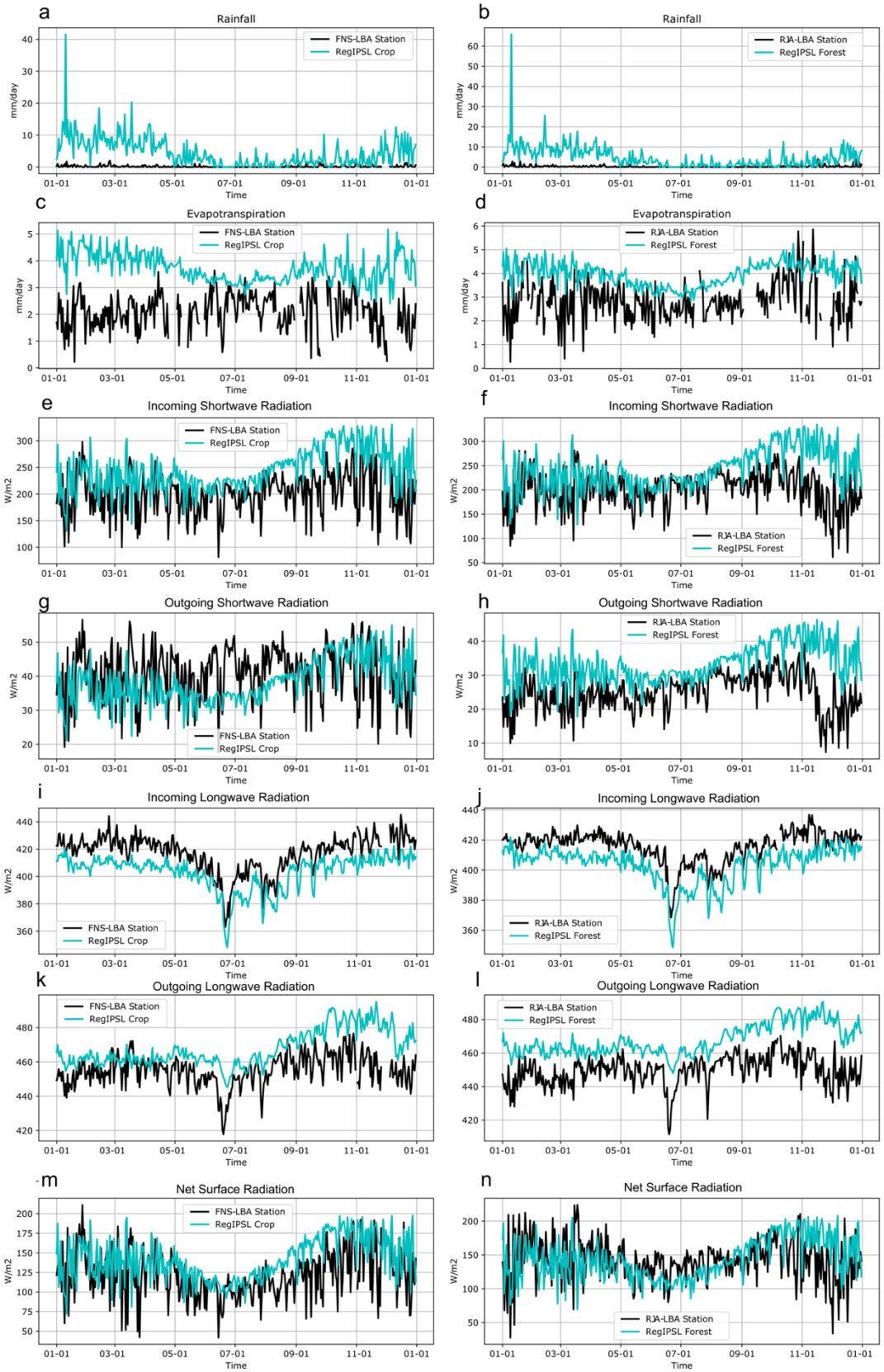

Fig. A.1 *Mean annual cycle in LBA stations Fazenda Nossa Senhora de Aparecida (FNS, deforested area) and Rondonia Jaru Biological Reserve Aparecida (RJA, forested area) in black lines, and RegIPSL-Control in cyan lines, for: rainfall over* ***a*** *cropland/grassland and* ***b*** *forest in mm day-1;*

*evapotranspiration over **c** cropland/grassland and **d** forest in mm day-1; incoming shortwave radiation over **e** cropland/grassland and **f** forest in W m-2; ; outgoing shortwave radiation over **g** cropland/grassland and **h** forest in W m^{-2}; ; incoming longwave radiation over **i** cropland/grassland and **j** forest in W m^{-2}; outgoing longwave radiation over **k** cropland/grassland and **l** forest in W m^{-2}; net surface radiation over **m** cropland/grassland and **n** forest in W m^{-2}. The period 2001-2002 is used for both model and observations. RegIPSL-Control values are computed as the spatial mean of surface variables over an area of 100 km x 100 km surrounding the two stations but masking over forest and non-forest.*

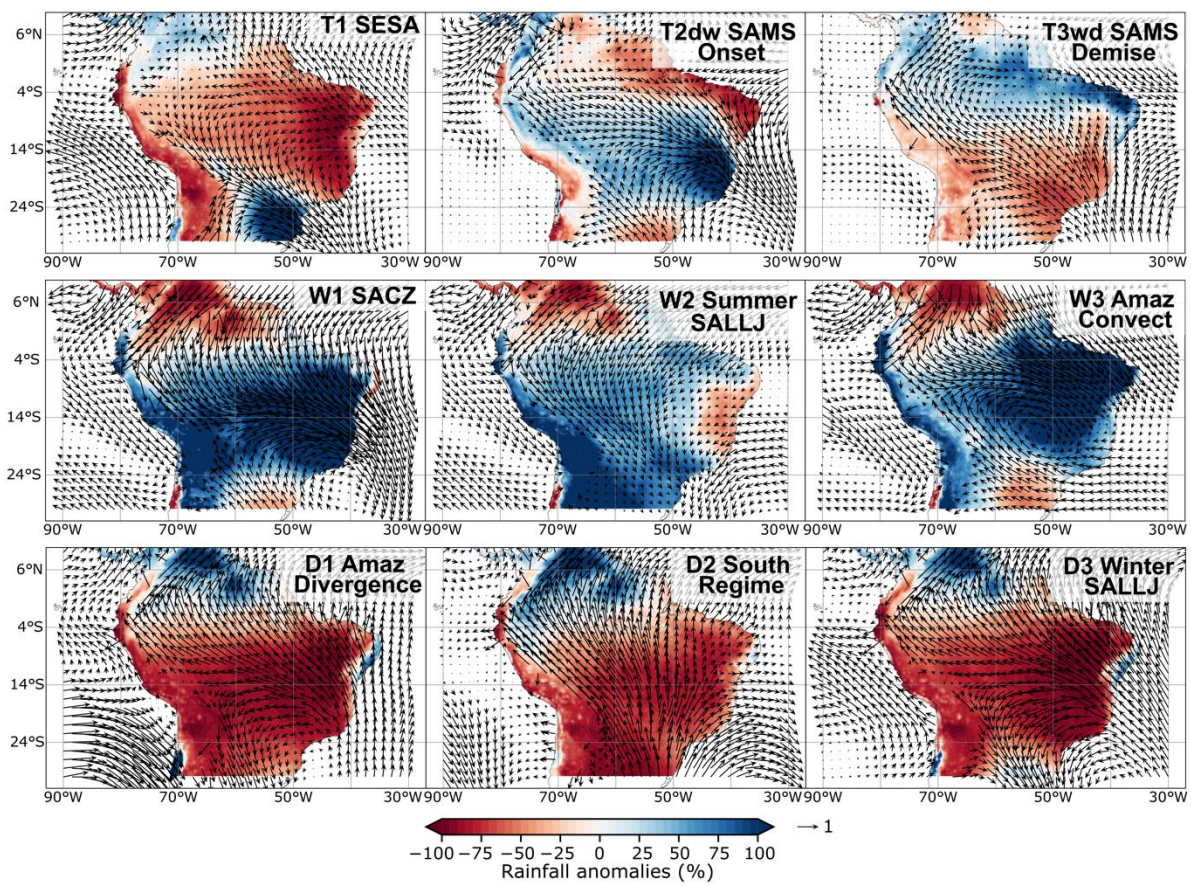

Fig. A.2 Rainfall and 850 hPa horizontal wind anomalies composites (vs the annual mean) for the 9 circulation patterns (CPs) defined from the k-means clustering analysis using ERA5 for winds and CHIRPS for rainfall. Rainfall (shaded) is in percentage respect to the inter-annual mean and horizontal winds at 850 hPa (vectors) are adimensional. Magenta box shows the southern Amazon domain (5°S-15°S, 70°W-50°W).

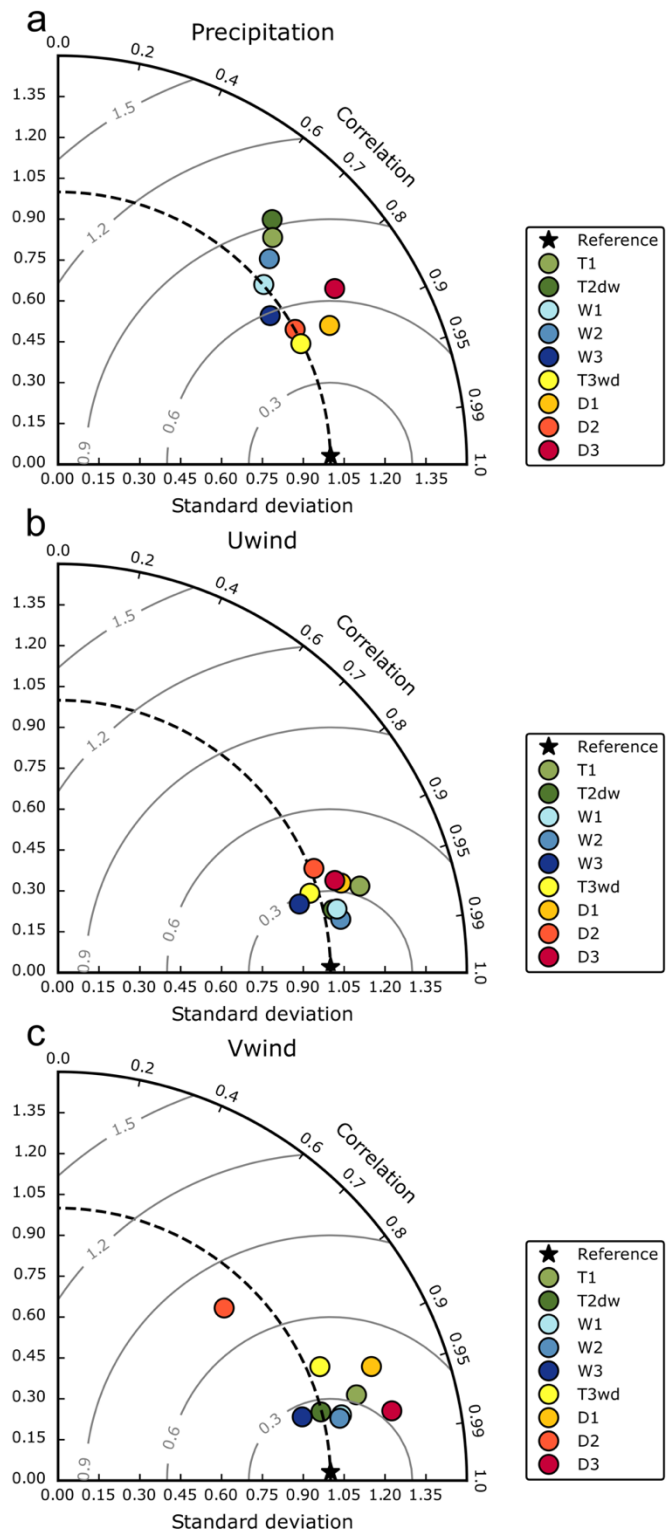

Fig. A.3 *Taylor diagrams of the spatial patterns of: a rainfall anomalies b zonal component anomalies at 850 hPa (denoted as 'Uwind'), and c meridional component anomalies at 850 hPa (denoted as 'Vwind') for the nine circulation patterns (CPs) as represented by RegIPSL-Control. The reference datasets are ERA5 for horizontal low-level winds at 850 hPa and CHIRPS for rainfall anomalies.*

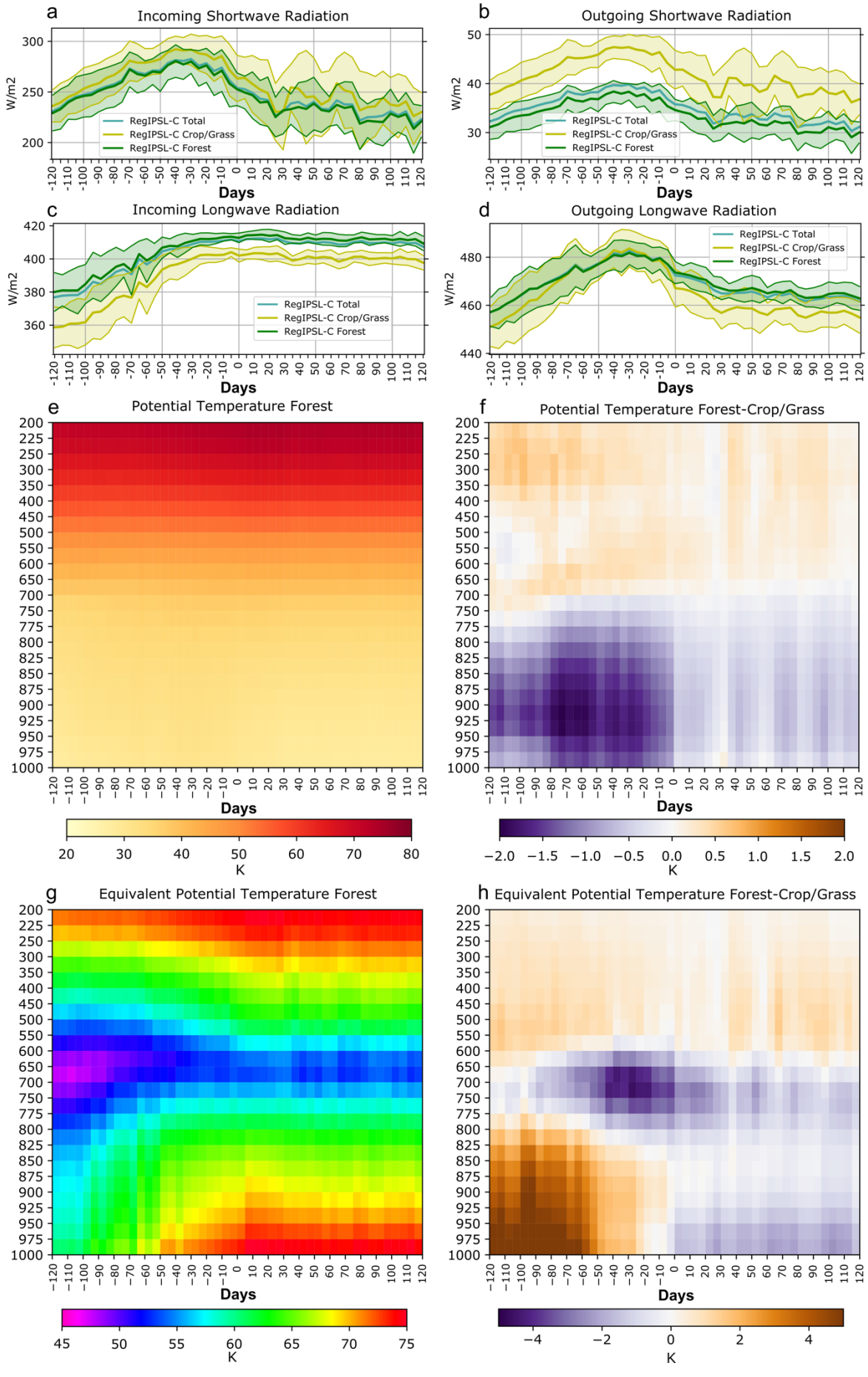
a
Incoming Shortwave Radiation
W/m2
Days
RegIPSL-C Total
RegIPSL-C Crop/Grass
RegIPSL-C Forest
b
Outgoing Shortwave Radiation
c
Incoming Longwave Radiation
d
Outgoing Longwave Radiation
e
Potential Temperature Forest
K
f
Potential Temperature Forest-Crop/Grass
g
Equivalent Potential Temperature Forest
h
Equivalent Potential Temperature Forest-Crop/Grass

Fig. A.4 Composite time series of: **a** incoming shortwave radiation, **b** outgoing shortwave radiation, **c** incoming longwave radiation), **d** outgoing longwave radiation, over the total southern Amazon, forest and cropland areas (cyan, green and yellow lines, respectively) from RegIPSL-Control. Green and yellow envelopes represent the standard deviation for each land cover. All time series are in W m^{-2} . Vertical cross-sections of: **e** potential temperature over forest areas and **f** forest minus crop/grass potential temperature (K), **i** equivalent potential temperature over forest areas (m s^{-1}) and **j** forest minus crop/grass equivalent potential temperature difference (K). The x-axis represents the time, with negative (positive) values for days before (after) the onset.

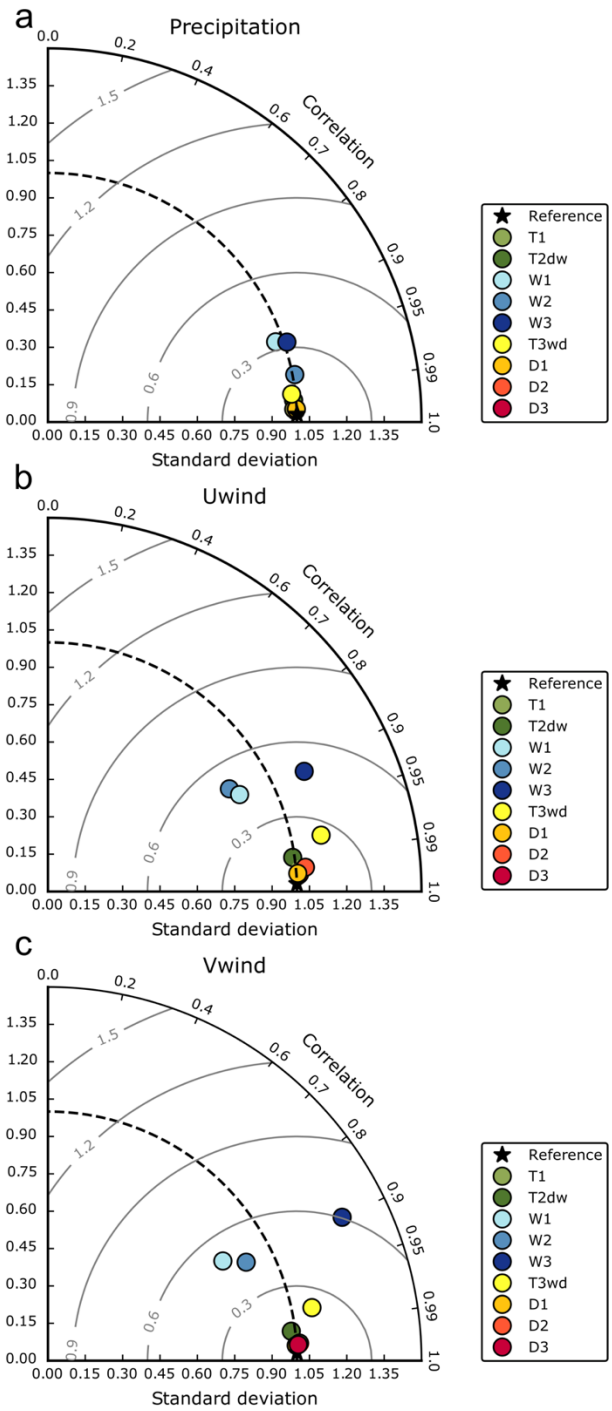

Fig. A.5 Taylor diagrams of the spatial patterns of: a rainfall anomalies b zonal component anomalies at 850 hPa (denoted as 'Uwind'), and c meridional component anomalies at 850 hPa (denoted as 'Vwind') for the nine circulation patterns (CPs) as represented by RegIPSL-Deforested, taking as a reference dataset RegIPSL-Control.

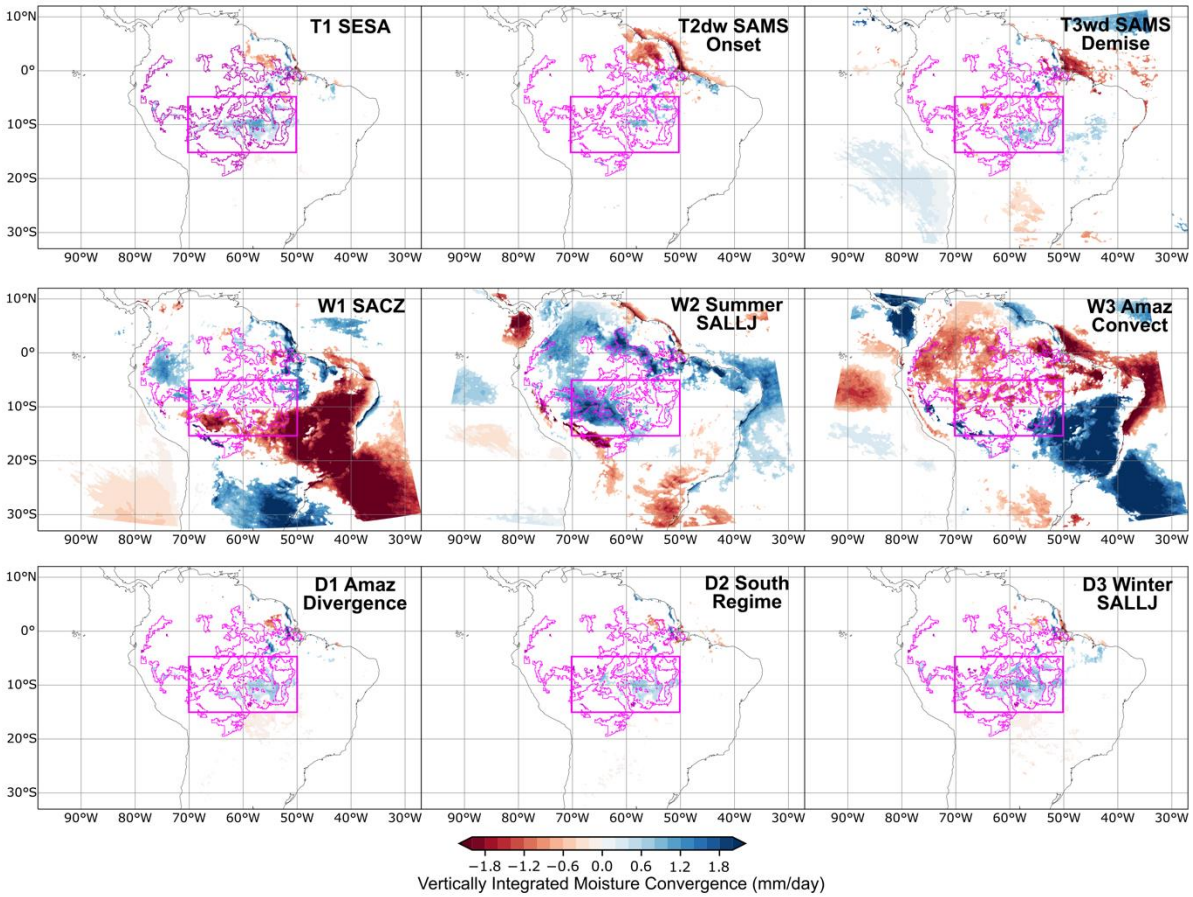

Fig. A.6 Differences RegIPSL-Deforested minus RegIPSL-Control in vertically integrated moisture convergence composites for the 9 circulation patterns (CPs) defined from the k-means clustering analysis. Differences are in mm/day. Only significant vertically integrated moisture convergence differences are shown (t-test, $p<0.05$). Magenta box shows the southern Amazon region (5°S-15°S, 70°W-50°W). The magenta line highlights the deforested area.

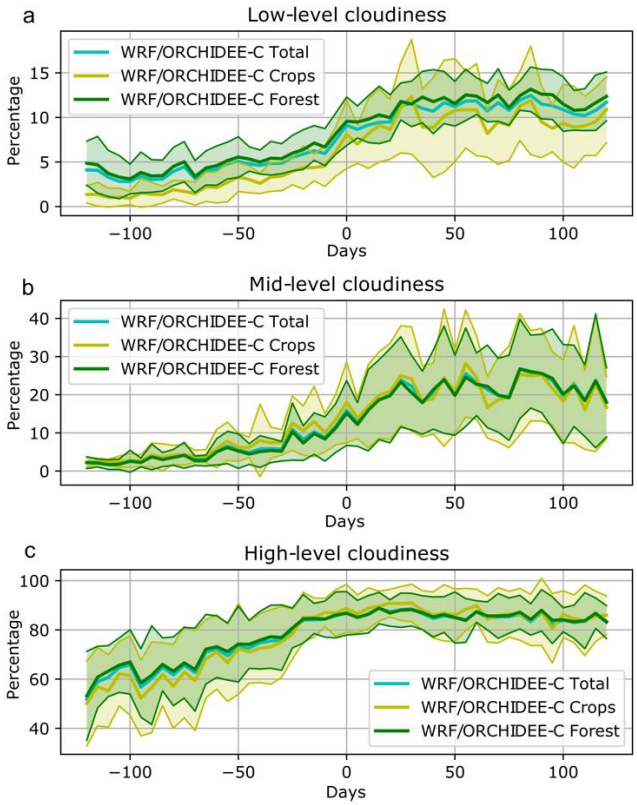

Fig. A.7 Composite time series of: **a** low-level cloudiness, **b** mid-level cloudiness, **c** high-level cloudiness over the total southern Amazon, forest and cropland areas (cyan, green and yellow lines, respectively) from RegIPSL-Control. Green and yellow envelopes represent the standard deviation for each land cover. All time series are in percentage. The x-axis represents the time, with negative (positive) values for days before (after) the onset.

A.1.3. Tables

Table A1. Absolute error (expressed as numbers of days) in the representation of the climatological frequency of occurrence of the identified circulation patterns (CPs) by RegIPSL-Control during the dry-to-wet transition period (July to November) with respect to ERA5 reanalysis.

CP	**T1**	**$T2_{DW}$**	**$T3_{WD}$**	**W1**	**W2**	**W3**	**D1**	**D2**	**D3**
Error metric	0.73	0.70	0.39	0.07	0.22	0.12	0.53	0.60	0.67

B. Appendix: Chapter 4

Abstract, figures and tables from Chapter 4

B.1. Deforestation impacts on Amazon-Andes hydroclimatic connectivity

Juan Pablo Sierra, Clementine Junquas, Jhan Carlo Espinoza, Hans Segura, Thomas Condom, Marcos Andrade, Jorge Molina-Carpio, Laura Ticona, Valeria Mardoñez, Luis Blacutt, Jan Polcher, Antoine Rabatel, Jean Emmanuel Sicart

Article published on the journal Climate Dynamics on the 21th of October 2021

B.1.1. Abstract

Amazonian deforestation has accelerated during the last decade, threatening an ecosystem where almost one third of the regional rainfall is transpired by the local rainforest. Due to precipitation recycling, the southwestern Amazon, including the Amazon-Andes transition region, is particularly sensitive to forest loss. This study evaluates the impacts of Amazonian deforestation on the hydro-climatic connectivity between the Amazon and the eastern tropical Andes during the austral summer (December-January-February) in terms of hydrological and energetic balances. Using 10-year high-resolution simulations (2001-2011) with the Weather Research and Forecasting Model, we analyze control and deforestation scenario simulations. Regionally, deforestation leads to a reduction in the surface net radiation, evaporation, moisture convergence and precipitation (~20%) over the entire Amazon basin. In addition, during this season, deforestation increases the atmospheric subsidence over the southern Amazon and weakens the regional Hadley cell. Atmospheric stability increases over the western Amazon and the tropical Andes inhibiting convection in these areas. Consequently, major deforestation impacts are observed over the hydro-climate of the Amazon-Andes transition region. At local scale, nighttime precipitation decreases in Bolivian valleys (~20-30%) due to a strong reduction in the humidity transport from the Amazon plains towards the Andes linked to the South American low-level jet. Over these valleys, a weakening of the daytime upslope winds is caused by local deforestation, which reduces the turbulent fluxes at lowlands. These alterations in rainfall and atmospheric circulation could impact the rich Andean ecosystems and its tropical glaciers.

B.1.2. Figures

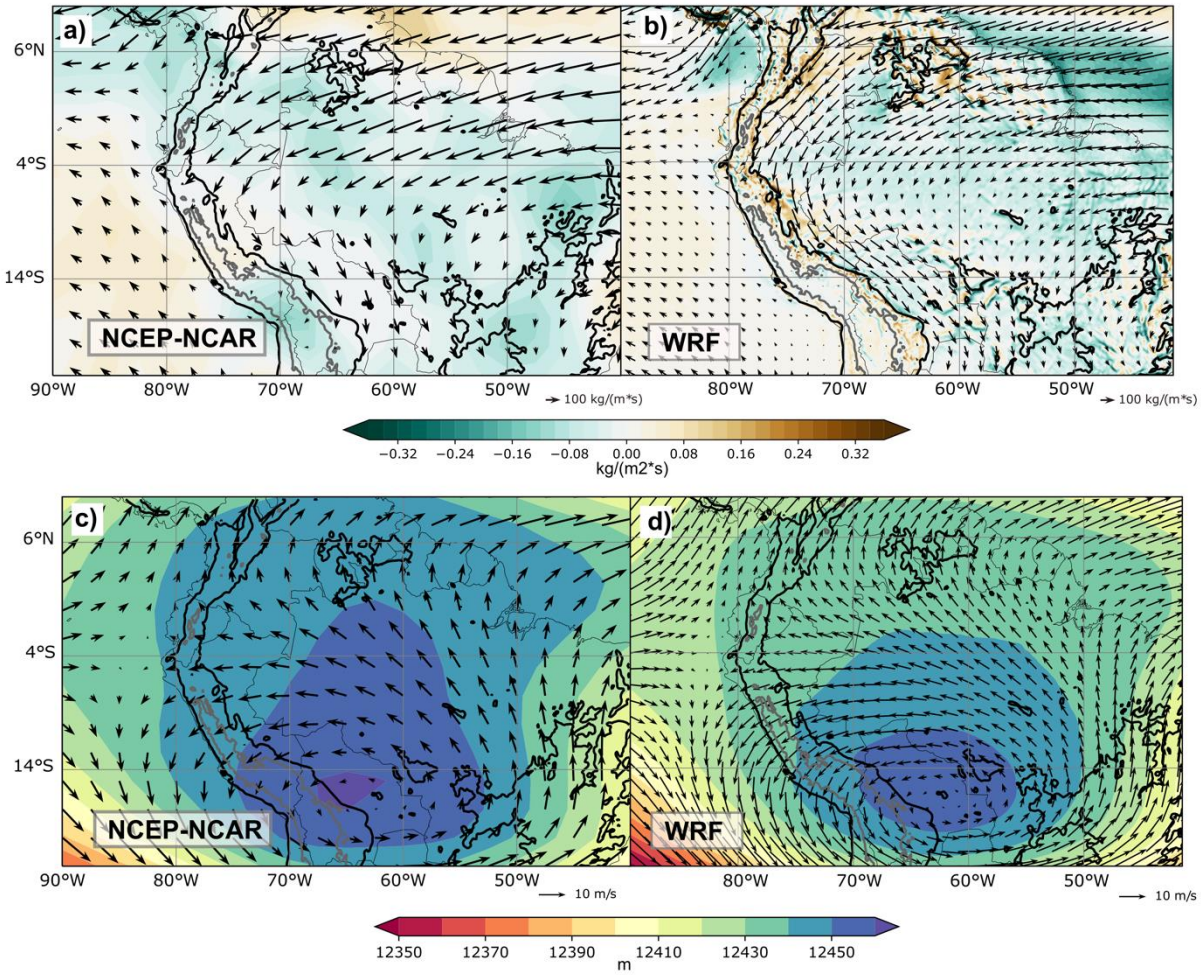

Fig. B.1 Same as Fig. 4.2c-f but comparing with NCEP-NCAR.

B.1.3. Tables

Table B1. Same as Table 4.3 but for geographic location and elevation of rain-gauge stations from field campaigns by the authors.

Name of station	**Location (latitude, longitude)**	**Elevation (m a.s.l.)**
Plataforma	16° 16' 55.0" S, 68° 07' 17.6" W	4730
Tiquimani	16° 12' 27.0" S, 68° 07' 23.8" W	3997

Botijlaca	16° 11' 32.2" S, 68° 08' 26.0" W	3557
Cuticucho	16° 08' 31.8" S, 68° 06' 57.3" W	2790
Santa Rosa	16° 07' 55.0" S, 68° 06' 33.5" W	2659
Sainani	16° 07' 25.9" S, 68° 05' 24.9" W	2224
Chururaqui	16° 06' 26.2" S, 68° 04' 14.4" W	1867
Harca	16° 05' 20.3" S, 68° 02' 39.1" W	1546
Cahua	16° 03' 23.4" S, 68° 00' 52.5" W	1271
Huaji	16° 02' 28.7" S, 67° 58' 37.0" W	1043

C. Appendix: Chapter 4

Figures from Chapter 5

C.1. Figures

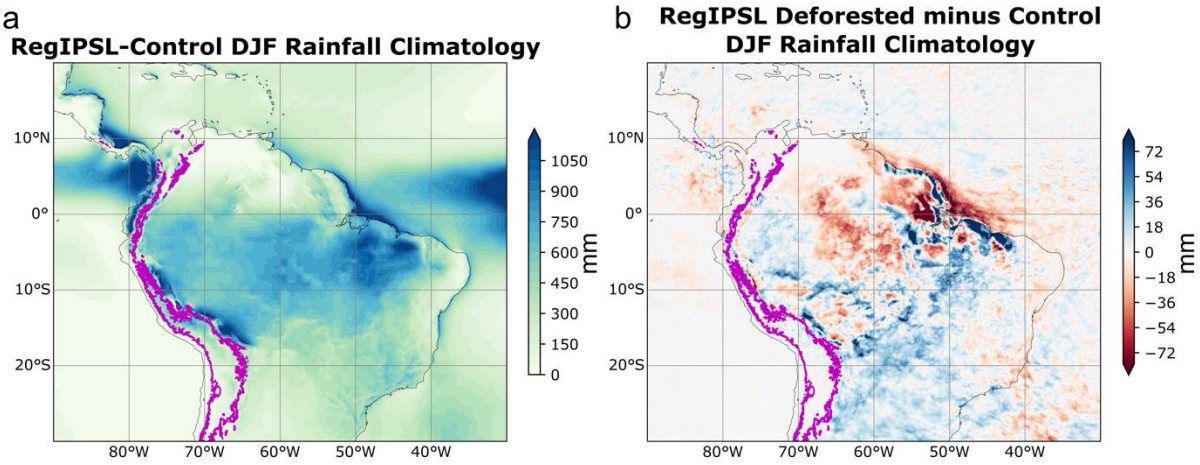

Fig. C.1 DJF total rainfall climatology during the period 2001-2019 for: **a** RegIPSL-Control and **b** RegIPSLDeforested minus Control. Precipitation values in **a** and **b** are in mm. The magenta line highlights the 3000 m elevation contour.

List of figures

List of Tables